New conformal bootstrap solutions and percolation models on the torus

Nina Javerzat

Thèse de doctorat

NNT : 2020UPASP062

université PARIS-SACLAY

New conformal bootstrap solutions and percolation models on the torus

Thèse de doctorat de l'université Paris-Saclay

École doctorale n° 564, Physique en Île-de-France (EDPIF)
Spécialité de doctorat : Physique
Unité de recherche : Université Paris-Saclay, CNRS, LPTMS, 91405, Orsay, France
Référent : Faculté des sciencesd'Orsay

Thèse présentée et soutenue à Orsay, le 20 Octobre 2020, par

Nina Javerzat

Composition du jury :

Malte Henkel Professeur, Université de Lorraine Laboratoire de Physique et Chimie Théoriques	Président, rapporteur & examinateur
Erik Tonni Professeur associé, Scuola Internazionale Superiore di Studi Avanzati	Rapporteur & examinateur
Bertrand Duplantier Directeur de recherche, Université Paris-Saclay, CEA Institut de Physique Théorique	Examinateur
Eveliina Peltola Professeure, University of Bonn Institute for Applied Mathematics	Examinatrice
Marco Picco Directeur de recherche, Sorbonne Université Laboratoire de Physique Théorique et Hautes Énergies	Examinateur
Sylvain Ribault Chargé de recherche, Université Paris-Saclay, CEA Institut de Physique Théorique	Examinateur
Jacopo Viti Professeur, Universidade Federal do Rio Grande do Norte International Institute of Physics	Examinateur
Raoul Santachiara Chargé de recherche, Université Paris-Saclay Laboratoire de Physique Théorique et Modèles Statistiques	Directeur de thèse

À Anaïs, que tout ça aurait bien fait rigoler.

REMERCIEMENTS

Mes premiers remerciements vont bien sûr, du fond du coeur, à mon directeur de thèse Raoul. Je suis très heureuse d'avoir eu la chance de te rencontrer, d'apprendre à connaître la belle personne que tu es, débordante d'idées et d'enthousiasme. Je suis très reconnaissante pour toutes ces heures passées à travailler ensemble, pour le temps que tu as pris, et au cours duquel j'ai tellement appris, à la fois sur la physique pure et dure que sur les mécanismes de la recherche, et sur comment communiquer la science (et aussi sur la physico-chimie de la *carbonara*, ce qui n'est pas négligeable). Vraiment, merci Raoul, c'est grâce à toi si ces trois années furent une si belle aventure !

Je souhaite ensuite remercier chaleureusement les membres du jury, Malte, Erik, Bertrand, Evelina, Jacopo, Marco et Sylvain, pour l'intérêt et la curiosité empreints de bienveillance qu'ils ont portés à mon travail. Je remercie aussi Marco et Sylvain pour les nombreuses discussions au cours desquelles j'ai beaucoup appris, Malte et Sylvain pour leurs commentaires détaillés sur le manuscrit.

Je remercie Alberto Rosso pour son éternelle bonne humeur et son incroyable gentillesse ; ce fut un grand plaisir et très enrichissant de travailler ensemble. Je remercie aussi Sebastian Grijalva avec qui, de même, je fus très contente de collaborer. J'aurais aimé pouvoir remercier Omar Foda, pour sa présence attentionnée et son soutien, constants malgré la distance. Je voudrais aussi remercier Christian Hagendorf qui m'a fait prendre conscience de l'importance de spécifier quelles sont les observables que décrit une CFT donnée (cf. les discussions pages 18 et 81), ainsi qu'Hugo Vanneuville pour nos échanges enthousiasmants et son aide précieuse avec la littérature mathématique.

Je remercie mon tuteur Benoît Estienne ainsi que mon parrain Satya Majumdar pour leurs conseils avisés. Je souhaite remercier l'ensemble des membres du LPTMS ; il semblerait que les interactions collectives de tant de personnes fantastiques créent une atmosphère particulièrement enrichissante, stimulante et épanouissante, et cela a joué un rôle primordial dans le déroulement de ma thèse. Je remercie en particulier Emmanuel Trizac pour son soutien discret mais bien présent, Claudine Le Vaou et Karolina Kolodziej pour leur efficacité et leur sympathie légendaires, ainsi que Véronique Terras pour son aide administrative fort appréciée. Je remercie également Nicolas Pavloff avec qui il fut très agréable d'enseigner, ainsi que Natasha Kirova qui, par son retour très positif sur un de mes séminaires m'a permis de prendre confiance en mes capacités à faire de la recherche. Pour les mêmes raisons je remercie aussi Stéphane Ouvry et Alberto Rosso. Et bien sûr, car tout aurait été différent sans eux, je remercie tous ces doctorants, devenus des amis durant ces trois années : Mathieu, Nadia, Hao, Luca, Ivan, Thibault, Samuel, Antonio, Sebastian, Alexandre, et aussi Aurélien, Bertrand, Kirill, Inés.

Un grand merci à mes parents, à ma petite soeur, à ma tante, pour leur amour et leur soutien, leurs encouragements, ainsi qu'à Lydia, Christel, Alain et Camille, Clotilde et Léopoldine, Dominique et Michel. Pour tout ça aussi, merci à mes amis, à Louisiane, Lara, Maxime (et merci pour les 120 samoussas, et le reste !) Baptiste, Léo, Guilhem, Clara, Yegor ; merci à Vaiana pour son magnifique dessin de la page 161 (promis je t'expliquerai un jour).

Enfin, merci à Thibault, un peu pour les belles figures en TikZ mais surtout pour tout l'amour et le bonheur que tu me donnes.

CONTENTS

MODULUS-SQUARE NOTATIONS

$$|f(z,\Delta)|^2 = f(z,\Delta)\times f(\bar{z},\bar{\Delta}) \tag{0.1}$$

For left and right conformal weights:

$$\begin{aligned}(\Delta) &\equiv \Delta,\bar{\Delta}\\ (\Delta,Y) &\equiv \Delta,Y;\bar{\Delta},\bar{Y}\end{aligned} \tag{0.2}$$

For OPE coefficients:

$$D^{(\Delta_3,Y_3)}_{(\Delta_1,Y_1),(\Delta_2,Y_2)} = \langle V_{(\Delta_3,Y_3)}(\infty)V_{(\Delta_1,Y_1)}(1)V_{(\Delta_2,Y_2)}(0)\rangle = D^{\Delta_3,Y_3}_{\Delta_1,Y_1;\Delta_2,Y_2}D^{\bar{\Delta}_3,\bar{Y}_3}_{\bar{\Delta}_1,\bar{Y}_1;\bar{\Delta}_2,\bar{Y}_2}. \tag{0.3}$$

PARAMETRISATIONS OF THE CENTRAL CHARGE

In terms of the background charge Q and coupling constant b:

$$c = 1+6Q^2, \qquad Q = b+\frac{1}{b} \tag{0.4}$$

$$c = 1-6(\beta-\frac{1}{\beta})^2, \qquad \beta = ib. \tag{0.5}$$

Central charge of minimal models $\mathcal{M}_{p,q}$:

$$c = c_{p,q} = 1-6\frac{(p-q)^2}{pq}, \quad \begin{cases} p,q \text{ coprime integers }, \\ 2\leq p<q\ , \end{cases} \tag{0.6}$$

PARAMETRISATIONS OF THE CONFORMAL DIMENSION

Parametrisation of the conformal dimension in terms of the momentum P (defined up to reflection $P\to -P$) or the charge α (defined up to $\alpha\to Q-\alpha$):

$$\Delta = \frac{Q^2}{4}-P^2 \tag{0.7a}$$

$$\Delta = \alpha(Q-\alpha) \tag{0.7b}$$

$$\alpha = P+\frac{Q}{2}. \tag{0.7c}$$

Degenerate representations have momentum, charge and dimension:

$$P_{r,s} = \frac{r}{2}b+\frac{s}{2}b^{-1} \tag{0.8a}$$

$$\alpha_{r,s} = \frac{1-r}{2}b+\frac{1-s}{2}b^{-1} \tag{0.8b}$$

$$\Delta_{r,s} = \frac{1}{4}\left((b+b^{-1})^2-(rb+sb^{-1})^2\right) \tag{0.8c}$$

RÉSUMÉ EN FRANÇAIS

CONTEXTE GÉNÉRAL

Les phénomènes critiques fascinent les physiciens depuis de nombreuses années [1], et pour de bonnes raisons : l'existence de l'universalité, la présence d'invariances, et, surtout, parce que leur description ne cesse de soulever de nouveaux défis et de nouvelles questions. En effet, ces phénomènes émergent du comportement collectif de nombreux degrés de liberté, et ne peuvent être compris à partir de l'analyse d'un petit nombre de ces derniers. Selon Anderson [2] «More is different », et la description de «more »a nécessité le développement de nouvelles idées en physique théorique. Même aujourd'hui, de nouvelles questions émergent, dont certaines sont au coeur de ce travail de thèse.
Afin d'illustrer pourquoi «l'universalité»et «les invariances»sont si attrayantes, considérons l'un des premiers phénomènes critiques observé expérimentalement, il y a environ deux siècles [3] : l'opalescence critique. Ce phénomène a lieu lorsqu'un fluide transparent est soumis à des conditions précises de pression et de température ; il prend alors subitement un aspect laiteux[1]. En effet, en ce point critique du diagramme de phase, les densités de fluctuations ont lieu à des longueurs d'onde suffisament grandes pour diffuser la lumière visible, rendant le fluide opaque. En fait, ces fluctuations ont lieu à toutes les échelles de longueurs, de telle façon que le système est statistiquement invariant d'échelle : si nous pouvions examiner le fluide au microscope, quel que soit le grossissement, nous verrions le même motif fluctuant de régions de hautes et basses densités. Ces régions sont des fractales aléatoires[2]. Quantitativement, il en découle que les observables physiques ont un comportement en loi de puissance. Par exemple, la chaleur spécifique d'un fluide diverge algébriquement lorsque la température approche sa valeur critique : $C \sim |T - T_c|^{-\alpha}$. L'exposant critique α, ainsi que tous les autres exposants donnant le comportement critique des autres fonctions thermodynamiques, encode ainsi les propriétés macroscopiques du système. De façon remarquable, ces exposants ne dépendent pas des détails microscopiques du système en question. Ainsi, différents fluides au point critique, mais aussi les aimants au point de transition ferromagnétique, sont décrits par les mêmes exposants [6]. Cette universalité du comportement critique macroscopique suggère des mécanismes fondamentaux identiques dans des systèmes différents au niveau microscopique.

La prédiction théorique des exposants critiques, et donc la caractérisation des phénomènes critiques, est un défi. Les approches dites de champ moyen sont parvenues à donner une description qualitative, et à prédire les valeurs des exposants critiques pour des systèmes pour lesquels les fluctuations peuvent être négligées. Les idées du groupe de renormalisation ont par la suite fourni un cadre théorique à l'étude des propriétés à grande échelle des modèles statistiques. En particulier, les idées du groupe de renormalisation suggèrent que les limites d'échelle des moyennes statistiques de certaines observables sur réseau existe, et correspondent à des fonctions de corrélation dans une théorie quantique des champs (voir par exemple la section 2 de [7]).

1 Des vidéos de réaisations expérimentales peuvent-être trouvées facilement, par exemple [4].
2 De telles fluctuations fractales ont été capturées et mesurées expérimentalement [5].

Pour les systèmes de basse dimension les fluctuations sont importantes, faisant échouer les approches de champ moyen et de groupe de renormalisation perturbatif. En deux dimensions la détermination exacte des exposants critiques de certaines classes d'universalité importantes (par exemple Ising et la percolation pure) a été accomplie à partir de solutions exactes des modèles sur réseau [8–12], et par les techniques du gaz de Coulomb [13–16]. En parallèle, il fut réalisé [17] que les systèmes critiques ne sont pas seulement invariants d'échelle, mais aussi, dans de nombreux cas, également invariants sous l'ensemble plus large des transformations conformes. A partir du fait que, en deux dimensions, il existe une infinité de transformations conformes, il a été montré [18] que l'on peut obtenir les solutions complètes des théories des champs quantiques en interactions qui décrivent les modèles critiques. Le principe de cette approche dite de «bootstrap »[19] est de trouver les solutions de théorie des champs qui soient cohérentes avec les principes généraux de théorie des champs et avec la symétrie conforme, à partir des contraintes mêmes imposées par cette cohérence. Appliquée au phénomènes critiques, cette approche permet de prédire exactement tous les exposants critiques, et plus généralement la limite d'échelle de toutes les moyennes statistiques des observables sur réseau. Ceci a été accompli pour les théories des champs conformes (CFTs) appelées modèles minimaux (voir par exemple [20–22]), qui ont été complètement classifiées [18, 23, 24] et résolues [18, 23, 25, 26]. Ces CFTs décrivent beaucoup (mais pas toutes) les classes d'universalité importantes, comme la fameuse classe d'universalité d'Ising. Les modèles sur réseau correspondant ont été construits [27, 28]. Ils comprennent en particulier les modèles définis par des interactions locales avec poids de Boltzmann positifs, décrits par des modèles minimaux unitaires.
Depuis lors, un intérêt croissant a été porté à la compréhension de la limite d'échelle des systèmes statistiques invariants conformes. Les mathématiciens y ont trouvé de nouveaux défis en théorie des probabilités [29, 30], notamment depuis la conjecture de Cardy [31, 32]. Ceux-ci incluent par exemple des preuves rigoureuses de l'invariance conforme des modèles statistiques [33, 34], ou de l'existence de la limite d'échelle [35–37], ainsi que des valeurs des exposants critiques [38, 39].

Cependant, il existe des modèles importants qui n'appartiennent pas à la classification ci-dessus. On peut citer notamment les modèles avec désordre, ainsi que les modèles décrivant les propriétés géométriques des transitions de phase critiques. Ces derniers sont en effet définis par des degrés de liberté non-locaux, et représentent le sujet principal de cette thèse. Pour donner un exemple concret, prenons l'un des modèles sur réseau les plus connus, le modèle d'Ising. Plutôt que de considérer les degrés de liberté locaux –les spins– considérons les amas (dits de Fortuin-Kasteleyn, FK) formés en plaçant des liens aléatoirement entre les sites de même spin. A la température critique une transition de percolation a lieu, où un amas de la taille du système émerge. Les fluctuations du système sont encodées dans la mesure de probabilité des amas, qui est invariante conforme. Caractériser ces fluctuations revient donc à déterminer complètement les propriétés statistiques des amas de percolation. L'approche de CFT a donné avec succès de nombreuses prédictions sur les amas FK d'Ising, et plus généralement sur les aspects géométriques des phénomènes critiques. On peut citer par exemple la formule de Cardy pour la percolation critique [31], et la détermination des dimensions fractales des amas des modèles $O(n)$ et des modèles de Potts à Q états [40, 41]. Malgré ces succès, des propriétés statistiques importantes sont restées hors de portée, même pour le modèle le plus simple de la percolation pure (non-corrélée). Par exemple, alors qu'il est connu depuis longtemps que la probabilité que deux points à distance r appartiennent à un même amas (connectivité à deux points) décroît comme $r^{-5/24}$ [11, 12, 42], la limite d'échelle de la probabilité que trois points appartiennent au même amas (connectivité à

trois points) a été conjecturée relativement récemment [43]. De façon plus générale, une solution complète de CFT décrivant les propriétés de connectivité des amas de la percolation pure a été un problème ouvert pendant une trentaine d'années, et seulement récemment une solution presque complète a été trouvée [44–49]. C'est une des nouvelles solutions de bootstrap que nous allons discuter dans cette thèse.

CE TRAVAIL: MOTIVATION ET RÉSUMÉ DES RÉSULTATS

La motivation à l'origine de ce travail de thèse était d'explorer les nouvelles solutions de bootstrap suggérées par les phénomènes critiques géométriques et désordonnés. J'ai travaillé dans deux directions principales :

i) L'implémentation de méthodes de bootstrap numérique en deux dimensions : j'ai examiné des questions techniques sur des subtilités dans le calcul récursif des blocs conformes de Virasoro.

ii) L'étude de modèles de percolation sur une topologie toroïdale : les amas aléatoires du modèle de Potts à Q états et la percolation de surface aléatoires. J'ai trouvé que les connectivités des amas (la probabilité que des points appartiennent au même amas) sur le tore sont un très bon outil pour tester des résultats récents sur les CFTs de ces modèles, et en établir de nouveaux.

Les résultats principaux sont résumés ci-dessous.

Structure anaytique de la représentation récursive des blocs conformes

Un ingrédient crucial du bootsrap conforme est le calcul des blocs conformes, dans l'espace des paramètres (dimensions d'échelle et/ou charge centrale). En deux dimensions les blocs conformes sont des fonctions compliquées de ces paramètres, qui ne sont pas connues sous forme fermée. On peut néammoins les calculer récursivement. Cependant, il se trouve que cette représentation récursive diverge à certains points de l'espace des paramètres. Ceci est assez problématique en pratique car le but du bootstrap est justement de scanner cet espace, à la recherche de solutions cohérentes. J'ai donc cherché à répondre aux questions suivantes : d'où viennent ces divergences ? Pouvons-nous trouver une formule manifestement finie pour les blocs conformes bidimensionels ?
J'ai compris que ces divergences sont des artefacts de la représentation récursive. J'ai pu comprendre systématiquement comment elles apparaissent pour des blocs plus simples, sur la topologie du tore. J'ai calculé explicitement leur limite finie pour un niveau arbitraire de l'expansion, donnée par l'équation (5.36) dans l'Article I. En revanche, trouver une représentation qui soit manifestement finie pour le bloc conforme à quatre points est toujours une question ouverte.

> Nina Javerzat, Raoul Santachiara, and Omar Foda. "Notes on the solutions of Zamolodchikov-type recursion relations in Virasoro minimal models." In: *JHEP* 08 (2018), p. 183. DOI: 10.1007/JHEP08(2018)183. arXiv: 1806.02790 [hep-th]

→Inclus comme Article I au Chapitre 3.

Amas aléatoires du modèle de Potts à Q états

A partir des solutions proposées dans [44–46], j'ai utilisé l'approche CFT pour déterminer analytiquement les corrections universelles dominantes dues à la toplogie du tore pour les connectivités à deux, trois et quatre points, pour toute valeur de $Q \in [1, 4]$, et comparé à des simulations Monte Carlo. La figure ci-dessous montre les points de données pour la connectivité à deux points dans la limite de percolation pure $Q \to 1$. Un de mes résultats principaux est également tracé, donné par (4.5) dans l'Article II. Sur cette figure on peut voir trois régimes : des effets non-universels quand la distance entre les points est de l'ordre de quelques pas du réseau, le régime du plan infini où la probabilité décroît comme une loi de puissance avec l'exposant bien connu $\eta = 5/24$, et un régime où les effets toplogiques dominent. En effet on peut clairement voir sur cette figure que lorsque $r \gtrsim N/2$ la probabilité dévie significativement d'une loi de puissance. Cet effet est universel. Bien que sont origine soit facilement expliquée (la probabilité prend des contributions des chemins connectant les deux points en faisant le tour du tore, voir la figure sur la droite), aucune prédiction théorique n'avait été donnée jusqu'à présent.

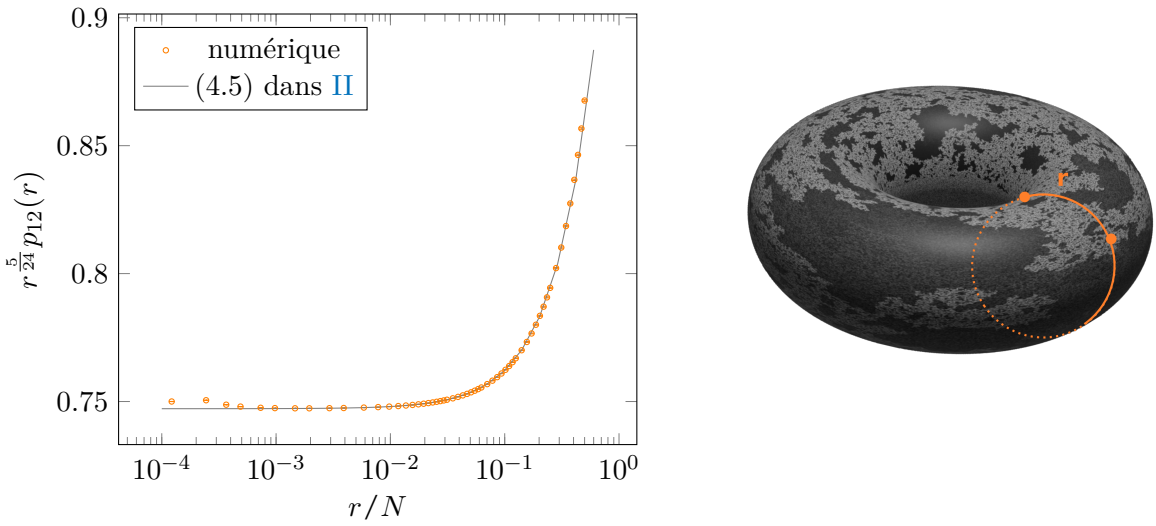

Données numériques et prédiction analytique pour la probabilité p_{12} que deux points à distance r appartiennent au même amas, sur un tore de taille $N \times N$.

L'intérêt pour la géométrie du tore a été motivée par le fait que les analyses numériques sont souvent réalisées avec des conditions au bord périodiques, et donc la connaissance des corrections induites par cette topologie est importante pour l'étude du problème sur le plan. En particulier, j'ai donnée aussi des expressions pour les corrections auparavant inconnues du ratio des connectivités à trois points et à deux points, (5.6) de l'Article III. Ces résultats fournissent de plus un test de conjectures sur la CFT décrivant les connectivités des amas, en particulier du fait que certaines des constantes de structure sont données par les constantes de structure de la théorie de Liouville.

Nina Javerzat, Marco Picco, and Raoul Santachiara. “Two-point connectivity of two-dimensional critical Q-Potts random clusters on the torus.” In: *Journal of Statistical Mechanics: Theory and Experiment* 2020.2 (2020), p. 023101. DOI: 10.1088/1742-5468/ab6331. arXiv: 1907.11041 [hep-th]

Nina Javerzat, Marco Picco, and Raoul Santachiara. “Three- and four-point connectivities of two-dimensional critical Q-Potts random clusters on the torus.” In: *Journal of Statistical Mechanics: Theory and Experiment* 2020.5 (2020), p. 053106. DOI: 10.1088/1742-5468/ab7c5e. arXiv: 1912.05865 [hep-th]

→Inclus comme Article II et Article III au Chapitre 4.

Percolation de surfaces aléatoires

J'ai étudié une famille de modèles de percolation corrélée à longue distance, définis à partir des «excursion sets »(ensemble des sites où la hauteur est plus grande qu'une certaine valeur) de surfaces aléatoires de rugosité négative. Pour ces modèles, la plupart des exposants critique est inconnue, et l'existence même de l'invariance conforme est débattue. J'ai utilisé l'anisotropie induite par une topologie de tore rectangulaire pour tester l'existence des deux composantes du tenseur impulsion-énergie, qui est l'une des conséquences les plus directes de l'invariance conforme. Pour cela, j'ai émis d'une part des prédictions sur la connectivité à deux points sur une telle géométrie, en utilisant une approche CFT et des hypothèses raisonnables, et comparé d'autre part avec les simulations numériques. De cette façon j'ai obtenu des signatures fortes de l'invariance conforme (voir les figures ci-dessous, expliquées en détails au Chapitre 5).

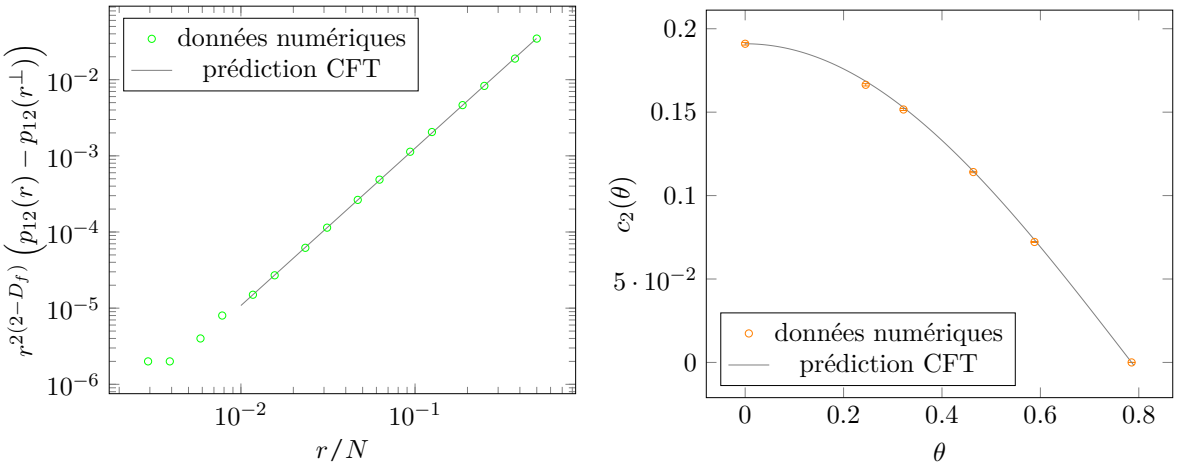

Effet de l'anisotropie sur la connectivité à deux points, pour une valeur de la rugosité $H = -2/3$. A gauche : la pente 2 correspond à la dimension d'échelle du tenseur énergie-impulsion. A droite : θ est l'angle auquel p_{12} est mesurée et c_2 est le coefficient dominant dans la différence $p_{12}(r,\theta) - p_{12}(r,\theta+\pi/2)$. Son comportement en $\cos(2\theta)$ correspond au spin 2 du tenseur énergie-impulsion.

De plus, j'ai obtenu les premières estimations de certaines quantités impliquant des données importantes de la CFT, telles que son spectre, les multiplicités, la charge centrale et les constantes

de structure. J'ai aussi montré que le champ thermique de cette CFT n'est pas dégénéré. Ces résultats combinés à ceux de l'Article II renforcent la conjecture [53] selon laquelle les amas sont ceux de la percolation pure pour certaines valeurs de la rugosité.

> Nina Javerzat et al. "Topological effects and conformal invariance in long-range correlated random surfaces." In: *SciPost Phys.* 9 (4 2020), p. 50. DOI: 10.21468/SciPostPhys.9.4.050. arXiv: 2005.11830

→Inclus comme Article IV au Chapitre 5.

APERÇU

La première partie détaille les implications générales de l'invariance conforme, en examinant ses conséquences au niveau des fonctions de corrélation. Dans le Chapitre 1 il est montré comment la symétrie et l'auto-cohérence contraignent les fonctions de corrélation. En particulier il est montré que toute corrélation peut être calculée comme une certaine expansion exacte. La structure analytique de cette expansion est étudiée, comme fonction des paramètres de la CFT. Dans le Chapitre 2 une approche bootstrap similaire est suivie pour dérivée des expressions générales pour les fonctions de corrélation sur la topologie du tore. Dans le Chapitre 3 les propriétés analytiques des fonctions de symétrie (les blocs conformes) dans leur représentation récursive sont examinées.
Ces résultats généraux sont appliqués dans la seconde partie de la thèse à l'étude des amas aléatoires du modèle de Potts au Chapitre 4 et à la percolation des surfaces aléatoires au Chapitre 5.

INTRODUCTION

GENERAL CONTEXT

Critical phenomena have fascinated physicists for a long time [1], and for good reasons: the existence of universality, the presence of invariances, and maybe above all because they keep raising new questions and challenges in their description. Indeed such phenomena emerge from the collective behaviour of many degrees of freedom, and cannot be understood from the analysis of a few of them: as coined by Anderson [2] "More is different", and the description of "more" has required the development of new ideas in theoretical physics. Even today, new questions still emerge, some of which are at the heart of the present research work.
To illustrate why "universality" and "invariance" are so appealing, let us consider one of the first critical phenomenon to be observed, about 200 years ago [3]: critical opalescence. Take a transparent fluid and submit it to precise conditions of pressure and temperature, it will suddenly become cloudy[1]: at this critical point of the phase diagram, density fluctuations occur at long enough wavelengths to scatter visible light and the fluid becomes opaque. These fluctuations actually occur at all length scales, in such a way that the system is statistically scale invariant: if we could examine such a fluid with a microscope, upon changing the magnification we would see the same pattern of fluctuating regions of high and low densities. These regions are random fractals[2]. Quantitatively, it follows that the physical observables behave as power laws. For instance the specific heat of the fluid diverges algebraically as the temperature approaches its critical value: $C \sim |T - T_c|^{-\alpha}$. The critical exponent α, together with the ones governing the decay of the other thermodynamic functions, encode thereby the macroscopic properties of the system. Remarkably, such exponents do not depend on microscopic details: not only different fluids have the same behaviour at criticality, but also magnets at their ferromagnetic transition are described by these same numbers [6]. This universality of long-distance critical behaviours hints at identical fundamental mechanisms in microscopically different systems.

The theoretical prediction of the critical exponents, and hence the characterisation of critical phenomena, is a challenge. Mean field approaches succeeded in giving a qualitative description, and in predicting the values of the critical exponents for systems in which fluctuations can be neglected. The renormalisation group ideas further provided a framework for the study of the long-distance properties of statistical models. In particular, renormalisation suggests that the scaling limit of the statistical averages of certain lattice observables exist and is given by the correlation functions of a quantum field theory (see for instance Section 2 of [7]).
For systems of low dimension, fluctuations are strong and mean field as well as perturbative renormalisation group techniques fail. In two dimensions the exact determination of the critical exponents of important universality classes (for instance Ising and pure percolation) was achieved instead from exact solutions of the lattice models [8–12], and Coulomb-gas techniques [13–16]. Meanwhile, it was argued [17] that critical systems are not only scale invariant, but in many cases also invariant under the larger set of conformal transformations. From the observation

1 Videos of experimental realisations can be easily found online, for instance [4].
2 Such fractal fluctuations have been captured and measured experimentally in [5].

that, in two dimensions, there is an infinity of conformal transformations, it was shown [18] that complete solutions can be obtained for the interacting quantum field theories which describe critical models. The principle of this so-called "bootstrap" approach [19] is to find quantum field theory solutions which are consistent with general field theory principles and with conformal symmetry, from the very constraints imposed by this consistency (here the reader is invited to imagine a theory pulling itself up by its own bootstraps). Applied to critical phenomena, this approach allows to predict exactly all critical exponents and more generally the scaling limit of all expectation values of lattice observables. This program was completed for the conformal field theories called minimal models (see for instance [20–22]), which have been fully classified [18, 23, 24] and solved [18, 23, 25, 26, 55]. These CFTs describe many (but not all) important universality classes, such as the celebrated Ising universality class. The lattice models which fall in these universality classes have been constructed [27, 28]. They include in particular the models defined by local interactions with positive Boltzmann weights, which are described by the unitary minimal models.
Since then, there has been an increasing interest in understanding the scaling limit of conformally invariant statistical systems. Mathematicians found there new challenges in probability theory [29, 30], triggered by Cardy's conjecture [31, 32]. These include putting on rigorous grounds the physicists' convictions of conformal invariance [33, 34], or of the existence of scaling limits of specific lattice models [35–37], as well as providing proofs of the values of critical exponents [38, 39].

However, there exist important models which do not fall into the above classification. Notably, models with disorder, as well as models which describe the geometric properties of critical phase transitions. These latter are indeed defined by non-local degrees of freedom, and they represent the main focus of this thesis. To give a concrete example let us take one of of the most well-known lattice models, the Ising model. Its phase transition can be described geometrically by putting bonds randomly between sites of like spins, forming so-called Fortuin-Kasteleyn (FK) clusters. At the critical temperature a percolation transition occurs, where a cluster spanning the whole system emerges. The fluctuations of the system are encoded in the probability measure of the clusters, which is conformallly invariant. Characterising these fluctuations amounts to determine the complete statistical properties of the percolation clusters. The CFT approach has been successful in giving numerous predictions on the Ising FK clusters, and more generally on geometrical aspects of critical phenomena. We can cite for instance the crossing formula for critical percolation [31], and the determination of the fractal dimensions of the clusters of the $O(n)$ and $Q-$state Potts models [40, 41]. Despite this success, important statistical properties have remained out of reach, even for the simplest model of pure (uncorrelated) percolation. For instance, while the probability that two points at distance r belong to the same cluster (two-point connectivity) has been known for a long time to decay as $\sim r^{-5/24}$ [11, 12, 42], the scaling limit of the probability that three points belong to the same cluster (three-point connectivity) was only conjectured fairly recently [43]. More generally, a full CFT solution describing the connectivity properties of the clusters of pure percolation has been an open problem for about 30 years, and only recently an almost complete solution was found [44–49]. This is one of the new bootstrap solutions which we are going to discuss in this thesis.

THE PRESENT WORK: MOTIVATION AND SUMMARY OF RESULTS

The motivation at the origin of this work was to explore the new bootstrap solutions pinpointed by such geometric and disordered critical phenomena. We have worked in two main directions:

i) The implementation of numerical bootstrap methods in two dimensions: we have investigated technical questions on subtelties in the recursive computation of the Virasoro conformal blocks.

ii) The study of percolation models on toroidal topology: the random clusters $Q-$state Potts model and the percolation of random surfaces. We found that the clusters connectivities (the probabilities that points belong to the same cluster) on the torus are an excellent tool to test recent results on the CFTs of these models, and to establish new ones.

We summarise our main results below.

Analytic structure of the recursion representation of conformal blocks

A crucial ingredient of the conformal bootstrap is the computation of so-called conformal blocks, in the space of parameters (scaling dimensions and/or central charge). In two dimensions the conformal blocks are complicated functions of these parameters, which are not known in closed form. We can nevertheless compute them recursively. However it turns out that this recursive representation diverges at some points of the parameter space. This is quite problematic since the aim of the bootstrap is precisely to scan this space, in search of consistent solutions. We have therefore tried to answer the following questions: where do these divergences come from ? Can we find a manifestly finite formula for two-dimensional conformal blocks ?
We understood that these divergences are artefacts of the recursive representation. We could understand systematically how they arise for simpler conformal blocks, on a torus topology. We computed explicitely their finite limit for arbitrary level of the expansion, given by equation (5.36) in Article I. Finding a manifestly finite representation for the four-point conformal blocks on the plane is however still an open question.

> Nina Javerzat, Raoul Santachiara, and Omar Foda. "Notes on the solutions of Zamolodchikov-type recursion relations in Virasoro minimal models." In: *JHEP* 08 (2018), p. 183. DOI: 10.1007/JHEP08(2018)183. arXiv: 1806.02790 [hep-th]

→Included as Article I in Chapter 3.

The random cluster $Q-$state Potts model

Based on the solutions proposed in [44–46], we use the CFT approach to determine analytically the universal dominant torus corrections to the two-, three- and four-point connectivities for all values of $Q \in [1, 4]$, and compare to Monte Carlo simulations. We show in the figure below data points for the two-point connectivity in the pure percolation limit $Q \to 1$. We plot as well one of our main results, given by (4.5) in Article II. On this figure one can see three regimes: non-universal effects when the distance between the points is of the order of a few lattice spacings,

the infinite plane regime where the probability decays with the well-known exponent $\eta = 5/24$, and a regime where topological effects dominate. Indeed one can clearly see on that figure that when $r \gtrsim N/2$ the probability deviates significantly from a power law. This effect is universal. Although its origin is easily explained (the probability takes contributions from paths connecting the two points by going around the torus, see the figure on the right), no theoretical prediction had been given so far.

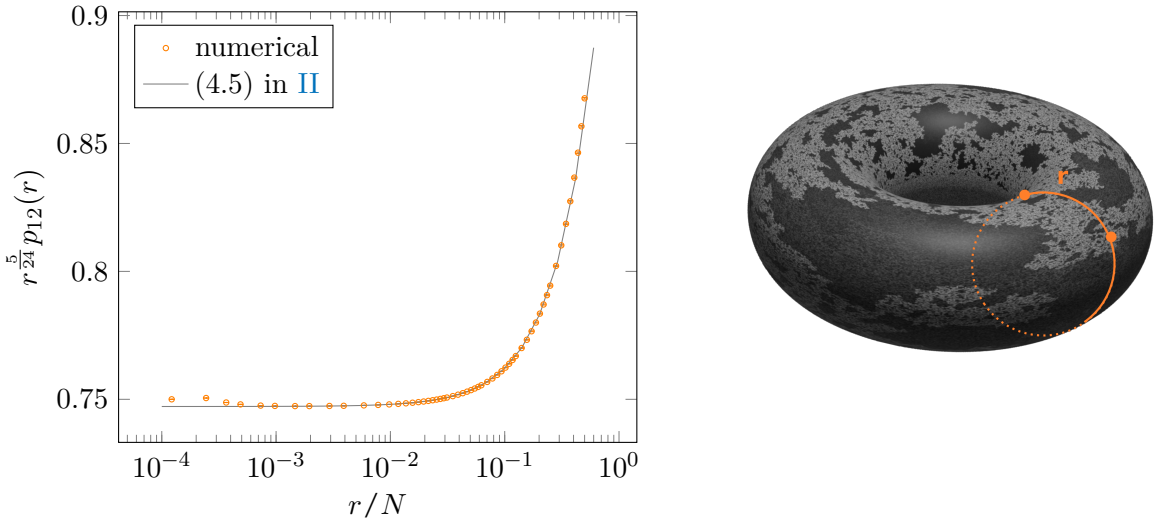

Numerical data and analytic prediction for the probability p_{12} that two points at distance r belong to the same cluster, rescaled by the plane limit decay, on a $N \times N$ torus.

The interest for the torus geometry was motivated by the fact that numerical investigations are often performed with periodic boundary conditions, so that the knowledge of the corrections induced by the topology is important for the studies of the planar problem. In particular we give also expressions for the previously unkown corrections to the ratio of three- to two-point connectivities, (5.6) in Article III. The results furthermore provide a test of conjectures on the CFT describing the clusters connectivities, in particular of the fact that some of the structure constants are given by the Liouville structure constants.

> Nina Javerzat, Marco Picco, and Raoul Santachiara. "Two-point connectivity of two-dimensional critical Q-Potts random clusters on the torus." In: *Journal of Statistical Mechanics: Theory and Experiment* 2020.2 (2020), p. 023101. DOI: 10.1088/1742-5468/ab6331. arXiv: 1907.11041 [hep-th]
>
> Nina Javerzat, Marco Picco, and Raoul Santachiara. "Three- and four-point connectivities of two-dimensional critical Q-Potts random clusters on the torus." In: *Journal of Statistical Mechanics: Theory and Experiment* 2020.5 (2020), p. 053106. DOI: 10.1088/1742-5468/ab7c5e. arXiv: 1912.05865 [hep-th]

→Included as Article II and Article III in Chapter 4.

Percolation of random surfaces

We study a family of long-range correlated percolation models, which are defined from the excursion sets (set of sites where the height is larger than a fixed level) of random surfaces with negative roughness. For these models most critical exponents are unknown, and the existence of conformal symmetry even debated. We use the anisotropy induced by a rectangular torus topology to probe the existence of the two components of the stress-energy tensor, which is the most direct consequence of conformal invariance. Specifically, we make predictions for the two-point connectivity on such geometries, using a CFT approach and reasonable assumptions, and compare with numerical simulations. We provide in this way strong evidence for conformal invariance (see the figures below, explained in details in Chapter 5).

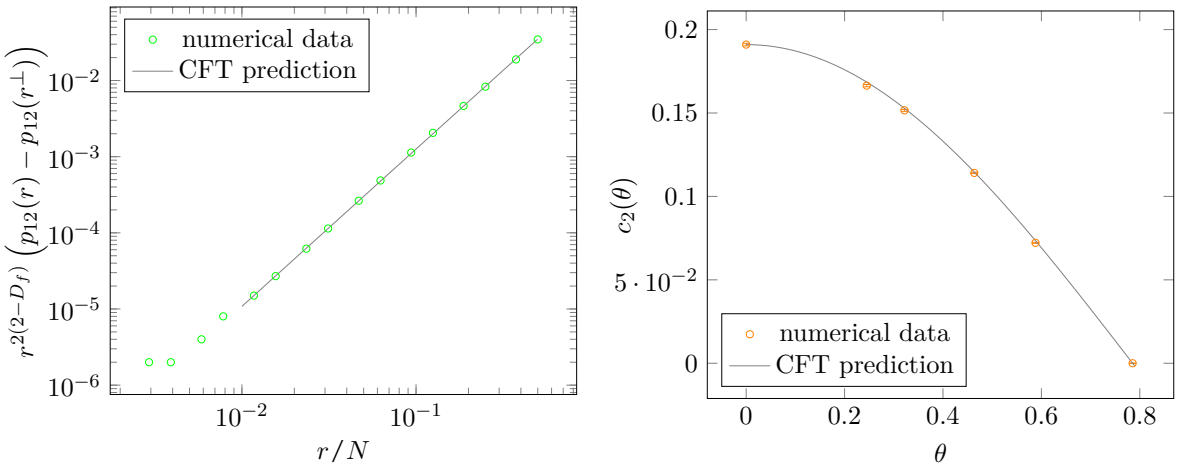

Effect of anisotropy on the two-point torus connectivity, for an example value of the roughness $H = -2/3$. Left: the slope 2 corresponds to the scaling dimension of the stress-energy tensor. Right: θ is the angle at which p_{12} is measured and c_2 the dominant coefficient in the difference $p_{12}(r,\theta) - p_{12}(r,\theta+\pi/2)$. Its behaviour in $\cos(2\theta)$ corresponds to the spin 2 of the stress-energy tensor.

Moreover we obtain the first numerical estimates of quantities involving important CFT data, such as the spectrum, the multiplicities, the central charge and the structure constants. We also show that the energy field of this CFT is not degenerate. Based on the results obtained in Article II we strengthen the conjecture [53] that for certain values of the roughness, the clusters are those of pure percolation.

> Nina Javerzat et al. "Topological effects and conformal invariance in long-range correlated random surfaces." In: *SciPost Phys.* 9 (4 2020), p. 50. DOI: 10.21468/SciPostPhys.9.4.050. arXiv: 2005.11830

→Included as Article IV in Chapter 5.

OUTLINE

The first part details the general implications of conformal invariance, by examining its consequences on correlation functions. In Chapter 1 we show how symmetry and self-consistency constrain correlation functions. In particular we show that any correlation function can be computed as a particular exact expansion. We further study the analytic structure of this expansion, as a function of the CFT parameters. In Chapter 2 we follow a similar bootstrap approach to derive general expressions for correlation functions on the torus topology. We examine in Chapter 3 the analytic properties of the symmetry functions, the conformal blocks, in their recursive representation.
These general results are applied in the second part of the thesis to the study of the random cluster $Q-$state Potts model in Chapter 4 and of the percolation of random surfaces in Chapter 5.

Part I

CONFORMAL FIELD THEORY

1

CONFORMAL FIELD THEORY ON THE PLANE

In this first chapter we explain what are the consequences of conformal symmetry at the level of our main object of study, the correlation functions. In two-dimensions the algebra of conformal symmetry is the infinite dimensional Virasoro algebra. This translates into an infinite number of constraints on the correlation functions. Are these constraints sufficient to determine all correlators ? Actually no, because correlation functions also incorporate model-dependent data, in a way which is not fixed by conformal symmetry. This results in a rich space of possible different theories.

Correlation functions in a quantum field theory are in general complicated objects. They are difficult to compute exactly and one usually resorts to perturbative methods. However, in a CFT it is always possible to write an arbitrary correlation as a certain exact expansion, by using the bootstrap approach. This expansion does not rely on anything about the theory but on its self-consistency and on conformal invariance. Self-consistency of the theory tells that correlation functions can be expanded, because in any consistent theory there must exist so-called operator product expansions. Conformal symmetry restricts the form of this expansion, to be built from basic units called conformal blocks. These are functions whose form is completely determined by conformal invariance: they are the symmetry functions of the Virasoro algebra. How conformal blocks arrange to form a given correlation function is determined by model-dependent data. Solving a theory, namely being able to compute all correlation functions, amounts then to determine this model-dependent data. Again, the bootstrap idea is that this data must be constrained: not all sets of model-dependent data give consistent correlation functions. For some CFTs, this constraint of consistency alone allows to solve completely the theory. This is the case for instance of the minimal models and of Liouville theory (see [20] for a review, as well as [21]). In other cases this is not restrictive enough, but numerical conformal bootstrap techniques can be used to determine part of the model-dependent data (see the example of the Potts model in Chapter 4).

In Sections 1.1 and 1.2 we give the algebraic aspects of CFT. We introduce the Virasoro algebra and its representations, and the model-independent data which enters the correlation functions under the form of conformal blocks. Correlation functions are discussed in Section 1.4, especially their conformal block expansion. Sections 1.5 and 1.6 deal with the analytic properties of the conformal block expansion: the conformal blocks themselves are very peculiar functions with a rich pole structure. Physical correlation functions are expected to be smooth functions, which implies a subtle interplay between the model-dependent and algebraic data. In Section 1.7 we make precise the consistency constraint on correlation functions, by deriving the crossing-symmetry equation.

1.1 FROM CONFORMAL TRANSFORMATIONS TO THE VIRASORO ALGEBRA

Let us consider the Euclidean space, equipped with a metric $g_{\mu\nu}$, which we take to be the flat metric $g_{\mu\nu} = \delta_{\mu\nu}$. *Conformal transformations* are defined (see for instance [22], Chapter 4) as

the transformations of $x^\mu \to x'^\mu$ which leave the distance $ds^2 = dx^\mu dx_\mu$ invariant, up to a position-dependent factor:

$$ds^2 \to \lambda^2(\mathbf{x}) ds^2. \tag{1.1}$$

In other words, conformal transformations are the transformations which correspond to a local (position-dependent) rescaling.
In two dimensions we can define the complex coordinates:

$$\begin{aligned} z &= x_1 + i x_2 \\ \bar{z} &= x_1 - i x_2. \end{aligned} \tag{1.2}$$

With these coordinates, the metric is:

$$ds^2 = dz\, d\bar{z}. \tag{1.3}$$

Under a transformation $z \to z' = f(z)$, where f is an analytic function, it becomes:

$$ds'^2 = dz'\, d\bar{z}' = \frac{df(z)}{dz}\frac{df(\bar{z})}{d\bar{z}} dz\, d\bar{z} = \left|\frac{df}{dz}\right|^2 ds^2. \tag{1.4}$$

Comparing with (1.1), any analytic function f is therefore a conformal transformation of the complex plane. Actually, we work on the complex plane enlarged with the point at infinity, that is, the Riemann sphere $\mathbb{C} \cup \{\infty\}$ (see for instance [20], Section 1.3). On this sphere, the transformations which are globally defined (everywhere invertible), are:

$$f(z) = z + b \quad \text{translation} \tag{1.5a}$$

$$f(z) = az \quad \begin{cases} \text{scaling if } a \in \mathbb{R} \\ \text{rotation if } |a| = 1 \end{cases} \tag{1.5b}$$

$$f(z) = \frac{z}{cz+1} \quad \begin{cases} \text{special conformal transformation: composition of} \\ \text{an inversion } f(z) = z^{-1}, \text{ a translation and another inversion.} \end{cases} \tag{1.5c}$$

They are special cases of the Möbius transformations:

$$f(z) = \frac{az+b}{cz+d}, \quad a, b, c, d \in \mathbb{C}, \quad ad - bc \neq 0. \tag{1.6}$$

An infinitesimal transformation can be written $f(z) = z + \epsilon(z)$ with [21]:

$$\epsilon(z) = \sum_{n=-1}^{\infty} \epsilon_n z^{n+1}. \tag{1.7}$$

Expanding (1.6) around the identity ($a = d$ and $c, b \ll d$), we see that the global transformations (1.5) are generated respectively by $n = \{-1, 0, 1\}$. The other modes of ϵ generate conformal transformations which are only defined locally.
Let us now consider a quantum field $V(z, \bar{z})$. It transforms under $f(z) = z + \epsilon(z)$ as [18]:

$$\delta_\epsilon V(0) = \frac{1}{2\pi i} \oint_C dz \epsilon(z) T(z) V(0) \tag{1.8}$$

where C is the contour of the region where ϵ is analytic [21]. T is the *stress-energy tensor*, which is the Noether current associated to conformal symmetry. We can formally write $T\,V$ as an expansion over the modes of T:

$$T(z)V(0) = \sum_{n\in\mathbb{Z}} \frac{L_n^{(0)}}{z^{n+2}} V(0). \tag{1.9}$$

The L_n's act on the field V. By replacing in the contour integral (1.8) one obtains:

$$\delta_\epsilon V(0) = \frac{1}{2\pi i}\oint_C dz \sum_n \sum_m \epsilon_n L_m^{(0)} z^{n-m-1} V(0) = \sum_n \epsilon_n L_n^{(0)} V(0). \tag{1.10}$$

The L_ns generate therefore the conformal transformations of fields. Adding also the antiholomorphic part we find:

$$\delta V(0) = \delta_\epsilon V(0) + \delta_{\bar\epsilon} V(0) = \sum_n \left(\epsilon_n L_n^{(0)} + \bar\epsilon_n \bar L_n^{(0)}\right) V(0). \tag{1.11}$$

For the global transformations we find for instance:

$$\delta V = \begin{cases} \epsilon_0 \left(L_0 + \bar L_0\right) V & \epsilon_0 \in \mathbb{R} \quad \text{rescaling} \\ \epsilon_0 \left(L_0 - \bar L_0\right) V & \epsilon_0 \in i\mathbb{R} \quad \text{rotation} \\ \epsilon_{-1} \left(L_{-1} + \bar L_{-1}\right) V & \epsilon_{-1} \in \mathbb{R} \quad \text{translation.} \end{cases} \tag{1.12}$$

Primary fields are those which transform covariantly under conformal transformations $z \to z' = f(z)$ [18]:

$$V'(z', \bar z') = f'(z)^{-\Delta} \bar f'(\bar z)^{-\bar\Delta} V(z, \bar z) \tag{1.13}$$

where $\Delta, \bar\Delta$ are called the holomorphic and anti-holomorphic *conformal dimensions*. These numbers partly characterise a given field[1] so that in the following we use the notation $V_{\Delta,\bar\Delta}$. We have in particular:

- Under scaling $z \to \lambda z$:

$$V_{\Delta,\bar\Delta}(\lambda z, \lambda \bar z) = \lambda^{-(\Delta+\bar\Delta)} V_{\Delta,\bar\Delta}(z, \bar z), \tag{1.14}$$

  so that the total scaling dimension is $\Delta + \bar\Delta$.

- Under rotations $z \to e^{i\theta} z$:

$$V_{\Delta,\bar\Delta}(e^{i\theta} z, e^{-i\theta} \bar z) = e^{-i\theta(\Delta-\bar\Delta)} V_{\Delta,\bar\Delta}(z, \bar z), \tag{1.15}$$

  so that the spin is $s = \Delta - \bar\Delta$.

Under an infinitesimal transformation $f(z) = z + \epsilon(z)$, (1.13) gives to first order:

$$V'(z') = \left(1 + \partial\epsilon(z)\right)^{-\Delta} V(z) = \left(1 - \Delta\partial\epsilon(z)\right) V(z). \tag{1.16}$$

1 We will see in the following that the conformal dimensions are not sufficient to fully characterise a field, and that the additional information of its fusion with other fields is needed.

Expanding the left-hand side:

$$V'(z') = V'(z) + \epsilon(z)\partial V(z) \tag{1.17}$$

we get

$$\delta V(z) = V(z) - V'(z) = (\epsilon(z)\partial + \Delta\partial\epsilon(z))\, V(z). \tag{1.18}$$

With $\epsilon(z)$ given by (1.7):

$$\delta V(0) = (\epsilon_{-1}\partial + \Delta\epsilon_0)\, V(0). \tag{1.19}$$

This is obtained from (1.8) if:

$$T(z)V(0) = \frac{\Delta V(0)}{z^2} + \frac{\partial V(0)}{z} + \cdots \tag{1.20}$$

as can be checked by inserting this product in the contour integral. The $\cdots$ stand for non-singular terms which therefore do not contribute to the contour integral (1.8).
The stress-energy tensor on the other hand is not a primary field and transforms as [18]:

$$T'(z') = [f'(z)]^{-2}\left(T(z) - \frac{c}{12}\{f, z\}\right). \tag{1.21}$$

$\{f, z\}$ is the Schwarzian derivative:

$$\{f, z\} = \frac{f'''(z)}{f'(z)} - \frac{3}{2}\left(\frac{f''(z)}{f'(z)}\right)^2 \tag{1.22}$$

and c is the *central charge*. The central charge corresponds to a quantum anomaly, which arises from the soft breaking of conformal invariance by the introduction of a length (see eg. [22], Chapter 5). For instance, the transformation $f(z) = -i\frac{N}{2\pi}\ln z$ maps the plane to the infinite cylinder of radius $N/2\pi$. On the cylinder, using (1.21) T becomes:

$$T'(z') = \left(\frac{2\pi}{N}\right)^2\left(\frac{c}{24} - z^2 T(z)\right). \tag{1.23}$$

We see that, whereas the expectation of T is zero on the plane: $\langle T\rangle_{\text{plane}} = 0$, (1.23) implies that it is non-zero on the cylinder and is proportional to the central charge: $\langle T\rangle_{\text{cylinder}} = \frac{\pi^2 c}{6N^2}$.
The central charge is an important parameter which characterises a conformal field theory. For instance $c = 1/2$ for the Ising model, and $c = 4/5$ for the 3−state Potts model [22]. However as mentioned in the introduction of this chapter, a CFT is also determined by model-dependent data, so that different theories may have the same central charge. To pursue with an example given in the general introduction, the correlation functions of the Ising spin variables, and the connectivities of the Ising FK clusters are described by CFTs which, albeit having the same central charge $c = 1/2$, are not the same theory. Indeed, the Ising spin variables are described by the minimal model $\mathcal{M}(4, 3)$ (in the notation [22]) which is a unitary CFT containing a finite number of fields, whereas the Ising FK clusters are described by the non-unitary, non-rational, logarithmic CFT that we study in Chapter 4.
Let us now make an infinitesimal transformation $f(z) = z + \epsilon(z)$, for which (1.21) becomes, at first order:

$$T'(z') = T(z) - 2T(z)\partial\epsilon(z) - \frac{c}{12}\partial'''\epsilon(z). \tag{1.24}$$

With

$$T'(z') = T'(z) + \epsilon(z)\partial T(z), \tag{1.25}$$

we get:

$$\delta T(0) = 2\epsilon_0 T + \epsilon_{-1}\partial T(0) + \frac{c}{2}\epsilon_2. \tag{1.26}$$

From the contour integral (1.8), upon taking $V = T$ (1.26) is equivalent to:

$$T(z)T(0) = \frac{c/2}{z^4} + \frac{2T(0)}{z^2} + \frac{\partial T(0)}{z} + \cdots \tag{1.27}$$

The modes L_n defined by (1.9) can be written as a contour integral:

$$L_n^{(z)} = \frac{1}{2\pi i}\oint_{\mathcal{C}_z} dy\,(y-z)^{n+1}\,T(y), \quad n \in \mathbb{Z}. \tag{1.28}$$

The expansion (1.27) is then equivalent to the following commutation relations (see for instance Chapter 3 in [21]):

$$[L_m, L_n] = (n-m)L_{m+n} + \frac{c}{12}n(n+1)(n-1)\delta_{n+m,0}. \tag{1.29}$$

These commutation relations define the algebra of two-dimensional conformal symmetry, called the Virasoro algebra Vir. The anti-holomorphic modes are defined analogously and we have

$$[L_m, \bar{L}_n] = 0. \tag{1.30}$$

In the next section we study the highest-weight representations of the Virasoro algebra. These representations are made of states $|\Delta\rangle$, which in a CFT are related to the fields V_Δ [18]:

$$|\Delta\rangle = \lim_{z\to 0} V_\Delta(z)\,|0\rangle\,, \tag{1.31}$$

where $|0\rangle$ is the vacuum state. The full conformal algebra of the CFT is the tensor product $Vir \otimes \overline{Vir}$. In a given theory only a subset of all possible representations of $Vir \otimes \overline{Vir}$ appear. This model-dependent data defines the full *spectrum* of the theory, $S = \{V_\Delta\}$. As will be made manifest in Section 1.4, the knowledge of the spectrum is crucial to compute the correlation functions.

1.2 HIGHEST WEIGHT REPRESENTATIONS OF THE VIRASORO ALGEBRA

In this section we recall basic facts about the highest weight representations of the Virasoro algebra. For a detailed presentation see for instance Chapter 4 of [56]. The highest-weight states $|\Delta\rangle$ of the Virasoro algebra (for a detailed presentation of the) are the eigenstates of the mode L_0, with eigenvalue Δ :

$$L_0\,|\Delta\rangle = \Delta\,|\Delta\rangle \tag{1.32}$$

which are annihilated by all positive modes:

$$L_n\,|\Delta\rangle = 0, \quad \forall n > 0. \tag{1.33}$$

Acting on $|\Delta\rangle$ with the negative modes $L_n, \quad n<0$ produces all other – so-called *descendant*– states in the representation $\mathcal{R}_\Delta$. We denote $Y=\{n_1,n_2,\cdots\}, \quad n_i\in\mathbb{N}, \quad n_i\leq n_{i+1}$, a partition of the integer $|Y|=\sum_i n_i$. All independent descendants of $|\Delta\rangle$ can then be written:

$$L_{-Y}\,|\Delta\rangle = L_{-n_1}L_{-n_2}\cdots|\Delta\rangle\,. \tag{1.34}$$

Such a descendant state has conformal weight $\Delta+|Y|$, as is seen by applying the L_0 operator onto the descendant state, and using the commutation relations (1.29). $|Y|$ is called the level of the descendant. For general Δ, the number of independent descendants at level $|Y|$ is therefore the number of integer partitions of $|Y|$.
The inner products between states are defined as the matrix elements of the Gram matrix H [22]:

$$H_{Y,Y'}(\Delta) = \langle\Delta L_{Y'}|L_{-Y}\Delta\rangle\,. \tag{1.35}$$

They are computed by applying the commutation relations (1.29), with the inner product of primary states normalised to one:

$$\langle\Delta|\Delta\rangle = 1. \tag{1.36}$$

The matrix H is block diagonal, since inner products between descendants of different levels vanish:

$$H(\Delta) = \begin{pmatrix} 1 & 0 & 0 & 0 & \cdots \\ 0 & 2\Delta & 0 & 0 & \cdots \\ 0 & 0 & 4\Delta(2\Delta+1) & 6\Delta & \cdots \\ 0 & 0 & 6\Delta & 4\Delta+c/2 & \cdots \\ \vdots & \vdots & \vdots & \vdots & \ddots \end{pmatrix} \tag{1.37}$$

in the basis $\{\{L_{-1}\,|\Delta\rangle\},\{L_{-1}^2\,|\Delta\rangle\,,L_{-2}\,|\Delta\rangle\},\cdots\}$.
The representation $\mathcal{R}_\Delta$ is irreducible if and only if there are no primary states among the descendants $L_{-Y}\,|\Delta\rangle$. Indeed, such a state, called *null state* or *singular state*, and such that:

$$|\chi\rangle = L_{-Y}\,|\Delta\rangle \tag{1.38a}$$
$$L_n\,|\chi\rangle = 0, \forall n>0, \tag{1.38b}$$

spans its own representation $\mathcal{R}_\chi$, which is a subrepresentation of $\mathcal{R}_\Delta$. Note that, by definition, singular states have vanishing norm:

$$\langle\chi|\chi\rangle = 0. \tag{1.39}$$

An irreducible representation is obtained by quotienting out the subrepresentation(s):

$$\mathcal{R}_\Delta \to \mathcal{R}_\Delta/\mathcal{R}_\chi, \tag{1.40}$$

and is called a *degenerate representation* at level $|Y|$. Given a level $|Y|=r\,s$, the representation with highest-weight state $|\Delta_{r,s}\rangle$ is degenerate at level rs, with the weight $\Delta_{r,s}$ given by:

$$\Delta_{r,s} = \frac{1}{4}\left((1+r)b+(1+s)b^{-1}\right)\left((1-r)b+(1-s)b^{-1}\right). \tag{1.41}$$

In this equation we use the following notation for the central charge (0.4):

$$c = 1 + 6\left(b + \frac{1}{b}\right)^2 . \tag{1.42}$$

We denote $\mathcal{R}_{\Delta_{r,s}} \equiv \mathcal{R}_{r,s}$ such a degenerate representation.
Note that setting the singular state to zero creates linear dependance between the states in the representation. For example, the null state in the representation $\mathcal{R}_{1,2}$ is:

$$|\chi\rangle \propto \left(L_{-1}^2 + b^{-2}L_{-2}\right)|\Delta_{1,2}\rangle = 0 \Rightarrow L_{-1}^2|\Delta_{1,2}\rangle = -b^{-2}L_{-2}|\Delta_{1,2}\rangle . \tag{1.43}$$

Using the notation (1.41), the inverse of the matrix of inner products (1.37) may be written:

$$H^{-1}(\Delta) = \begin{pmatrix} 1 & 0 & 0 & 0 & \cdots \\ 0 & \frac{1}{2(\Delta-\Delta_{1,1})} & 0 & 0 & \cdots \\ 0 & 0 & \frac{4\Delta+c/2}{32\Delta(\Delta-\Delta_{1,2})(\Delta-\Delta_{2,1})} & \frac{-6\Delta}{32\Delta(\Delta-\Delta_{1,2})(\Delta-\Delta_{2,1})} & \cdots \\ 0 & 0 & \frac{-6\Delta}{32\Delta(\Delta-\Delta_{1,2})(\Delta-\Delta_{2,1})} & \frac{4\Delta(2\Delta+1)}{32\Delta(\Delta-\Delta_{1,2})(\Delta-\Delta_{2,1})} & \cdots \\ \vdots & \vdots & \vdots & \vdots & \ddots \end{pmatrix} \tag{1.44}$$

In this expression it is manifest that $\Delta = \Delta_{1,1}$ or $\Delta = \Delta_{1,2}, \Delta_{2,1}$, the matrix H^{-1} is not well-defined. More generally, when $\Delta = \Delta_{r,s}$ the corresponding block of $H(\Delta)$ is not invertible. This happens of course when $\mathcal{R}_\Delta$ is degenerate, $\mathcal{R}_\Delta = \mathcal{R}_{r,s}$. In that case, the singularities are removed by the existence of fusion rules (see next section). However, it is important to note that $H(\Delta)$ may also be non-invertible for non-degenerate representations $\mathcal{R}_\Delta$, at values of the central charge c such that $\Delta(c) = \Delta_{r,s}(c)$ (see Section 1.6.2).
We now define the following factors, which will appear in the computation of correlation functions:

$$\Gamma^{\Delta_3,Y_3}_{\Delta_1,Y_1;\Delta_2,Y_2} \equiv \frac{\langle V_{\Delta_3,Y_3}(\infty)V_{\Delta_1,Y_1}(1)V_{\Delta_2,Y_2}(0)\rangle}{\langle V_{\Delta_3}(\infty)V_{\Delta_1}(1)V_{\Delta_2}(0)\rangle}. \tag{1.45}$$

Because the V_{Δ_i,Y_i}'s are descendant states, $\langle V_{\Delta_3,Y_3}(\infty)V_{\Delta_1,Y_1}(1)V_{\Delta_2,Y_2}(0)\rangle$ is completely determined from $\langle V_\Delta(\infty)V_{\Delta_1}(1)V_{\Delta_2}(0)\rangle$ by the conformal algebra. An efficient way to compute it is by using the following recursions [57]:

$$\langle L_{-n}^{(\infty)}V_{\Delta_3}(\infty)V_{\Delta_1}(1)V_{\Delta_2}(0)\rangle = \langle V_{\Delta_3}(\infty)\left(nL_0^{(1)} + \sum_{i=1}^{n}\frac{(n+1)!}{(i+1)!(n-i)!}L_i^{(1)}\right)V_{\Delta_1}(1)V_{\Delta_2}(0)\rangle \tag{1.46a}$$
$$+ \langle L_0^{(\infty)}V_{\Delta_3}(\infty)V_{\Delta_1}(1)V_{\Delta_2}(0)\rangle + \langle V_{\Delta_3}(\infty)V_{\Delta_1}(1)\left(L_n^{(0)} - L_0^{(0)}\right)V_{\Delta_2}(0)\rangle$$

$$\langle V_{\Delta_3}(\infty)L_{-n}^{(1)}V_{\Delta_1}(1)V_{\Delta_2}(0)\rangle = (-1)^n\langle V_{\Delta_3}(\infty)L_0^{(1)}V_{\Delta_1}(1)V_{\Delta_2}(0)\rangle \tag{1.46b}$$
$$+ \langle\left((-1)^{n+1}(L_0^{(\infty)} - L_1^{(\infty)}) + L_n^{(\infty)} + \sum_{i=0}^{\infty}\frac{(n-1+i)!}{(i+1)!(n-2)!}L_{n+1+i}^{(\infty)}\right)V_{\Delta_3}(\infty)V_{\Delta_1}(1)V_{\Delta_2}(0)\rangle$$
$$+ (-1)^n\langle V_{\Delta_3}(\infty)V_{\Delta_1}(1)\left(nL_0^{(0)} + \sum_{i=1}^{\infty}\frac{(n-1+i)!}{(i+1)!(n-2)!}L_i^{(0)}\right)V_{\Delta_2}(0)\rangle$$

$$\langle V_{\Delta_3}(\infty)V_{\Delta_1}(1)L_{-n}^{(0)}V_{\Delta_2}(0)\rangle = \langle\left(L_n^{(\infty)} - L_0^{(\infty)}\right)V_{\Delta_3}(\infty)V_{\Delta_1}(1)V_{\Delta_2}(0)\rangle \tag{1.46c}$$
$$+ \langle V_{\Delta_3}(\infty)V_{\Delta_1}(1)L_0^{(0)}V_{\Delta_2}(0)\rangle + \langle V_{\Delta_3}(\infty)\left(nL_0^{(1)} + \sum_{i=1}^{\infty}\frac{(-1)^i(n-1+i)!}{(i+1)!(n-2)!}L_i^{(1)}\right)V_{\Delta_1}(1)V_{\Delta_2}(0)\rangle.$$

In particular we see that $\langle V_{\Delta_3,Y_3}(\infty)V_{\Delta_1,Y_1}(1)V_{\Delta_2,Y_2}(0)\rangle$ is proportional to $\langle V_{\Delta}(\infty)V_{\Delta_1}(1)V_{\Delta_2}(0)\rangle$, so that the ratios (1.45) are completely fixed by conformal symmetry and are therefore independent of the particular theory.

1.3 THE OPERATOR PRODUCT EXPANSION

In the bootstrap approach (see for eg. [20]), we assume that the product of two fields can be expanded over the other fields in the spectrum, namely, that the following *operator product expansion* (OPE) exists [18] (see also Chapter 5 of [58]):

$$\begin{aligned} V_{\Delta_1,\bar{\Delta}_1}(z_1,\bar{z}_1)V_{\Delta_2,\bar{\Delta}_2}(z_2,\bar{z}_2) &\overset{z_1\sim z_2}{=} \sum_{(\Delta_3)} \left|z_{12}^{-\Delta_1-\Delta_2+\Delta_3}\right|^2 \left|\sum_{Y_3} D^{\Delta_3,Y_3}_{\Delta_1,\Delta_2} z_{12}^{|Y_3|} V_{\Delta_3,Y_3}\right|^2 \\ &= \sum_{(\Delta_3)} \left|z_{12}^{-\Delta_1-\Delta_2+\Delta_3}\right|^2 D^{(\Delta_3)}_{(\Delta_1),(\Delta_2)} \left(V_{(\Delta_3)} + O(z_{12})\right). \end{aligned} \tag{1.47}$$

Here we introduced the short-hand notation :

$$(\Delta) \equiv (\Delta, \bar{\Delta}), \tag{1.48}$$

as well as the modulus-square notation:

$$|f(z,\Delta)|^2 = f(z,\Delta) \times f(\bar{z},\bar{\Delta}). \tag{1.49}$$

The coefficient $D^{\Delta_3,Y_3}_{\Delta_1,\Delta_2}$ can be factorised in the following way:

$$D^{\Delta_3,Y_3}_{\Delta_1,\Delta_2} = D^{\Delta_3}_{\Delta_1,\Delta_2} \left(\sum_{\substack{Y \\ |Y|=|Y_3|}} H^{-1}_{Y,Y_3}(\Delta_3)\Gamma^{\Delta_3,Y}_{\Delta_1,\Delta_2} \right) \tag{1.50}$$

which makes apparent what depends on the particular model and what is fixed by conformal invariance:

- The sum encodes the contribution of descendants in (1.47), and is therefore completely determined by the symmetry algebra, with H^{-1}_{Y,Y_3} the matrix elements of (1.44) and the Gamma factors given by (1.45).
- The number

  $$D^{(\Delta_3)}_{(\Delta_1),(\Delta_2)} = \langle V_{\Delta_3,\bar{\Delta}_3}(\infty)V_{\Delta_1,\bar{\Delta}_1}(1)V_{\Delta_2,\bar{\Delta}_2}(0)\rangle = D^{\Delta_3}_{\Delta_1,\Delta_2} D^{\bar{\Delta}_3}_{\bar{\Delta}_1,\bar{\Delta}_2}, \tag{1.51}$$

  is called *structure constant*. Looking back at (1.47), it encodes the fusion of two primary fields onto another primary field. The set of structure constants is a model-dependent set of data, in the sense that it is not fixed by conformal symmetry[2].

  We normalise the structure constants involving an identity field to 1:

  $$D^{(\Delta_3)}_{(\Delta_{\mathrm{Id}}),(\Delta_2)} = 1. \tag{1.52}$$

2 Nevertheless, the structure of this set of constants may reflect the presence of possible extra symmetries, as discussed in Section 1.6.

Note that the OPE (1.47) extends straightforwardly to descendant fields: $(\Delta_1) \to (\Delta_1, Y_1)$, $(\Delta_2) \to (\Delta_2, Y_2)$. In particular expression (1.20) of Section 1.1 is the OPE between a primary field and the stress-energy tensor, which is the level-2 descendant of the Identity field.
Seen as a function of the scaling dimension, the coefficient $D^{\Delta_3,Y_3}_{\Delta_1,\Delta_2}$ (1.50) has poles whenever the dimension Δ_3 is of the type $\Delta_{m,n}$ (0.8c). As seen above, the block of the matrix $H(\Delta_3)$ corresponding to level mn is indeed non-invertible in that case. For example, at level 1:

$$\left.\begin{aligned} H^{-1}_{\{1\},\{1\}}(\Delta_3) &= \frac{1}{2\Delta_3} \\ \Gamma^{\Delta_3,\{1\}}_{\Delta_1,\Delta_2} &= \Delta_3 - \Delta_2 + \Delta_1 \end{aligned}\right\} \qquad D^{\Delta_3,\{1\}}_{\Delta_1,\Delta_2} = D^{\Delta_3}_{\Delta_1,\Delta_2}\frac{\Delta_3 - \Delta_2 + \Delta_1}{2\Delta_3}. \tag{1.53}$$

For generic values of Δ_1, Δ_2, this is singular as $\Delta_3 \to \Delta_{1,1} = 0$, which means that the field V_{Δ_3} cannot appear in the OPE $V_{\Delta_1}V_{\Delta_2}$. However, if $\Delta_1 = \Delta_2$, then $\lim_{\Delta_3\to\Delta_{1,1}} D^{\Delta_3,\{1\}}_{\Delta_1,\Delta_2} = \frac{1}{2}$. In general, fields with degenerate dimension cannot appear in the OPE expansion, except if the dimensions Δ_1 and Δ_2 satisfy algebraic relations, called *fusion rules*.
Let us take now $V_{(\Delta_1)}$ or $V_{(\Delta_2)}$ to be degenerate. For simplicity let us take $V_{\Delta_1} = V_{1,1}$. Then, because the null state $L_{-1}V_{1,1}$ is set to zero:

$$D^{\Delta_3}_{\Delta_1,\{1\};\Delta_2} = \langle V_{\Delta_3}(\infty)L_{-1}V_{1,1}(1)V_{\Delta_2}(0)\rangle = 0. \tag{1.54}$$

Using relation (1.46a):

$$\langle V_{\Delta_3}(\infty)L_{-1}V_{1,1}(1)V_{\Delta_2}(0)\rangle = (\Delta_3 - \Delta_2)\, D^{\Delta_3}_{1,1;\Delta_2}, \tag{1.55}$$

so that $D^{\Delta_3}_{1,1;\Delta_2} \neq 0 \Rightarrow \Delta_2 = \Delta_3$. The degenerate field $V_{1,1}$ imposes therefore the fusion:

$$\mathcal{R}_{1,1} \times \mathcal{R}_\Delta = \mathcal{R}_\Delta. \tag{1.56}$$

More generally, the fusion rule with a degenerate representation is, in terms of the conformal charge α (0.7b) [18]:

$$\mathcal{R}_{r,s} \times \mathcal{R}_\alpha = \sum_{i=0}^{r-1}\sum_{j=0}^{s-1} \mathcal{R}_{\alpha+\alpha_{r,s}+ib+jb^{-1}}. \tag{1.57}$$

1.4 CORRELATION FUNCTIONS

In this section we give the form of the two-, three- and four-point functions on the plane. The spatial dependence of the two- and -three-point is fixed by global conformal invariance. The four-point function on the other hand, combines in a non-trivial way model-dependent data with data fixed by local conformal invariance. By using the OPE we show how to write an arbitrary four-point function as a channel expansion, over the spectrum of the theory. This is the technique we will use throughout this thesis to compute correlation functions. Applying the OPE in a similar way reduces higher point-functions to combinations of two-point functions, with coefficients determined by the spectrum and the structure constants. Therefore the necessary ingredients to determine all correlation functions are the set of scaling dimensions and the set of structure constants. A CFT is completely defined by these two sets of data. Four-point functions are in this respect a central object of study in a CFT: on the one hand they depend non-trivially

on the model-dependent data, and on the other hand they describe physical observables of a (statistical) model.

Consider first the two-point function. It is fixed by global conformal invariance to [18]:

$$\langle V_{\Delta_1,\bar{\Delta}_1}(z_1,\bar{z}_1)V_{\Delta_2,\bar{\Delta}_2}(z_2,\bar{z}_2)\rangle = \frac{\delta_{\Delta_1,\Delta_2}\delta_{\bar{\Delta}_1,\bar{\Delta}_2}}{z_{12}^{\Delta_1+\Delta_2}\bar{z}_{12}^{\bar{\Delta}_1+\bar{\Delta}_2}}. \tag{1.58}$$

Translation and rotation invariance imply a $|z_{12}|$ dependence, while scale invariance implies a power law decay. The special conformal transformation (1.5c) imposes that two-point functions vanish unless the fields have the same dimension.

The three-point function, on the other hand, is fixed –also by global symmetry, up to a constant [18]:

$$\langle V_{\Delta_1,\bar{\Delta}_1}(z_1,\bar{z}_1)V_{\Delta_2,\bar{\Delta}_2}(z_2,\bar{z}_2)V_{\Delta_3,\bar{\Delta}_3}(z_3,\bar{z}_3)\rangle = \frac{D^{(\Delta_3)}_{(\Delta_1),(\Delta_2)}}{\left|z_{12}^{\Delta_1+\Delta_2-\Delta_3}z_{23}^{-\Delta_1+\Delta_2+\Delta_3}z_{13}^{\Delta_1-\Delta_2+\Delta_3}\right|^2}. \tag{1.59}$$

The constant $D^{(\Delta_3)}_{(\Delta_1),(\Delta_2)}$ is the structure constant appearing in the OPE (1.47): this can be found by inserting the OPE say of V_{Δ_1} and V_{Δ_2} in the left-hand side of (1.59). It is easily seen that the OPE expansion corresponds to the series of the right-hand side of (1.59) when $z_1 \sim z_2$. This is done explicitely in Section 2.5.2 where the three-point function is studied on the torus.

The four-point function is conveniently written in the form [18]:

$$\begin{aligned}\langle\prod_{i=1}^{4} V_{(\Delta_i)}(z_i,\bar{z}_i)\rangle = &\left|z_{13}^{-2\Delta_1}z_{23}^{\Delta_1-\Delta_2-\Delta_3+\Delta_4}z_{24}^{-\Delta_1-\Delta_2+\Delta_3-\Delta_4}z_{34}^{\Delta_1+\Delta_2-\Delta_3-\Delta_4}\right|^2 \\ &\times\langle V_{\Delta_1,\bar{\Delta}_1}(z,\bar{z})V_{\Delta_2,\bar{\Delta}_2}(0)V_{\Delta_3,\bar{\Delta}_3}(\infty)V_{\Delta_4,\bar{\Delta}_4}(1)\rangle,\end{aligned} \tag{1.60}$$

where we defined:

$$\begin{aligned}&\langle V_{\Delta_1,\bar{\Delta}_1}(z,\bar{z})V_{\Delta_2,\bar{\Delta}_2}(0)V_{\Delta_3,\bar{\Delta}_3}(\infty)V_{\Delta_4,\bar{\Delta}_4}(1)\rangle \\ &= \lim_{Z\to\infty} Z^{2\Delta_3}\bar{Z}^{2\bar{\Delta}_3}\langle V_{\Delta_1,\bar{\Delta}_1}(z,\bar{z})V_{\Delta_2,\bar{\Delta}_2}(0)V_{\Delta_3,\bar{\Delta}_3}(Z,\bar{Z})V_{\Delta_4,\bar{\Delta}_4}(1)\rangle,\end{aligned} \tag{1.61}$$

which depends on the *cross-ratio*:

$$z \equiv \frac{z_{12}z_{34}}{z_{13}z_{24}}. \tag{1.62}$$

The four-point function can be expanded as a sum over the fields in the spectrum S, in a so-called *s-channel expansion*, as follows. Inserting the OPE (1.47) of $V_{(\Delta_1)}$ and $V_{(\Delta_2)}$, and using (1.50) we obtain:

$$\begin{aligned}&\langle V_{(\Delta_1)}(z,\bar{z})V_{(\Delta_2)}(0)V_{(\Delta_3)}(\infty)V_{(\Delta_4)}(1)\rangle \\ &= \sum_{(\Delta_s)\in S_s}\left|z^{-\Delta_1-\Delta_2+\Delta_s}\right|^2 D^{(\Delta_s)}_{(\Delta_1),(\Delta_2)}D^{(\Delta_3)}_{(\Delta_s),(\Delta_4)}\left|\sum_{Y_s} z^{Y_s}\Gamma^{\Delta_3}_{\Delta_4;\Delta_s,Y_s}\sum_{\substack{Y_s'\\|Y_s'|=|Y_s|}} H^{-1}_{Y_s,Y_s'}(\Delta_s)\,\Gamma^{\Delta_s,Y_s'}_{\Delta_1,\Delta_2}\right|^2 \\ &= \sum_{(\Delta_s)\in S_s} D^{(\Delta_s)}_{(\Delta_1),(\Delta_2)}D^{(\Delta_3)}_{(\Delta_s),(\Delta_4)}\left|\mathcal{F}^{(s)}_{\Delta_s}(\Delta_i|z)\right|^2\end{aligned} \tag{1.63}$$

where $\Delta_i = \Delta_1, \Delta_2, \Delta_3, \Delta_4$, and Δ_s is called the internal dimension. The *s-channel spectrum* S_s is a subset of the full spectrum S, namely the set of fields V_{Δ_s} in S for which the structure constants $D^{(\Delta_s)}_{(\Delta_1),(\Delta_2)}$, $D^{(\Delta_s)}_{(\Delta_1),(\Delta_2)}$ are non-zero. In the last line we introduced the s-channel *four-point conformal block* on the plane, $\mathcal{F}^{(s)}_{\Delta_s}$ (see eg. [20], Section 2.4). It corresponds to the expansion $z \to 0$, which can be represented diagrammatically as:

$$\mathcal{F}^{(s)}_{\Delta_s} = \quad \begin{array}{ccccc} V_{\Delta_2}(0) & & & & V_{\Delta_3}(\infty) \\ & \diagdown & & \diagup & \\ & & V_{\Delta_s} & & \\ & \diagup & & \diagdown & \\ V_{\Delta_1}(z) & & & & V_{\Delta_4}(1) \end{array} \tag{1.64}$$

The conformal block contains the contributions of all descendants of the field $V_{(\Delta)}$ to the four-point function:

$$\begin{aligned} \mathcal{F}^{(s)}_{\Delta}(\Delta_i|z) &= z^{-\Delta_1-\Delta_2+\Delta} \sum_{Y} z^{Y} \Gamma^{\Delta_3}_{\Delta_4;\Delta,Y} \sum_{\substack{Y' \\ |Y'|=Y}} H^{-1}_{Y,Y'}(\Delta)\, \Gamma^{\Delta,Y'}_{\Delta_1,\Delta_2} \\ &= z^{-\Delta_1-\Delta_2+\Delta} \Bigg\{ 1 + \Gamma^{\Delta_3}_{\Delta_4;\Delta,\{1\}} H^{-1}_{\{1\},\{1\}}(\Delta) \Gamma^{\Delta,\{1\}}_{\Delta_1,\Delta_2}\, z \\ &+ \Big[\Gamma^{\Delta_3}_{\Delta_4;\Delta,\{1,1\}} \left(H^{-1}_{\{1,1\},\{1,1\}}(\Delta) \Gamma^{\Delta,\{1,1\}}_{\Delta_1,\Delta_2} + H^{-1}_{\{1,1\},\{2\}}(\Delta) \Gamma^{\Delta,\{2\}}_{\Delta_1,\Delta_2} \right) \\ &+ \Gamma^{\Delta_3}_{\Delta_4;\Delta,\{2\}} \left(H^{-1}_{\{2\},\{1,1\}}(\Delta) \Gamma^{\Delta,\{1,1\}}_{\Delta_1,\Delta_2} + H^{-1}_{\{2\},\{2\}}(\Delta) \Gamma^{\Delta,\{2\}}_{\Delta_1,\Delta_2} \right) \Big] z^2 + O(z^3) \Bigg\}. \end{aligned} \tag{1.65}$$

It is therefore completely determined by symmetry. The s-channel expansion (1.63) is then a model-dependent (spectrum and structure constants) linear combination of model-independent functions (the conformal blocks).

1.5 ANALYTIC STRUCTURE OF THE CONFORMAL BLOCKS

While some models may live at a particular value of the central charge (for instance the Ising spin model at $c = 1/2$), CFTs can be defined on a (continuous) range of the central charge. This is the case of Liouville theory and of the generalised minimal models (see for instance Chapter 3 in [20]), as well as of the CFTs describing the continuous families of models studied in this thesis. Scaling dimensions and structure constants are then (a priori unknown) functions of the central charge. It is manifest from the conformal block expansion (1.63) that the behaviour of the four-point function with the central charge depends on the interplay between the analytic properties of the structure constants and the ones of the conformal blocks. In this section we investigate the structure of these latter.

1.5.1 *Recursion relation for the conformal blocks*

Although the four-point conformal block (1.65) is completely determined by the commutation relations (1.29), there exist no closed form formula for $\mathcal{F}^{(s)}_{\Delta}(\Delta_i|z)$, for generic values of the dimensions Δ_i. This is not very surprising, given that the conformal blocks are the symmetry functions associated to an infinite dimensional algebra. By comparison, the conformal blocks

in (even) dimension greater than two are given in terms of hypergeometric functions (see for instance [59]).
The expansion (1.65) may be computed level by level using relations (1.46a), but this is not very efficient, since the number of descendants grows quickly. Let us look at the analytic structure of the expansion (1.65), as a function of the internal dimension. Similarly to the OPE expansion (1.47), the conformal block $\mathcal{F}_\Delta^{(s)}$ has a pole whenever the internal dimension Δ takes degenerate values $\Delta = \Delta_{m,n}$. This means that the block will be well-defined only if the external dimension Δ_1, Δ_2 or/and Δ_3, Δ_4 satisfy the corresponding fusion rules. In the simple example (1.53) at level $mn = 1$:

$$\left.\begin{aligned} H^{-1}_{\{1\},\{1\}}(\Delta) &= \frac{1}{2\Delta} \\ \Gamma^{\Delta,\{1\}}_{\Delta_1,\Delta_2} &= \Delta - \Delta_2 + \Delta_1 \\ \Gamma^{\Delta_3}_{\Delta_4;\Delta,\{1\}} &= -\Delta_3 + \Delta + \Delta_4 \end{aligned}\right\} \qquad \Gamma^{\Delta_3}_{\Delta_4;\Delta,\{1\}} H^{-1}_{\{1\},\{1\}}(\Delta) \Gamma^{\Delta,\{1\}}_{\Delta_1,\Delta_2} = \frac{(\Delta_1 - \Delta_2 + \Delta)(\Delta_4 - \Delta_3 + \Delta)}{2\Delta}. \tag{1.66}$$

When $\Delta \to \Delta_{1,1} = 0$, the limit will be either finite if the fusion rule is satisfied by one of the two nodes in diagram (1.64): $\Delta_1 = \Delta_2$ or $\Delta_3 = \Delta_4$, or zero if the two nodes satisfy the fusion: $\Delta_1 = \Delta_2$ and $\Delta_3 = \Delta_4$. Note that the null state $L_{-1}|\Delta_{1,1}\rangle$ has descendants at levels 2, 3, ..., and therefore there will be simple poles also at higher orders in the expansion of the block $\mathcal{F}^{(s)}_{\Delta_{1,1}}$. From the example at order 1 above, we know that the residues of these poles must vanish when $\Delta_1 = \Delta_2$ and when $\Delta_3 = \Delta_4$. We can then deduce that each residue is proportional to $(\Delta_1 - \Delta_2)(\Delta_3 - \Delta_4)$. More generally,

$$\mathrm{res}_{\Delta=\Delta_{m,n}} \mathcal{F}^{(s)}_\Delta(\Delta_i|z) \propto \mathcal{F}^{(s)}_{\Delta_{m,n}+mn}(\Delta_i|z). \tag{1.67}$$

This observation leads to a very efficient way to compute the Virasoro conformal blocks, given by Zamolodchikov's recursion representation [60, 61]:

$$\mathcal{F}^{(s)}_\Delta(\Delta_i|z) = (16q)^{\Delta - \frac{Q^2}{4}} z^{\frac{Q^2}{4} - \Delta_1 - \Delta_2} (1-z)^{\frac{Q^2}{4} - \Delta_1 - \Delta_4} \theta_3(q)^{3Q^2 - 4\sum_i \Delta_i} H_\Delta(\Delta_i|q). \tag{1.68}$$

In this expression, Q refers to notation (0.4) for the central charge. The recursion parameter q is a function of z:

$$q = \frac{1}{16}\left(z + \frac{1}{2}z^2 + \cdots\right), \tag{1.69}$$

which follows from inverting

$$z = \left(\frac{\theta_2(q)}{\theta_3(q)}\right)^4, \tag{1.70}$$

where θ_2 and θ_3 are the Jacobi theta functions (A.1). The analytic structure (1.67) of the conformal block appears in the function $H_\Delta(\Delta_i|q)$, as made manifest in its recursive form:

$$H_\Delta(\Delta_i|q) = 1 + \sum_{mn \geq 1} (16q)^{mn} \frac{R_{m,n}(\Delta_i)}{\Delta - \Delta_{m,n}} H_{\Delta_{m,n}+mn}(\Delta_i|q). \tag{1.71}$$

To express the coefficients $R_{m,n}$, it is convenient to parametrise the conformal dimension with the momentum P (0.7a,0.8a), in terms of which:

$$R_{m,n}(P_i) = \frac{2P_{0,0}P_{m,n}}{\prod_{r=1-m}^{m-1}\prod_{s=1-n}^{n-1} 2P_{r,s}} \prod_{r\overset{2}{=}1-m}^{m-1} \prod_{s\overset{2}{=}1-n}^{n-1} \prod_{\pm} (P_2 \pm P_1 + P_{r,s})\,(P_3 \pm P_4 + P_{r,s})\,. \quad (1.72)$$

For instance,

$$R_{1,1} = \frac{1}{2}(P_2^2 - P_1^2)(P_3^2 - P_4^2) = \frac{(\Delta_1 - \Delta_2)(\Delta_4 - \Delta_3)}{2}, \quad (1.73)$$

which is indeed the residue when $\Delta \to \Delta_{1,1}$ of the coefficient at order 1 (1.66).
We point out that further, non-physical singularities arise in the representation (1.71). Indeed, using that

$$\Delta_{m,n} + mn = \Delta_{m,-n} \quad (1.74)$$

(cf. (0.8c)) we have:

$$H_{\Delta_{m,n}+mn}(\Delta_i|q) = H_{\Delta_{m,-n}}(\Delta_i|q) = 1 + \sum_{rs\geq 1} (16q)^{rs} \frac{R_{r,s}(\Delta_i)}{\Delta_{m,-n} - \Delta_{r,s}} H_{\Delta_{r,-s}}(\Delta_i|q). \quad (1.75)$$

The denominator vanishes if there are positive integers r, s such that:

$$\Delta_{m,-n} = \Delta_{r,s} \Leftrightarrow mb - \frac{n}{b} = \pm rb \pm \frac{s}{b}, \quad (1.76)$$

where b is parametrisation of the central charge (0.4). For generic b, this implies $r, s = \pm m, \mp n$, so that $rs < 0$. Therefore, for generic central charge, no such singularities arise. However, if b is such that:

$$mb - \frac{n}{b} = \pm rb \pm \frac{s}{b} \Leftrightarrow b^2 = \pm\frac{n+s}{m \mp r}, \quad (1.77)$$

that is if b^2 is a rational number, then expression (1.71) develops singularities. In particular, these values of b include the values of the central charge:

$$c = c_{p,q} = 1 - 6\frac{(p-q)^2}{pq}, \quad \begin{cases} p, q \text{ coprime integers }, \\ 2 \leq p < q\ , \end{cases} \quad (1.78)$$

These values correspond to the central charges of A-type minimal models [20], among which the Ising model, the 3−states Potts model, etc. It has been conjectured in [50, 62] that these unphysical poles cancel each other in the sum (1.71). Nevertheless, they prevent accurate numerical analysis at rational values of the central charge, as remarked for instance in Section 4.3 of [47]. Obtaining a recursion which would be manifestly smooth as a function of the central charge is a difficult problem, which we study in Chapter 3.

1.6 CONFORMAL BLOCKS AND STRUCTURE CONSTANTS TOGETHER

In this section we would like to point at two subtle aspects of the channel expansion, which arise when putting structure constants and conformal blocks together. In Section 1.6.1 we explain what happens when the symmetry algebra is larger than the Virasoro algebra, through the simple but instructive example of the 3−state Potts model. In Section 1.6.2 we comment on further singularities which can appear both in the conformal blocks and in the structure constants.

1.6.1 *s-channel expansions in the* 3*−state Potts model*

The 3-state Potts model is a well-known spin model which is a generalisation of the Ising model: the spin variables can take 3 values instead of 2 (see for instance Chapter 7 in [22]. In Chapter 4 we define precisely the general $Q-$state Potts model in its random cluster formulation). This model is conformally invariant and possesses the additional permutational symmetry S_3. The CFT is then based on the extended algebra $\mathcal{W}_3$, formed by the stress-energy tensor and a spin-3 field W (see for instance [63] for an introduction to the $\mathcal{W}_3$ algebra and its representations). The modes W_n of the field W are defined in strict analogy with the Virasoro ones (1.28):

$$W_n^{(z)} = \frac{1}{2\pi i}\oint_{\mathcal{C}_z} dy\,(y-z)^{n+2}\,W(y), \quad n \in \mathbb{Z}. \tag{1.79}$$

The spectrum of the 3$-$Potts model contains seven scalar Virasoro primaries [22][3]:

Field	$V_{1,1} = \mathrm{Id}$	$V_{3,3} = \sigma^{\pm}$	$V_{1,2} = \varepsilon$	$V_{3,1}$	$V_{1,3}$	$V_{1,4}$
Δ	0	1/15	2/5	2/3	7/5	3

The field $V_{3,3}$ has multiplicity 2: there are two spin fields $\sigma^{\pm}$ with the same dimension but different fusion rules, as seen below. Among these fields, only the identity Id, the two spin fields $\sigma^{\pm}$, the energy ε and the $V_{3,1}$ fields are primaries of the full $\mathcal{W}_3$ algebra, the others being $\mathcal{W}_3$ descendants:

$$\begin{aligned} V_{1,4} &= W = W_{-3}\mathrm{Id} \\ V_{1,3} &= W_{-1}\bar{W}_{-1}\varepsilon. \end{aligned} \tag{1.80}$$

Let us now consider the spin four-point function. Note that one can define several different four-point spin correlators due to its 2-fold multiplicity. These four-point functions typically have different s-channel expansions, since σ^+ et σ^- have different fusions:

$$\sigma^+ \times \sigma^+ = \sigma^- + V_{3,1} \tag{1.81a}$$
$$\sigma^+ \times \sigma^- = \mathrm{Id} + \varepsilon. \tag{1.81b}$$

Then we have for instance the following s-channel conformal block expansions:

$$\langle\sigma^+(z)\sigma^+(0)\sigma^+(\infty)\sigma^+(1)\rangle = \sum_{V=\sigma^-,Z}\left[D^V_{\sigma^+,\sigma^+}\right]^2 |\mathcal{F}_{\Delta_V}(\Delta_\sigma|z)|^2 \tag{1.82a}$$

$$\langle\sigma^+(z)\sigma^-(0)\sigma^+(\infty)\sigma^-(1)\rangle = \sum_{\substack{V=\mathrm{Id},\varepsilon,\\ V_{1,3},W}}\left[D^V_{\sigma^+,\sigma^-}\right]^2 |\mathcal{F}_{\Delta_V}(\Delta_\sigma|z)|^2\,. \tag{1.82b}$$

It is clear from the above expansions that these two correlators are not the same object, although they are both four-point functions of fields with the same dimension. This is a crucial point in the study of the more general $Q-$Potts model of Chapter 4.
Let us consider the second correlator (1.82b). In this "naive" conformal block expansion, only conformal symmetry is taken into account: the fields $V_{1,3}$ and W are considered as primaries, since they are indeed Virasoro primaries. But if we know that the symmetry is actually larger, we

3 NB: the convention for the field indices m, n in [22] is switched with respect to ours $m \leftrightarrow n$.

can rewrite this expansion by regrouping the terms according to the full algebra representations, instead of the Virasoro representations. Using (1.80) we obtain:

$$\begin{aligned}\langle\sigma^+(z)\sigma^-(0)\sigma^+(\infty)\sigma^-(1)\rangle = &\left(\left|\mathcal{F}_{\Delta_{\mathrm{Id}}}\left(\Delta_\sigma|z\right)\right|^2+\left[D^{W}_{\sigma^+,\sigma^-}\right]^2\left|\mathcal{F}_{\Delta_W}\left(\Delta_\sigma|z\right)\right|^2\right)\\ &+\left[D^{\varepsilon}_{\sigma^+,\sigma^-}\right]^2\left(\left|\mathcal{F}_{\Delta_\varepsilon}\left(\Delta_\sigma|z\right)\right|^2+\left[\frac{D^{V_{1,3}}_{\sigma^+,\sigma^-}}{D^{\varepsilon}_{\sigma^+,\sigma^-}}\right]^2\left|\mathcal{F}_{\Delta_{1,3}}\left(\Delta_\sigma|z\right)\right|^2\right)\end{aligned} \tag{1.83}$$

with the structure constant of the identity normalised to one (1.52). Because W and $V_{1,3}$ are W_3 descendants, it means that the ratios of structure constants $D^{W}_{\sigma^+,\sigma^-}/D^{\mathrm{Id}}_{\sigma^+,\sigma^-}$ and $D^{V_{1,3}}_{\sigma^+,\sigma^-}/D^{\varepsilon}_{\sigma^+,\sigma^-}$ are fixed by the full, W_3 symmetry, exactly as the Gamma factors of Section 1.2. These ratios can be computed recursively as well [57]. Defining the $\mathcal{W}_3$ blocks $\mathcal{W}$, the expansion (1.83) becomes:

$$\langle\sigma^+(z)\sigma^-(0)\sigma^+(\infty)\sigma^-(1)\rangle = \left|\mathcal{W}_{\Delta_{\mathrm{Id}}}\left(\Delta_\sigma|z\right)\right|^2+\left[D^{\varepsilon}_{\sigma^+,\sigma^-}\right]^2\left|\mathcal{W}_{\Delta_\varepsilon}\left(\Delta_\sigma|z\right)\right|^2. \tag{1.84}$$

This is a very simple example in which the symmetry function of the full symmetry algebra (here the $\mathcal{W}_3$ block) assembles the contributions of different Virasoro primaries. An important point is that the presence of this extra symmetry implies relations between some structure constants: in that case $D^{W}_{\sigma^+,\sigma^-}$ and $D^{V_{1,3}}_{\sigma^+,\sigma^-}$ can be determined recursively from $D^{\mathrm{Id}}_{\sigma^+,\sigma^-}$ and $D^{\varepsilon}_{\sigma^+,\sigma^-}$. A similar structure is present in the more involved $Q-$Potts model under the form of interchiral blocks, as will be seen in Chapter 4.

1.6.2 *Analytic structure of four-point functions*

In Section 1.5 we have seen that a conformal block $\mathcal{F}_{\Delta_s}(\Delta_i)$ is well-defined if $\Delta_s \neq \Delta_{r,s}$ with $r,s\in\mathbb{N}$, or if $\Delta_s=\Delta_{r,s}$ and the external dimensions Δ_i satisfy fusion rules.
Let us consider the s-channel expansion of a generic four-point function (for simplicity the four external fields are taken to have the same dimension):

$$\langle V_{(\Delta)}(z)V_{(\Delta)}(0)V_{(\Delta)}(\infty)V_{(\Delta)}(1)\rangle = \sum_{(\Delta_s)\in S_s}\left[D^{(\Delta_s)}_{(\Delta),(\Delta)}\right]^2\left|\mathcal{F}^{(s)}_{\Delta_s}(\Delta|z)\right|^2. \tag{1.85}$$

In particular $V_{(\Delta)}$ and the $V_{(\Delta_s)}$'s are not degenerate. Δ and Δ_s are functions of the central charge c, so that there can exist values of c at which $\Delta_s=\Delta_{r,s}$ for some integers r,s. The dimension Δ is arbitrary so that the conformal block $\mathcal{F}^{(s)}_{\Delta_s}$ has a pole at order rs. This happens in particular in the four-point functions of the random cluster $Q-$Potts model. In that case it turns out that the poles coming from the conformal blocks are cancelled by poles in the structure constants. The CFT of the $Q-$Potts model is fully detailed in Chapter 4. To give an example of such analytic behaviour of the four-point function, let us assume for now that this CFT is defined for continuous values of the central charge, and contains a field with dimension $\Delta=\Delta_{0,1/2}$, whose four-point function has the following s-channel expansion:

$$\langle V_{(0,\frac{1}{2})}(z,\bar z)V_{(0,\frac{1}{2})}(0)V_{(0,\frac{1}{2})}(\infty)V_{(0,\frac{1}{2})}(1)\rangle = \left[D^{(0,\frac{1}{2})}_{(0,\frac{1}{2})(0,\frac{1}{2})}\right]^2\left|\mathcal{F}_{0,\frac{1}{2}}(z)\right|^2+\cdots \tag{1.86}$$

The conformal block is:

$$\mathcal{F}_{0,\frac{1}{2}}(z) = |z|^{2\Delta_{(0,\frac{1}{2})}}\left(1+f_1(\Delta_{0,\frac{1}{2}})z+f_2(\Delta_{0,\frac{1}{2}})z^2+\cdots\right) \tag{1.87}$$

and the structure constant $D^{(0,\frac{1}{2})}_{(0,\frac{1}{2})(0,\frac{1}{2})}$ is known to be well-defined on the considered range of c (cf. Section 4.2).
At central charge $c = 1/2$ we have $\Delta_{0,\frac{1}{2}}(c = 1/2) = \Delta_{2,1}(c = 1/2)$, which corresponds to a level 2 degenerate dimension. $V_{0,1/2}$ is however not a degenerate field, for any c. The fusion rules are thereby not satisfied and there is a pole in the conformal block at level 2:

$$f_2(\Delta_{0,\frac{1}{2}}) \sim \frac{1}{c - 1/2}. \tag{1.88}$$

However (1.86) takes also a contribution from a non-diagonal field with dimensions $(\Delta, \bar{\Delta}) = (\Delta_{2,-1}, \Delta_{2,1}) = (\Delta_{2,1} + 2, \Delta_{2,1})$, so that:

$$(1.86) = \left[D^{(0,\frac{1}{2})}_{(0,\frac{1}{2})(0,\frac{1}{2})}\right]^2 \mathcal{F}_{\Delta_{0,\frac{1}{2}}}(z)\bar{\mathcal{F}}_{\Delta_{0,\frac{1}{2}}}(\bar{z}) + \left[D^{(2,-1),(2,1)}_{(0,\frac{1}{2})(0,\frac{1}{2})}\right]^2 \mathcal{F}_{\Delta_{2,1}+2}(z)\bar{\mathcal{F}}_{\Delta_{2,1}}(\bar{z}) + \cdots \tag{1.89}$$

where $\bar{\mathcal{F}}_{0,\frac{1}{2}} \overset{c=1/2}{=} \bar{\mathcal{F}}_{2,1}$. The smoothness of the four-point function at $c = 1/2$ then requires:

$$\mathrm{res}_{c=1/2}\left[D^{(2,-1),(2,1)}_{(0,\frac{1}{2})(0,\frac{1}{2})}\right]^2 \mathcal{F}_{\Delta_{2,1}+2} = -\left[D^{(0,\frac{1}{2})}_{(0,\frac{1}{2})(0,\frac{1}{2})}\right]^2 \mathrm{res}_{c=1/2}\mathcal{F}_{\Delta_{0,\frac{1}{2}}}. \tag{1.90}$$

However from the structure of conformal blocks we have (cf. Section 1.5):

$$\mathrm{res}_{c=1/2}\mathcal{F}_{\Delta_{0,\frac{1}{2}}} = \mathrm{res}_{\Delta=\Delta_{2,1}}\mathcal{F}_{\Delta} \propto \mathcal{F}_{\Delta_{2,1}+2}. \tag{1.91}$$

Therefore condition (1.90) becomes:

$$\begin{aligned}\mathrm{res}_{c=1/2}\left[D^{(2,-1),(2,1)}_{(0,\frac{1}{2})(0,\frac{1}{2})}\right]^2 &\propto \left[D^{(0,\frac{1}{2})}_{(0,\frac{1}{2})(0,\frac{1}{2})}\right]^2 \\ &= -\left[D^{(0,\frac{1}{2})}_{(0,\frac{1}{2})(0,\frac{1}{2})}\right]^2 \mathrm{res}_{c=1/2} f_2(\Delta_{0,\frac{1}{2}}).\end{aligned} \tag{1.92}$$

The structure constant $D^{(2,-1),(2,1)}_{(0,\frac{1}{2})(0,\frac{1}{2})}$, obtained from numerical conformal bootstrap has indeed a pole at $c = 1/2$ (see Figure 8 a) in [47]).
More generally in the random clusters Potts model, the smoothness of physical observables is ensured by a similar precise interplay between the analytic properties of both conformal blocks and structure constants.

1.7 CROSSING SYMMETRY

Crossing-symmetry is a consistency constraint on the four-point functions, which allow to determine the model-dependent data: the spectrum and the structure constants. It comes from assuming commutativity of fields:

$$V_{(\Delta_1)}(z_1)V_{(\Delta_2)}(z_2) = V_{(\Delta_2)}(z_2)V_{(\Delta_1)}(z_1). \tag{1.93}$$

Expression (1.63) for the four-point function, was derived by taking the OPE between fields $V_{(\Delta_1)}(z)$ and $V_{(\Delta_2)}(0)$, yielding the s-channel expansion $z \to 0$ of the four-point correlator. We could have instead chosen to let z approach 1 (resp.∞) by taking the OPE $V_{(\Delta_1)} \times V_{(\Delta_4)}$

(resp.$V_{(\Delta_1)} \times V_{(\Delta_3)}$), yielding the t- (resp. u-) channel expansions. For instance we could have written:

$$\langle V_{(\Delta_1)}(z,\bar{z})V_{(\Delta_2)}(0)V_{(\Delta_3)}(\infty)V_{(\Delta_4)}(1)\rangle = \sum_{(\Delta_t)\in S_t} D^{(\Delta_t)}_{(\Delta_1),(\Delta_4)} D^{(\Delta_3)}_{(\Delta_t),(\Delta_2)} \left|\mathcal{F}^{(t)}_{\Delta_t}(\Delta_i|1-z)\right|^2 , \quad (1.94)$$

with the four-point t-channel conformal block:

$$\mathcal{F}^{(t)}_{\Delta}(\Delta_i|1-z) = (1-z)^{-\Delta_1-\Delta_4+\Delta_t} \sum_{Y} (1-z)^{Y} \Gamma^{\Delta_3}_{\Delta_t,Y;\Delta_2} \sum_{\substack{Y' \\ |Y'|=Y}} H^{-1}_{Y,Y'}(\Delta_t)\, \Gamma^{\Delta_t,Y'}_{\Delta_1,\Delta_4}$$

$$= \quad (1.95)$$

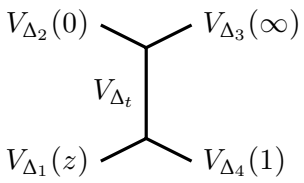

Note that the s-channel and t-channel spectra can be in general different.
Commutativity implies that we can equate the s-expansion (1.63) with the above t-expansion (1.94). It gives the following crossing-symmetry equation:

$$\sum_{(\Delta_s)\in S_s} D^{(\Delta_s)}_{(\Delta_1),(\Delta_2)} D^{(\Delta_3)}_{(\Delta_s),(\Delta_4)} \left|\mathcal{F}^{(s)}_{\Delta_s}(\Delta_i|z)\right|^2 = \sum_{(\Delta_t)\in S_t} D^{(\Delta_t)}_{(\Delta_1),(\Delta_4)} D^{(\Delta_3)}_{(\Delta_t),(\Delta_2)} \left|\mathcal{F}^{(t)}_{\Delta_t}(\Delta_i|1-z)\right|^2 . \quad (1.96)$$

This equation condenses all consistency and symmetry constraints: existence of an associative OPE and conformal block decomposition. It must be satisfied by any four-point function in a consistent theory. This restricts the allowed model-dependent data: a spectrum and a set of structure constants are consistent if they lead to crossing-symmetric four-point functions.
Exploitation of crossing-symmetry is especially powerful when applied to correlation functions which involve degenerate fields. In that case the fusion rules (1.57) impose that the spectra S_s and S_t contain finitely many terms. Such a bootstrap approach allowed for instance to determine analytically all structure constants of diagonal Liouville theory [64] and was applied more recently to non-diagonal Liouville [65, 66]. In the random cluster $Q-$Potts model a similar approach allowed to determine shift relations between some of the structure constants [47] (cf. Chapter 4).
When the sum in (1.96) contains a large (potentially infinite) number of terms, numerical bootstrap techniques allow to check crossing-symmetry of a given spectrum and to determine part of the set of structure constants.

2

CONFORMAL FIELD THEORY ON THE TORUS

In this Chapter we derive general formulas for the correlation functions of fields living on a torus topology, from a conformal bootstrap approach. In general, correlation functions on the torus are extremely complicated objects, for which exact expressions are known only in a few cases (for example Ising and Ashkin-Teller models [67–69]). However it is always possible to obtain a general expansion, similar to the s-channel expansion of the plane four-point function seen in Chapter 1.

We first derive the expressions of the conformal generators in Section 2.1. In Section 2.2 we define correalations on the torus. We derive the general expressions for the one-point function and the partition function in Sections 2.3 and 2.4. In Section 2.5 we derive the s-channel expansions of the two-, three- and four-point functions. Alhough they follow from standard CFT techniques, to our knowledge they do not appear in the literature. We therefore give here their derivation in full details.

2.1 CONFORMAL GENERATORS ON THE CYLINDER

Following [70], we express the Virasoro generators on the plane as the modes of the stress-energy tensor (1.28):

$$L_n^{(z)} = \frac{1}{2\pi i}\oint_{\mathcal{C}_z} dy\,(y-z)^{n+1}\,T(y), \quad n\in\mathbb{Z}. \tag{2.1}$$

The stress-tensor transforms under a general conformal map $z\mapsto f(z)$ according to equation (1.21):

$$T(y) = [f'(y)]^2\,T(f(y)) + \frac{c}{12}\{f,y\} = [f'(y)]^2\sum_{m\in\mathbb{Z}}\frac{L_m^{(f(z))}}{[f(y)-f(z)]^{m+2}} + \frac{c}{12}\{f,y\} \tag{2.2}$$

where $\{f,y\}$ is the Schwarzian derivative (1.22). Expanding $[f(y)-f(z)]^{-m-2}$ around $y\sim z$, and replacing in (1.28) we get:

$$\begin{aligned} L_n^{(z)} &= \frac{c}{12}\frac{1}{2\pi i}\oint_{\mathcal{C}_z} dy\,(y-z)^{n+1}\,\{f,y\} \\ &+ \frac{1}{2\pi i}\sum_m \frac{L_m^{(f(z))}}{[f'(z)]^{m+2}}\oint_{\mathcal{C}_z} dy\,\frac{[f'(y)]^2}{(y-z)^{-n+m+1}}\left(1+\sum_{l\geq 1}\frac{(-1)^l}{l!}\frac{(m+l+1)!}{(m+1)!}\left[\sum_{k\geq 2}\frac{f^{(k)}(z)}{k!f'(z)}(y-z)^{k-1}\right]^l\right). \end{aligned} \tag{2.3}$$

The second contour integral gives non-zero terms for $m=n,n+1,\cdots$. Collecting the residues from the different order poles in the sum, we get for the first values of m:

$$\begin{aligned} L_n^{(z)} &= \frac{c}{12}\frac{1}{2\pi i}\oint_{\mathcal{C}_z} dy\,(y-z)^{n+1}\,\{f,y\} + [f'(z)]^{-n}\,L_n^{(f(z))} + \frac{1-n}{2}\frac{f''(z)}{[f'(z)]^{n+2}}L_{n+1}^{(f(z))} \\ &+ [f'(z)]^{-n-4}\left(\frac{2-n}{6}f'''(z)f'(z) + \frac{n^2+n-4}{8}[f''(z)]^2\right)L_{n+2}^{(f(z))} + \cdots \end{aligned} \tag{2.4}$$

An explicit check is obtained using the transformation $f(y) = y^2$:

$$\begin{aligned}
&\frac{1}{2\pi i}\oint_{\mathcal{C}_z} dy\,(y-z)^{n+1}\,[f'(y)]^2 \sum_{m\in\mathbb{Z}} \frac{L_m^{(f(z))}}{[f(y)-f(z)]^{m+2}} \\
&= \frac{1}{2\pi i}\oint_{\mathcal{C}_z} dy\,(2y)^2(y-z)^{n+1} \sum_{m\in\mathbb{Z}} \frac{L_m^{(z^2)}}{[y^2-z^2]^{m+2}} \\
&= \frac{1}{2\pi i}\oint_{\mathcal{C}_z} dy\,(2y)^2 \left(\frac{L_n^{(z^2)}(y+z)^{-n-2}}{y-z} + \frac{L_{n+1}^{(z^2)}(y+z)^{-n-3}}{(y-z)^2} + \frac{L_{n+2}^{(z^2)}(y+z)^{-n-4}}{(y-z)^3} + \cdots \right) \\
&= \frac{1}{(2z)^n} L_n^{(z^2)} + \frac{1-n}{(2z)^{n+2}} L_{n+1}^{(z^2)} + \frac{n^2+n-4}{2} \frac{1}{(2z)^{n+4}} L_{n=2}^{(z^2)} + \cdots
\end{aligned} \tag{2.5}$$

We take now f to be the map:

$$z \mapsto w = -i\frac{N}{2\pi}\ln z \tag{2.6}$$

from the plane to a finite cylinder of length M and radius N, as pictured in Figure 2.1.

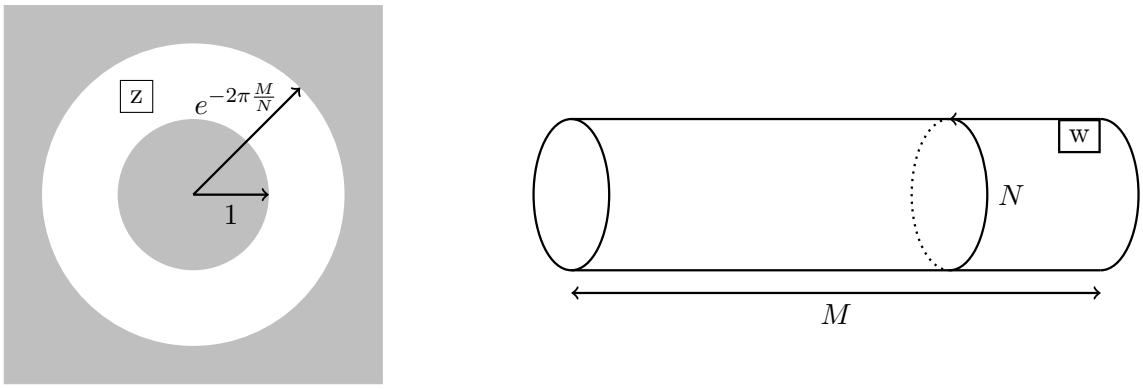

Figure 2.1: The coordinate z on an annulus is mapped to the coordinate w on the finite cylinder.

The Schwarzian is $\{f, z\} = \frac{1}{2z^2}$, and we obtain from (2.4) for finite $w = f(z)$:

$$L_0^{(z)} = L_0^{\mathcal{C},(w)} \tag{2.7a}$$

$$L_{-1}^{(z)} = z^{-1}\left(\frac{N}{2\pi i}\right)\left(L_{-1}^{\mathcal{C},(w)} - \frac{2\pi i}{N} L_0^{\mathcal{C},(w)}\right) \tag{2.7b}$$

$$L_{-2}^{(z)} = z^{-2}\left(\frac{N}{2\pi i}\right)^2\left(L_{-2}^{\mathcal{C},(w)} - \frac{3}{2}\frac{2\pi i}{N} L_{-1}^{\mathcal{C},(w)} + \frac{13}{12}\left(\frac{2\pi i}{N}\right)^2 L_0^{\mathcal{C},(w)} + \left(\frac{2\pi i}{N}\right)^2 \frac{c}{24}\right) \tag{2.7c}$$

$$\cdots$$

The modes with $L_n^{\mathcal{C},(w=\infty)}$, obtained from $L_n^{(z=0)}$ are instead related to contour integrals that are non-contractible on the cylinder. One finds for instance:

$$L_{-n}^{(0)} = L_{-n}^{\mathcal{C},(\infty)} + \frac{c}{24}\delta_{n,0}. \tag{2.8}$$

2.2 EXPECTATIONS ON THE TORUS

Consider now a statistical model with Hamiltonian H, defined on a $M \times N$ lattice with periodic boundary conditions in, say, the N direction. We can think of spin degrees of freedom $S_{i,j}$ living at each site of the lattice, so that each row is a state $|S_t\rangle = \{S_{t,0}, \cdots S_{t,N-1}\}$. This state is obtained from the state $|S_0\rangle$ by evolution with H over a distance –or time, t: $|S_t\rangle = e^{-tH}|S_0\rangle$. Such evolution on the cylinder corresponds, by conformal mapping to the plane, to radial evolution (cf. Figure 2.2) and so the Hamiltonian is given by the dilation operator (see eg. [56], Chapter 8):

$$H = L_0^{\mathcal{C},(\infty)} + \bar{L}_0^{\mathcal{C},(\infty)}. \tag{2.9}$$

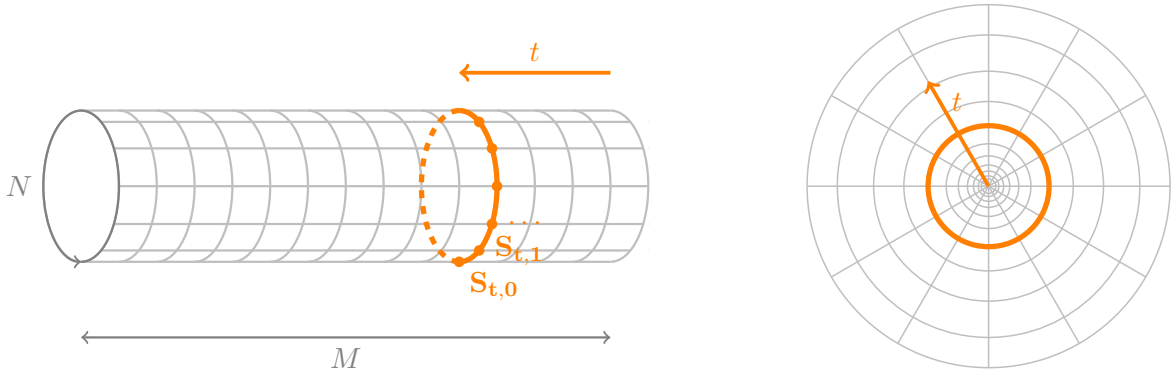

Figure 2.2: A state $|S_t\rangle$ propagating on the cylinder (left) and on the plane (right).

The partition function of the system on the cylinder is therefore:

$$Z = \sum_{|S_0\rangle,|S_M\rangle} \langle S_M| e^{-M\left(L_0^{\mathcal{C},(\infty)} + \bar{L}_0^{\mathcal{C},(\infty)}\right)} |S_0\rangle. \tag{2.10}$$

Imposing periodic boundary conditions also in the M direction: $|S_0\rangle = |S_M\rangle$ we get the partition function on a torus:

$$Z = \mathrm{tr}_S e^{-M\left(L_0^{\mathcal{C},(\infty)} + \bar{L}_0^{\mathcal{C},(\infty)}\right)} \tag{2.11}$$

where the trace is over the set of states, aka the spectrum S. Gluing the ends of the cylinder this way does not create the most general torus one can design: as shown in Figure 2.3 this torus corresponds to the case $\tau_1 = 0$ drawn in grey. A general torus would have complex modular parameter $\tau = \tau_1 + i\tau_2$. In addition we can use the modular transformations

$$\tau \mapsto \frac{a\tau + b}{c\tau + d}, \quad ad - bc = 1 \tag{2.12}$$

to get an equivalent torus with $\tau = \tau_1 + i\frac{M}{N}$. To create such a torus from the cylinder, we need to first translate the edges by τ_1 before gluing them together.
The translation operator on the cylinder is $L_0^{\mathcal{C}} - \bar{L}_0^{\mathcal{C}}$ (see again [56], 8.4), so that the partition function on the torus with modular parameter τ is:

$$Z = \mathrm{tr}_S e^{-2\pi\tau_2\left(L_0^{\mathcal{C},(\infty)} + \bar{L}_0^{\mathcal{C},(\infty)}\right)} e^{2\pi i\tau_1\left(L_0^{\mathcal{C},(\infty)} - \bar{L}_0^{\mathcal{C},(\infty)}\right)} = \mathrm{tr}_S q^{L_0^{\mathcal{C},(\infty)}} \bar{q}^{\bar{L}_0^{\mathcal{C},(\infty)}}, \tag{2.13}$$

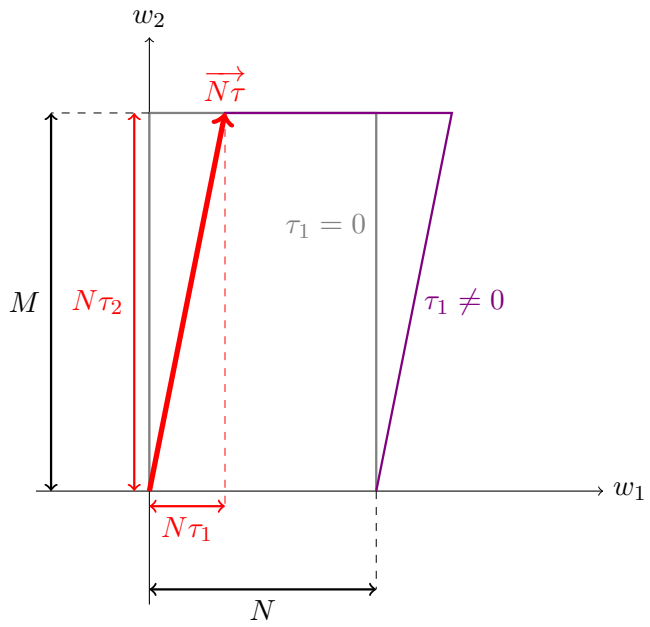

Figure 2.3: To make a torus of complex modular parameter τ we glue the edges of length M together to make a cylinder, and twist it by $N\tau_1$ before gluing its ends.

where we introduced the elliptic nome:

$$q = e^{2\pi i \tau}. \tag{2.14}$$

2.3 ONE-POINT FUNCTION

The one-point function of a field $V_{\Delta,\bar{\Delta}}$ corresponds to the trace (2.13) with a field insertion:

$$\langle V_{\Delta,\bar{\Delta}} \rangle_\tau = \frac{1}{Z_\tau} \mathrm{tr}_{S_{\mathrm{int}}} \left(q^{L_0^{\mathcal{C},\infty}} \bar{q}^{\bar{L}_0^{\mathcal{C},\infty}} V_{\Delta,\bar{\Delta}}(0) \right) \tag{2.15}$$

and is normalised by the partition function on the torus Z_τ (see next Section 2.4). By translation invariance, we can choose to insert the field at $w = 0$. This torus correlation function can be associated with diagram 2.4, where $S_{\mathrm{int}} \subseteq S$ is the set of representations which satisfy the fusion:

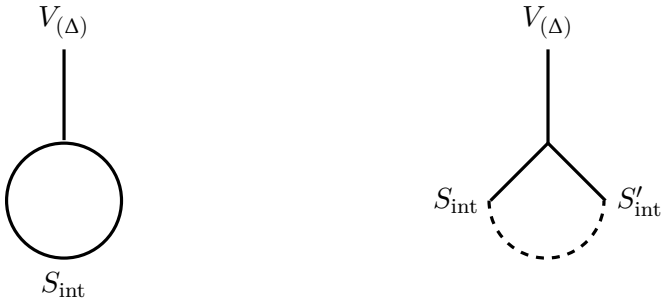

Figure 2.4: Diagrammatic representation of the torus one-point function.

$$\mathcal{R}_\Delta \times \mathcal{R}_{\mathrm{int}} \to \mathcal{R}_{\mathrm{int}} \tag{2.16}$$

pictured in Figure 2.4. We now map (2.15) to the plane using (2.6). The generators at infinity transform as (2.8):

$$\begin{aligned} L_0^{(\mathcal{C},\infty)} &= L_0^{(0)} - \frac{c}{24} \\ \bar{L}_0^{(\mathcal{C},\infty)} &= \bar{L}_0^{(0)} - \frac{c}{24}, \end{aligned} \tag{2.17}$$

while the field tranforms as (1.13):

$$V_{\Delta,\bar{\Delta}}(0) = i^{\Delta-\bar{\Delta}} \left(\frac{2\pi}{N}\right)^{\Delta+\bar{\Delta}} V_{\Delta,\bar{\Delta}}(1). \tag{2.18}$$

Considering for simplicity the one-point function of spinless fields, we get from (2.15) using (2.17) and (2.18):

$$\langle V_{\Delta,\bar{\Delta}} \rangle_\tau = \frac{1}{Z_\tau} \left(\frac{2\pi}{N}\right)^{\Delta+\bar{\Delta}} \mathrm{tr}_{S_{\mathrm{int}}} \left(q^{L_0^{(0)} - \frac{c}{24}} \bar{q}^{\bar{L}_0^{(0)} - \frac{c}{24}} V_{\Delta,\bar{\Delta}}(1) \right). \tag{2.19}$$

Performing the trace over the conformal families $\mathcal{R}_{\Delta_{\mathrm{int}}}$,

$$\begin{aligned} \langle V_{\Delta,\bar{\Delta}} \rangle_\tau &= \frac{1}{Z_\tau} \left(\frac{2\pi}{N}\right)^{\Delta+\bar{\Delta}} \sum_{(\Delta_{\mathrm{int}}, Y_{\mathrm{int}})} \langle V_{(\Delta_{\mathrm{int}}, Y_{\mathrm{int}})}(\infty) q^{L_0^{(0)} - \frac{c}{24}} q^{\bar{L}_0^{(0)} - \frac{c}{24}} V_{(\Delta)}(1) V_{(\Delta_{\mathrm{int}}, Y_{\mathrm{int}})}(0) \rangle \\ &= \frac{1}{Z_\tau} \left(\frac{2\pi}{N}\right)^{\Delta+\bar{\Delta}} \sum_{(\Delta_{\mathrm{int}})} q^{\Delta_{\mathrm{int}} - \frac{c}{24}} \bar{q}^{\bar{\Delta}_{\mathrm{int}} - \frac{c}{24}} \sum_{Y_{\mathrm{int}}, \bar{Y}_{\mathrm{int}}} D^{(\Delta_{\mathrm{int}}, Y_{\mathrm{int}})}_{(\Delta_{\mathrm{int}}, Y_{\mathrm{int}}),(\Delta)} q^{|Y_{\mathrm{int}}|} \bar{q}^{|\bar{Y}_{\mathrm{int}}|}, \end{aligned} \tag{2.20}$$

where we used the notation (0.3). The sum over $Y_{\mathrm{int}}, \bar{Y}_{\mathrm{int}}$ is the contribution of descendants, and can be wrapped up into the one-point conformal block on the torus:

$$\langle V_{\Delta,\bar{\Delta}} \rangle_\tau = \frac{1}{Z_\tau} \left(\frac{2\pi}{N}\right)^{\Delta+\bar{\Delta}} \sum_{(\Delta_{\mathrm{int}})} D^{(\Delta_{\mathrm{int}})}_{(\Delta_{\mathrm{int}}),(\Delta)} q^{\Delta_{\mathrm{int}} - \frac{c}{24}} \bar{q}^{\bar{\Delta}_{\mathrm{int}} - \frac{c}{24}} \left| \mathcal{F}^{(1)}_{\Delta_{\mathrm{int}}}(\Delta|q) \right|^2, \tag{2.21}$$

with:

$$\begin{aligned} \mathcal{F}^{(1)}_{\Delta_{\mathrm{int}}}(\Delta|q) &= \sum_{Y=0}^{\infty} q^Y \sum_{\substack{Y_L, Y_R \\ |Y_L|=|Y_R|=Y}} \Gamma^{\Delta_{\mathrm{int}}, Y_R}_{\Delta_{\mathrm{int}}, Y_L; \Delta} H^{-1}_{Y_L, Y_R}(\Delta_{\mathrm{int}}) \\ &= 1 + \frac{2\Delta_{\mathrm{int}} + \Delta(\Delta-1)}{2\Delta_{\mathrm{int}}} q + O(q^2). \end{aligned} \tag{2.22}$$

As for the four-point conformal block on the plane (1.65), there exist a recursion relation to compute efficiently one-point conformal blocks on the torus [71]:

$$\begin{aligned} \mathcal{F}^{(1)}_{\Delta_{\mathrm{int}}}(\Delta_{\mathrm{ext}}|q) &= \frac{q^{1/24}}{\eta} \left(1 + \sum_{N \geq 1} H^{(N)}_{\Delta_{\mathrm{int}}}(\Delta_{\mathrm{ext}}) q^N \right) \\ &= 1 + \left(1 + H^{(1)}_{\Delta_{\mathrm{int}}}(\Delta_{\mathrm{ext}})\right) q + \left(2 + H^{(1)}_{\Delta_{\mathrm{int}}}(\Delta_{\mathrm{ext}}) + H^{(2)}_{\Delta_{\mathrm{int}}}(\Delta_{\mathrm{ext}})\right) q^2 + \cdots \end{aligned} \tag{2.23}$$

with

$$H^{(N)}_{\Delta_{\mathrm{int}}}(\Delta_{\mathrm{ext}}) = \sum_{mn=1}^{N} \frac{R^{\mathbb{T}}_{m,n}(\Delta_{\mathrm{ext}})}{\Delta_{\mathrm{int}} - \Delta_{m,n}} H^{(N-mn)}_{\Delta_{m,-n}}(\Delta_{\mathrm{ext}}). \tag{2.24}$$

The coefficients $R^{\mathbb{T}}_{m,n}$ are given, in terms of the momenta (0.7a,0.8a), by:

$$R^{\mathbb{T}}_{m,n}(P_{\text{ext}}) = \frac{2P_{0,0}P_{m,n}}{\prod_{r=1-m}^{m}\prod_{s=1-n}^{n} 2P_{r,s}} \prod_{r\overset{2}{=}1-2m}^{2m-1} \prod_{s\overset{2}{=}1-2n}^{2n-1} (P_{\text{ext}} - P_{r,s})\,. \tag{2.25}$$

The recursion makes manifest that the one-point block has an analytic structure similar to the four-point block, with poles at degenerate values of the internal dimension, $\Delta_{\text{int}} = \Delta_{m,n}$. The combination of the fusion (2.16) with the one imposed by the degenerate channel (1.57) leads to:

$$\mathcal{R}_{P_{\text{int}}} \times \mathcal{R}_{P_{\text{ext}}} = \mathcal{R}_{m,n} \times \mathcal{R}_{P_{\text{ext}}} \to \mathcal{R}_{m,n}, \tag{2.26}$$

implying that the external field is degenerate, $P_{\text{ext}} = P_{k,l}$, $|k| = 1, 3, \cdots 2m-1$, $|l| = 1, 3, \cdots 2n-1$. It follows that the coefficient $R^{\mathbb{T}}_{m,n}(P_{k,l})$ vanishes. Writing:

$$\begin{aligned} P_{\text{ext}} &= P_{k,l} + \epsilon_{\text{ext}} \\ P_{\text{int}} &= P_{m,n} + \epsilon_{\text{int}}, \end{aligned} \tag{2.27}$$

the limit $(\epsilon_{\text{ext}}, \epsilon_{\text{int}}) \to (0,0)$ of

$$\frac{R^{\mathbb{T}}_{m,n}(P_{\text{ext}})}{\Delta_{\text{int}} - \Delta_{m,n}} \propto \frac{\epsilon_{\text{ext}}}{\epsilon_{\text{int}}} \tag{2.28}$$

depends on how the limit is reached. We will illustrate this point in Section 2.4, when dealing with the analogous formula for the partition function.

As an example, let us consider the one-point function of the energy field in the Ising model $\mathcal{M}_{4,3}$. The Ising spectrum consists of three degenerate fields:

$$\begin{aligned} &\text{Id} = V_{1,1}, \quad \varepsilon = V_{1,2} = V_{3,2} \\ &\sigma = V_{2,1} = V_{2,2} \end{aligned} \tag{2.29}$$

Therefore the fusion of the energy field with another degenerate field is dictated by the fusion of $\mathcal{R}_{1,2}$:

$$\mathcal{R}_{1,2} \times \mathcal{R}_{r,s} = \mathcal{R}_{r,s\pm1}. \tag{2.30}$$

The fields entering the internal channel of the energy one-point function should further satisfy the fusion (2.16). There is only one such field which is the spin σ, and we obtain:

$$\langle \varepsilon \rangle_\tau = \frac{1}{Z_\tau} \left(\frac{2\pi}{N}\right)^{2\Delta_\varepsilon} D^{\sigma}_{\sigma,\varepsilon}\, |q|^{2\Delta_\sigma - c/12} \left|\mathcal{F}_{\Delta_\varepsilon,\Delta_\sigma}(q)\right|^2 . \tag{2.31}$$

Using the expansion (2.22) of the conformal block as well as the values of dimensions, central charge and structure constant:

$$\begin{aligned} \Delta_\varepsilon &= \frac{1}{2}, & c &= \frac{1}{2}, \\ \Delta_\sigma &= \frac{1}{16}, & D^{\sigma}_{\sigma,\varepsilon} &= \frac{1}{2}, \end{aligned} \tag{2.32}$$

we obtain:

$$\langle\varepsilon\rangle_\tau = \frac{1}{N}\frac{\pi}{Z_\tau}\,|q|^{1/12}\left|1-q+O(q^2)\right|. \tag{2.33}$$

The exact expression on the torus with $N=1$ is given by the following expression [69] in terms of the Dedekind eta function (A.5):

$$\langle\varepsilon\rangle = \frac{\pi|\eta|^2}{Z} = \frac{\pi}{Z}\,|q|^{1/12}\left|(1-q)(1-q^2)\cdots\right|^2. \tag{2.34}$$

It matches the expansion (2.33) up to the factor of $1/N$, which comes from the transformation between a cylinder of length N and a cylinder of length 1:

$$\langle V_{(\Delta)}\rangle_{\tau_1+iM/N} = \frac{1}{N^{\Delta+\bar\Delta}}\langle V_{(\Delta)}\rangle_{\tau_1+iM} \equiv \frac{1}{N^{\Delta+\bar\Delta}}\langle V_{(\Delta)}\rangle. \tag{2.35}$$

Finally, let us consider the one-point functions of descendant fields, and in particular of level 1 and 2 descendants. Coming back to definition (2.15), and this time transforming both the field with (2.18) and the generator with (2.7b):

$$\langle L_{-1}^{\mathcal{C},(w=0)}V_{\Delta,\bar\Delta}\rangle_\tau = i^{\Delta-\bar\Delta+1}\left(\frac{2\pi}{N}\right)^{\Delta+\bar\Delta+1}\mathrm{tr}_{S_{\mathrm{int}}}\left\{q^{L_0^{(0)}-\frac{c}{24}}\bar q^{\bar L_0^{(0)}-\frac{c}{24}}\left(L_{-1}^{(z=1)}+L_0^{(z=1)}\right)V_{\Delta,\bar\Delta}(1)\right\}. \tag{2.36}$$

When computing the trace, we evaluate the Virasoro matrix elements (1.45) of $(L_{-1}+L_0)\,V_{\Delta,\bar\Delta}$. Using the recursions (1.46a) these evaluate to:

$$\langle V_{\Delta_{\mathrm{int}}}(\infty)\,(L_{-1}+L_0)\,V_{\Delta,\bar\Delta}(1)V_{\Delta_{\mathrm{int}}}(0)\rangle = 0. \tag{2.37}$$

Therefore, any one-point function of a level 1 descendant field vanishes on the torus.
At level 2, using (2.7c):

$$\begin{aligned}
&\langle L_{-2}^{\mathcal{C},(w=0)}V_{\Delta,\bar\Delta}\rangle_\tau \\
&= -\left(\frac{2\pi}{N}\right)^{\Delta+\bar\Delta+2}\mathrm{tr}_{S_{\mathrm{int}}}\left\{q^{L_0^{(0)}-\frac{c}{24}}\bar q^{\bar L_0^{(0)}-\frac{c}{24}}\left(L_{-2}^{(z=1)}-\frac{13}{12}L_0^{(z=1)}-\frac{c}{24}\right)V_{\Delta,\bar\Delta}(1)\right\} \\
&= \left(\frac{2\pi}{N}\right)^{\Delta+\bar\Delta+2}\sum_{(\Delta_{\mathrm{int}},Y_{\mathrm{int}})}\left(\frac{\Delta}{12}-\Delta_{\mathrm{int}}-|Y_{\mathrm{int}}|+\frac{c}{24}\right)D^{(\Delta_{\mathrm{int}},Y_{\mathrm{int}})}_{(\Delta_{\mathrm{int}},Y_{\mathrm{int}}),(\Delta)}q^{\Delta_{\mathrm{int}}+|Y_{\mathrm{int}}|-\frac{c}{24}}\bar q^{\bar\Delta_{\mathrm{int}}+|\bar Y_{\mathrm{int}}|-\frac{c}{24}}.
\end{aligned} \tag{2.38}$$

This expression will be useful to evaluate for instance the one-point function of an important level 2 descendant, the stress-energy tensor.

2.4 THE PARTITION FUNCTION ON THE TORUS

The partition function is the one-point function of the identity,

$$Z_\tau = \mathrm{tr}_S\left(q^{L_0^{\mathcal{C}}}\bar q^{\bar L_0^{\mathcal{C}}}\mathrm{Id}\right). \tag{2.39}$$

From the general expression (2.21), and using the normalisation of the identity structure constant (1.52), we can write it as:

$$Z_\tau = \sum_{(\Delta_{\text{int}})\in S} q^{\Delta_{\text{int}}-\frac{c}{24}}\bar{q}^{\bar{\Delta}_{\text{int}}-\frac{c}{24}}\left|\lim_{\Delta_{\text{ext}}\to 0}\mathcal{F}^{(1)}_{\Delta_{\text{int}}}(\Delta_{\text{ext}}|q)\right|^2. \tag{2.40}$$

If the representations $\mathcal{R}_{\text{int}}$ entering the sum are not degenerate, the matrix of inner products $H(\Delta_{\text{int}})$ appearing in the conformal block expansion (2.22) is invertible. We can then simply take the limit

$$\lim_{\Delta_{\text{ext}}\to 0}\Gamma^{\Delta_{\text{int}},Y_R}_{\Delta_{\text{int}},Y_L;\Delta_{\text{ext}}} = H_{Y_L,Y_R}(\Delta_{\text{int}}), \tag{2.41}$$

and the blocks assume the simple form:

$$\mathcal{F}^{(1)}_{\Delta_{\text{int}}}(\Delta_{\text{ext}}=0|q) = \sum_{Y=0}^{\infty} q^Y p(Y), \tag{2.42}$$

where $p(Y)$ is the number of partitions of the integer Y. This sum can be written in terms of the η function (A.5) :

$$\mathcal{F}^{(1)}_{\Delta_{\text{int}}}(\Delta_{\text{ext}}=0|q) = \sum_{n=1}^{\infty}\frac{1}{1-q^n} = \frac{q^{\frac{1}{24}}}{\eta(q)}. \tag{2.43}$$

Plugging in (2.40) we obtain the partition function of a free boson (see for intstance [22], Chapter 10):

$$Z_\tau = \frac{1}{|\eta(q)|}\sum_{(\Delta_{\text{int}})\in S} q^{\Delta_{\text{int}}}\bar{q}^{\bar{\Delta}_{\text{int}}}. \tag{2.44}$$

If there are degenerate representations $\mathcal{R}_{\text{int}} = \mathcal{R}_{m,n}$ in the spectrum, the block of the matrix $H(\Delta_{m,n})$ corresponding to level mn is non-invertible. The simplest example is a degenerate representation at level 1:

$$\begin{aligned}\Gamma^{\Delta_{\text{int}},\{1\}}_{\Delta_{\text{int}},\{1\};\Delta_{\text{ext}}} &= 2\Delta_{\text{int}} + \Delta_{\text{ext}}(\Delta_{\text{ext}}-1)\\ H^{-1}_{\{1\},\{1\}}(\Delta_{\text{int}}) &= \frac{1}{2\Delta_{\text{int}}}\end{aligned} \tag{2.45}$$

and the expansion of the conformal block (2.22) is:

$$\mathcal{F}^{(1)}_{\Delta_{\text{int}}}(\Delta_{\text{ext}}|q) = 1 + \frac{2\Delta_{\text{int}}+\Delta_{\text{ext}}(\Delta_{\text{ext}}-1)}{2\Delta_{\text{int}}}q + O(q^2). \tag{2.46}$$

The limit $\lim_{\Delta_{\text{ext}},\Delta_{\text{int}}\to 0}\mathcal{F}^{(1)}_{\Delta_{\text{int}}}(\Delta_{\text{ext}}|q)$ can be reached in different ways. Let us parametrise the conformal dimension using the momentum α, and use the regularisation parameters ϵ_{ext} and ϵ_{int}:

$$\alpha_{\text{ext}} = 2\epsilon_{\text{ext}} \tag{2.47a}$$

$$\alpha_{\text{int}} = \alpha_{1,1} + \epsilon_{\text{int}} = \epsilon_{\text{int}}. \tag{2.47b}$$

Then,

$$\frac{2\Delta_{\text{int}} + \Delta_{\text{ext}}(\Delta_{\text{ext}} - 1)}{2\Delta_{\text{int}}} = 1 - \frac{\epsilon_{\text{ext}} + O(\epsilon_{\text{ext}}^2)}{\epsilon_{\text{int}} + O(\epsilon_{\text{int}}^2)}. \tag{2.48}$$

The limit $(\epsilon_{\text{ext}}, \epsilon_{\text{int}}) \to (0,0)$ depends therefore on the way one reaches the point $(\epsilon_{\text{ext}}, \epsilon_{\text{int}}) = (0,0)$. If $\epsilon_{\text{ext}} > \epsilon_{\text{int}}$ we get back expression (2.44). Setting instead $\epsilon_{\text{ext}} = \epsilon_{\text{int}}$ one finds,

$$\begin{aligned} &\frac{2\Delta_{\text{int}} + \Delta_{\text{ext}}(\Delta_{\text{ext}} - 1)}{2\Delta_{\text{int}}} = 0 \\ &\mathcal{F}^{(1)}_{\Delta_{\text{ext}},\Delta_{\text{int}}}(q) = 1 + O(q^2). \end{aligned} \tag{2.49}$$

This corresponds to removing the null state at level 1. The general case $\alpha_{\text{int}} = \alpha_{m,n}$ is more easily worked out by using the recursion formula (2.23) of the conformal blocks. Using the same regularisation scheme

$$\alpha_{\text{ext}} = 2\epsilon_{\text{ext}} \tag{2.50a}$$

$$\alpha_{\text{int}} = \alpha_{(m,n)} + \epsilon_{\text{int}}, \tag{2.50b}$$

the residues (2.25) become:

$$R^{\mathbb{T}}_{m,n}(2\epsilon_{\text{ext}}) = \epsilon_{\text{ext}} \frac{\prod_{i=1-2m}^{2m-1} \prod_{j=1-2n}^{2n-1} \frac{i-1}{2} b + \frac{j-1}{2} b^{-1}}{\prod_{k=1-m}^{m} \prod_{l=1-n}^{n} (-kb - lb^{-1})} + O(\epsilon_{\text{ext}}^2), \quad (k,l) \neq (0,0), (m,n), \tag{2.51}$$

and relabelling indices leads to:

$$R^{\mathbb{T}}_{m,n}(2\epsilon_{\text{ext}}) = -\epsilon_{\text{ext}}(mb + \frac{n}{b}) + O(\epsilon_{\text{ext}}^2). \tag{2.52}$$

With

$$\Delta_{\text{int}} - \Delta_{m,n} = \epsilon_{\text{int}}(mb + \frac{n}{b}) + O(\epsilon_{\text{int}}^2), \tag{2.53}$$

we get:

$$\lim_{\substack{\epsilon \to 0 \\ \epsilon_{\text{int}} \to 0}} \frac{R^{\mathbb{T}}_{m,n}(2\epsilon_{\text{ext}})}{\Delta_{\text{int}} - \Delta_{m,n}} = \lim_{\substack{\epsilon \to 0 \\ \epsilon_{\text{int}} \to 0}} -\frac{\epsilon_{\text{ext}} + O(\epsilon_{\text{ext}}^2)}{\epsilon_{\text{int}} + O(\epsilon_{\text{int}}^2)} = -1, \tag{2.54}$$

if we set $\epsilon = \epsilon_{\text{int}}$. Again, this amounts to quotienting out the null representation $\mathcal{R}_{m,n}$, and the expansion of the conformal block becomes:

$$\mathcal{F}^{(1)}_{0,\Delta_{\text{int}}}(q) = 1 + \cdots + \Big(p(mn) - 1\Big) q^{mn} + \cdots + \Big(p(mn+N) - p(N)\Big) q^{mn+N} + \cdots \tag{2.55}$$

Similarly to the recursion representation for the four-point blocks of Section 1.5, the recursion formula (2.23) develops non-physical singularities at rational values of the central charge $c = c_{p,q}$ (0.6). The structure of these singularities and their cancellation is studied in Chapter 3.

2.4.1 *One-point function of the stress-energy tensor*

An important quantity is the expectation value of the stress-energy tensor. On the torus it is given by [70]:

$$\langle T\rangle_\tau = \frac{2\pi i}{N^2}\partial_\tau \log Z. \tag{2.56}$$

For example, the Ising partition function on the torus takes the form [69]:

$$Z = \frac{1}{2\,|\eta|}\sum_{\nu=2}^{4}|\theta_\nu(0|\tau)|\,, \tag{2.57}$$

in terms of the elliptic theta functions defined in Appendix A. Taking the derivative,

$$\langle T\rangle = \frac{1}{8\,|\eta|\,Z}\sum_{\nu=2}^{4}|\theta_\nu|\left(\frac{\theta_\nu''}{\theta_\nu}-\frac{1}{3}\frac{\theta_1'''}{\theta_1'}\right). \tag{2.58}$$

We will most often use (2.56) as an expansion in q:

$$\begin{aligned}\langle T\rangle_\tau &= \left(\frac{2\pi i}{N}\right)^2 q\partial_q \log Z \\ &= -\frac{1}{Z}\left(\frac{2\pi}{N}\right)^2\sum_{(\Delta_{\rm int},Y_{\rm int})}\left(\Delta_{\rm int}+|Y_{\rm int}|-\frac{c}{24}\right)D^{(\Delta_{\rm int},Y_{\rm int})}_{(\Delta_{\rm int},Y_{\rm int}),0}q^{\Delta_{\rm int}+|Y_{\rm int}|-\frac{c}{24}}\bar q^{\bar\Delta_{\rm int}+\left|\bar Y_{\rm int}\right|-\frac{c}{24}}.\end{aligned} \tag{2.59}$$

Note that this is expansion (2.38) which we derived in Section 2.3, since T is the level 2 descendant of the identity.
In the limit $\frac{M}{N}\to\infty$, ie in the limit $q\to 0$, the torus becomes a cylinder, and (5.28) becomes:

$$\langle T\rangle_{M/N\to\infty} = \langle T\rangle_{\mathcal{C}} = \frac{\pi^2 c}{6N^2}, \tag{2.60}$$

which can also be derived from the transformation of T under the map between the plane and the cylinder (2.6). The stress-energy tensor gives the variation of the Hamiltonian (see eg. [58], Chapter 11):

$$\delta H = \frac{1}{2\pi}\int_0^N dw_2\langle T\rangle_{\mathcal{C}} + \langle\bar T\rangle_{\mathcal{C}} = \frac{\pi\, c}{6N}. \tag{2.61}$$

This variation is compensated by a change in the free energy [58], so that the free energy density is:

$$E = -\frac{\pi c}{6N}\overset{N=2\pi}{=\!=} -\frac{c}{12}. \tag{2.62}$$

When $c=1$ this is the famous Casimir energy of a free boson on a circle.

2.5 HIGHER POINT FUNCTIONS ON THE TORUS

We derived the general expression (2.20) of the torus one-point function in the preceding section. In this section we derive the expression of the two, three and four point-functions on the torus. We will see that the terms induced by the torus topology are determined by the structure of the CFT, namely the fusion rules and structure constants. These are the expressions which will be applied in Part II to the study of percolation models.

2.5.1 *Two-point function*

Similarly to the zero- and one-point functions, the two-point function on the torus is defined as the trace over the spectrum with field insertions:

$$\langle V_{(\Delta_1)}(w_1,\bar{w}_1)V_{(\Delta_2)}(w_2,\bar{w}_2)\rangle_\tau = \frac{1}{Z}\mathrm{tr}_S\left(q^{L_0^{\mathcal{C},\infty}}\bar{q}^{\bar{L}_0^{\mathcal{C},\infty}}V_{(\Delta_1)}(w_1,\bar{w}_1)V_{(\Delta_2)}(w_2,\bar{w}_2\right). \tag{2.63}$$

When the insertion points get close, ie $w_1 \to w_2$, we can insert the OPE (1.47) of the two fields in the expression above, giving the s-channel expansion of the two-point function:

$$\begin{aligned}\langle V_{(\Delta_1)}(w_1,\bar{w}_1)V_{(\Delta_2)}(w_2,\bar{w}_2)\rangle_\tau = \sum_{(\Delta_{\mathrm{top}},Y_{\mathrm{top}})\in S} D^{(\Delta_3,Y_3)}_{(\Delta_1),(\Delta_2)} w_{12}^{\Delta_3+|Y_3|-\Delta_1-\Delta_2}\bar{w}_{12}^{\bar{\Delta}_3+|\bar{Y}_3|-\bar{\Delta}_1-\bar{\Delta}_2} \\ \times \mathrm{tr}_S\left(q^{L_0^{\mathcal{C},\infty}}\bar{q}^{\bar{L}_0^{\mathcal{C},\infty}}V_{(\Delta_{\mathrm{top}},Y_{\mathrm{top}})}(w_2,\bar{w}_2)\right).\end{aligned} \tag{2.64}$$

The trace gives the one-point function (2.15) on a torus of length N. We find convenient to express the two- (and higher) point functions in terms of the one-point functions on a torus of length $N=1$:

$$\langle V_{(\Delta)}\rangle_{\tau_1+iM/N} = \frac{1}{N^{\Delta+\bar{\Delta}}}\langle V_{(\Delta)}\rangle_{\tau_1+iM} \equiv \frac{1}{N^{\Delta+\bar{\Delta}}}\langle V_{(\Delta)}\rangle. \tag{2.65}$$

This makes explicit the plane limit and the $\frac{w_{12}}{N}$ topological corrections of the two-point function:

$$\begin{aligned}&\langle V_{(\Delta_1)}(w_1,\bar{w}_1)V_{(\Delta_2)}(w_2,\bar{w}_2)\rangle_\tau \\ &= \frac{1}{w_{12}^{\Delta_1+\Delta_2}\bar{w}_{12}^{\bar{\Delta}_1+\bar{\Delta}_2}}\sum_{(\Delta_{\mathrm{top}},Y_{\mathrm{top}})} D^{(\Delta_{\mathrm{top}},Y_{\mathrm{top}})}_{(\Delta_1),(\Delta_2)}\left(\frac{w_{12}}{N}\right)^{\Delta_{\mathrm{top}}+|Y_{\mathrm{top}}|}\left(\frac{\bar{w}_{12}}{N}\right)^{\bar{\Delta}_{\mathrm{top}}+|\bar{Y}_{\mathrm{top}}|}\langle V_{(\Delta_{\mathrm{top}},Y_{\mathrm{top}})}\rangle \\ &= \frac{1}{w_{12}^{\Delta_1+\Delta_2}\bar{w}_{12}^{\bar{\Delta}_1+\bar{\Delta}_2}}\left[\delta_{(\Delta_1),(\Delta_2)} + f^{(2)}_\tau\left(\frac{w_{12}}{N}\right)\right]\end{aligned} \tag{2.66}$$

where we defined the function $f^{(2)}_\tau$ which accounts for the torus expansion:

$$f^{(2)}_\tau = \sum_{(\Delta_{\mathrm{top}},Y_{\mathrm{top}})} a^{(2)}_{(\Delta_{\mathrm{top}},Y_{\mathrm{top}})}(\tau)\left(\frac{w_{12}}{N}\right)^{\Delta_{\mathrm{top}}+Y_{\mathrm{top}}}\left(\frac{\bar{w}_{12}}{N}\right)^{\bar{\Delta}_{\mathrm{top}}+\bar{Y}_{\mathrm{top}}}, \tag{2.67}$$

with

$$a^{(2)}_{(\Delta,Y)}(\tau) = D^{(\Delta,Y)}_{(\Delta_1),(\Delta_2)}\langle V_{(\Delta,Y)}\rangle. \tag{2.68}$$

Expansion (2.66) can be represented diagramatically as in Figure 2.5.

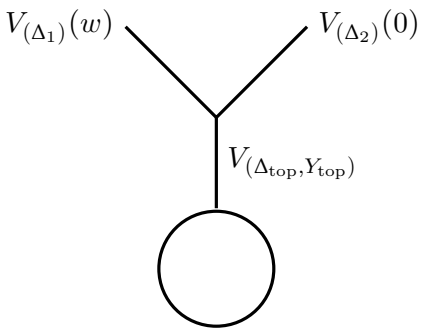

Figure 2.5: Diagrammatic representation of the torus two-point function.

Remark that on the plane the expansion (2.66) reduces to the simple power-law decay (1.58). This is due to the fact that all one-point functions (but the identity) vanish on the plane. But on the torus, two-point functions contain, similarly to four-point functions on the plane, information on the fusion of fields through their dependence on the structure constants. Note also that, although the two-point function of two different fields is zero on the plane, it might be non-zero on the torus, with $\frac{w_{12}}{N}$ terms coming from the contributions of the fields in their fusion which are different from the identity.

As an explicit example, let us consider the two-point function of the Ising spin fields (2.29). Their fusion rule is:

$$\mathcal{V}_{(2,1)} \times \mathcal{V}_{(2,1)} = \mathcal{V}_{(1,1)} + \mathcal{V}_{(3,1)}, \tag{2.69}$$

and therefore the two channels in the expansion (2.66) are the identity and the energy field. The contribution of each primary and its descendants give:

$$\begin{aligned}\langle\sigma(w)\sigma(0)\rangle_\tau = |w|^{-4\Delta_\sigma} \Bigg(\left[1 + D^{(0,\{2\})}_{\sigma,\sigma} \left(\left(\frac{w}{N}\right)^2 \langle T\rangle + \left(\frac{\bar{w}}{N}\right)^2 \langle \bar{T}\rangle \right) + O\left(\frac{w^4}{N^4}\right)\right] \\ + D^{\varepsilon}_{\sigma,\sigma} \left|\frac{w}{N}\right|^{2\Delta_\varepsilon} \left[\langle\varepsilon\rangle + O\left(\frac{w^{2\Delta_\varepsilon+4}}{N^{2\Delta_\varepsilon+4}}\right)\right] \Bigg)\end{aligned} \tag{2.70}$$

where we took into account that the one-point functions of total derivatives vanish (see (2.36) and (2.37)), and that the energy is degenerate at level 2 (2.38). From (1.50) and using relations (1.46a) one finds that $D^{(0,\{2\})}_{\sigma,\sigma} = \frac{2\Delta_\sigma}{c}$. With the dimensions (2.32) of the Ising model,

$$\langle\sigma(w)\sigma(0)\rangle_\tau = |w|^{-1/4} \left(1 + \frac{1}{2}\left|\frac{w}{N}\right| \langle\varepsilon\rangle + \frac{1}{4}\left(\left(\frac{w}{N}\right)^2 \langle T\rangle + \left(\frac{\bar{w}}{N}\right)^2 \langle \bar{T}\rangle\right) + O\left(\frac{w^4}{N^4}\right)\right). \tag{2.71}$$

The exact two-point function is [68, 69]:

$$\langle\sigma(w)\sigma(0)\rangle = \frac{1}{2|\eta|Z} \frac{[\theta_1'(0)|^{1/4}}{|\theta_1(w)|^{1/4}} \sum_{i=1}^{4} |\theta_i\left(\frac{w}{2}\right)|. \tag{2.72}$$

Expanding around $w \sim 0$, and using the identity (A.8):

$$\begin{aligned}\langle\sigma(w)\sigma(0)\rangle = |w|^{-1/4}\Bigg\{1 + \frac{1}{2}\frac{\pi\,|\eta|^2}{Z}\,|w| \\ + \frac{1}{4}\frac{1}{8\,|\eta|\,Z}\sum_{\nu=2}^{4}|\theta_\nu|\left[\left(\frac{\theta_\nu''}{\theta_\nu} - \frac{1}{3}\frac{\theta_1'''}{\theta_1'}\right)w^2 + \left(\frac{\bar\theta_\nu''}{\bar\theta_\nu} - \frac{1}{3}\frac{\bar\theta_1'''}{\bar\theta_1'}\right)\bar w^2\right] + O(w^4)\Bigg\}.\end{aligned} \tag{2.73}$$

The terms of order w and w^2 are respectively the contributions of the energy and the stress-energy tensor. With their one-point functions given by (2.33) and (2.58), we recover expansion (2.71) [1].

2.5.2 *Three-point function*

The derivation of the $s-$channel expansion of the three-point function $\langle V_{(\Delta_1)}(w_1)V_{(\Delta_2)}(w_2)V_{(\Delta_3)}(w_3)\rangle_\tau$ of spin-less fields[2] follows what we did in the previous section for the two-point function. Inserting the OPE $V_{(\Delta_1)}(w_1)V_{(\Delta_2)}(w_2)$:

$$\frac{\langle V_{(\Delta_1)}(w_1)V_{(\Delta_2)}(w_2)V_{(\Delta_3)}(w_3)\rangle_\tau}{|w_{12}|^{-2\Delta_1-2\Delta_2}} = \sum_{\substack{(\Delta_L)\in S\\ Y_L,\bar Y_L}} D^{(\Delta_L,Y_L)}_{(\Delta_1),(\Delta_2)}\, w_{12}^{\Delta_L+|Y_L|}\,\bar w_{12}^{\bar\Delta_L+|\bar Y_L|}\left\langle V_{(\Delta_L,Y_L)}(w_2)V_{(\Delta_3)}(w_3)\right\rangle_\tau . \tag{2.74}$$

The plane limit corresponds to the internal channel $V_{(\Delta_L)} = V_{(\Delta_3)}$ as shown in diagram 2.6a, while the topological corrections are associated to diagram 2.6b. Inserting the expansion (2.66)

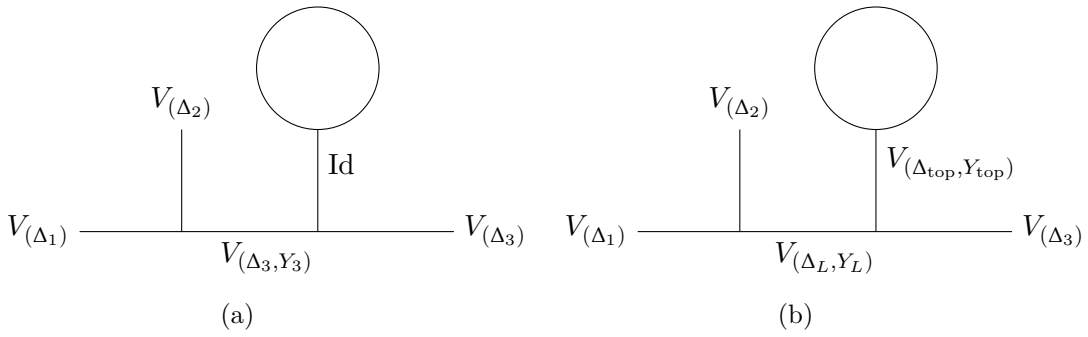

Figure 2.6: Diagrammatic representations of the plane limit (a) and the topological corrections (b) of the torus three-point function.

1 up to the powers of N: (2.72) is the two-point function on a torus of length 1. Transforming the coordinate: $w' = Nw$, and the field σ using (2.35), we find exactly (2.71).

2 for simplicity of notation we derive the result for spin-less fields; it is straightforward to extend it to fields with spin.

of the two-point $\left\langle V_{(\Delta_L,Y_L)}(w_2)V_{(\Delta_3)}(w_3)\right\rangle_\tau$ we get:

$$\begin{aligned}\frac{\langle V_{(\Delta_1)}(w_1)V_{(\Delta_2)}(w_2)V_{(\Delta_3)}(w_3)\rangle_\tau}{|w_{12}|^{-2\Delta_1-2\Delta_2}\,|w_{23}|^{-2\Delta_3}} &= \sum_{\substack{(\Delta_L)\in S\\ Y_L,\bar{Y}_L}} D^{(\Delta_L,Y_L)}_{(\Delta_1),(\Delta_2)}\left(\frac{w_{12}}{w_{23}}\right)^{\Delta_L+|Y_L|}\left(\frac{\bar{w}_{12}}{\bar{w}_{23}}\right)^{\bar{\Delta}_L+|\bar{Y}_L|}\\ &\quad\times\sum_{(\Delta),Y,\bar{Y}} D^{(\Delta,Y)}_{(\Delta_L,Y_L),(\Delta_3)}\left(\frac{w_{23}}{N}\right)^{\Delta+|Y|}\left(\frac{\bar{w}_{23}}{N}\right)^{\bar{\Delta}+|\bar{Y}|}\langle V_{(\Delta,Y)}\rangle.\end{aligned} \tag{2.75}$$

We can separate explicitely the plane limit:

$$\begin{aligned}\frac{\langle V_{(\Delta_1)}(w_1)V_{(\Delta_2)}(w_2)V_{(\Delta_3)}(w_3)\rangle_\tau}{|w_{12}|^{-2\Delta_1-2\Delta_2}\,|w_{23}|^{-2\Delta_3}} &= \left|\frac{w_{12}}{w_{23}}\right|^{2\Delta_3}\sum_{Y_3} D^{(\Delta_3,Y_3)}_{(\Delta_1),(\Delta_2)}D^{(0)}_{(\Delta_3,Y_3),(\Delta_3)}\left(\frac{w_{12}}{w_{23}}\right)^{|Y_3|}\left(\frac{\bar{w}_{12}}{\bar{w}_{23}}\right)^{|\bar{Y}_3|}\\ &\quad+f^{(3)}_\tau\left(\frac{w_{12}}{w_{23}},\frac{w_{23}}{N}\right),\end{aligned} \tag{2.76}$$

with the function $f^{(3)}_\tau$ accounting for the topological corrections:

$$f^{(3)}_\tau\left(\frac{w_{12}}{w_{23}},\frac{w_{23}}{N}\right)=\sum_{(\Delta_{\text{top}},Y_{\text{top}})} a^{(3)}_{(\Delta_{\text{top}},Y_{\text{top}})}\left(\frac{w_{12}}{w_{23}};\tau\right)\left(\frac{w_{23}}{N}\right)^{\Delta_{\text{top}}+|Y_{\text{top}}|}\left(\frac{\bar{w}_{23}}{N}\right)^{\bar{\Delta}_{\text{top}}+|\bar{Y}_{\text{top}}|}, \tag{2.77}$$

where we define:

$$\begin{aligned}a^{(3)}_{(\Delta_{\text{top}})}\left(\frac{w_{12}}{w_{23}}\middle|\tau\right) &= \langle V_{(\Delta_{\text{top}})}\rangle\sum_{(\Delta_L,Y_L)} D^{(\Delta_L,Y_L)}_{(\Delta_1),(\Delta_2)}D^{(\Delta_{\text{top}})}_{(\Delta_L,Y_L),(\Delta_3)}\left(\frac{w_{12}}{w_{23}}\right)^{\Delta_L+|Y_L|}\left(\frac{\bar{w}_{12}}{\bar{w}_{23}}\right)^{\bar{\Delta}_L+|\bar{Y}_L|}\\ &= \langle V_{(\Delta_{\text{top}})}\rangle\sum_{(\Delta_L)} D^{(\Delta_L)}_{(\Delta_1),(\Delta_2)}D^{(\Delta_{\text{top}})}_{(\Delta_L),(\Delta_3)}\left(\frac{w_{12}}{w_{23}}\right)^{\Delta_L}\left(\frac{\bar{w}_{12}}{\bar{w}_{23}}\right)^{\bar{\Delta}_L}\left|\mathcal{F}^{(3)}_{\Delta_L}\left(\Delta_i\middle|\frac{w_{12}}{w_{23}}\right)\right|^2.\end{aligned} \tag{2.78}$$

For convenience we defined the three-point conformal block:

$$\mathcal{F}^{(3)}_{\Delta_L}\left(\Delta_i\middle|\frac{w_{12}}{w_{23}}\right)=\sum_{Y_L}\left(\frac{w_{12}}{w_{23}}\right)^{|Y_L|}\Gamma^{\Delta_{\text{top}}}_{\Delta_L,Y_L;\Delta_3}\sum_{\substack{Y\\ |Y|=|Y_L|}} H^{-1}_{Y,Y_L}(\Delta_L)\,\Gamma^{\Delta_L,Y}_{\Delta_1,\Delta_2}. \tag{2.79}$$

By definition the function $f^{(3)}_\tau$ vanishes in the limit $\frac{w_{23}}{N}\to 0$, which is the plane limit regime. Note that, contrary to the two-point analog $f^{(2)}_\tau$, the three-point topological function depends on the ratio $\frac{w_{12}}{w_{23}}$ which encodes the geometry of the fields insertion points.
The first sum in (2.76) adds up to:

$$\begin{aligned}&\frac{1}{D^{(\Delta_3)}_{(\Delta_1),(\Delta_2)}}\sum_{Y_3} D^{(\Delta_3,Y_3)}_{(\Delta_1),(\Delta_2)}D^{(0)}_{(\Delta_3,Y_3),(\Delta_3)}\left(\frac{w_{12}}{w_{23}}\right)^{|Y_3|}\left(\frac{\bar{w}_{12}}{\bar{w}_{23}}\right)^{|\bar{Y}_3|}\\ &=\left|1+\beta^{(\Delta_3,\{-1\})}_{\Delta_1,\Delta_2}\beta^0_{(\Delta_3,\{-1\}),\Delta_3}\frac{w_{12}}{w_{23}}+\left(\beta^{(\Delta_3,\{-1,-1\})}_{\Delta_1,\Delta_2}\beta^0_{(\Delta_3,\{-1,-1\}),\Delta_3}+\beta^{(\Delta_3,\{-2\})}_{\Delta_1,\Delta_2}\beta^0_{(\Delta_3,\{-2\}),\Delta_3}\right)\frac{w_{12}^2}{w_{23}^2}+\cdots\right|^2\\ &=\left|1-(\Delta_1-\Delta_2+\Delta_3)\frac{w_{12}}{w_{23}}+\frac{1}{2}(\Delta_1-\Delta_2+\Delta_3)(1+\Delta_1-\Delta_2+\Delta_3)\frac{w_{12}^2}{w_{23}^2}+\cdots\right|^2\\ &=\left|1+\frac{w_{12}}{w_{23}}\right|^{-2\Delta_1+2\Delta_2-2\Delta_3}=\left|\frac{w_{23}}{w_{13}}\right|^{2\Delta_1-2\Delta_2+2\Delta_3}\end{aligned}$$

where the beta coefficients are (cf. Section 1.3):

$$\beta^{\Delta_3,Y_3}_{\Delta_1,Y_1;\Delta_2,Y_2} = \sum_{|Y|=|Y_3|} H^{-1}_{Y,Y_3}(\Delta_3)\Gamma^{\Delta_3,Y}_{\Delta_1,Y_1;\Delta_2,Y_2} \tag{2.80}$$

and are computed using the relations (1.46a). Finally,

$$\begin{aligned}&\langle V_{(\Delta_1)}(w_1)V_{(\Delta_2)}(w_2)V_{(\Delta_3)}(w_3)\rangle \\ &= \frac{D^{(\Delta_3)}_{(\Delta_1),(\Delta_2)}}{|w_{12}|^{2\Delta_1+2\Delta_2-2\Delta_3}\,|w_{23}|^{-2\Delta_1+2\Delta_2+2\Delta_3}\,|w_{13}|^{2\Delta_1-2\Delta_2+2\Delta_3}} + \frac{f^{(3)}_\tau\left(\frac{w_{12}}{w_{23}},\frac{w_{23}}{N}\right)}{|w_{12}|^{2\Delta_1+2\Delta_2}\,|w_{23}|^{2\Delta_3}}.\end{aligned} \tag{2.81}$$

2.5.3 *Four-point function*

The $s-$channel expansion of the four-point function $\langle V_{(\Delta_1)}(w_1)V_{(\Delta_2)}(w_2)V_{(\Delta_3)}(w_3)V_{(\Delta_4)}(w_4)\rangle_\tau$ of four (primary, spin-less) fields is derived by inserting the OPEs of $V_{(\Delta_1)}(w_1)V_{(\Delta_2)}(w_2)$ and $V_{(\Delta_3)}(w_3)V_{(\Delta_4)}(w_4)$:

$$\begin{aligned}&\frac{\langle V_{(\Delta_1)}(w_1)V_{(\Delta_2)}(w_2)V_{(\Delta_3)}(w_3)V_{(\Delta_4)}(w_4)\rangle_\tau}{|w_{12}|^{-2\Delta_1-2\Delta_2}\,|w_{34}|^{-2\Delta_3-2\Delta_4}} = \langle \sum_{(\Delta_L,Y_L)} D^{(\Delta_L,Y_L)}_{(\Delta_1),(\Delta_2)} w_{12}^{\Delta_L+|Y_L|}\bar{w}_{12}^{\bar{\Delta}_L+|\bar{Y}_L|}V_{(\Delta_L,Y_L)}(w_2) \\ &\times \sum_{(\Delta_R,Y_R)} D^{(\Delta_R,Y_R)}_{(\Delta_3),(\Delta_4)} w_{34}^{\Delta_R+|Y_R|}\bar{w}_{34}^{\bar{\Delta}_R+|\bar{Y}_R|}V_{(\Delta_R,Y_R)}(w_4)\rangle_\tau.\end{aligned} \tag{2.82}$$

Inserting the expansion (2.66) of $\langle V_{(\Delta_L,Y_L)}(w_2)V_{(\Delta_R,Y_R)}(w_4)\rangle_\tau$,

$$\begin{aligned}&\frac{\langle V_{(\Delta_1)}(w_1)V_{(\Delta_2)}(w_2)V_{(\Delta_3)}(w_3)V_{(\Delta_4)}(w_4)\rangle_\tau}{|w_{12}|^{-2\Delta_1-2\Delta_2}\,|w_{34}|^{-2\Delta_3-2\Delta_4}} \\ &= \sum_{\substack{(\Delta_L,Y_L)\\(\Delta_R,Y_R)}} D^{(\Delta_L,Y_L)}_{(\Delta_1),(\Delta_2)} D^{(\Delta_R,Y_R)}_{(\Delta_3),(\Delta_4)} \left(\frac{w_{12}}{w_{24}}\right)^{\Delta_L+|Y_L|}\left(\frac{\bar{w}_{12}}{\bar{w}_{24}}\right)^{\bar{\Delta}_L+|\bar{Y}_L|}\left(\frac{w_{34}}{w_{24}}\right)^{\Delta_R+|Y_R|}\left(\frac{\bar{w}_{34}}{\bar{w}_{24}}\right)^{\bar{\Delta}_R+|\bar{Y}_R|} \\ &\sum_{(\Delta_{\text{top}},Y_{\text{top}})} D^{(\Delta_{\text{top}},Y_{\text{top}})}_{(\Delta_L,Y_L),(\Delta_R,Y_R)} \left(\frac{w_{24}}{N}\right)^{\Delta_{\text{top}}+|Y_{\text{top}}|}\left(\frac{\bar{w}_{24}}{N}\right)^{\bar{\Delta}_{\text{top}}+|\bar{Y}_{\text{top}}|}\langle V_{(\Delta_{\text{top}},Y_{\text{top}})}\rangle.\end{aligned} \tag{2.83}$$

The plane limit P_0 is given by the terms with $\Delta_{\text{top}} = 0$ and $\Delta_L = \Delta_R$, corresponding to diagrams 2.7a. It can be written as a function of the cross-ratio (1.62) z:

$$\begin{aligned}P_0(z) &= \sum_{(\Delta,Y)} D^{(\Delta,Y)}_{(\Delta_1),(\Delta_2)} D^{(\Delta,Y)}_{(\Delta_3),(\Delta_4)} \left(\frac{w_{12}w_{34}}{w_{24}^2}\right)^{\Delta+|Y|}\left(\frac{\bar{w}_{12}\bar{w}_{34}}{\bar{w}_{24}^2}\right)^{\bar{\Delta}+|\bar{Y}|} \\ &= \sum_{(\Delta)} D^{(\Delta)}_{(\Delta_1),(\Delta_2)} D^{(\Delta)}_{(\Delta_3),(\Delta_4)} \left|\mathcal{F}^{(4)}_{(\Delta)}(\Delta_i|z)\right|^2,\end{aligned} \tag{2.84}$$

where $\mathcal{F}^{(4)}_{(\Delta)}(\Delta_i|z)$ is the $s-$ channel four-point conformal block (1.65). We obtain:

$$\begin{aligned}&\langle V_{(\Delta_1)}(w_1)V_{(\Delta_2)}(w_2)V_{(\Delta_3)}(w_3)V_{(\Delta_4)}(w_4)\rangle_\tau \\ &= \frac{1}{|w_{12}|^{2\Delta_1+2\Delta_2}\,|w_{34}|^{2\Delta_3+2\Delta_4}}\left[P_0(z) + f^{(4)}_\tau\left(\frac{w_{12}}{w_{24}},\frac{w_{34}}{w_{24}},\frac{w_{24}}{N}\right)\right],\end{aligned} \tag{2.85}$$

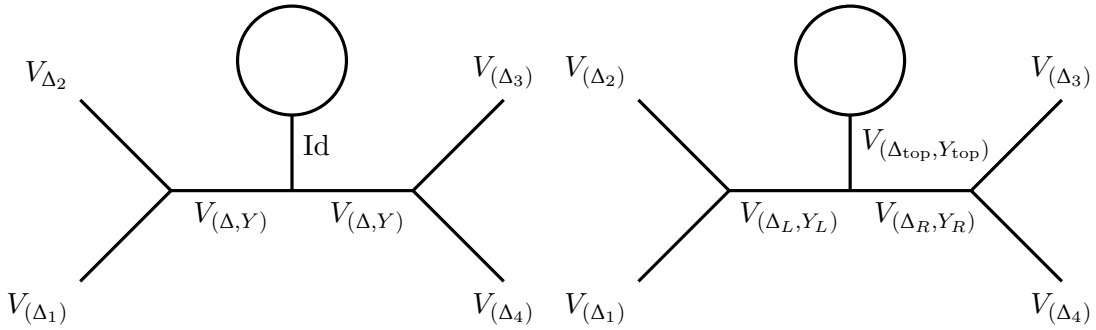

(a) Diagrammatic representation of the plane limit of the torus four-point function.

(b) Diagrammatic representation of the torus corrections.

where we define:

$$f_\tau^{(4)}\left(\frac{w_{12}}{w_{24}},\frac{w_{34}}{w_{24}},\frac{w_{24}}{N}\right)=\sum_{(\Delta_{\text{top}},Y_{\text{top}})}a^{(4)}_{(\Delta_{\text{top}},Y_{\text{top}})}\left(\frac{w_{12}}{w_{24}},\frac{w_{34}}{w_{24}};\tau\right)\left(\frac{w_{24}}{N}\right)^{\Delta_{\text{top}}+|Y_{\text{top}}|}\left(\frac{\bar{w}_{24}}{N}\right)^{\bar{\Delta}_{\text{top}}+|\bar{Y}_{\text{top}}|}. \tag{2.86}$$

$f_\tau^{(4)}$ accounts for the topological corrections represented by diagrams 2.7b, with:

$$\begin{aligned}a^{(4)}_{(\Delta,Y)}\left(\frac{w_{12}}{w_{24}},\frac{w_{34}}{w_{24}};\tau\right)=\langle V_{(\Delta,Y)}\rangle\sum_{\substack{(\Delta_L,Y_L),\\(\Delta_R,Y_R)}}&D^{(\Delta_L,Y_L)}_{(\Delta_1),(\Delta_2)}D^{(\Delta_R,Y_R)}_{(\Delta_3),(\Delta_4)}D^{(\Delta,Y)}_{(\Delta_L,Y_L),(\Delta_R,Y_R)}\\&\times\left(\frac{w_{12}}{w_{24}}\right)^{\Delta_L+|Y_L|}\left(\frac{\bar{w}_{12}}{\bar{w_{24}}}\right)^{\bar{\Delta}_L+|\bar{Y}_L|}\left(\frac{w_{34}}{w_{24}}\right)^{\Delta_R+|Y_R|}\left(\frac{\bar{w}_{34}}{\bar{w}_{24}}\right)^{\bar{\Delta}_R+|\bar{Y}_R|}.\end{aligned} \tag{2.87}$$

Note that it depends on the two geometric ratios $\frac{w_{12}}{w_{24}}$ and $\frac{w_{34}}{w_{24}}$.

3

ANALYTIC STRUCTURE OF THE RECURSION REPRESENTATION OF CONFORMAL BLOCKS

In Section 1.5 we introduced the recursion representation of the four-point conformal blocks. We discussed the poles of the block, seen as a function of the internal dimension Δ or of the central charge:

- "physical" poles when $\Delta = \Delta_{m,n}$. These poles are also present in the level-by-level representation (1.65), they reflect the structure of the Virasoro representations. The block is well-defined if V_Δ is degenerate, namely if the external dimensions satisfy the corresponding fusion rule.
- "unphysical poles" for values of the central charge corresponding to $b^2 \in \mathbb{Q}$ and for any value of Δ: they come from resonances of the dimensions $\Delta_{m,-n} = \Delta_{r,s}$. They do not appear in the level-by-level expansion (1.65) and are observed to cancel out.

In this chapter we are concerned with the second type of poles. In principle one could content oneself with the fact that the poles are unphysical and that the block are still well defined for $b^2 \in \mathbb{Q}$ and arbitrary internal and external dimensions. The problem is practical: in a numerical bootstrap study, the conformal blocks must be computed accurately to check crossing-symmetry of four-point functions, and obtain accurate estimates of the structure constants. The most efficient known way to compute conformal blocks is the recursion representation. It is then needed to regularise the blocks at the (dense set of) points where the unphysical poles appear, by taking the central charge slightly away from the rational value. While this regularisation scheme works, the cancellation of two very large terms leads to non-negligible numerical error, which can prevent the bootstrap analysis near these values of the central charge (see for instance note 20 in Section 4.3 of [47]).
Finding a representation of the four-point conformal blocks which is both computationally efficient and manifestly finite for any Δ's and any c seems difficult. In this chapter we study the function (1.71):

$$H_\Delta(\Delta_i|q) = 1 + \sum_{mn\geq 1} (16q)^{mn} \frac{R_{m,n}(\Delta_i)}{\Delta - \Delta_{m,n}} H_{\Delta_{m,n}+mn}(\Delta_i|q) = \sum_{mn\geq 0} q^{mn} H_{mn}\left(\Delta|\Delta_i\right) \tag{3.1}$$

when the central charge becomes rational, $b^2 \in \mathbb{Q}$. From explicit checks at the lowest orders in q we conjecture that cancellations occur at each order. In particular the poles are seen to be artificial in the sense that this particular representation splits finite terms from the level-by-level expansion (1.65) into sums of divergent terms. Indeed, writing the conformal block as:

$$\mathcal{F}_\Delta\left(\Delta_i|z\right) = \sum_{|Y|} f_{|Y|}\left(\Delta, \Delta_i\right) z^{|Y|}, \tag{3.2}$$

the coefficient at a given level $|Y|$ is:

$$f_{|Y|} = \Gamma^{\Delta_3}_{\Delta_4;\Delta,Y} \sum_{\substack{Y' \\ |Y'|=Y}} H^{-1}_{Y,Y'}(\Delta)\, \Gamma^{\Delta,Y'}_{\Delta_1,\Delta_2}. \tag{3.3}$$

For instance the order 2 term is

$$f_2 = \frac{\Gamma^{\Delta_3}_{\Delta_4;\Delta,\{1,1\}}\left((4\Delta+c/2)\,\Gamma^{\Delta,\{1,1\}}_{\Delta_1,\Delta_2} - 6\Delta\Gamma^{\Delta,\{2\}}_{\Delta_1,\Delta_2}\right) + \Gamma^{\Delta_3}_{\Delta_4;\Delta,\{2\}}\left(-6\Delta\Gamma^{\Delta,\{1,1\}}_{\Delta_1,\Delta_2} + 4\Delta(2\Delta+1)\Gamma^{\Delta,\{2\}}_{\Delta_1,\Delta_2}\right)}{32\Delta(\Delta-\Delta_{1,2})(\Delta-\Delta_{2,1})} \tag{3.4}$$

where the inverse matrix elements $H^{-1}_{Y,Y'}$ have been replaced by the entries of (1.44). For generic Δ's, it is finite at rational c. In terms of the coefficients H_i of the recursion (3.1):

$$f_2 = \mathcal{P}_2^{(0)}\left(\Delta|\Delta_i,c\right) + \mathcal{P}_2^{(1)}\left(\Delta|\Delta_i,c\right)H_1 + \mathcal{P}_2^{(2)}\left(\Delta|\Delta_i,c\right)H_2 \tag{3.5}$$

where

$$\mathcal{P}_2^{(0)}\left(\Delta|\Delta_i,c\right) = \frac{1}{256}\Bigg(-3b^{-2}-3b^2-6+8(-7(\Delta_2+\Delta_3)+9(\Delta_1+\Delta_4) \tag{3.6}$$
$$+4(\Delta_1-\Delta_2-\Delta_3+\Delta_4)^2)+4\Delta\left(13+16(\Delta_1-\Delta_2-\Delta_3+\Delta_4)\right)+32\Delta^2\Bigg)$$

$$\mathcal{P}_2^{(1)}\left(\Delta|\Delta_i,c\right) = \frac{1}{8}\left(1+\Delta_1-\Delta_2-\Delta_3+\Delta_4+\Delta\right) \tag{3.7}$$

$$\mathcal{P}_2^{(2)}\left(\Delta|\Delta_i,c\right) = \frac{1}{256} \tag{3.8}$$

as can be found by expanding (1.68) in z. The H's are by construction sums of rational functions of Δ, for instance:

$$\begin{aligned} H_1 &= \frac{R_{1,1}}{\Delta} \\ H_2 &= \frac{R_{1,1}^2}{\Delta} + \frac{R_{1,2}}{\Delta-\Delta_{1,2}} + \frac{R_{2,1}}{\Delta-\Delta_{2,1}} \\ &\dots \end{aligned} \tag{3.9}$$

The rewriting (3.5) corresponds then to a decomposition in partial fraction of (3.4). In the general case at level $|Y|$ it is this decomposition which introduces artificial divergences. Sketchily, a rational term in $f_{|Y|}$ is decomposed as:

$$\begin{aligned} \frac{\mathcal{P}(\Delta|\Delta_i,c)}{(\Delta-\Delta_{r_1,s_1})(\Delta-\Delta_{r_2,s_2})} &= \frac{\mathcal{P}_1(\Delta|\Delta_i,c)}{\Delta-\Delta_{r_1,s_1}} + \frac{\mathcal{P}_2(\Delta|\Delta_i,c)}{\Delta-\Delta_{r_2,s_2}} + \text{ finite terms} \\ &= \frac{(\Delta-\Delta_{r_2,s_2})\mathcal{P}_1(\Delta|\Delta_i,c)+(\Delta-\Delta_{r_1,s_1})\mathcal{P}_2(\Delta|\Delta_i,c)}{(\Delta-\Delta_{r_1,s_1})(\Delta-\Delta_{r_2,s_2})} + \text{ finite} \end{aligned} \tag{3.10}$$

where all $\mathcal{P}$'s are polynomials in Δ. The left-hand side is finite when the central charge is rational. Namely $\mathcal{P}$ is finite in the limit $\epsilon \to 0$ of central charge $b_\epsilon^2 = \mathbb{Q}+\epsilon$. Artificial poles are however introduced by writing it instead as:

$$\mathcal{P}(\Delta) = \mathcal{P}(\Delta) + \frac{\mathcal{P}_\epsilon(\Delta)-\mathcal{P}_\epsilon(\Delta)}{\epsilon} \tag{3.11}$$

for some polynomial $\mathcal{P}_\epsilon$. Then the polynomials $\mathcal{P}_1(\Delta)$ and $\mathcal{P}_2(\Delta)$ in the right-hand side of (3.10) are both divergent when $\epsilon \to 0$:

$$(\Delta-\Delta_{r_2,s_2})\mathcal{P}_1(\Delta) = \epsilon^{-1}\mathcal{P}_\epsilon(\Delta) + \text{finite} \tag{3.12}$$

$$(\Delta-\Delta_{r_1,s_1})\mathcal{P}_2(\Delta) = -\epsilon^{-1}\mathcal{P}_\epsilon(\Delta) + \text{finite}. \tag{3.13}$$

An explicit computation of the order 3 coefficient f_3 is performed in Appendix A of Article I, both in the level-by-level and recursive representations. Taking the limit $c \to -2$ ($b^2 = -1/2$) shows explicitely the mechanism sketched above.
In Article I the main object of study is the one-point block on the torus $\mathcal{F}^{(1)}_{\Delta_{\text{int}}}(\Delta_{\text{ext}})$, for which a similar recursion representation exists (cf. Chapter 2). This block is simpler than the four-point block on the sphere, but its recursion shows the same cancellation structure at rational c. In particular, explicit expressions could be found when the external field is set to the Identity, namely when the one-point block $\mathcal{F}^{(1)}_{\Delta_{\text{int}}}(q)$ becomes the character of the representation $\mathcal{R}_{\Delta_{\text{int}}}$. It is an expansion in q where the (integer) coefficient at each order gives the number of descendants at the corresponding level. In that case the recursion has no poles. Instead, the recursion splits the integer coefficients into sums of fractional terms. How these fractional terms combine to give integer numbers shows the same structure as the pole cancellation in the four-point block.

Published for SISSA by Springer

Received: *July 3, 2018*
Accepted: *August 25, 2018*
Published: *August 28, 2018*

Notes on the solutions of Zamolodchikov-type recursion relations in Virasoro minimal models

Nina Javerzat,[a] **Raoul Santachiara**[a] **and Omar Foda**[b]

[a] *LPTMS, CNRS, Université Paris-Sud, Université Paris-Saclay, 91405 Orsay, France*
[b] *School of Mathematics and Statistics, University of Melbourne, Parkville, Victoria 3010, Australia*

E-mail: Nina.Javerzat@lptms.u-psud.fr, Raoul.Santachiara@lptms.u-psud.fr, omar.foda@unimelb.edu.au

Abstract: We study Virasoro minimal-model 4-point conformal blocks on the sphere and 0-point conformal blocks on the torus (the Virasoro characters), as solutions of Zamolodchikov-type recursion relations. In particular, we study the singularities due to resonances of the dimensions of conformal fields in minimal-model representations, that appear in the intermediate steps of solving the recursion relations, but cancel in the final results.

Keywords: Conformal Field Theory, Lattice Integrable Models

ArXiv ePrint: 1806.02790

https://doi.org/10.1007/JHEP08(2018)183

JHEP08(2018)183

Contents

JHEP08(2018)183

1 Introduction

1.1 The conformal bootstrap and Virasoro conformal blocks

In spite of the enormous progress in our understanding of 2D conformal field theories over the past 35 years, important classes of two-dimensional conformal field theories remain to be discovered, or at least better-understood. An outstanding example is critical percolation, which is known to be a CFT with Virasoro central charge $c = 0$, but the correlation functions of this CFT remain to be computed. Recently, new numerical 2D conformal bootstraps that fully exploit the full 2D local conformal symmetries were developed and new 2D CFT's were discovered [8, 12]. These 2D bootstraps are based on Virasoro conformal blocks, and the corresponding solutions are functions of infinite-dimensional representations of local conformal transformations, as opposed to bootstraps that are valid in *any* dimension, which are based on *global* conformal blocks, and the corresponding solutions are functions of finite-dimensional representations of global conformal transformations.

1.2 Zamolodchikov's recursion relation

To implement the new 2D bootstraps numerically, one needs to compute the 4-point conformal blocks on the sphere efficiently. The most efficient known method to compute 4-point conformal blocks on the sphere is Zamolodchikov's recursion relation. In fact, solving the 2D bootstrap efficiently is what motivated Al. Zamolodchikov to develop the recursion relations in the first place [14, 15]. There are two versions of Zamolodchikov's recursion relation, a hypergeometric version [14], and an elliptic version [15]. The elliptic version is particularly efficient, and will be the focus of the present work, and to fully understand this recursion relation, we will find it useful to consider a related recursion relation for the 1-point conformal block on the torus, and its 0-point conformal block limit, which is a Virasoro character.

1.3 The singularities

The 4-point conformal block on the sphere is a function of six parameters: the Virasoro central charge, the conformal dimension of the Virasoro representation that flows in the internal channel, and the conformal dimensions of the four external fields. The solution of

the elliptic recursion relation displays a rich structure of poles. These poles are physical in the sense that they correspond to the propagation of states for suitable choices of the central charge and conformal dimensions. In a numerical 2D bootstrap based on Virasoro conformal blocks that are computed using the elliptic recursion relation, one must deal with these poles when exploring the space of possible crossing-symmetric CFT solutions. This happens, for example, in studies of percolation in the 2D Ising model [9]. When the central charge is such that one deals with minimal-model conformal blocks, additional poles appear. These additional poles are non-physical and appear due to resonances of conformal dimensions (see equation (2.11)) at rational values of the central charge. This complication requires a careful study of the pole structure of the elliptic recursion relation in the case of Virasoro minimal models, which is the aim of the present work.

1.4 The present work

We study the cancellation of the non-physical poles in computations of minimal-model conformal blocks using Zamolodchikov's elliptic recursion relation for the 4-point conformal block on the sphere. But the 4-point conformal block on the sphere is not the only or the simplest conformal block that can be computed using a recursion relation. In 2009, Poghossian [10], and independently Fateev and Litvinov [3] proposed recursion relations to compute Liouville 1-point conformal blocks on the torus. These recursion relations are equivalent [6], and we use the Fateev-Litvinov version to study minimal-model 1-point functions on the torus, and their 0-point limits (when the vertex operator insertion is the identity) which are Virasoro minimal-model characters, as the simplest examples of solutions of a Zamolodchikov-type elliptic recursion relation.

1.5 Outline of contents

In section 2, we recall basic facts related to the Virasoro algebra, its representations, and conformal blocks. In section 3, we consider the 4-point conformal blocks on the sphere as solutions of the recursion relation, study their singularities and their behaviour in the context of the Virasoro generalized minimal models and minimal models. In section 4, we consider the 1-point conformal block on the torus as solutions of the Fateev-Litvinov recursion relation. In section 5, we study the solutions of the Fateev-Litvinov recursion relations for the Virasoro minimal-model 1-point functions on the torus in the special case where the inserted vertex operator is the identity and the 1-point function reduces to the character of the irreducible highest-weight representation that flows in the torus. In appendix A, we include the details of an explicit computation, and in appendix B, we include technical details related to coefficients that appear in the recursion relations.

2 Virasoro algebra, representations and conformal blocks

We recall basic definitions related to the Virasoro algebra, representation theory, and conformal blocks. We refer the reader to the review [13].

2.1 The Virasoro algebra, generators and central charge

A Virasoro CFT is based on the Virasoro algebra,

$$[L_n, L_m] = (n-m)L_{n+m} + \frac{c}{12} n(n^2-1)\delta_{n+m,0}, \quad n, m \in \mathbb{Z}, \tag{2.1}$$

JHEP08(2018)183

where the Virasoro generators $L_n, n \in \mathbb{Z}$ are the modes of the stress-energy tensor and c is the central charge. The Liouville parametrization of the central charge is,

$$c = 1 + 6\,Q^2, \quad Q = b + b^{-1}, \quad c \in \mathbb{C} \tag{2.2}$$

2.2 Verma modules

Given a highest-weight state $|\Delta\rangle$, with highest weight Δ, $L_0|\Delta\rangle = \Delta\,|\Delta\rangle$, the descendant states $L_{-n_1}\cdots L_{-n_N}|\Delta\rangle$, $n_1 \geqslant n_2 \geqslant \cdots \geqslant n_N$, form a basis of the Verma module $\mathcal{V}_\Delta$. A general element in this basis is $L_{-Y}\,|\,\Delta\,\rangle$, labeled by a Young diagram $Y = (n_1, \cdots, n_N)$, that has N non-zero parts, and,

$$L_0\,|L_{-Y}\Delta\rangle = (\Delta + |Y|)\,|L_{-Y}\Delta\rangle, \tag{2.3}$$

where $|Y| = \sum_{i=1}^{N} n_i$ is the number of cells in the Young diagram Y. Using the state-field correspondence, we use $\Phi_\Delta\,(x)$ for the primary field of conformal dimension Δ, and $L_{-Y}\,\Phi_\Delta(x)$ for the descendant fields. We parametrize the conformal dimension Δ by the parameter Q, (2.2), and the charge α,

$$\Delta = \alpha\,(Q - \alpha) \tag{2.4}$$

2.3 Degenerate representations

A degenerate representation has a highest weight $\Delta_{m,n}$,

$$\Delta_{m,n} = \alpha_{m,n}\,(Q - \alpha_{m,n})\,, \quad \alpha_{m,n} = -\frac{1}{2}\,(m-1)\;b - \frac{1}{2}\,(n-1)\;b^{-1}, \tag{2.5}$$

and has a null state $|\,\chi_{mn}\,\rangle$ at level mn, $\langle\,\chi_{mn}\,|\,\chi_{mn}\rangle = 0$. When a representation with highest weight Δ_{mn} appears in the spectrum of a given CFT model, two situations can occur.

2.3.1 Null states vanish

The corresponding representation module $\mathcal{V}_{m,n}$ is the quotient of a reducible Verma module by a non-trivial submodule,

$$\mathcal{V}_{mn} = \frac{\mathcal{V}_{\Delta_{mn}}}{\mathcal{V}_{\Delta_{mn}+mn}} \tag{2.6}$$

The representations $\mathcal{V}_{mn}$ form the spectrum of the Virasoro generalized minimal as well as the minimal models. The vanishing of the null state implies the fusion rules. The fusions of products of $\mathcal{V}_{mn}$ have simple expressions in the parametrization (2.4). For instance, the fusion of $\mathcal{V}_{mn}$ with a Verma module $\mathcal{V}_\alpha$ is a sum of mn Verma modules and takes the form,

$$\mathcal{V}_{mn} \times \mathcal{V}_\alpha = \sum_{i=\frac{1}{2}\,(1-m)}^{\frac{1}{2}\,(m-1)} \sum_{j=\frac{1}{2}\,(1-n)}^{\frac{1}{2}\,(n-1)} \mathcal{V}_{\alpha+ib+jb^{-1}}\,, \tag{2.7}$$

where the sums are in steps of 1.

JHEP08(2018)183

2.3.2 Null states do not vanish

Representations with non-vanishing null-states appear in Liouville field theory at $c \leqslant 1$ [12], and in computations of probabilities of non-local critical objects such as the left-right passage probability of an SLE interface. We will not deal with this case in the present work.

2.4 The Virasoro minimal models

$\mathcal{M}_{pp'}$, are labeled by two positive co-prime integers p and p', such that $0 < p < p'$. The space of chiral states of $\mathcal{M}_{pp'}$ is generated by a Virasoro algebra with central charge,

$$b = \left(-\frac{p'}{p}\right)^{\frac{1}{2}} \tag{2.8}$$

The space of chiral states splits into (typically finitely-many) fully-degenerate irreducible highest-weight modules $\mathcal{V}_{mn}$ labeled by two integers m and n, such that $0 < m < p$, and $0 < n < p'$. From (2.5), $\Delta_{m\,n}$ satisfies the negation relation, and the periodicity relation,

$$\Delta_{m\,n} = \Delta_{-m,\,-n}, \quad \Delta_{m,n} = \Delta_{m+p,\,n+p'}, \tag{2.9}$$

which combine to give,

$$\Delta_{m,n} = \Delta_{m',\,n'}, \quad m' = p - m, \quad n' = p' - n, \tag{2.10}$$

as well as an infinite chain of relations that involve *'resonant'* conformal dimensions,

$$\Delta_{m,n} = \Delta_{p+m,\,p'+n} = \cdots \tag{2.11}$$

Two pairs of indexes (m, n) and (r, s) are resonant if there are linked by a finite chain of transformations (2.9). In this case we use the notation,

$$(m, n) \leftrightarrow (r, s)_l^{\pm}\,, \tag{2.12}$$

to indicate that there exists an integer l such that,

$$(m, n) \leftrightarrow (r, s)_l^{\pm} \implies r = l\,p \pm m, \quad s = l\,p' \pm n, \quad l \in \mathbb{N} \tag{2.13}$$

2.4.1 Remark

In our notation, $0 < p < p'$, and $b = \sqrt{-p'/p}$ is pure imaginary such that $|b| > 0$. One can think of $|b|$ as the magnitude of the positive screening charge $\alpha_+ > 0$. We normally take the negative screening charge $\alpha_- < 0$, and the background charge,

$$-\,2\alpha_0 = -\,(\alpha_+ + \alpha_-)\,, \tag{2.14}$$

that is, the background charge can be screened by the sum of a single α_+ and a single α_-.

JHEP08(2018)183

2.5 The Virasoro conformal blocks

The conformal blocks are special functions of the Virasoro representations. We consider the 4-point conformal blocks on the sphere, the 1-point conformal blocks on the torus, and the 0-point conformal blocks on the torus, which are Virasoro characters. In all generality, these conformal blocks are defined in terms of the $p_{|Y|} \times p_{|Y|}$ matrix $S_{|Y|}(Y, Y')$ of inner products of descendants at level $|Y|$, where $p_{|Y|}$ is the number of partitions of $|Y|$,

$$S_{|Y|}\left(Y, Y'\right) = \langle L_{-Y}\Delta | L_{-Y'}\Delta \rangle, \quad |Y| = |Y'|, \tag{2.15}$$

and the matrix elements,

$$\langle L_{-Y_1}\Delta_1 | L_{-Y_2}\Phi_{\Delta_2}(1) | L_{-Y_3}\Delta_3 \rangle \tag{2.16}$$

In Virasoro CFT's, the Shapolavov matrix and the 3-point functions are completely determined by the Virasoro algebra (2.1). Note that this is not true anymore for more general conformal chiral algebras such as the $\mathcal{W}^N$ algebras [1, 2].

3 The 4-point conformal blocks on the sphere

We outline Zamolodchikov's computation of the 4-point conformal block on the sphere, and study its poles.

3.1 The 4-point conformal block on the sphere

Global conformal symmetry determines the dependences of four-point blocks on three of the four positions z_i, and we assume $(z_i) = (x, 0, \infty, 1)$. The conformal block is a function of six parameters, the central charge, the cross-ratio x, the conformal dimensions of the four external fields Δ_i, $i = 1, \cdots, 4$, and the conformal dimension of the representation that flows in the internal channel Δ_{int}. In terms of the vertex-operators charges,

$$\Delta_i = \alpha_i \left(Q - \alpha_i\right), \quad \Delta_{\text{int}} = \alpha_{\text{int}} \left(Q - \alpha_{\text{int}}\right) \tag{3.1}$$

The 4-point conformal block on the sphere has an x-series expansion,

$$\mathcal{B}\left(\mathbf{\Delta}, x\right) = x^{-\Delta_1 - \Delta_2 + \Delta_{int}} \left(1 + \mathcal{B}_1\left(\mathbf{\Delta}\right) x + \mathcal{B}_2\left(\mathbf{\Delta}\right) x^2 + \cdots\right), \tag{3.2}$$

where $\mathbf{\Delta}$ for the set of external and internal conformal dimensions $(\Delta_1, \Delta_2, \Delta_3, \Delta_4, \Delta_{\text{int}})$, and,

$$\mathcal{B}_{|Y|}\left(\mathbf{\Delta}\right) = \sum_{\substack{Y, Y' \\ |Y| = |Y'|}} S^{(-1)}_{|Y|}\left(Y, Y'\right) \langle \Delta_2 \left| \Phi_1(1) \right| L_{-Y'}\Delta_{int} \rangle \langle L_{-Y}\, \Delta_{\text{int}} \left| \Phi_3(1) \right| \Delta_4 \rangle, \tag{3.3}$$

where Y' is *any* Young diagram such that $|Y'| = |Y|$, and Φ_i is a primary field of conformal dimension Δ_i.

JHEP08(2018)183

3.2 The elliptic recursion relation

In [15], Zamolodchikov introduced an elliptic recursion relation of the same 4-point conformal blocks on the sphere.[1] The recursion parameter q is a function of x

$$q = \frac{1}{16}\left(x + \frac{1}{2}x^2 + \frac{21}{64}x^3 + \frac{31}{128}x^4 + \mathcal{O}\left(x^5\right)\right), \tag{3.4}$$

which follows from inverting,

$$x = \frac{\theta_2^4(q)}{\theta_3^4(q)}, \tag{3.5}$$

where $\theta_2(q)$ and $\theta_3(q)$ are Jacobi theta functions,

$$\theta_2(q) = \sum_{n=-\infty}^{\infty} q^{(n+1/2)^2}, \quad \theta_3(q) = \sum_{n=-\infty}^{\infty} q^{n^2}, \tag{3.6}$$

The conformal blocks can be written as,

$$\begin{aligned}\mathcal{B}(\boldsymbol{\Delta}, c, x) = {} & x^{\frac{c-1}{24}-\Delta_1-\Delta_2}(1-x)^{\frac{c-1}{24}-\Delta_2-\Delta_3}(16q)^{\Delta_{\rm int}-\frac{Q^2}{4}}\theta_3(q)^{3Q^2-4(\Delta_1+\Delta_2+\Delta_3+\Delta_4)} \\ & \times \mathcal{H}^{\rm sph}(\boldsymbol{\Delta}_{\rm ext}, \Delta_{\rm int}, c, x),\end{aligned} \tag{3.7}$$

where the elliptic variable q and function $\theta_3(q)$ are defined in (3.4) and in (3.6) and we use $\boldsymbol{\Delta}_{\rm ext}$ for the set of external dimensions $(\Delta_1, \Delta_2, \Delta_3, \Delta_4)$. The analytic structure of the function $\mathcal{H}^{\rm sph}(\boldsymbol{\Delta}_{\rm ext}, \Delta_{\rm int}, c, x)$ is manifest in the following expansion,[2]

$$\mathcal{H}^{\rm sph}(\boldsymbol{\Delta}_{\rm ext}, \Delta_{\rm int}, c, x) = 1 + \sum_{rs\geqslant 1}(16q)^{rs}\frac{R^{\rm sph}_{r,s}(\boldsymbol{\Delta}_{\rm ext}, c)}{\Delta_{\rm int} - \Delta_{r,s}}\mathcal{H}^{\rm sph}(\boldsymbol{\Delta}_{\rm ext}, \Delta_{r,-s}, c, x), \tag{3.8}$$

where,

$$R^{\rm sph}_{m,n}(\boldsymbol{\Delta}, c) = \frac{1}{r_{m,n}}P_{m,n}(\Delta_1, \Delta_2)P_{m,n}(\Delta_3, \Delta_4) \tag{3.9}$$

The factors $P_{m,n}$ carries all dependence in $R^{\rm sph}_{m,n}(\boldsymbol{\Delta})$ on the external conformal dimensions $\Delta_i, i = 1, \cdots, 4$. It is convenient to parametrize the conformal dimensions in terms of the momenta λ_i and $\lambda_{m,n}$,

$$\Delta_i = \frac{c-1}{24} + \lambda_i^2, \quad \Delta_{m,n} = \frac{c-1}{24} + \lambda_{m,n}^2 \tag{3.10}$$

In terms of these variables, one has,

$$\begin{aligned}P_{m,n}(\Delta_1, \Delta_2) = {} & \prod_{\rho,\sigma}(\lambda_1 + \lambda_2 - \lambda_{\rho,\sigma})(\lambda_1 - \lambda_2 - \lambda_{\rho,\sigma}) \\ & \rho = 1-m, 3-m, \cdots, m-1, \quad \sigma = 1-n, 3-n, \cdots, n-1\end{aligned} \tag{3.11}$$

The factor $r_{m,n}$ is given by,

$$\begin{aligned}r_{m,n} = {} & -\frac{1}{2}\prod_{\rho,\sigma}2\lambda_{\rho,\sigma}, \\ & \rho = 1-m, 2-m, \cdots, m, \quad \sigma = 1-n, 2-n, \cdots, n, \quad (\rho,\sigma) \neq (0,0), \ (m,n)\end{aligned} \tag{3.12}$$

[1] In [11], Poghossian extended Zamolodchikov's elliptic recursion relation to a class of $\mathcal{W}_3$ Toda 4-point conformal blocks on the sphere.

[2] Note that some closed form expression has been found in [7].

JHEP08(2018)183

3.3 The generalized minimal model

When the central charge is non-rational, but a degenerate representation $\mathcal{V}_{\Delta_{m,n}}$ flows in the channel, the recursion relation (3.8) has a pole related to the presence of a null-state at level mn in $\mathcal{V}_{\Delta_{m,n}}$, and the corresponding Shapovalov matrix has a vanishing eigenvalue that produces the singularity in the expansion (3.3).

3.3.1 The regularization ϵ

We introduce a regularization parameter ϵ,

$$\Delta_{\text{int}} = \Delta^{(\epsilon)}_{m,n} = \Delta_{mn} + \epsilon \tag{3.13}$$

The limit $\epsilon \to 0$ in (3.8) exists only if the polynomial $P_{m,n}(\Delta_1, \Delta_2)$ and/or $P_{m,n}(\Delta_3, \Delta_4)$, defined in (3.9) and in (3.11), vanish. Recall that $P_{m,n}(\Delta_1, \Delta_2)$ vanishes when $(\mathcal{V}_{\Delta_1}, \mathcal{V}_{\Delta_2}, \mathcal{V}_{m,n})$ satisfy the fusion rules (2.7), that is to say when $\alpha_2 = \alpha_1 + ib + jb^{-1}$, with $i \in \{(1-m)/2, (3-m)/2, \cdots, (m-1)/2\}$ and $j \in \{(1-n)/2, (3-m)/2, \cdots, (n-1)/2\}$. The generalized minimal model has a non-rational central charge, $c \notin \mathbb{Q}$, and a spectrum formed by all the degenerate representations $\mathcal{V}_{m,n}$ with $(m,n) \in \mathbb{N}_+$. All the fields in the spectrum satisfy the fusion rules (2.7), imposed by the condition $\chi_{mn} = 0$. The conformal blocks of the generalized minimal model can be obtained by using the recursion relation with a simple limiting procedure. This consists in setting,

$$\Delta_i = \Delta^{(\epsilon_i)}_{r_i,s_i} = \Delta_{r_i,s_i} + \epsilon_i, \quad i = 1, \cdots, 4, \tag{3.14}$$

with $\epsilon_i \to 0$, $i = 1, \cdots, 4$ of the same order of ϵ, $\epsilon_i = \mathcal{O}(\epsilon)$, and take the limit $\epsilon \to 0$. Using,

$$\frac{H^{\text{sph}}_{m,n}(\mathbf{\Delta}, c, x)}{\Delta_{\text{int}} - \Delta_{m,n}} \propto \frac{P_{m,n}\left(\Delta^{(\epsilon)}_{r_1,s_1}\Delta^{(\epsilon_2)}_{r_2,s_2}\right) P_{m,n}\left(\Delta^{(\epsilon_3)}_{r_3,s_3}\Delta^{(\epsilon_4)}_{r_4,s_4}\right)}{\Delta^{\epsilon}_{m,n} - \Delta_{m,n}} \sim O(\epsilon), \tag{3.15}$$

it is straightforward to see that the term $\mathcal{H}^{sph}_{m,n}(\mathbf{\Delta}, c, x)$in (3.8) do not contribute. In the generalized minimal models therefore, the conformal block with $\Delta_{\text{int}} = \Delta_{m,n}$ is obtained using the sum in (3.8) where the term $(r,s) = (m,n)$ is omitted. We stress that, in this procedure limit, the final result is independent of the exact relation between the regularization parameters ϵ_i and ϵ. The only thing that matters is the fact that the ϵ_i and ϵ are of the same order. As we will see later, this will not be the case for the computation of the characters.

3.4 Minimal-model conformal blocks.

We address here the problem of how to obtain the conformal blocks of minimal models $\mathcal{M}_{p,p'}$ from the recursion relation (3.8). The main observation is that, with respect to the generalized minimal models, there are new poles appearing in (3.8). The location of these extra poles do not depend neither on the internal channel field nor on the external fields. They originate from the resonances in the conformal dimensions that occur when $c \in \mathbb{Q}$.

JHEP08(2018)183

Let us consider for instance one conformal block of the Ising minimal model, $\mathcal{M}_{4,3}$. At level 7, two terms appear,

$$\frac{R^{\text{sph}}_{2,1}\left(\boldsymbol{\Delta}_{\text{ext}},c\right)}{\Delta_{\text{int}}-\Delta_{2,1}}\frac{R^{\text{sph}}_{1,5}\left(\boldsymbol{\Delta}_{\text{ext}},c\right)}{\Delta_{2,-1}-\Delta_{1,5}},\quad\text{and}\quad\frac{R^{\text{sph}}_{1,3}\left(\boldsymbol{\Delta}_{\text{ext}},c\right)}{\Delta_{\text{int}}-\Delta_{1,3}}\frac{R^{\text{sph}}_{4,1}\left(\boldsymbol{\Delta}_{\text{ext}},c\right)}{\Delta_{-1,3}-\Delta_{4,1}},\tag{3.16}$$

that are singular due to the fact that at $c=1/2$, $(2,-1)\to(1,5)^{-}$ and $(-1,3)\to(4,1)^{-}$. Differently from the poles that originate when $\Delta_{\text{int}}=\Delta_{m,n}$, which are related to the null-state at level mn, these other singularities can be considered an artifact of the recursion relation in the sense that they are not related to any special properties of descendant states. In the appendix we better explain this point with an explicit example.

3.4.1 The regularization ϵ'

In addition to (3.13), we introduce a regularization parameter ϵ' to the central charge c,

$$b^2=-\frac{p'}{p}+\epsilon',\tag{3.17}$$

that is of the same order of ϵ, $\epsilon'=O\left(\epsilon\right)$.

3.5 Conjecture

We conjecture that, by setting (3.13), (3.14) and (3.17), the limit $\epsilon\to 0$ in the recursion relation (3.8) exists and provides the correct minimal model conformal block.

3.6 Further example

We have checked that the two terms (3.16) combine to give a finite contribution. Another example, at level 20, is the combination of the following five singular terms,

$$\begin{aligned}
&\frac{R^{\text{sph}}_{1,1}\left(\boldsymbol{\Delta}_{\text{ext}},c\right)}{\left(\Delta^{(\epsilon)}_{1,1}-\Delta_{1,1}\right)}\frac{R^{\text{sph}}_{4,3}\left(\boldsymbol{\Delta}_{\text{ext}},c\right)}{\left(\Delta_{1,-1}-\Delta_{4,3}\right)}\frac{R^{\text{sph}}_{7,1}\left(\boldsymbol{\Delta}_{\text{ext}},c\right)}{\left(\Delta_{4,-3}-\Delta_{7,1}\right)}\\
&\quad+\frac{R^{\text{sph}}_{1,1}\left(\boldsymbol{\Delta}_{\text{ext}},c\right)}{\left(\Delta^{(\epsilon)}_{1,1}-\Delta_{1,1}\right)}\frac{R^{\text{sph}}_{2,5}\left(\boldsymbol{\Delta}_{\text{ext}},c\right)}{\left(\Delta_{1,-1}-\Delta_{2,5}\right)}\frac{R^{\text{sph}}_{1,9}\left(\boldsymbol{\Delta}_{\text{ext}},c\right)}{\left(\Delta_{2,-5}-\Delta_{1,9}\right)}\\
&\quad+\frac{R^{\text{sph}}_{2,3}\left(\boldsymbol{\Delta}_{\text{ext}},c\right)}{\left(\Delta^{(\epsilon)}_{1,1}-\Delta_{2,3}\right)}\frac{R^{\text{sph}}_{5,1}\left(\boldsymbol{\Delta}_{\text{ext}},c\right)}{\left(\Delta_{2,-3}-\Delta_{5,1}\right)}\frac{R^{\text{sph}}_{1,9}\left(\boldsymbol{\Delta}_{\text{ext}},c\right)}{\left(\Delta_{5,-1}-\Delta_{1,9}\right)}\\
&\quad+\frac{R^{\text{sph}}_{2,3}\left(\boldsymbol{\Delta}_{\text{ext}},c\right)}{\left(\Delta^{(\epsilon)}_{1,1}-\Delta_{2,3}\right)}\frac{R^{\text{sph}}_{1,7}\left(\boldsymbol{\Delta}_{\text{ext}},c\right)}{\left(\Delta_{2,-3}-\Delta_{1,7}\right)}\frac{R^{\text{sph}}_{7,1}\left(\boldsymbol{\Delta}_{\text{ext}},c\right)}{\left(\Delta_{1,-7}-\Delta_{7,1}\right)}+\frac{R^{\text{sph}}_{4,5}\left(\boldsymbol{\Delta}_{\text{ext}},c\right)}{\left(\Delta^{(\epsilon)}_{1,1}-\Delta_{4,5}\right)}
\end{aligned}\tag{3.18}$$

to a finite contribution. If we can predict the singular terms that, at a given level, provide finite contributions, we have not been able to obtain a compact formula for these. As we will see in the following, we can control the contribution of these type of singularities in the computation of a simpler symmetry function, the character.

JHEP08(2018)183

4 1-point conformal blocks on the torus

We recall the Fateev-Litvinov recursion relation for the 1-point conformal block on the torus, and introduce the structure of its poles.

4.1 The 1-point conformal block on the torus

The Virasoro 1-point conformal block on the torus consists of a single vertex-operator insertion in a torus geometry, and a Virasoro irreducible highest-weight representation flows in the single internal channel of the torus. This is a function of four parameters, the central charge, the torus parameter q, the conformal dimension of the external field Δ_{ext}, and the conformal dimension of the internal channel Δ_{int}. The conformal dimension of the external vertex-operator is,

$$\Delta_{\text{ext}} = \alpha_{\text{ext}} \left(Q - \alpha_{\text{ext}} \right), \tag{4.1}$$

and similarly, the conformal dimension of the representation that flows in the torus is,

$$\Delta_{\text{int}} = \alpha_{\text{int}} \left(Q - \alpha_{\text{int}} \right) \tag{4.2}$$

The torus 1-point conformal block has the q-series expansion,

$$\mathcal{F} \left(\boldsymbol{\Delta}, q \right) = 1 + \mathcal{F}_1 \left(\boldsymbol{\Delta} \right) q + \mathcal{F}_2 \left(\boldsymbol{\Delta} \right) q^2 + \cdots , \tag{4.3}$$

where $\boldsymbol{\Delta}$ is a pair of conformal dimensions $(\Delta_{\text{ext}}, \Delta_{\text{int}})$, and,

$$\mathcal{F}_{|Y|} \left(\boldsymbol{\Delta} \right) = \sum_{\substack{Y, Y' \\ |Y| = |Y'|}} S^{(-1)}_{|Y|} \left(Y, Y' \right) \langle L_{-Y} \Delta_{\text{int}} \,|\, \Phi_{\text{ext}}(1) \,|\, L_{-Y'} \Delta_{\text{int}} \rangle \tag{4.4}$$

4.2 The recursion relation of Fateev and Litvinov [3]

The 1-point conformal block on the torus is,

$$\mathcal{F} \left(\boldsymbol{\Delta} \,|\, q \right) = \frac{q^{1/24}}{\eta(q)} \mathcal{H} \left(\boldsymbol{\Delta} \,|\, q \right), \tag{4.5}$$

where,

$$\frac{q^{1/24}}{\eta(q)} = \prod_{i=1}^{\infty} \frac{1}{1 - q^i} = 1 + q + \cdots + p_N \, q^N + \cdots , \tag{4.6}$$

p_N is the number of partitions of $N \in \mathbb{N}$, and,

$$\mathcal{H} \left(\boldsymbol{\Delta} \,|\, q \right) = \sum_{N=0}^{\infty} H_N \left(\alpha_{\text{ext}}, \Delta_{\text{int}} \right) q^N \tag{4.7}$$

4.2.1 Remark

The factor $q^{1/24}/\eta(q)$ is the character of the Fock space of a free boson, and in (4.5), the 1-point function on the torus is written in terms of the free-boson of Feigin and Fuks [4, 5]. This will become clear once we take the $\alpha_{\text{ext}} \to 0$ limit, and 1-point function becomes a character, in section 5.

JHEP08(2018)183

4.2.2 The recursion relation

The recursion comes in the definition of H_N, the coefficients of the numerator of the conformal block,

$$H_N\left(\alpha_{\rm ext},\Delta_{\rm int}\right)=\sum_{rs=1}^{N}\frac{R^{\rm tor}_{r,s}\left(\alpha_{\rm ext}\right)}{\left(\Delta_{\rm int}-\Delta_{r,s}\right)}H_{N-rs}\left(\alpha_{\rm ext},\Delta_{-r,s}\right),H_0\left(\alpha_{\rm ext},\Delta_{\rm int}\right)=1 \tag{4.8}$$

4.2.3 The $R^{\rm tor}_{r,s}$ numerators

$$\begin{aligned}R^{\rm tor}_{r,s}\left(\alpha_{\rm ext}\right)&=\frac{1}{4r_{r,s}}\prod_k\prod_l\left(\frac{k-1}{2}\,b+\frac{l-1}{2}\,b^{-1}+\alpha_{\rm ext}\right),\\ &k=1-2r,3-2r,\cdots,2r-1,\quad l=1-2s,3-2s,\cdots,2s-1,\end{aligned} \tag{4.9}$$

$r_{r,s}$ is given by formula (3.12).

4.2.4 Examples

The simplest coefficients H_N, $N=1,2,\cdots$, in (4.7) are,

$$\begin{aligned}H_1\left(\alpha_{\rm ext},\Delta_{\rm int}\right)&=\frac{R^{\rm tor}_{1,1}\left(\alpha_{\rm ext}\right)}{\left(\Delta_{\rm int}-\Delta_{1,1}\right)},\\ H_2\left(\alpha_{\rm ext},\Delta_{\rm int}\right)&=\frac{R^{\rm tor}_{1,1}\left(\alpha_{\rm ext}\right)}{\left(\Delta_{\rm int}-\Delta_{1,1}\right)}H_1\left(\alpha_{\rm ext},\Delta_{-1,1}\right)\\ &\quad+\frac{R^{\rm tor}_{1,2}\left(\alpha_{\rm ext}\right)}{\left(\Delta_{\rm int}-\Delta_{1,2}\right)}+\frac{R^{\rm tor}_{2,1}\left(\alpha_{\rm ext}\right)}{\left(\Delta_{\rm int}-\Delta_{2,1}\right)},\\ H_3\left(\alpha_{\rm ext},\Delta_{\rm int}\right)&=\frac{R^{\rm tor}_{1,1}\left(\alpha_{\rm ext}\right)}{\left(\Delta_{\rm int}-\Delta_{1,1}\right)}H_2\left(\alpha_{\rm ext},\Delta_{-1,1}\right)+\frac{R^{\rm tor}_{1,2}\left(\alpha_{\rm ext}\right)}{\left(\Delta_{\rm int}-\Delta_{1,2}\right)}H_1\left(\alpha_{\rm ext},\Delta_{-1,2}\right)\\ &\quad+\frac{R^{\rm tor}_{2,1}\left(\alpha_{\rm ext}\right)}{\left(\Delta_{\rm int}-\Delta_{2,1}\right)}H_1\left(\alpha_{\rm ext},\Delta_{-2,1}\right)+\frac{R^{\rm tor}_{1,3}\left(\alpha_{\rm ext}\right)}{\left(\Delta_{\rm int}-\Delta_{1,3}\right)}+\frac{R^{\rm tor}_{3,1}\left(\alpha_{\rm ext}\right)}{\left(\Delta_{\rm int}-\Delta_{3,1}\right)}\end{aligned} \tag{4.10}$$

and so on.

4.3 Remark

Expanding (4.5), we obtain,

$$\begin{aligned}\mathcal{F}\left(\Delta_{\rm ext},\Delta_{\rm int}\,|\,q\right)&=\left(H_0\right)q^0+\left(H_0+H_1\right)q+\left(2H_0+H_1+H_2\right)q^2+\cdots\\ &=\sum_{N=0}^{\infty}\sum_{k=0}^{N}p(N-k)H_kq^N\end{aligned} \tag{4.11}$$

From (4.11), the structure of the conformal block $\mathcal{F}\left(\boldsymbol{\Delta}\,|\,q\right)$ is clear. In particular, if $\Delta_{\rm ext}=0$, and $H_N=0$, for all $N=1,2,\cdots$, we recover the character of the Fock space of a free boson, which is the character of a generic non-minimal conformal field theory. If $\Delta_{\rm ext}=0$, and $H_N=\pm1$, for appropriate values of N, null states and their descendants are removed and one obtains the character of an irreducible fully-degenerate highest-weight module. This will be discussed in detail in section 5.

5 The 0-point functions on the torus: the characters

We discuss the derivation of the character of the representation corresponding to $\Delta_{\rm int}$ *using the recursion relation and a particular limiting procedure, in three cases:* **1.** *general central charge and general* $\Delta_{\rm int}$ *,* **2.** *general central charge and degenerate representation* $\Delta_{\rm int} = \Delta_{m,n}$*, and* **3.** *minimal models* $\mathcal{M}_{p,p'}$ *characters.*

5.1 General central charge and general $\Delta_{\rm int}$

We introduce regularization parameter ϵ that we set to 0 at the end. We set the inserted vertex-operator to be the identity, in the limit ϵ to zero,

$$\alpha_{\rm ext} = 2\epsilon \tag{5.1}$$

The factor 2 in the above definition is for convenience. For general $r, s \in \mathbb{N}$, the term,

$$R^{\rm tor}_{r,s} \frac{(\alpha_{\rm ext} = 2\epsilon)}{(\Delta_{\rm int} - \Delta_{r,s})} = -\epsilon \frac{(Q - 2\alpha_{r,s})}{(\Delta_{\rm int} - \Delta_{r,s})} + \mathcal{O}\left(\epsilon^2\right), \tag{5.2}$$

vanishes in the limit $\epsilon \to 0$, provided that $\lim_{\epsilon\to 0} \Delta_{\rm int} \neq \Delta_{r,s}$. All the H_i are then zero and the expansion is given by (4.6). As expected, one finds the character $\chi_{\Delta_{\rm int}}(q)$ of an irreducible Verma module of dimension $\Delta_{\rm int}$.

5.2 General central charge, $\Delta_{\rm int} = \Delta_{m,n}$

First we set $\alpha_{\rm ext} = 2\epsilon$. Differently from the previous case, here we encounter the pole coming from the denominator $(\Delta_{\rm int} - \Delta_{m,n})$.

5.2.1 Internal field regularization

We need to regularize the dimension of the internal field, and we set,

$$\alpha_{\rm int} = \alpha_{m,n} + \epsilon', \tag{5.3}$$

and we define,

$$\Delta^{(\epsilon')}_{m,n} = \alpha_{\rm int}\left(Q - \alpha_{\rm int}\right) = \Delta_{m,n} + \epsilon'\left(Q - 2\alpha_{m,n}\right) + \mathcal{O}\left(\epsilon'^2\right) \tag{5.4}$$

For $\epsilon, \epsilon' \ll 1$, the term,

$$\frac{R^{\rm tor}_{m,n}(2\epsilon)}{\left(\Delta^{(\epsilon')}_{m,n} - \Delta_{m,n}\right)} = -\frac{\epsilon + \mathcal{O}\left(\epsilon^2\right)}{\epsilon' + \mathcal{O}\left(\epsilon'^2\right)} \tag{5.5}$$

The result of the limit $(\epsilon, \epsilon') \to (0,0)$ depends therefore on the way one reaches the point $(\epsilon, \epsilon') = (0,0)$. For instance, if one first sends $\epsilon \to 0$ and then $\epsilon' \to 0$, all the H_i are zero and the character of a general Verma module is found. This result can be interpreted by saying that the null-state at level nm is not vanishing. Interestingly, such representation appears for instance in the construction of the Liouville theory for $c \leqslant 1$ [12]. By setting $\epsilon' = \epsilon$ one finds instead that,

$$\lim_{\epsilon\to 0} \frac{R^{\rm tor}_{m,n}(\alpha_{\rm ext} = 2\epsilon)}{\left(\Delta^{(\epsilon)}_{m,n} - \Delta_{m,n}\right)} = -1, \tag{5.6}$$

JHEP08(2018)183

for general b. The contribution (5.6) is the only non-zero term in H_{mn}, which is itself the only non-zero H_i. This contribution $H_{mn} = -1$ at level mn corresponds to removing the null state. From equation (4.11), you can see that the expansion is (keeping only the non-zero terms),

$$\begin{aligned}\mathcal{F}(\boldsymbol{\Delta}\,|\,q) = 1 + \cdots + (p_{mn} - 1)\; q^{mn} + (p_{mn+1} - 1)\; q^{mn+1} \\ + \cdots + (p_{mn+N} - p_N)\; q^{mn+N} + \cdots\end{aligned} \tag{5.7}$$

This corresponds to quotienting out the module of the null state.We observe that the condition $\epsilon' = \epsilon$, providing the character of a degenerate representation $\mathcal{V}_{m,n}$, assures that the Coulomb gas fusion condition $\alpha_{\text{int}} + \alpha_{\text{int}} = \alpha_{\text{ext}}$ is satisfied for any value of ϵ.

5.3 Characters in minimal models

In the case of the minimal models, $b^2 = -\frac{p'}{p}$, where p and p' are coprime positive integers, $0 < p < p'$, we know that a fully-degenerate highest-weight module $\mathcal{V}_{m,n}$ has a null-state at level mn, and another at level $(p-m)(p'-n)$. We need first to solve the new poles appearing in the term $H_{m'n'} = \frac{R^{\text{tor}}_{m',n'}(2\epsilon)}{\left(\Delta^{(\epsilon')}_{m,n} - \Delta_{m',n'}\right)}$, where $\Delta^{(\epsilon')}_{m,n}$ is defined in (5.3), $0 < m < p$ and $0 < n < p'$, and $m' = p - m$, and $n' = p' - n$.

5.3.1 The regularization ϵ''

We introduce a third regularization parameter ϵ'' to move away from the minimal model point by setting

$$b = \sqrt{-\frac{p'}{p}\,(1 + \epsilon'')} \tag{5.8}$$

For $\epsilon, \epsilon', \epsilon'' \ll 1$,

$$\frac{R^{\text{tor}}_{m',n'}(2\epsilon)}{\left(\Delta^{(\epsilon')}_{m,n} - \Delta_{m',n'}\right)} = -\frac{\epsilon + \mathcal{O}\left(\epsilon^2\right)}{-\epsilon' + \frac{1}{2}\sqrt{-pp'}\,\epsilon'' + \mathcal{O}\left(\epsilon'^2, \epsilon''^2, \epsilon'\,\epsilon''\right)} \tag{5.9}$$

Again, the final result depends on how we approach the point $(\epsilon, \epsilon', \epsilon'') = (0,0,0)$. In order to obtain the minimal model character we have first to remove the null state at level $(p-m)(p'-n)$. This is obtained by setting,

$$\epsilon' \to \epsilon, \quad \epsilon'' \to \frac{4}{\sqrt{-p\,p'}}\epsilon, \tag{5.10}$$

and taking the limit $\epsilon \to 0$. Then both (5.6) and,

$$\lim_{\epsilon \to 0} \frac{R^{\text{tor}}_{m',n'}(2\epsilon)}{\left(\Delta^{(\epsilon)}_{m,n} - \Delta_{m',n'}\right)} = -1, \tag{5.11}$$

are satisfied at the same time. The results (5.6) and (5.11) are not sufficient to prove that one obtains in the limit the minimal model character. One has to consider that there are

JHEP08(2018)183

other terms, of the form,

$$\frac{R^{\rm tor}_{m_1,n_1}(2\epsilon)}{\left(\Delta^{(\epsilon)}_{m_1,n_1}-\Delta_{m_1,n_1}\right)}\frac{R^{\rm tor}_{m_2,n_2}(2\epsilon)}{(\Delta_{-m_1,n_1}-\Delta_{m_2,n_2})}, \tag{5.12}$$

that will contribute when "resonances" in the conformal dimension, such as $\Delta_{-m_1,n_1} = \Delta_{m_2,n_2}$, occur. The fact that there is an infinite number of resonances, or equivalently, infinitely-many pairs (r,s) that correspond to the same conformal dimension $\Delta_{r,s}$, and that the recursion relation expression for H_N includes all resonances (r,s) such that $rs \leqslant N$ will thus play an important role. We are now in the position to give the exact contribution of all the terms which do not vanish in the limit $\epsilon \to 0$ (see appendix B for the derivation of the following results). In the following we always assume that the integers (m,n) belong to the minimal model $\mathcal{M}_{p,p'}$ Kac table, $0 < m < p$, $0 < n < p'$. Concerning the terms in the recursion that have at the denominator the dimension of the internal field $\Delta^{(\epsilon)}_{m,n}$, we show in appendix B that,

$$\text{if}\,(m,n) \leftrightarrow (r,s)^{\pm}_{l} \implies \lim_{\epsilon\to 0}\frac{R^{\rm tor}_{r,s}(2\epsilon)}{\Delta^{(\epsilon)}_{m,n}-\Delta_{r,s}} = -\frac{1}{2^{2l-1\pm 1}(2l\pm 1)}\prod_{k=1}^{l-\frac{1}{2}\pm\frac{1}{2}}\frac{4k^2-1}{k^2} \tag{5.13}$$

We consider now the terms of the type $R^{\rm tor}_{r,s}(2\epsilon)\,/\left(\Delta_{m',-n'}-\Delta_{r,s}\right)$. We define two integers (l_1,l_2) from the Euclidean division of (r,s), $(r,s) = (l_1 p + m,\ l_2 p' + n)$. We have,

$$\begin{aligned}&\text{if}\left(m',-n'\right) \leftrightarrow (r,s)^{\pm}_{l'} \implies\\ &\lim_{\epsilon\to 0}\frac{R^{\rm tor}_{r,s}}{\Delta_{m',-n'}-\Delta_{r,s}} = -\frac{1}{2^{2\,l+1}\,l'}\prod_{k=1}^{l}\frac{4k^2-1}{k^2},\quad l=\min(l_1,l_2)\end{aligned} \tag{5.14}$$

We will provide below the complete combinatorial structure of all the terms that contribute to the character. All these terms are finite, but they are fractional and add up to integral values.

5.4 Example 1. The Ising model, $(p',p) = (4,3)$, $(m,n) = (1,1)$

We give here an explicit application of the previous formulas to the identity character of the $\mathcal{M}_{4,3}$ minimal model. We set $\alpha_{est} = 2\epsilon$, $\alpha_{\rm int} = \epsilon$ and $b = b^{\epsilon}$ given by (5.10).

$$\begin{aligned}H_1 &= \frac{R^{\rm tor}_{1,1}(2\epsilon)}{\left(\Delta^{(\epsilon)}_{1,1}-\Delta_{1,1}\right)},\quad \lim_{\epsilon\to 0}H_1 = -1,\quad H_6 = \frac{R^{\rm tor}_{2,3}(2\epsilon)}{\left(\Delta^{(\epsilon)}_{1,1}-\Delta_{2,3}\right)},\quad \lim_{\epsilon\to 0}H_6 = -1\\ H_{11} &= \frac{R^{\rm tor}_{1,1}(2\epsilon)}{\left(\Delta^{(\epsilon)}_{1,1}-\Delta_{1,1}\right)}\frac{R^{\rm tor}_{2,5}(2\epsilon)}{(\Delta_{1,-1}-\Delta_{2,5})} + \frac{R^{\rm tor}_{2,3}(2\epsilon)}{\left(\Delta^{(\epsilon)}_{1,1}-\Delta_{2,3}\right)}\frac{R^{\rm tor}_{5,1}(2\epsilon)}{(\Delta_{2,-3}-\Delta_{5,1})}\end{aligned} \tag{5.15}$$

Using the fact that $(1,1)$ and $(2,3)$ are in the Kac table and that $(1,-1) \to (2,5)^{-}_{1}$, $(2,-3) \to (5,1)^{+}_{1}$, one has from (5.13) and (5.14),

$$\lim_{\epsilon\to 0}H_{11} = \left(-1\times -\frac{1}{2}\right)+\left(-1\times -\frac{1}{2}\right) = 1 \tag{5.16}$$

$$H_{13} = \frac{R^{\rm tor}_{1,1}(2\epsilon)}{\left(\Delta^{(\epsilon)}_{1,1}-\Delta_{1,1}\right)}\frac{R^{\rm tor}_{4,3}(2\epsilon)}{(\Delta_{-1,1}-\Delta_{4,3})} + \frac{R^{\rm tor}_{2,3}(2\epsilon)}{\left(\Delta^{(\epsilon)}_{1,1}-\Delta_{2,3}\right)}\frac{R_{1,7}{}^{\rm tor}(2\epsilon)}{(\Delta_{2,-3}-\Delta_{1,7})} \tag{5.17}$$

From $(1,-1) \to (4,3)_1^+$, $(2,-3) \to (1,7)_1^-$

$$\lim_{\epsilon\to 0} H_{13} = \left(-1 \times -\frac{1}{2}\right) + \left(-1 \times -\frac{1}{2}\right) = 1, \tag{5.18}$$

These two terms correspond to adding again the null states at level 11 and 13, which are contained into the modules of both the null states at level 1 and 6, and were therefore subtracted twice. Let us make another example at level 20,

$$\begin{aligned} H_{20} = & \frac{R^{\text{tor}}_{1,1}(2\epsilon)}{\left(\Delta^{(\epsilon)}_{1,1} - \Delta_{1,1}\right)} \frac{R^{\text{tor}}_{4,3}(2\epsilon)}{(\Delta_{1,-1} - \Delta_{4,3})} \frac{R^{\text{tor}}_{7,1}(2\epsilon)}{(\Delta_{4,-3} - \Delta_{7,1})} \\ & + \frac{R^{\text{tor}}_{1,1}(2\epsilon)}{\left(\Delta^{(\epsilon)}_{1,1} - \Delta_{1,1}\right)} \frac{R^{\text{tor}}_{2,5}(2\epsilon)}{(\Delta_{1,-1} - \Delta_{2,5})} \frac{R^{\text{tor}}_{1,9}(2\epsilon)}{(\Delta_{2,-5} - \Delta_{1,9})} \\ & + \frac{R^{\text{tor}}_{2,3}(2\epsilon)}{\left(\Delta^{(\epsilon)}_{1,1} - \Delta_{2,3}\right)} \frac{R^{\text{tor}}_{5,1}(2\epsilon)}{(\Delta_{2,-3} - \Delta_{5,1})} \frac{R^{\text{tor}}_{1,9}(2\epsilon)}{(\Delta_{5,-1} - \Delta_{1,9})} \\ & + \frac{R^{\text{tor}}_{2,3}(2\epsilon)}{\left(\Delta^{(\epsilon)}_{1,1} - \Delta_{2,3}\right)} \frac{R^{\text{tor}}_{1,7}(2\epsilon)}{(\Delta_{2,-3} - \Delta_{1,7})} \frac{R^{\text{tor}}_{7,1}(2\epsilon)}{(\Delta_{1,-7} - \Delta_{7,1})} + \frac{R^{\text{tor}}_{4,5}(2\epsilon)}{\left(\Delta^{(\epsilon)}_{1,1} - \Delta_{4,5}\right)} \end{aligned} \tag{5.19}$$

From (5.13) and (5.14),

$$\begin{aligned} \lim_{\epsilon\to 0} H_{20} = & \left(-1 \times -\frac{1}{2} \times -\frac{1}{2}\right) + \left(-1 \times -\frac{1}{2} \times -\frac{1}{2}\right) \\ & + \left(-1 \times -\frac{1}{2} \times -\frac{1}{4}\right) + \left(-1 \times -\frac{1}{2} \times -\frac{1}{4}\right) - \frac{1}{4} = -1 \end{aligned} \tag{5.20}$$

Notice that this sum of terms which add up to an integer has exactly the same structure as equation (3.18).

5.5 General case

We consider the character of a representation indexed by (m,n), $0 < m < p$, $0 < n < p'$. We provide here the explicit procedure to find all the terms that, in the limit (5.10), have a finite fraction contribution that sums up, at a given level, to 1 or -1. We want to give a procedure that takes into account all the singular terms appearing in the one-point torus recursion relation in the minimal model limit. Given a pair of indices (m,n), we want to find the set of pairs (r,s), that are resonant with $(m,-n)$, $(m,-n) \leftrightarrow (r,s)_l^+$, or with $(-m,n)$, $(-m,n) \leftrightarrow (r,s)_l^+$, where we used the notation defined in (2.13). These pairs are obtained respectively by the two transformations,

$$v_1^{(l)}: \quad (m,n) \to \big(r = lp + m, s = lp' - n\big) \quad (m,-n) \leftrightarrow (r,s)_l^+ \tag{5.21}$$

$$v_2^{(l)}: \quad (m,n) \to \big(r = lp - m, s = lp' + n\big) \quad (-m,n) \leftrightarrow (r,s)_l^+ \tag{5.22}$$

JHEP08(2018)183

By using these transformations we generate the following diagram,

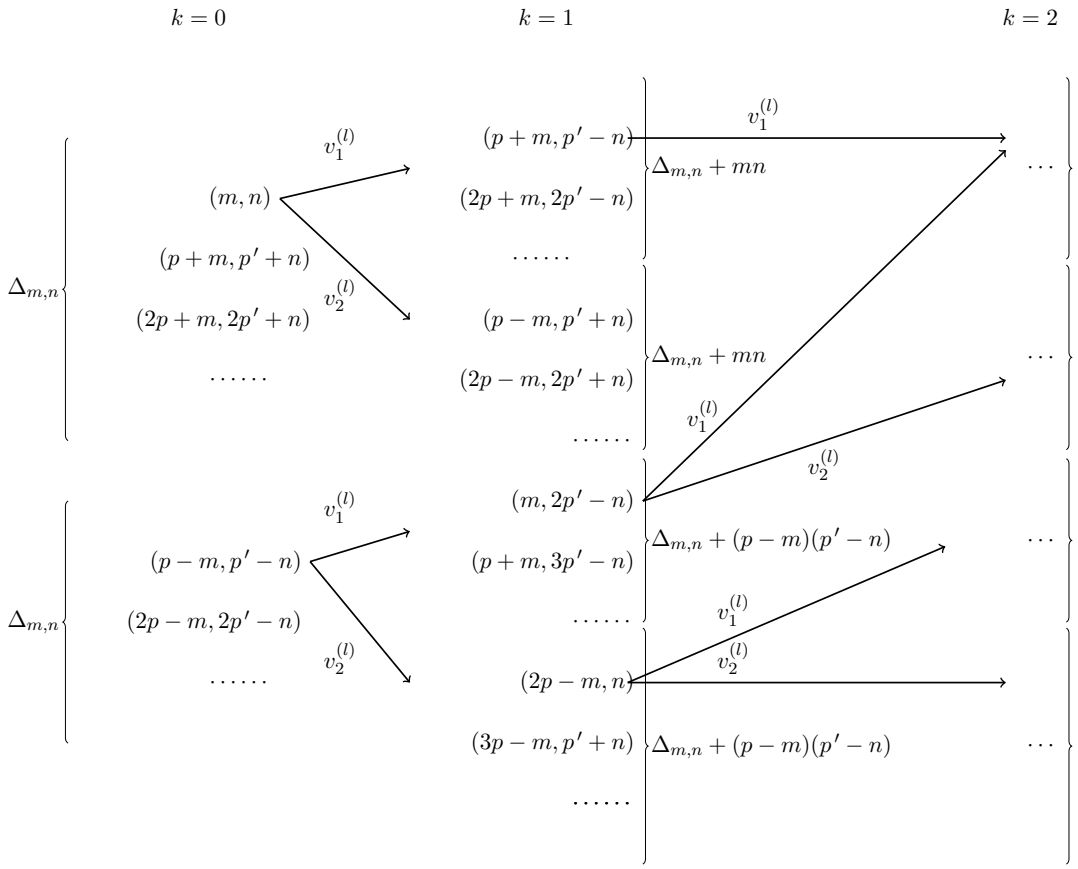

In the $k=0$ column, we place the two groups of pairs, (r,s), which are resonant with (m,n), $(m,n) \leftrightarrow (r,s)_l^+$ and $(m,n) \leftrightarrow (r,s)_l^-$. The column $k=1$ is generated by applying the transformations $v_1^{(l)}$ and $v_2^{(l)}$ to (m,n) and $(p'-m,p-n)$. One obtains four families, corresponding to the two set of pairs (r,s) resonant with $(m,-n)$, $(m,-n) \leftrightarrow (r,s)_l^+$ and $(m,-n) \leftrightarrow (r,s)_l^-$ and associated to representation with dimension $\Delta_{m,n}+mn$, plus the two sets of pairs in resonance with $(p-m,n-p')$, $(p-m,n-p') \leftrightarrow (r,s)_l^+$ and $(p-m,n-p') \leftrightarrow (r,s)_l^-$ and associated to representation with dimension $\Delta_{m,n}+(p'-m)(p-n)$. The column $k=2$ is obtained by applying the transformations $v_1^{(l)}$ and $v_2^{(l)}$ to $(p+m,p'-n)$, $(p-m,p'+n)$, $(m,2p'-n)$ and $(2p-m,n)$ and so on. At each column one can therefore identify four families of pairs that we indicate with the letters U^1,D^1 and U^2,D^2. Any pair of indices appearing in the diagram is identified by its family and by two non-negative integers k and l, indicating respectively the column and the position in the interior of each family,

$$U^1(k,l) \to \left((k+l)p+m,(-1)^k n+lp'+\frac{1-(-1)^k}{2}p'\right)$$
$$D^1(k,l) \to \left((1+l)p-m,(-1)^{k+1} n+(l+k)p'+\frac{1-(-1)^{k+1}}{2}p'\right)$$

JHEP08(2018)183

$$
\begin{aligned}
U^2(k,l) &\to \left(lp+m, (-1)^k n + (l+k)p' + \frac{1-(-1)^k}{2}p'\right) \\
D^2(k,l) &\to \left((1+l+k)p-m, (-1)^{k+1} n + lp' + \frac{1-(-1)^{k+1}}{2}p'\right)
\end{aligned} \tag{5.23}
$$

It is straightforward to obtain the action of the transformations $v_1^{(l)}$ and $v_2^{(l)}$ on each index,

$$
\begin{aligned}
v_1^{(l')} &: U^1(k,l) \to U^1(k+2l+1,l'), \qquad & U^2(k,l) &\to U^1(k+2l+1,l') \\
v_1^{(l')} &: D^1(k,l) \to D^2(k+2l+1,l'), \qquad & D^2(k,l) &\to D^2(k+2l+1,l') \\
v_2^{(l')} &: U^1(k,l) \to D^1(k+2l+1,l'), \qquad & U^2(k,l) &\to D^1(k+2l+1,l') \\
v_2^{(l')} &: D^1(k,l) \to U^2(k+2l+1,l'), \qquad & D^2(k,l) &\to U^2(k+2l+1,l').
\end{aligned} \tag{5.24}
$$

The above rules allow to write the chains of resonant terms in the recursion relation in terms of words formed by the letters $U^{1,2}$ and $D^{1,2}$, whose sequences have to satisfy the connections above. For instance, the terms in the example in (5.19), correspond to the following words,

$$
\begin{aligned}
&U^1(0,0)U^1(1,0)U^1(2,0) \\
&U^1(0,0)D^1(1,0)U^2(2,0) \\
&D^1(0,0)D^2(1,0)U^2(2,0) \\
&D^1(0,0)U^2(1,0)U^1(2,0) \\
&U^1(0,1)
\end{aligned}
$$

As seen in this example, the words corresponding to a certain level N will all end either with U or with D. The reason is that the last arrows of the chains must point to the same dimension, so they must all point either to the 1 sector or all point to the 2 sector. From (5.24), all U labels transform to a label in the 1 sector, while all D labels transform to labels in the 2 sector. Since there always exists either a $U^1(0,0)U^1(1,0)\cdots U^1(K,0)$ or a $D^2(0,0)D^2(1,0)\cdots D^2(K,0)$ chain, of length $K+1$, the level N is either,

$$
N_U(K) = \sum_{k=0}^{K} (kp+m)\left((-1)^k n + \left(1-(-1)^k\right)\frac{p'}{2}\right), \tag{5.25}
$$

or

$$
N_D(K) = \sum_{k=0}^{K} ((k+1)p-m)\left((-1)^{k+1} n + \left(1-(-1)^{k+1}\right)\frac{p'}{2}\right) \tag{5.26}
$$

Then, the contribution of each word is obtained by using formulas (5.13) and (5.14). For instance,

$$
\begin{aligned}
U^1(k_1,l_1)U^1(k_1+2l_1+1,l_2) &\to \lim_{\epsilon\to 0} \frac{R^{\text{tor}}_{r_2,s_2}(2\epsilon)}{\Delta_{r_1,-s_1}-\Delta_{r_2,s_2}}, \\
\textit{with} \quad (r_1,s_1) &= U^1(k_1,l_1), \quad (r_2,s_2) = U^1(k_1+2l_1+1,l_2)
\end{aligned} \tag{5.27}
$$

JHEP08(2018)183

Applying (5.14) with $l' = l_1 + l_2 + 1$ and $l = l_2$, one has,

$$U^1(k_1, l_1)U^1(k_1 + 2l_1 + 1, l_2) \to -\frac{1}{2^{2l_2+1}(l_1 + l_2 + 1)} \prod_{j=1}^{l_2} \frac{4\lambda^2 - 1}{\lambda^2} \tag{5.28}$$

In the same way, we find,

$$\begin{aligned} U^2(k_1, l_1)D^1(k_1 + 2l_1 + 1, l_2) &= D^1(k_1, l_1)U^2(k_1 + 2l_1 + 1, l_2) \\ &= D^2(k_1, l_1)D^2(k_1 + 2l_1 + 1, l_2) \\ &= U^1(k_1, l_1)U^1(k_1 + 2l_1 + 1) \\ &= -\frac{1}{2^{2l_2+1}(l_1 + l_2 + 1)} \prod_{\lambda=1}^{l_2} \frac{4\lambda^2 - 1}{\lambda^2} \end{aligned} \tag{5.29}$$

and

$$\begin{aligned} U^2(k_1, l_1)U^1(k_1 + 2l_1 + 1) &= D^1(k_1, l_1)D^2(k_1 + 2l_1 + 1, l_2) \\ &= D^2(k_1, l_1)U^2(k_1 + 2l_1 + 1, l_2) \\ &= U^1(k_1, l_1)D^1(k_1 + 2l_1 + 1, l_2) \\ &= -\frac{1}{2^{2l_2+1}(k_1 + l_1 + l_2 + 1)} \prod_{\lambda=1}^{l_2} \frac{4\lambda^2 - 1}{\lambda^2} \end{aligned} \tag{5.30}$$

The non-trivial contribution at level $N(K)$ is given by all possible chains starting with $U^1(0, l_0)$ or $D^1(0, l_0)$, with constraint on the last terms: U^1 or U^2 if $N = N_1$, D^1 or D^2 if $N = N_2$. Note that given equalities (5.29) and (5.30), for fixed K and fixed $\{l_i\}$, the contributions at levels $N_1(K)$ and $N_2(K)$ are equal. Therefore, to compute the contribution at level $N_1(K)$ (resp. at level $N_2(K)$), instead of constraining the chains to end by U (resp. D), we can leave the ends of the chains free and divide by 2 at the end. The first terms of the chains involve the internal dimension $\Delta^{\epsilon}_{m,n}$,

$$\begin{aligned} U^1(0, l_0) &= \frac{R^{\text{tor}}_{l_0 p+m, l_0 p'+n}}{\Delta^{\epsilon}_{m,n} - \Delta_{l_0 p+m, l_0 p'+n}} = -\frac{1}{2^{2l_0}(2l_0 + 1)} \prod_{\lambda=1}^{l_0} \frac{4\lambda^2 - 1}{\lambda^2}, \\ D^1(0, l_0) &= \frac{R^{\text{tor}}_{(l_0+1)p-m, (l_0+1)p'-n}}{\Delta^{\epsilon}_{m,n} - \Delta_{(l_0+1)p-m, (l_0+1)p'-n}} = -\frac{1}{2^{2l_0}(2l_0 + 1)} \prod_{\lambda=1}^{l_0} \frac{4\lambda^2 - 1}{\lambda^2} \end{aligned} \tag{5.31}$$

We now need to specify the set $\{l_i\}$. Let us denote I the cardinal of this set. We then have the constraint,

$$I + \sum_{i=0}^{I-1} 2l_i = K + 1 \tag{5.32}$$

By writing $I = K + 1 - 2a$, the constraint is,

$$\sum_{i=0}^{K-2a} l_i = a, \tag{5.33}$$

JHEP08(2018)183

and the set $\{l_0, l_1, \cdots, l_{K-2a}\}$ is therefore a partition of size $K-2a+1$ of the integer a, $\{l_0, l_1, \cdots, l_{K-2a}\} = \tilde{p}_{K-2a+1}(a)$ in which zeroes are included, as well as all permutations. For example the set of the partitions of size 3 of 3 is,

$$\{(3,0,0),(0,3,0),(2,1,0),(2,0,1),(1,2,0),(1,0,2),(0,1,2),(0,2,1),(1,1,1)\}. \tag{5.34}$$

a then runs from 0 to a maximal a. If K is odd, $K+1$ is even and $I_{\min} = K+1-2a_{\max}$ is even. Therefore $I_{\min} = 2$, and $a_{\max} = (K-1)/2$. If K is even, $K+1$ is odd and $I_{\min} = K+1-2a_{\max}$ is odd and equals 1. Therefore $a_{\max} = K/2$ and $l_0 = a_{\max}$, all other l_i being 0, and this chain consists of the single term (5.31). We can now give the final formula for the contribution $C_{N(K)}$ that takes into account all the non-zero terms at a given level $N(K)$,

$$\begin{aligned} C_{N(K)} = \frac{1}{2} \sum_{a=0}^{[\frac{K-1}{2}]} & \sum_{\{l_0,\cdots,l_{K-2a}\}=\tilde{p}_{K-2a+1}(a)} \sum_{\{X_0,\cdots,X_{K-2a}\}} X_0\left(0,l_0\right) \\ & \times \prod_{j=0}^{K-1-2a} X_j\left(2\sum_{i=0}^{j-1} l_i + j, l_j\right) X_{j+1}\left(2\sum_{i=0}^{j} l_i + j + 1, l_{j+1}\right) \\ & + \delta_{K(\text{mod }2),0} X_0\left(0, K/2\right), \end{aligned} \tag{5.35}$$

where the $X_{j>1}$'s are $U^{1,2}$ or $D^{1,2}$, X_0 is U^1 or D^1. From (5.29), (5.30) and (5.31),

$$\begin{aligned} C_{N(K)} = & -\delta_{K(\text{mod }2),0} \frac{\prod_{\lambda=1}^{K/2} \frac{4\lambda^2-1}{\lambda^2}}{2^K(K+1)} + \sum_{a=0}^{[\frac{K-1}{2}]} \sum_{\{l_0,\ldots,l_{K-2a}\}=\tilde{p}_{K-2a+1}(a)} -\frac{\prod_{\lambda=1}^{l_0} \frac{4\lambda^2-1}{\lambda^2}}{2^{2l_0}(2l_0+1)} \\ & \times \prod_{j=0}^{K-1-2a} -\frac{\prod_{\lambda=1}^{l_{j+1}} \frac{4\lambda^2-1}{\lambda^2}}{2^{2l_{j+1}+1}} \left(\frac{1}{l_j + l_{j+1} + 1} + \frac{1}{l_j + l_{j+1} + 1 + 2\sum_{i=0}^{j-1} l_i + j}\right). \end{aligned} \tag{5.36}$$

We have checked numerically — up to order $N \sim 300$ — that $C_{N(K)} = (-1)^{K+1}$.

6 Conclusions

We extended Zamolodchikov's elliptic recursion relation for 4-point conformal blocks on the sphere [15], and its analogue for 1-point functions on the torus [3, 10], originally derived for conformal blocks in Liouville theory with non-rational central charge, to conformal field theories with rational central charges, including the generalized minimal and minimal models. When the central charge is rational, solutions of the recursion relation have additional poles that appear on a term by term basis. These poles are non physical in the sense that they are artifacts of the recursion which splits perfectly well-defined terms into terms that can be singular on their own but add up to finite contributions. We studied the structure

JHEP08(2018)183

of these non physical poles in two situations. **1.** In 4-point conformal blocks on the sphere, where we found that the singular terms add up to finite terms on the basis of examples, and conjectured that this is the case in general, and that regularizing properly all the parameters entering the conformal block, one obtains the minimal model conformal block. **2.** In 1-point conformal blocks on the torus, in the limit where the vertex operator insertion is the identity operator and the 1-point conformal block reduces to a 0-point conformal block, which is a Virasoro character. In this case, the contributions of the non-physical poles are fractions, and explicit expressions of these fractions were derived in (5.13) and (5.14). We unveiled the combinatorial structure of these fractions found it to be reminiscent of that in the Feigin-Fuks construction of minimal model characters [4], and used it to show that the contribution of the non-physical poles add up to ± 1. The non-physical poles of the 4-point conformal blocks also follow this combinatorial structure. A fine regularization of the central charge is needed in the case of the 0-point functions, whereas the 4-point function is not sensitive to the regularization used.

Acknowledgments

We thank Kenji Iohara, Santiago Migliaccio, Rubik Poghossian and Sylvain Ribault for discussions. OF wishes to thank Profs K Lechner, M Matone and D Sorokin for hospitality in the Physics Department, University of Padova, while this work was in progress, and the organizers of "*Supersymmetric Quantum Field Theories in the Non-perturbative Regime*", and Prof A Dabholkar for hospitality at the Galileo Galilei Institute for Theoretical Physics, Arcetri, Firenze, Italy, and at the Abdus Salam Center for Theoretical Physics, Trieste, respectively, where it was finalized. OF is supported by a Special Studies Program grant from the Faculty of Science, University of Melbourne, and the Australian Research Council.

A A direct computation at $c = -2$

At $c = -2$, which we can consider as the $\mathcal{M}(2,1)$ minimal model, the first extra pole appear at order 3 in the expansion of the conformal block. It is therefore possible to compare the recursion result to the result one gets by hand, ie by computing the Shapovalov matrix of inner products and the "matrix elements",

$$\begin{aligned} &\langle L_{-Y}\Delta|\Phi_{\Delta_1}(x)\Phi_{\Delta_2}(0)\rangle/\langle\Delta|\Phi_{\Delta_1}(x)\Phi_{\Delta_2}(0)\rangle, \\ &\langle\Phi_{\Delta_3}(1)\Phi_{\Delta_4}(\infty)|L_{-Y'}\Delta\rangle/\langle\Phi_{\Delta_3}(1)\Phi_{\Delta_4}(\infty)|\Delta\rangle \end{aligned} \tag{A.1}$$

which appear in (3.3). In the basis $\{L_{-1}^3|\Delta\rangle, L_{-1}|Q_2\rangle, |Q_3\rangle\}$ where,

$$\begin{aligned} |Q_2\rangle &= \left(L_{-1}^2 - \frac{2(2\Delta+1)}{3}L_{-2}\right)|\Delta\rangle, \\ |Q_3\rangle &= \left(L_{-1}^3 - 2(\Delta+1)L_{-2}L_{-1} + \Delta(\Delta+1)L_{-3}\right)|\Delta\rangle \end{aligned} \tag{A.2}$$

are the quasi-primary states at levels 2 and 3, the Shapovalov matrix at level 3 is diagonal,

$$\begin{aligned} S_{(3)} = \mathrm{diag}\,(&24\Delta(\Delta+1)(2\Delta+1),\\ &\frac{64}{9}(\Delta+2)(2\Delta+1)(\Delta-\Delta_{1,2})(\Delta-\Delta_{2,1}),\\ &6\Delta(\Delta+1)(\Delta+2)(\Delta-\Delta_{1,3})(\Delta-\Delta_{3,1})) \end{aligned} \tag{A.3}$$

Then the contribution of the quasi-primary at level 3 is,

$$\frac{P_L\,(Q_3\,;\,\Delta_1,\Delta_2)\,P_R\,(Q_3\,;\,\Delta_3,\Delta_4)}{\langle Q_3|Q_3\rangle} = \frac{\mathcal{P}_2\,(\Delta\,;\,\Delta_i)}{6\Delta(\Delta+1)(\Delta+2)(\Delta-\Delta_{1,3})(\Delta-\Delta_{3,1})} \tag{A.4}$$

where $\mathcal{P}_2\,(\Delta\,;\,\Delta_i)$ is a polynomial of order 2 in the internal dimension Δ:

$$\begin{aligned} \mathcal{P}_2\,(\Delta\,;\,\Delta_i) = &(\Delta_1-\Delta_2)(\Delta_3-\Delta_4)(\Delta_1+\Delta_2-1)(\Delta_3+\Delta_4-1)\Delta^2\\ &+(\Delta_1-\Delta_2)(\Delta_3-\Delta_4)\Big\{\,(1-(\Delta_1+\Delta_2))\left((\Delta_3-\Delta_4)^2-(\Delta_3+\Delta_4)\right)\\ &+(1-(\Delta_3+\Delta_4))\left((\Delta_1-\Delta_2)^2-(\Delta_1+\Delta_2)\right)\Big\}\Delta\\ &+(\Delta_1-\Delta_2)(\Delta_3-\Delta_4)\left((\Delta_1-\Delta_2)^2-(\Delta_1+\Delta_2)\right)\\ &\times\left((\Delta_3-\Delta_4)^2-(\Delta_3+\Delta_4)\right) \end{aligned} \tag{A.5}$$

When $c=-2$, we have,

$$\Delta_{1,3}=0,\quad \Delta_{3,1}=3, \tag{A.6}$$

and the contribution (A.4) of $|Q_3\rangle$ is well-defined. However, if we decompose it in partial fractions,

$$\frac{\langle Q_3|\Phi_{\Delta_1}(0)|\Delta_2\rangle\langle\Delta_3|\Phi_{\Delta_4}(\infty)|Q_3\rangle}{\langle Q_3|Q_3\rangle} = \frac{A}{\Delta-\Delta_{1,1}}+\frac{B}{\Delta-\Delta_{1,3}}+\frac{C}{\Delta-\Delta_{3,1}}+\frac{A\Delta+D}{(\Delta+1)(\Delta+2)}, \tag{A.7}$$

we find,

$$\begin{aligned} A &= \frac{f_{1,1}\,(\Delta_1,\Delta_2)\,f_{1,1}\,(\Delta_3,\Delta_4)}{2\Delta_{1,3}\Delta_{3,1}},\\ B &= \frac{f_{1,3}\,(\Delta_1,\Delta_2)\,f_{1,3}\,(\Delta_3,\Delta_4)}{\Delta_{1,3}(\Delta_{1,3}-\Delta_{3,1})(1+\Delta_{1,3})(2+\Delta_{1,3})},\\ C &= \frac{f_{3,1}\,(\Delta_1,\Delta_2)\,f_{3,1}\,(\Delta_3,\Delta_4)}{\Delta_{3,1}(\Delta_{1,3}-\Delta_{3,1})(1+\Delta_{3,1})(2+\Delta_{3,1})}, \end{aligned} \tag{A.8}$$

where we defined the function,

$$f_{r,s}\,(\Delta_i,\Delta_j) = (\Delta_i-\Delta_j)\left((\Delta_i-\Delta_j)^2-(\Delta_i+\Delta_j)(1+\Delta_{r,s})+\Delta_{r,s}\right) \tag{A.9}$$

Notice that given equations (A.6), A and B become singular for $c=-2$. In fact we have,

$$\lim_{c\to-2} A \propto \frac{R_{1,1}(\Delta_i)R_{2,1}(\Delta_i)}{\Delta_{1,-1}-\Delta_{2,1}},\quad \lim_{c\to-2} B \propto R_{1,3}(\Delta_i),\quad \lim_{c\to-2} C \propto R_{3,1}(\Delta_i) \tag{A.10}$$

A and B are the terms that add to a finite contribution. In that sense, the extra poles are artifacts of the recursion relation rewrites a well-defined quantity as a sum of terms that are individually singular.

JHEP08(2018)183

B About $R^{\text{tor}}_{m,n}$

We prove that

$$R^{\text{tor}}_{m,n}(2\epsilon) = -\epsilon\left(mb + nb^{-1}\right) + \mathcal{O}\left(\epsilon^2\right), \tag{B.1}$$

for general b and for all (m,n).

$$\begin{aligned} R^{\text{tor}}_{m,n}(\alpha) &= \frac{1}{4r_{m,n}} \prod_{k,l} \left(\frac{1-k}{2}\, b + \frac{1-l}{2}\, b^{-1} - \alpha \right), \\ & k = 1-2m, 3-2m, \cdots, 2m-1, \quad l = 1-2n, 3-2n, \cdots, 2n-1 \end{aligned} \tag{B.2}$$

and,

$$\begin{aligned} r_{m,n} =& -\frac{1}{2} \prod_{\rho,\sigma} 2\lambda_{\rho,\sigma}, \\ & \rho = 1-m, 2-m, \cdots, m, \quad \sigma = 1-n, 2-n, \cdots, n, \quad (\rho,\sigma) \neq (0,0),\ (m,n) \end{aligned} \tag{B.3}$$

which can be rewritten as,

$$r_{m,n} = \frac{1}{2} \prod_{i=1-m}^{m} \prod_{j=1-n}^{n} \left(i\, b + j\, b^{-1}\right), \quad (i,j) \neq (0,0), \quad (i,j) \neq (m,n), \tag{B.4}$$

When the inserted operator is the identity, $\alpha = 2\epsilon$, we get,

$$R^{\text{tor}}_{m,n} = -\frac{\epsilon}{\prod_{ij}\left(i\, b + j\, b'\right)} \prod_{(k,l)\neq(1,1)} \left(\frac{1-k}{2}\, b + \frac{1-l}{2}\, b^{-1} \right) + \mathcal{O}\left(\epsilon^2\right) \tag{B.5}$$

We can call $\rho = \frac{1-k}{2}$ and $\sigma = \frac{1-l}{2}$, then ρ goes from $1-m, 2-m, \cdots, m$ and σ from $1-n, 2-n, \cdots, n$. $(k,l) \neq (1,1) \Leftrightarrow (\rho,\sigma) \neq (0,0)$ and we get,

$$\begin{aligned} R^{\text{tor}}_{m,n} =& -\epsilon \left(\prod_{(i,j)\neq(0,0),(i,j)\neq(m,n)} \left(ib + \frac{j}{b} \right) \right)^{-1} \left(\prod_{(\rho,\sigma)\neq(0,0)} \left(\rho b + \frac{\sigma}{b} \right) + \mathcal{O}\left(\epsilon^2\right) \right) \\ =& -\epsilon\left(m\, b + n\, b'\right) + \mathcal{O}\left(\epsilon^2\right) \end{aligned} \tag{B.6}$$

This also implies that,

$$\lim_{\epsilon\to 0} \frac{R_{m,n}(2\epsilon)}{\epsilon\left(mb + nb^{-1}\right)} = -1 \tag{B.7}$$

for all b, for all (m,n). When $c \in \mathbb{Q}$, it can happen that the denominator $r_{m,n}$ vanishes. We will show that the coefficients $R_{m,n}(2\epsilon)$ are always well-defined and express them in closed form. Let's first examine the space (m,n) for which $r_{m,n} \sim \epsilon^d$. Let us start with the case $d = 1$. $r_{m,n} = \epsilon \Rightarrow \exists (i_1, j_1)$ such that,

$$b^2 = -\frac{j_1}{i_1}, \quad 1-m \leqslant i_1 \leqslant m, \quad 1-n \leqslant j_1 \leqslant n, \quad (i_1,j_1) \neq (m,n), \tag{B.8}$$

so that,

$$r_{m,n} = \epsilon, \quad (m,n) \in \{p\}\times]p', \infty[\bigcup]p, \infty[\times\{p'\} \tag{B.9}$$

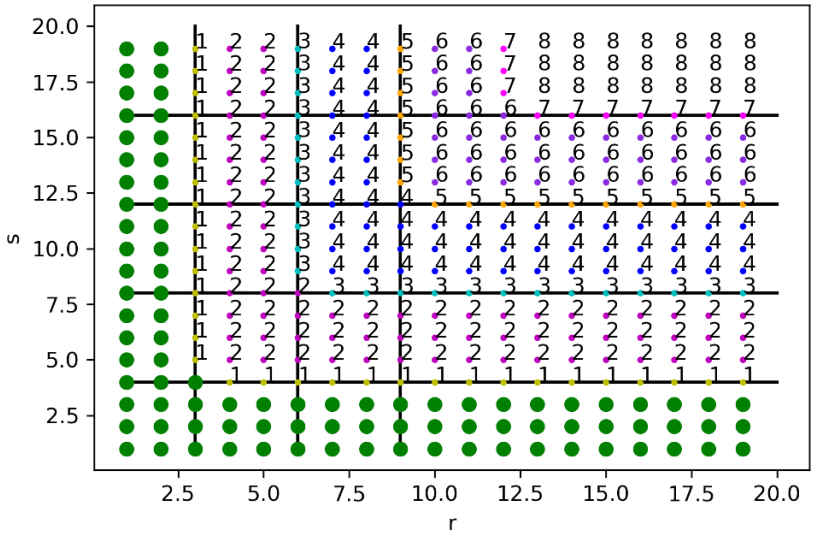

Figure 1. Degree d for the Ising model $p = 4$, $p' = 3$. Green dots are the values for which $D_{m,n} \neq 0$.

In the same way, $r_{m,n} = \epsilon^2 \Rightarrow \exists (i_1, j_1),\ (i_2, j_2)$ such that $b^2 = -\frac{j_1}{i_1} = -\frac{j_2}{i_2}$ with $(i_1, j_1) \neq (i_2, j_2)$, that is, $(i_1, j_1) = (p, p')$ and $(i_2, j_2) = (-p, -p')$, that is,

$$r_{m,n} = \epsilon^2, \quad (m,n) \in]p, \infty[\times]p', 2p'[\bigcup]p, 2p[\times]p', \infty[\tag{B.10}$$

We can generalize to $r_{m,n} = \epsilon^d$.

$$(m,n) \in \left\{\frac{d+1}{2}p\right\} \times]\frac{d+1}{2}p', \infty[\bigcup]\frac{d+1}{2}p, \infty[\times \left\{\frac{d+1}{2}p'\right\} \qquad d \text{ odd} \tag{B.11}$$

$$(m,n) \in]\frac{d}{2}p, \infty[\times]\frac{d}{2}p', \left(\frac{d}{2}+1\right)p'[\bigcup]\frac{d}{2}p, \left(\frac{d}{2}+1\right)p[\times]\frac{d}{2}p', \infty[\qquad d \text{ even} \tag{B.12}$$

This space is shown on figure 1 for the Ising model. Notice that odd d corresponds to the borders of the cells (the fundamental cell being the Kac table). The physical states are not located on the borders, so under the condition that $R^{\text{tor}}_{m,n}(2\epsilon)$ vanishes for odd d, we can restrict only to even d. For even d, the coefficient $R^{\text{tor}}_{m,n}$ is,

$$\begin{aligned} R^{\text{tor}}_{m,n}(2\epsilon) = & -2\epsilon \left(m\sqrt{-\frac{p'}{p}} + \frac{n}{\sqrt{-\frac{p'}{p}}} + \mathcal{O}(\epsilon) \right) \times \prod_{k=1}^{\frac{d}{2}} b^{-1} \left(\pm kpb^2 \pm kp' - 2\epsilon b \right) \\ & \times \prod{}' \left(\rho b + \sigma b^{-1} - 2\epsilon \right) \times \frac{1}{2\prod_{k=1}^{\frac{d}{2}} b^{-1}\left(\pm kpb^2 \pm kp'\right) \times \prod{}'\left(\rho b + \sigma b^{-1}\right)} \end{aligned} \tag{B.13}$$

where $\prod'$ is $\prod_{\rho=1-m}^{m}\prod_{\sigma=1-n}^{n}$ with $(0,0), (m,n)$ and $(\pm kp, \pm kp')$ excluded. Using the regularization for the b,

$$b = \sqrt{-\frac{p'}{p}\left(1 + \frac{4\epsilon}{\sqrt{-pp'}}\right)} \tag{B.14}$$

we have,

$$\pm kpb^2 \pm kp' = \pm 4\epsilon\, k \sqrt{-\frac{p'}{p}} + \mathcal{O}\left(\epsilon^2\right),$$
$$\pm kpb^2 \pm kp' - 2\epsilon b = 2\epsilon \sqrt{-\frac{p'}{p}}\,(\pm 2k-1) + \mathcal{O}\left(\epsilon^2\right) \tag{B.15}$$

which gives,

$$R^{\rm tor}_{m,n}(2\epsilon) = -\epsilon\left(m\sqrt{-\frac{p'}{p}} + \frac{n}{\sqrt{-\frac{p'}{p}}}\right) \times \frac{1}{2^d}\prod_{k=1}^{\frac{d}{2}} \frac{4k^2-1}{k^2} + \mathcal{O}\left(\epsilon^2\right) \tag{B.16}$$

for all (m,n) and d. For given (m,n), we can write $m = l_m p + m_0$, $n = l_n p' + n_0$ with $0 \leqslant m_0 < p$ and $0 \leqslant n_0 < p'$. Then,

$$d = 2\min\left(l_m, l_n\right) \equiv 2\,l \tag{B.17}$$

and we can write

$$R^{\rm tor}_{m,n}(2\epsilon) = -\epsilon\left(m\sqrt{-\frac{p'}{p}} + \frac{n}{\sqrt{-\frac{p'}{p}}}\right) \times \frac{1}{2^{2l}}\prod_{k=1}^{l} \frac{4k^2-1}{k^2} + \mathcal{O}\left(\epsilon^2\right) \tag{B.18}$$

$l = \min\left(l_m, l_n\right)$. We need to check that the coefficient also vanishes when d is odd. In that case,

$$\begin{aligned} R^{\rm tor}_{m,n}(2\epsilon) = & -\epsilon\left(m\sqrt{-\frac{p'}{p}} + \frac{n}{\sqrt{-\frac{p'}{p}}} + \mathcal{O}(\epsilon)\right) \times \left(\frac{d+1}{2}pb^2 + \frac{d+1}{2}p' - 2\epsilon b\right) \\ & \times \prod_{k=1}^{\frac{d-1}{2}} b^{-1}\left(\pm kpb^2 \pm kp' - 2\epsilon b\right) \times {\prod}'\left(\rho b + \sigma b^{-1} - 2\epsilon\right) \\ & \times \frac{1}{\left(\frac{d+1}{2}pb^2 + \frac{d+1}{2}p'\right)\prod_{k=1}^{\frac{d-1}{2}} b^{-1}\left(\pm kpb^2 \pm kp'\right) \times {\prod}'\left(\rho b + \sigma b^{-1}\right)} \end{aligned} \tag{B.19}$$

Using equation (B.15) we get,

$$R^{\rm tor}_{m,n}(2\epsilon) = -\epsilon\left(m\sqrt{-\frac{p'}{p}} + \frac{n}{\sqrt{-\frac{p'}{p}}}\right) \frac{d}{2^{d-1}(d+1)}\prod_{k=1}^{\frac{d-1}{2}} \frac{4k^2-1}{k^2} + \mathcal{O}\left(\epsilon^2\right) \tag{B.20}$$

Here $d = 2\min\left(l_m, l_n\right) - 1 \equiv 2\,l - 1$ which yields,

$$R^{\rm tor}_{m,n}(2\epsilon) = -\epsilon\left(m\sqrt{-\frac{p'}{p}} + \frac{n}{\sqrt{-\frac{p'}{p}}}\right) \frac{2l-1}{2^{2l-1}\,l}\prod_{k=1}^{l-1} \frac{4k^2-1}{k^2} + \mathcal{O}\left(\epsilon^2\right) \tag{B.21}$$

JHEP08(2018)183

These terms thus do not contribute in the computation of the character of a physical field. Now we can figure out expressions for the terms in the recursion. The non-vanishing terms that involve $\Delta_{\text{int}} = \Delta^{\epsilon}_{m,n}$ are of the type $\frac{R^{\text{tor}}_{r,s}(2\epsilon)}{\Delta^{\epsilon}_{m,n}-\Delta_{r,s}}$ with $(m,n) \to (r,s)^{\pm}_{l}$ Using the regularization of b, we have,

$$\Delta^{\epsilon}_{m,n} - \Delta_{r,s} = (\pm 2l+1)\left(m\sqrt{-\frac{p'}{p}} + \frac{n}{\sqrt{-\frac{p'}{p}}}\right)\epsilon + \mathcal{O}\left(\epsilon^2\right) \tag{B.22}$$

and using expression (4.9) with $\min(l_r, l_s) = l - \frac{1}{2} \pm \frac{1}{2}$, we get,

$$\lim_{\epsilon\to 0} \frac{R^{\text{tor}}_{r,s}(2\epsilon)}{\Delta^{\epsilon}_{m,n} - \Delta_{r,s}} = -\frac{1}{2^{2(l-\frac{1}{2}\pm\frac{1}{2})}(2l\pm 1)} \prod_{k=1}^{l-\frac{1}{2}\pm\frac{1}{2}} \frac{4k^2-1}{k^2} \tag{B.23}$$

The terms involving the extra poles are of the form $\frac{R^{\text{tor}}_{r,s}}{\Delta_{m',-n'}-\Delta_{r,s}}$ when $(m',-n') \to (r,s)^{\pm}_{l'}$. We get,

$$\lim_{\epsilon\to 0} \frac{R^{\text{tor}}_{r,s}}{\Delta_{m',-n'} - \Delta_{r,s}} = -\frac{1}{2^{2l+1}\, l'} \prod_{k=1}^{l} \frac{4k^2-1}{k^2}, \quad l = \min(l_r, l_s). \tag{B.24}$$

References

[1] V. Belavin, X. Cao, B. Estienne and R. Santachiara, *Second level semi-degenerate fields in $\mathcal{W}_3$ Toda theory: matrix element and differential equation*, *JHEP* **03** (2017) 008 [arXiv:1610.07993] [INSPIRE].

[2] V. Belavin, B. Estienne, O. Foda and R. Santachiara, *Correlation functions with fusion-channel multiplicity in $\mathcal{W}_3$ Toda field theory*, *JHEP* **06** (2016) 137 [arXiv:1602.03870] [INSPIRE].

[3] V.A. Fateev and A.V. Litvinov, *On AGT conjecture*, *JHEP* **02** (2010) 014 [arXiv:0912.0504] [INSPIRE].

[4] B.L. Feigin and D.B. Fuks, *Invariant skew-symmetric differential operators on the line and Verma modules over the Virasoro algebra*, *Funct. Anal. Appl.* **16** (1982) 114.

[5] B.L. Feigin and D.B. Fuks, *Verma modules over the Virasoro algebra*, *Funct. Anal. Appl.* **17** (1982) 241.

[6] L. Hadasz, Z. Jaskolski and P. Suchanek, *Recursive representation of the torus 1-point conformal block*, *JHEP* **01** (2010) 063 [arXiv:0911.2353] [INSPIRE].

[7] E. Perlmutter, *Virasoro conformal blocks in closed form*, *JHEP* **08** (2015) 088 [arXiv:1502.07742] [INSPIRE].

[8] M. Picco, S. Ribault and R. Santachiara, *A conformal bootstrap approach to critical percolation*, *SciPost* **1** (2016) 009.

JHEP08(2018)183

[9] M. Picco, S. Ribault and R. Santachiara, *A conformal bootstrap solution for critical Potts clusters*, in progress.

[10] R. Poghossian, *Recursion relations in CFT and $N = 2$ SYM theory*, *JHEP* **12** (2009) 038 [arXiv:0909.3412] [INSPIRE].

[11] R. Poghossian, *Recurrence relations for the $\mathcal{W}_3$ conformal blocks and $\mathcal{N} = 2$ SYM partition functions*, *JHEP* **11** (2017) 053 [*Erratum ibid.* **01** (2018) 088] [arXiv:1705.00629] [INSPIRE].

[12] S. Ribault and R. Santachiara, *Liouville theory with a central charge less than one*, *JHEP* **08** (2015) 109.

[13] S. Ribault, *Conformal field theory on the plane*, arXiv:1406.4290 [INSPIRE].

[14] Al.B. Zamolodchikov, *Conformal symmetry in two dimensions: an explicit recurrence formula for the conformal partial wave amplitude*, *Commun. Math. Phys.* **96** (1984) 419.

[15] Al.B. Zamolodchikov, *Conformal symmetry in two-dimensional space: recursion representation of conformal block*, *Theor. Math. Phys.* **73** (1987) 1088.

JHEP08(2018)183

Part II

RANDOM FRACTALS ON THE TORUS

This second part addresses the description of percolation models on the torus, using the conformal field theory approach presented in Part I. Before focusing on each specific model, we define the observables which will be studied in both cases. On a lattice, we define a general percolation model by activating the sites (or bonds) randomly with probability p. For uncorrelated percolation each site is activated independently of its neighbours [42], while for the models of Chapters 4 and 5 correlations are introduced. The connected sets of active sites or bonds are called clusters, see Figures ia and ic. Of course these clusters are random objects of which we show here particular configurations, and physical observables are obtained by averaging over many such configurations. As shown on Figure ib the emergence of a percolating cluster (connecting the top and bottom of the system as in Figure ic), at a critical value p_c of the occupation probability, defines the percolation phase transition. In the infinite size limit, the probability of an infinite cluster jumps from 0 to 1 at $p = p_c$. On the figure we have also plotted data points taken on a finite $N \times N$ lattice, where the transition has a finite width (see eg. Section 4.1 in [42]).

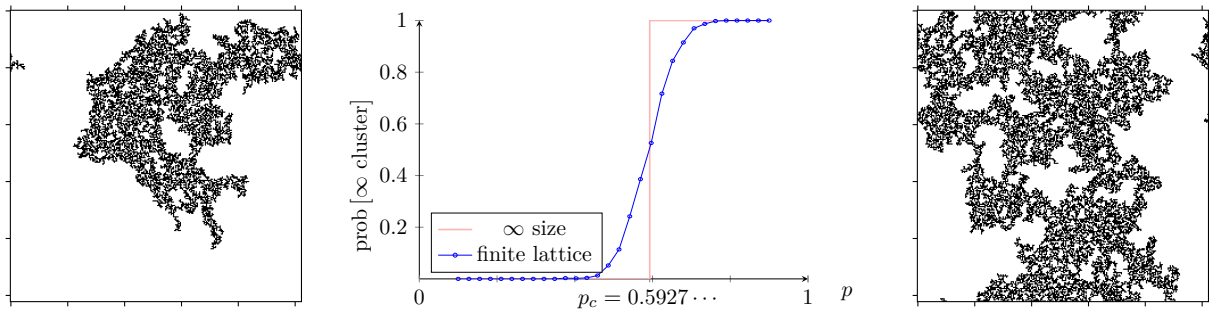

(a) a non-percolating configuration ($p = 0.58$). We show only the largest cluster.

(b) percolation transition

(c) a percolating cluster ($p = 0.596$)

Figure i: Cluster configurations and phase transition for uncorrelated site percolation on a 258×258 square lattice.

The clusters represent therefore the central object of study in percolation theory. More precisely, the study of the percolative behaviour of a system is the study of the *connectivity properties* of the clusters [72], namely of the probabilities that sites are connected to each others by clusters (examples are given in Figures ii, iii). The question we ask is wether there exist, and what is, the CFT which describes these probabilities in the scaling limit. The motivation to study such observables is also that it represents a front door to find a CFT which may also describe other observables. Taking again the example of pure percolation, it appears that several other probabilities can be obtained from the CFT which describes the connectivities, such as the probability that points lie on the boundary (perimeter) of the same cluster [73]. Nonetheless, for the correlated percolation model considered in Chapter 5 it is not clear if the clusters and their boundaries are described by the same CFT. We shall therefore focus on one type of observables,

and we define precisely the object of our study as "the CFT which describes the scaling limit of the clusters connectivities" of a given model.
As detailed in the first part, a CFT is defined by its spectrum (the set of fields) and its structure constants. In this introduction we show in which way the fact that connectivities are probabilities of geometric events constrains the CFT data. Ultimately, it will be made clear how their study – either on the plane or on the torus, allows to determine this data.

We denote $\text{prob}\,[\sigma]$ the probability that n given points fall into the cluster configuration σ. Consider the simplest case $n = 2$: either the two points belong to the same cluster $\sigma = 12$ or they do not, $\sigma = 1;2$ (Figure iia). Since $\text{prob}\,[12] + \text{prob}\,[1;2] = 1$ there is only one independent probability, say $\text{prob}\,[12]$. With three points one obtains the five possible configurations of Figure iib. They are not independent: for instance $\text{prob}\,[123] + \text{prob}\,[12;3] = \text{prob}\,[12]$. It can be shown that they can be all expressed in terms of $\text{prob}\,[12]$ and $\text{prob}\,[123]$ [74].

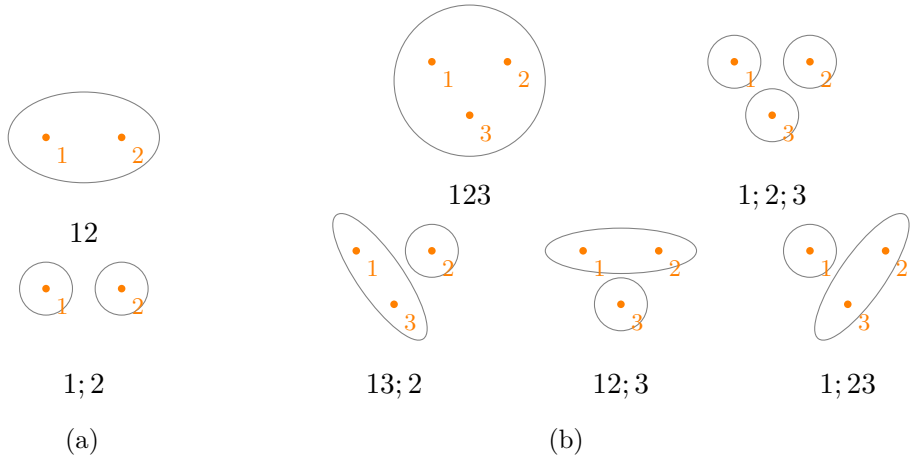

Figure ii: The different clusters configurations of two (left) and three (right) points.

The counting of independent probabilities in the general case has been worked out analogously in [74]. We will be interested in the two-, three- and four-point connectivities. The space of independent four-point connectivities is four-dimensional and is pictured in Figure iii.

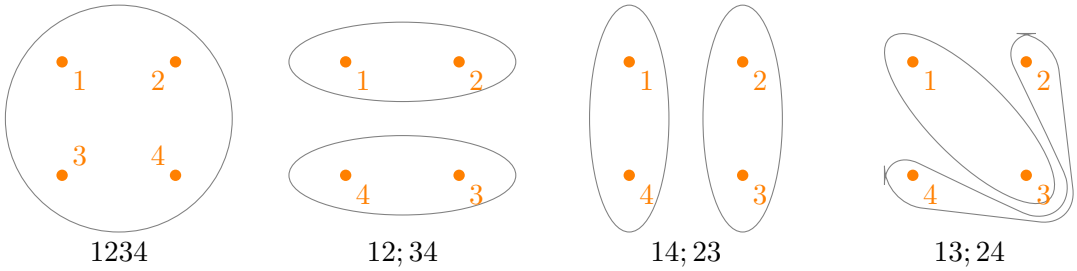

Figure iii: The four independent four-point connectivities.

We now assume that the scaling limit of the connectivities $\text{prob}\,[\sigma]$, denoted p_σ, exist and is given by the correlation functions of fields V_Δ in a CFT:

$$p_\sigma(z_1, z_2, \cdots, z_n) = d_0^{(n)} \langle V_\Delta(z_1) V_\Delta(z_2) \cdots V_\Delta(z_n) \rangle_\sigma, \tag{i}$$

with $d_0^{(n)}$ a non-universal constant. As will be made clear below, the correlation functions in the right-hand side must have different s-channel spectra S_σ, in order to describe the spaces of

connectivities of Figures ii and iii. We thus label them with an index σ. Consider first the case $n = 2$. From (i) and the general form of the two-point function (1.58):

$$p_{12}(z_1, z_2) = d_0^{(2)} \langle V_\Delta(z_1) V_\Delta(z_2) \rangle_{12} = \frac{d_0^{(2)}}{|z_1 - z_2|^{4\Delta}}. \tag{ii}$$

General percolation theory (see for instance Section 3.2 of [42]) tells us that the decay of p_{12} is governed by the critical exponent η:

$$p_{12}(z_1, z_2) \sim \frac{1}{|z_1 - z_2|^{\eta}}. \tag{iii}$$

Comparing with (ii) this fixes the dimension of the connectivity fields V_Δ to be:

$$\Delta = \frac{\eta}{4}. \tag{iv}$$

With three points we get:

$$p_{123}(z_1, z_2, z_3) = d_0^{(3)} \langle V_\Delta(z_1) V_\Delta(z_2) V_\Delta(z_3) \rangle_{123} = d_0^{(3)} \frac{D_{123}^{(\Delta)}}{|z_{12}|^{2\Delta} |z_{23}|^{2\Delta} |z_{13}|^{2\Delta}}. \tag{v}$$

We can already obtain non-trivial information on the CFT from the measurement of the two- and three-point connectivities on the plane: indeed from (ii) and (v) we get

$$\frac{p_{123}(z_1, z_2, z_3)}{\sqrt{p_{12}(z_1, z_2) p_{12}(z_2, z_3) p_{12}(z_1, z_3)}} = \frac{d_0^{(3)}}{\left[d_0^{(2)}\right]^{\frac{3}{2}}} D_{123}^{(\Delta)}. \tag{vi}$$

Provided that the non-universal constants can be determined, or that $d_0^{(3)} = \left[d_0^{(2)}\right]^{\frac{3}{2}}$, one obtains $D_{123}^{(\Delta)}$ from the measurement of this ratio. This has been applied notably to pure percolation [75] and to the $Q-$Potts model at different values of Q [76].

More CFT data can be obtained from measuring the two- and three-point connectivities on the torus. This will be detailed in Chapters 4 and 5, but one can already foresee from the expressions (2.66) and (2.81) of the two- and three-point functions on the torus, that more structure constants are going to appear in (ii) and (v).

We now concentrate on aspects which, although still general, will be especially useful in the discussion of the random cluster Potts model, in the next chapter. In Chapters 1 and 2 we labelled structure constants according to the dimensions of the fields. To describe connectivities we need to adopt the more precise notation $D_\sigma^{(\Delta')}$ which stands for the structure constant $D_{(\Delta),(\Delta)}^{(\Delta')}$ appearing in the expansion of p_σ. This is especially important for describing the four-point connectivities, where we can have $D_{\sigma_1}^{(\Delta')} \neq D_{\sigma_2}^{(\Delta')}$. Consider now $n = 4$:

$$p_\sigma(z_1, z_2, z_3, z_4) = d_0^{(4)} \langle V_\Delta(z_1) V_\Delta(z_2) V_\Delta(z_3) V_\Delta(z_4) \rangle_\sigma \tag{vii}$$

where σ can be one of the four cluster configurations of Figure iii: $\sigma = 1234,\ 12;34\ 13;24\ 14;23$. From (1.60) the four-point function of generic fields with the same dimension can be written:

$$\langle \prod_{i=1}^{4} V_\Delta(z_i, \bar{z}_i) \rangle = |z_{13} z_{24}|^{-4\Delta} \langle V_\Delta(z) V_\Delta(0) V_\Delta(\infty) V_\Delta(1) \rangle \tag{viii}$$

where z is the cross-ratio (1.62). The s-expansion $z_1 \to z_2$ of the four-point function in the right-hand side is given by (1.63):

$$\langle V_\Delta(z)V_\Delta(0)V_\Delta(\infty)V_\Delta(1)\rangle = \sum_{\Delta_s\in S}\left[D^{(\Delta_s)}_{(\Delta),(\Delta)}\right]^2\left|\mathcal{F}^{(s)}_{\Delta_s}(\Delta|z)\right|^2 \tag{ix}$$

with S the s-channel spectrum. Using expression (ix) in (vii) we then obtain:

$$p_\sigma(z_1,z_2,z_3,z_4) = d_0^{(4)}\,|z_{13}z_{24}|^{-4\Delta}\sum_{\Delta_s\in S_\sigma}\left[D^{(\Delta_s)}_{\sigma}\right]^2\left|\mathcal{F}^{(s)}_{\Delta_s}(\Delta|z)\right|^2 \tag{x}$$

where S_σ is the s-channel spectrum of the four-point function $\langle\prod_{i=1}^4 V_\Delta\rangle_\sigma$. Let us note a subtle but very important point. The expansion (x) over the standard conformal blocks of Chapter 1 follows from the assumption that the Hamiltonian, or equivalently L_0 is diagonalisable (cf. Section 1.2). It is now understood [48, 49, 77–79] (see also [80]) that the Potts CFT is a logarithmic CFT, that is a CFT in which states do not fall into the standard representations of Section 1.2, and where correlation functions, as a consequence, have logarithmic divergences (for reviews on logCFTs see for instance [81, 82]). Nonetheless, it seems that the four-point connectivities in the Potts model can be obtained using the standard conformal blocks expansion as in (x), as made manifest by the bootstrap studies [44, 47] and by our results on the torus [51, 52]. This expansion is not manifestly finite for all central charge: there are values of c at which structure constants and conformal blocks diverge. These divergences seem to cancel out [47] so that the expansion remains finite at all c. Indeed, as discussed in Section 1.6, by combining the usual Virasoro conformal blocks one can obtain various behaviours as a function of the central charge: in certain limits correlation functions might be finite, they might diverge, and they might also show logarithmic behaviour [83, 84]. In the following we will therefore make the extra assumption (x).

To see how the geometric behaviour of the connectivities leads to different spectra S_σ, let us consider the p_σ's when the points 1 and 2 are brought close together, $z_1 \to z_2$. We have for instance:

$$p_{12;34} \overset{1\to 2}{\sim} p_{12}p_{34} \sim \frac{1}{|z_{12}|^{4\Delta}}\frac{1}{|z_{34}|^{4\Delta}} \tag{xi}$$

where we used equation (ii). From (x) the s-channel expansion of the corresponding four-point function is, considering only the most dominant contribution:

$$\begin{aligned} p_{12;34}(z_1,z_2,z_3,z_4) &\sim |z_{13}z_{24}|^{-4\Delta}\left[D^{(\Delta_s)}_{12;34}\right]^2|z|^{-4\Delta+\Delta_s}+\cdots \\ &\sim \frac{\left[D^{(\Delta_s)}_{12;34}\right]^2}{|z_{12}z_{34}|^{4\Delta}}z^{\Delta_s}+\cdots \end{aligned} \tag{xii}$$

Comparing with (xi), the field with the lowest dimension in the spectrum $S_{12;34}$ must be the Identity: $S_{12;34} = \{\mathrm{Id},\cdots\}$, so that $\Delta_s = 0$ and $D^{(\Delta_s)}_{12;34} = 1$ in the equation above.

However if we consider say p_{1234} we get a different behaviour when $1 \to 2$. To see this, we follow the argument given in [46] and define the conditional probability $p_{ij|jk}$ which is the probability that i and j are in the same cluster, given that j and k are in the same cluster. We have for instance

$$p_{123} = p_{12|23}p_{23}. \tag{xiii}$$

When 1 is close to 2, the probability that 1 and 2 are in the same cluster does not depend much on the configuration of points 2, 3 and 4. In particular $p_{12|23} \overset{1\to 2}{\sim} p_{12|234}$ so that:

$$p_{1234} = p_{12|234}p_{234} \overset{1\to 2}{\sim} p_{12|23}p_{234} = \frac{p_{123}}{p_{234}}p_{23} \tag{xiv}$$

where we used (xiii). Using now (ii) and (v):

$$\begin{aligned} p_{1234} &\overset{1\to 2}{\sim} \frac{|z_{23}|^{4\Delta}}{|z_{12}z_{13}z_{23}|^{2\Delta}\,|z_{23}z_{34}z_{24}|^{2\Delta}} D^{(\Delta)}_{123}D^{(\Delta)}_{234} \\ &= |z_{13}z_{24}|^{-4\Delta}\; z^{-2\Delta} D^{(\Delta)}_{123}D^{(\Delta)}_{234}. \end{aligned} \tag{xv}$$

Comparing with the s-channel expansion (xi), the field with the lowest dimension in the spectrum S_{1234} must be V_Δ: $S_{1234} = \{V_\Delta, \cdots\}$. In particular this spectrum does not contain the Identity. We have that $\left[D^{(\Delta)}_{1234}\right]^2 = D^{(\Delta)}_{123}D^{(\Delta)}_{234} = \left[D^{(\Delta)}_{123}\right]^2$.
From these examples we conclude that the four-point s-channel spectra are in general different. As one can convince her · himself by looking at Figure iii, only three s-channel spectra are needed to write the expansions of the four-point connectivities in all possible channels. This is summarised in the table below.

	$s-$channel spectrum $(1 \to 2)$	$t-$channel spectrum $(1 \to 3)$	$u-$channel spectrum $(1 \to 4)$
p_{1234}	S_{1234}	S_{1234}	S_{1234}
$p_{12;34}$	$S_{12;34}$	$S_{13;24}$	$S_{13;24}$
$p_{13;24}$	$S_{13;24}$	$S_{12;34}$	$S_{13;24}$
$p_{14;23}$	$S_{13;24}$	$S_{13;24}$	$S_{12;34}$

Table 3.1: The spectra of the four independent four-point connectivities in the s-, t- and u-channels are given by the s-channel spectra S_{1234}, $S_{12;34}$ and $S_{13;24}$.

As we review in the next chapter, the study of the four-point connectivity on the plane allowed, under assumption (x) to make significant progress in the understanding of the random clusters Potts CFT, by determining a consequent amount of the CFT data. On the torus, similarly to the two- and three-point, the four-point connectivities allow to probe different structure constants.

4

THE RANDOM CLUSTERS $Q-$STATE POTTS MODEL

In this chapter, we present new predictions for the two-, three- and four-point connectivities of the Potts model on the torus. They are obtained as s-channel expansions using the general CFT techniques of Chapter 2, combined with the prediction of the s-channel spectra [45] and with conjectures on the structure constants [43, 46] which we review below. So far, predictions have been made for the connectivities on the infinite plane. To allow precise comparison with numerical simulations, made on doubly-periodic lattices, we aimed at predicting the exact form of the topological corrections. The importance of such topological effects was already pointed out in [75], where the ratio of three- to two-point connectivities was measured on large torii to extract the plane limit and check the conjecture [43]. We now understand and are able to predict such effects (equation (5.6) in Article III). Besides, these results test the overall consistency of the theory and the conjectures for the structure constants.
Most computations can be found in the published papers Article II and Article III, and we do not reproduce them here. We rather provide additional details not given in the articles and discuss our results in the light of very recent advances towards a full CFT solution. In the last section we discuss further interesting points which have not been investigated in Article II and Article III.

The random clusters $Q-$state Potts model is a family of geometrical models, defined on the lattice by the partition function:

$$Z = \sum_G p^{\#\text{bonds}}(1-p)^{\#\text{absent bonds}} Q^{\#\text{clusters}}. \tag{4.1}$$

The sum is over subsets G of edges randomly occupied with probability p. Occupied edges are called bonds. We will consider real[1] $Q \in [0,4]$ where there exists a second-order phase transition [86–88] of percolation type: namely there exists a value of $p = p_c$ at which a percolating cluster emerges. $Q = 1$ corresponds to pure (uncorrelated) percolation. When $Q \neq 1$, the factor $Q^{\#\text{clusters}}$ induces long-range correlations, since the weight of a configuration depends on the non-local organisation of the bonds into clusters (Figure 4.1).

1 Although we do not consider this case, the critical model can be defined also for complex values of Q [46, 48, 85].

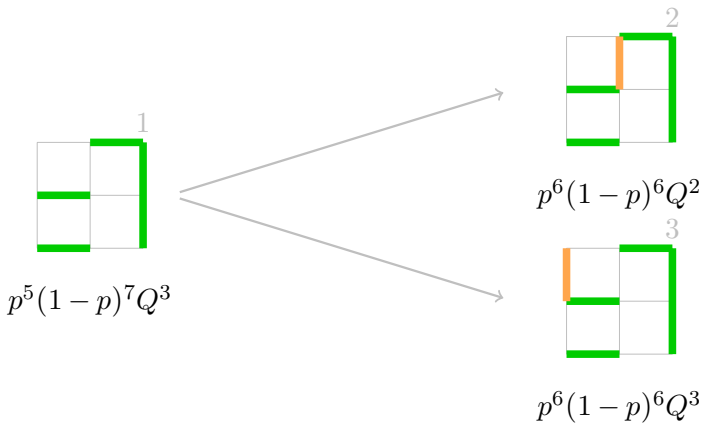

Figure 4.1: Starting from configuration 1, adding one bond may lead to configurations with different weights: if the bond connects two clusters (pivotal bond) the number of clusters is reduced (configuration 2). If the bond is not pivotal (configuration 3) the number of clusters remains the same.

It is a well-established fact that the random clusters have a conformally invariant measure, although rigorous proofs exist only at $Q = 1$ [33] and $Q = 2$ [34, 89].
The random cluster Potts model has two notable features. First it is integrable [90], and its transfer matrix is related to a Temperley-Lieb-type algebraic structure (see for instance Chapter 4 in [91]). The representations of this algebra are known ([45] and references therein). In the continuum limit they encode the spectrum of the Potts CFT. Secondly, some of the cluster configurations can be mapped to height configurations [92]. In the continuum limit this height becomes a scalar field described by the so-called Coulomb-gas CFT [22, 93, 94] (see also the reviews in [65, 91]). This CFT describes models with central charge $c \leq 1$ [95], and in particular the minimal models. It also describes some universal properties of the random clusters $Q-$Potts model, for generic Q: its spectrum, encoded in the torus partition function [94] (see Section 4.1.1) and many two-point functions, in particular the two-point connectivity. However, higher point connectivities cannot in general be described by the Coulomb-gas. Indeed, correlation functions in this CFT should obey so-called charge neutrality, which translates into the fact that the dimensions of the fields should satisfy specific relations for their correlator to be non-zero. This relation cannot be satisfied, for instance, for the three-point function of the connectivity field which is hence erroneously set to zero [96].
For a long time, which CFT describes the connectivities of the Potts clusters for all Q remained an open problem. Indeed, this CFT escaped all classifications:

- it must be non-unitary, since the only unitary CFTs with central charge less than one are the minimal models [22],
- it is non-rational: it involves an infinite number of Virasoro representations,
- only a subset of fields are degenerate, so that correlation functions do not satisfy in general any differential equation,
- it is logarithmic, as discussed in the introduction ii.

With the conjecture [43] for the three-point connectivity at $Q = 1$, which gave a meaning to "mysterious"[2] structure constants [97], a new line of research started, aiming at predicting the three- and four-point connectivities for all Q. In the pioneering work [44] the first proposal for consistent (crossing-symmetric) four-point functions describing the four-point connectivities was made, by direct application of the bootstrap approach. This solution was subsequently understood to describe a variation of the Potts model where some configurations have modified weights, and to be connected with RSOS models [47, 98]. The full s-channel spectra were determined from detailed study of the lattice algebra [45]. Very recent works [47, 48] provided significant progress towards the determination of all the structure constants entering the four-point connectivities.

4.1 THE POTTS MODEL SPECTRA

In Section 4.1.1 we discuss the spectrum of the Potts model given by its partition function. In Section 4.1.2 we give the s-channel spectra of the four-point connectivities.

4.1.1 *The torus partition function and the Potts spectrum*

The set of fields in the Potts CFT is known to be given by the following spectrum [45, 94, 99]:

$$S_{\text{Potts}} = S^{D,\text{quot}}_{1,\mathbb{N}^*} \bigcup S_{0,\mathbb{Z}+\frac{1}{2}} \bigcup_{\substack{M\geq 2 \\ N|M,(p,N)=1}} S_{M,\mathbb{Z}+\frac{p}{N}}. \tag{4.2}$$

$S^{D,\text{quot}}_{1,\mathbb{N}^*}$ contains the diagonal degenerate fields: $S^{D,\text{quot}}_{1,\mathbb{N}^*} = \left\{ V^{D,\text{quot}}_{(1,n)}, n = 1, 2, \cdots \middle| \Delta = \bar{\Delta} = \Delta_{1,n} \right\}$. The two other sectors contain non-diagonal, non degenerate fields: $S_{r,s} = \left\{ V_{(r,s)} \middle| \Delta, \bar{\Delta} = \Delta_{r,s}, \Delta_{r,-s} \right\}$. In this section we explain the different sectors of the spectrum 4.2 by examining the torus partition function which, as seen in Section 2.4 of Chapter 2 encodes the set of scaling dimensions and their multiplicities. For the Potts model it is given by [94]:

$$Z(q) = \hat{Z}(q) + \frac{1}{2}(Q-1)\left[Z_c(q|1) - Z_c(q|1/2)\right]. \tag{4.3}$$

The form most often encountered in the literature involves the exponents $x_{e,m}$:

$$\begin{aligned} Z_c(q|f) &= \frac{1}{|\eta(q)|^2} \sum_{\substack{e\in\mathbb{Z}/f \\ m\in\mathbb{Z}f}} q^{x_{e,m}} \bar{q}^{\bar{x}_{e,m}}, \\ x_{e,m}, \bar{x}_{e,m} &= \frac{1}{4}\left(\frac{e}{2\beta} \pm 2\beta m\right)^2 \end{aligned} \tag{4.4}$$

where β is the parametrisation of the central charge (0.5), and is related to Q by:

$$Q = 2 + 2\cos\left(2\pi(1-\beta^2)\right). \tag{4.5}$$

In terms of the conformal dimension we have:

$$\begin{aligned} x_{e,m} &= \Delta_{-2m,e/2} - \frac{c-1}{24} \\ \bar{x}_{e,m} &= x_{e,-m} = \Delta_{2m,e/2} - \frac{c-1}{24}, \end{aligned} \tag{4.6}$$

2 dixit Al. Zamolodchikov !

which allows to rewrite Z_c in the familiar form (2.40) of Section 2.4:

$$\begin{aligned} Z_c(q|f=1) &= q^{-c/24}\bar{q}^{-c/24}\sum_{\substack{m\in 2\mathbb{Z}\\ e\in\mathbb{Z}/2}} q^{\Delta_{m,e}}\bar{q}^{\bar{\Delta}_{m,e}}\,(1+q+\bar{q}+\cdots)\\ Z_c(q|f=\frac{1}{2}) &= q^{-c/24}\bar{q}^{-c/24}\sum_{m,e\in\mathbb{Z}} q^{\Delta_{m,e}}\bar{q}^{\bar{\Delta}_{m,e}}\,(1+q+\bar{q}+\cdots) \end{aligned} \tag{4.7}$$

where $\cdots$ indicate the contributions of the other descendants, given by the expansion of the η function in (4.4).
The function $\hat{Z}$ is given by:

$$\begin{aligned} \hat{Z}(q) &= \frac{1}{|\eta(q)|^2}\left[\sum_{p\in\mathbb{Z}}(q\bar{q})^{x_{e_0+2p,0}} + \sum_{\substack{M,N=1\\ N \text{ divides } M}}^{\infty}\Lambda(M,N)\sum_{\substack{p\in\mathbb{Z}\\ (p,N)=1}} q^{x_{2p/N,M/2}}\bar{q}^{\bar{x}_{2p/N,M/2}}\right]\\ e_0 &= 2(1-\beta^2). \end{aligned} \tag{4.8}$$

(p,N) denotes the greatest common divisor of p and N. The combinatorial coefficients $\Lambda(M,N)$ are polynomials in Q. Their expression is given in [94], and a `Mathematica` notebook to compute them can be found at [100]. Again we rewrite (4.8) in terms of the conformal dimensions:

$$\begin{aligned} \hat{Z}(q) = q^{-c/24}\bar{q}^{-c/24}\Bigg[&\sum_{p\in\mathbb{Z}} q^{\Delta_{1,p+1}}\bar{q}^{\Delta_{1,p+1}}(1+q+\cdots)\\ &+\sum_{\substack{M,N=1\\ N \text{ divides } M}}^{\infty}\Lambda(M,N)\sum_{\substack{p\in\mathbb{Z}\\ (p,N)=1}} q^{\Delta_{-M,p/N}}\bar{q}^{\bar{\Delta}_{-M,p/N}}(1+q+\cdots)\Bigg] \end{aligned} \tag{4.9}$$

where we used that $\Delta_{0,1-\beta^2+p}=\Delta_{1,p+1}$. The terms in the first sum of (4.9) with $p<-1$ can be rewritten as diagonal descendant states since, for all β:

$$\begin{aligned} &\Delta_{1,-n} = \Delta_{1,n}+n\\ &\Rightarrow \sum_{n\in\mathbb{N}_*} q^{\Delta_{1,-n}}\bar{q}^{\Delta_{1,-n}} = \sum_{n\in\mathbb{N}_*} q^{\Delta_{1,n}+n}\bar{q}^{\Delta_{1,n}+n}. \end{aligned} \tag{4.10}$$

The state with $n=0$ simply drops out from the partition function since its multiplicity is:

$$\underbrace{1}_{p=-1 \text{ in } \hat{Z}} + \underbrace{2\times -\frac{1}{2}(Q-1)}_{m,e=\pm 1,0 \text{ in } Z_c(1/2)} + \underbrace{\Lambda(1,1)}_{M=N=1,p=-1 \text{ in } \hat{Z}} = 0 \tag{4.11}$$

where we used that $\Lambda(1,1)=Q-2$. Therefore we can write (4.9) as:

$$\begin{aligned} \hat{Z}(q) = q^{-c/24}\bar{q}^{-c/24}\Bigg[&\sum_{n\in\mathbb{N}_*} q^{\Delta_{1,n}}\bar{q}^{\Delta_{1,n}}(1+q+\cdots)\\ &+\sum_{\substack{M,N=1\\ N \text{ divides } M}}^{\infty}\Lambda(M,N)\sum_{\substack{p\in\mathbb{Z}\\ (p,N)=1}} q^{\Delta_{-M,p/N}}\bar{q}^{\bar{\Delta}_{-M,p/N}}(1+q+\cdots)\Bigg] \end{aligned} \tag{4.12}$$

The first sum corresponds to the spectrum $S^{D,\text{quot}}_{1,\mathbb{N}^*}$ and indicates that the primaries have multiplicity one. This spectrum contains in particular the identity $V^{D,\text{quot}}_{1,1}$ and the energy $V^{D,\text{quot}}_{1,2}$. In the full partition function the correct multiplicity of their descendants is ensured by cancellations which occur between the different sums. Let us illustrate this in the simplest case of the identity, which is degenerate at level 1. The term $\bar{q}$ has multiplicity:

$$\underbrace{1}_{p=0 \text{ in } \hat{Z}} + \underbrace{2 \times -\frac{1}{2}(Q-1)}_{m,e=\pm 1 \text{ in } Z_c(1/2)} + \underbrace{\Lambda(1,1)}_{M=N=1,p=-1 \text{ in } \hat{Z}} = 0 \tag{4.13}$$

and similarly for the term q: $L_{-1}\text{Id}$ and $\bar{L}_{-1}\text{Id}$ are quotiented out. The existence of these degenerate fields in the spectrum has important consequences, as we will see in Sections 4.2 and 4.3.1.

The "magnetic" sector $S_{0,\mathbb{Z}+\frac{1}{2}} = \{V_{0,1/2}, V_{0,3/2}, \cdots\}$ contains states with scaling dimensions $\Delta = \bar{\Delta} = \Delta_{0,\mathbb{Z}+1/2}$. It contains notably the field $V_{0,1/2}$. For the Potts model the dimension of this field satisfies

$$\Delta_{0,\frac{1}{2}} = \frac{\eta}{4} \tag{4.14}$$

for all values of Q, where η is the exponent giving the decay of the two-point connectivity (see the Introduction ii). We therefore identify $V_{0,1/2}$ as the connectivity field. This identification is also natural in the Coulomb-gas construction, where the insertion of two such fields correspond to the propagation of a cluster. The fields in $S_{0,\mathbb{Z}+\frac{1}{2}}$ appear in the partition function $Z_c(f=1)$ where they are counted twice ($m=0$, $e=\pm(\mathbb{N}+1/2)$) so that their total multiplicity in (4.3) is $Q-1$. For instance in the 3−states Potts model there are $3-1=2$ connectivity fields $V^{\pm}_{0,\frac{1}{2}}$, which have the same dimension $\Delta_{0,1/2}$, but different fusion rules as has been discussed in Section 1.6.1. For generic value of Q the multiplicity $Q-1$ of the connectivity field is non-integer.

$S_{M,\mathbb{Z}+\frac{p}{N}}$ contains in particular non-scalar fields. For general Q their multiplicities are non-integer and non-positive.

The partition function (4.3) describes the spectrum of the random cluster Potts model for all values of Q, but also reduces to the spectrum of particular theories, due to subtle cancellations at specific values of Q. As a simple illustrative example, consider $Q=2$ where (4.3) becomes:

$$Z(q) = q^{-1/48}\bar{q}^{-1/48}\left(1 + q^{1/16}\bar{q}^{1/16} + q^{1/2}\bar{q}^{1/2} + q^{1/16+1}\bar{q}^{1/16} + \cdots\right). \tag{4.15}$$

This is the torus partition function of the Ising minimal model (2.57). Only three conformal families remain, spanned by the diagonal primaries: the identity $\Delta_{1,1}=0$, the spin $\Delta_{0,1/2} = \Delta_{2,2} = 1/16$ and the energy $\Delta_{1,2} = 1/2$. This is due to resonances between dimensions which occur at rational values of the central charge:

$$\Delta_{r,s} = \Delta_{\lambda q \pm r, \lambda p \pm s} \quad \forall \lambda \in \mathbb{R}, \quad \beta^2 = p/q \tag{4.16}$$

and which causes the cancellation of an infinite number of terms in the partition function.

4.1.2 *The spectra of the four-point connectivities*

The s-channel spectra of the four-point connectivities is given in the table below. The t- and u-channel spectra follow since the connectivities are related to each other by swapping the position of the points z_i, as explained in the introduction ii.

	$s-$channel spectrum
p_{1234}	$S_{0,\mathbb{Z}+\frac{1}{2}} \bigcup_{\substack{M\in 2\mathbb{Z} \\ Mp/N \text{ even}}} S_{M,\mathbb{Z}+\frac{p}{N}} = \left\{V_{(0,\frac{1}{2})}, V_{(2,0)}, V_{(0,\frac{3}{2})}, V_{(2,1)}, \cdots\right\}$
$p_{12;34}$	$S^{D,\text{quot}}_{1,\mathbb{N}^*} \bigcup S_{0,\mathbb{Z}+\frac{1}{2}} \bigcup_{\substack{M\in 2\mathbb{Z}_* \\ Mp/N \text{ even}}} S_{M,\mathbb{Z}+\frac{p}{N}} = \left\{V^{D,\text{quot}}_{(1,1)}, V_{(0,\frac{1}{2})}, V^{D,\text{quot}}_{(1,2)}, V_{(2,0)}, \cdots\right\}$
$p_{13;24}, p_{14;23}$	$\bigcup_{\substack{M\in 2\mathbb{Z}_* \\ Mp/N\in\mathbb{Z}}} S_{M,\mathbb{Z}+\frac{p}{N}} = \left\{V_{(2,0)}, V_{(2,\frac{1}{2})}, V_{(2,1)}, V_{(2,\frac{3}{2})}, \cdots\right\}$

Table 4.1: s-channel spectra of the different connectivities [45].

In Figure 4.2 we give the total dimensions of the fields in the full spectrum (4.2), which also appear in the spectra 4.1.

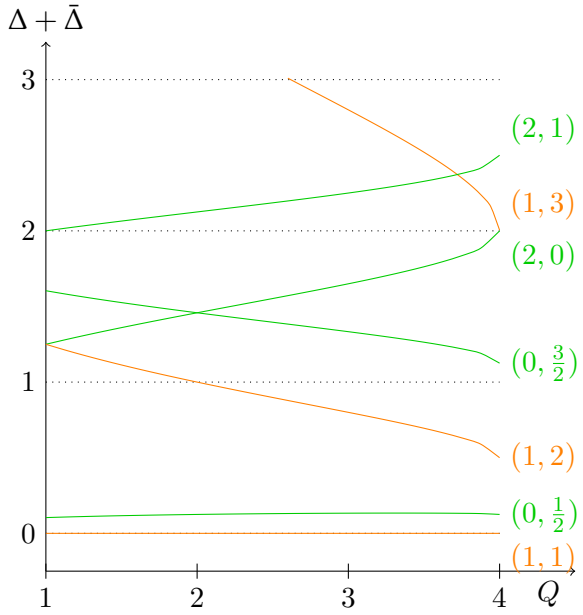

Figure 4.2: The total dimension of the fields in the Potts spectra (4.2) and 4.1. Dimensions in the non-diagonal sector (green) alternate with dimensions of diagonal fields (orange). This figure is inspired from [46].

To make an explicit example we write below the first terms in the s-channel expansion of p_{1234}. From the general expression (x) and using the spectrum 4.1 and Figure 4.2 we find:

$$p_{1234}(z_1,z_2,z_3,z_4) = \frac{1}{|z_{13}z_{24}|^{4\Delta_{0,\frac{1}{2}}}} \left(\left[D^{(0,\frac{1}{2})}_{1234}\right]^2 \left|\mathcal{F}^{(s)}_{\Delta_{(0,\frac{1}{2})}}\left(\Delta_{0,\frac{1}{2}}|z\right)\right|^2 + \left[D^{(2,0)}_{(1234)}\right]^2 \left|\mathcal{F}^{(s)}_{\Delta_{(2,0)}}\left(\Delta_{0,\frac{1}{2}}|z\right)\right|^2 + \left[D^{(0,\frac{3}{2})}_{1234}\right]^2 \left|\mathcal{F}^{(s)}_{\Delta_{(0,\frac{3}{2})}}\left(\Delta_{0,\frac{1}{2}}|z\right)\right|^2 + \cdots \right) \tag{4.17}$$

with the higher order terms $\cdots$ corresponding to contributions of primaries of higher dimension. Which contribution gives the subdominant term depends on the relative size of the dimensions $\Delta_{2,0}$ and $\Delta_{0,3/2}$, which varies with Q (cf. Figure 4.2). We can proceed similarly for the other connectivities p_σ. In the next section we explain which structure constants $D_\sigma^{(\Delta_{r,s})}$ are determined so far.
A very important feature of the Potts spectrum (4.2) and therefore 4.1, which made the analyses [44, 46, 47] and [51, 52] possible, is that it is discrete and it is sparse. Namely the values of the dimensions are well separated (except at some particular values of Q), which produces well separated contributions in the four-point connectivity, as in (4.17). This is also true of the connectivities on the torus as we will see below (4.24-4.26). It means that by measuring numerically the four-point connectivity on the plane or the two-, three-, four-point connectivities on the torus, one can access contributions of different orders and:

i check or determine numerically which fields contribute

ii estimate numerically the structure constants involved.

4.2 STRUCTURE CONSTANTS

The full set of structure constants of the CFT is not yet determined. To date:

- a subset of structure constants has been determined analytically [66]
- relations between the structure constants entering the different four-point connectivities have been uncovered [47, 48]
- some constants have been determined using numerical conformal bootstrap [44, 46–48].

In this section we compile the results from the works [43, 44, 46, 47, 66] to give a clear picture of which structure constants are known and which ones are not, so far. Most of this discussion involves structure constants of the type $D^{(r,s)}_{(0,1/2),(0,1/2)}$ which are the ones entering the s-channel spectra of the four-point connectivitiesand we adopt the notation introduced in the introduction ii:

$$D_\sigma^{(r,s)}, \quad \sigma = 12,\ 123,\ 1234,\ 12,34,\ 13,24,\ 14,23 \tag{4.18}$$

indicating which is the connectivity whose expansion involves this particular constant.
It has been known since the work [43] that some structure constants involved in the connectivities are related to the structure constants of Liouville theory. The first conjecture [43] was that the three-point connectivity is given –using the notation above– by :

$$D_{123}^{(0,\frac{1}{2})} = \sqrt{2} C^{(0,\frac{1}{2})}_{(0,\frac{1}{2}),(0,\frac{1}{2})} \tag{4.19}$$

where $C^{(0,\frac{1}{2})}_{(0,\frac{1}{2}),(0,\frac{1}{2})}$ is the structure constant of Liouville theory with central charge $c \leq 1$ [65, 66, 97, 101, 102]. This conjecture was checked numerically [75, 76] and very precisely recently [48].

In Liouville theory, there exist two degenerate fields $V^{D,\text{quot}}_{(1,2)}$ and $V^{D,\text{quot}}_{(2,1)}$. As a consequence the structure constants obey shift equations, and the following ratios are completely determined in terms of Gamma functions:

$$\frac{C^{(r+2,s)}_{(0,\frac{1}{2}),(0,\frac{1}{2})}}{C^{(r,s)}_{(0,\frac{1}{2}),(0,\frac{1}{2})}} = \frac{\gamma^2\left(\frac{1}{2}\left[1-r+(s+1)\beta^2\right]\right)}{\gamma\left(\frac{1}{2}\left[1+r-s\beta^2\right]\right)\gamma\left(\frac{1}{2}\left[1+r-(s+2)\beta^2\right]\right)} \tag{4.20a}$$
$$\times\left[\gamma\left(1-r+s\beta^2\right)\gamma\left(1-r+(s+1)\beta^2\right)\gamma\left(-r+(s+1)\beta^2\right)\gamma\left(-r+(s+2)\beta^2\right)\right]^{-\frac{1}{2}}$$
$$\frac{C^{(r,s+2)}_{(0,\frac{1}{2}),(0,\frac{1}{2})}}{C^{(r,s)}_{(0,\frac{1}{2}),(0,\frac{1}{2})}} = \frac{\gamma^2\left(\frac{1}{2}\left[1-r+\frac{s+1}{\beta^2}\right]\right)}{\gamma\left(\frac{1}{2}\left[1+r-\frac{s}{\beta^2}\right]\right)\gamma\left(\frac{1}{2}\left[1+r-\frac{s+2}{\beta^2}\right]\right)} \tag{4.20b}$$
$$\times\left[\gamma\left(1-r+\frac{s}{\beta^2}\right)\gamma\left(1-r+\frac{s+1}{\beta^2}\right)\gamma\left(-r+\frac{s+1}{\beta^2}\right)\gamma\left(-r+\frac{s+2}{\beta^2}\right)\right]^{-\frac{1}{2}}.$$

This is true for diagonal as well as non-diagonal fields [65, 66, 97, 101, 102]. The recursion relations can be solved leading to the analytic expression for the structure constant $C^{(r,s)}_{(0,\frac{1}{2}),(0,\frac{1}{2})}$, reported in Appendix B of Article III.

In the Potts model $V_{(2,1)}$ is not degenerate, only $V^{D,\text{quot}}_{(1,2)}$ is (cf. (4.2)). From this degeneracy, the structure constants with the second index shifted are related [47]:

$$\left[\frac{D^{(r,s+1)}_\sigma}{D^{(r,s)}_\sigma}\right]^2 = \begin{cases} \frac{\Gamma(-r-\frac{s}{\beta^2})\Gamma(1+r-\frac{1+s}{\beta^2})\Gamma(\frac{1-r}{2}+\frac{s}{2\beta^2})\Gamma(\frac{1+r}{2}+\frac{s}{2\beta^2})\Gamma(\frac{1-r}{2}+\frac{1+s}{2\beta^2})\Gamma(\frac{1+r}{2}+\frac{1+s}{2\beta^2})}{\Gamma(r+\frac{1+s}{\beta^2})\Gamma(1-r+\frac{s}{\beta^2})\Gamma(\frac{1+r}{2}-\frac{1+s}{2\beta^2})\Gamma(\frac{1-r}{2}-\frac{1+s}{2\beta^2})\Gamma(\frac{1+r}{2}-\frac{s}{2\beta^2})\Gamma(\frac{1-r}{2}-\frac{s}{2\beta^2})}, & s\neq 0 \\ \frac{\Gamma(r)\Gamma\left(1-r-\frac{1}{\beta^2}\right)\Gamma\left(\frac{1-r}{2}+\frac{1}{2\beta^2}\right)\Gamma\left(\frac{1+r}{2}+\frac{1}{2\beta^2}\right)}{\Gamma(1+r)\Gamma\left(-r+\frac{1}{\beta^2}\right)\Gamma\left(\frac{1-r}{2}-\frac{1}{2\beta^2}\right)\Gamma\left(\frac{1+r}{2}-\frac{1}{2\beta^2}\right)}, & s=0. \end{cases} \tag{4.21}$$

For diagonal fields:

$$\left[\frac{D^{(1,s+1)^D}_\sigma}{D^{(1,s)^D}_\sigma}\right]^2 = \frac{\gamma^2\left(\frac{1+s}{2\beta^2}\right)\gamma^2\left(\frac{s}{2\beta^2}\right)}{\gamma\left(\frac{s}{\beta^2}\right)\gamma\left(-1+\frac{1+s}{\beta^2}\right)}. \tag{4.22}$$

Applying recursively (4.21) and (4.22) we see that many structure constants can be obtained from a same structure constant. Namely:

$$D^{(1,n)^D}_\sigma = \left[(4.22)|_{s=n-1}\times(4.22)|_{s=n-2}\times\cdots(4.22)|_{s=1}\right]^{\frac{1}{2}} D^{(1,1)^D}_\sigma, \quad \forall n\in\mathbb{N}_*$$
$$D^{(0,k+\frac{1}{2})}_\sigma = \left[(4.21)|_{\substack{r=0\\ s=k-1+\frac{1}{2}}}\times(4.21)|_{\substack{r=0\\ s=k-2+\frac{1}{2}}}\times\cdots(4.21)|_{\substack{r=0\\ s=\frac{1}{2}}}\right]^{\frac{1}{2}} D^{(0,\frac{1}{2})}_\sigma, \quad \forall k\in\mathbb{Z}$$
$$D^{(2\mathbb{Z}_*,k+\frac{p}{M})}_\sigma = \left[(4.21)|_{\substack{r=2\mathbb{Z}_*\\ s=k-1+\frac{p}{M}}}\times(4.21)|_{\substack{r=2\mathbb{Z}_*\\ s=k-2+\frac{p}{M}}}\times\cdots(4.21)|_{\substack{r=2\mathbb{Z}_*\\ s=\frac{p}{M}}}\right]^{\frac{1}{2}} D^{(2\mathbb{Z}_*,\frac{p}{M})}_\sigma, \quad \forall k\in\mathbb{Z}.$$

In particular, as summarised in Table 4.2 all constants of the type $D^{(1,\mathbb{N}_*)^D}_\sigma$ and $D^{(0,\mathbb{Z}+\frac{1}{2})}_\sigma$ are known since they are related to the Liouville constants $C^{(1,1)^D}_{(0,\frac{1}{2}),(0,\frac{1}{2})}$ and $C^{(0,\frac{1}{2})}_{(0,\frac{1}{2}),(0,\frac{1}{2})}$. In addition it has been found [47] that there exist other universal ratios relating:

1. structure constants with the first index shifted

2. structure constants with different σ.

The existence of such relations has been established, and the ratios determined, for the structure constants of the first states in the spectrum [47]:

$$\left[\frac{D^{4,\frac{1}{2}}_{1234}}{D^{0,\frac{1}{2}}_{1234}}\right]^2 = \frac{(Q-2)(Q^2-4Q+2)}{Q(Q-3)^2}\left[\frac{C^{(4,\frac{1}{2})}_{(0,\frac{1}{2}),(0,\frac{1}{2})}}{C^{(0,\frac{1}{2})}_{(0,\frac{1}{2}),(0,\frac{1}{2})}}\right]^2$$
$$= \frac{(Q-2)(Q^2-4Q+2)}{Q(Q-3)^2} \times (4.20b)^2|_{\substack{r=2\\s=\frac{1}{2}}} \times (4.20b)^2|_{\substack{r=0\\s=\frac{1}{2}}} \tag{4.23a}$$

$$\left[\frac{D^{4,\frac{1}{2}}_{12;34}}{D^{4,\frac{1}{2}}_{1234}}\right]^2 = \frac{2-Q}{2} \tag{4.23b}$$

$$\left[\frac{D^{2,0}_{12;34}}{D^{2,0}_{1234}}\right]^2 = \frac{1}{1-Q} \tag{4.23c}$$

$$\left[\frac{D^{4,0}_{12;34}}{D^{4,0}_{1234}}\right]^2 = -\frac{Q^5-7Q^4+15Q^3-10Q^2+4Q-2}{2(Q^2-3Q+1)} \tag{4.23d}$$

$$\left[\frac{D^{2,\frac{1}{2}}_{13;24}}{C^{(0,\frac{1}{2})}_{(0,\frac{1}{2}),(0,\frac{1}{2})}}\right]^2 = \frac{Q-2}{2}\left[\frac{C^{(2,\frac{1}{2})}_{(0,\frac{1}{2}),(0,\frac{1}{2})}}{C^{(0,\frac{1}{2})}_{(0,\frac{1}{2}),(0,\frac{1}{2})}}\right]^2$$
$$= \frac{Q-2}{2} \times (4.20b)^2|_{\substack{r=0\\s=\frac{1}{2}}} \tag{4.23e}$$

$$\left[\frac{D^{4,\frac{1}{2}}_{13;24}}{D^{2,\frac{1}{2}}_{13;24}}\right]^2 = \frac{(Q-1)(Q-4)(Q^2-4Q+2)}{2Q(Q-3)^2}\left[\frac{C^{(4,\frac{1}{2})}_{(0,\frac{1}{2}),(0,\frac{1}{2})}}{C^{(2,\frac{1}{2})}_{(0,\frac{1}{2}),(0,\frac{1}{2})}}\right]^2$$
$$= \frac{(Q-1)(Q-4)(Q^2-4Q+2)}{2Q(Q-3)^2} \times (4.20b)^2|_{\substack{r=2\\s=\frac{1}{2}}} \times (4.20b)^2|_{\substack{r=0\\s=\frac{1}{2}}} \tag{4.23f}$$

$$\left[\frac{D^{2,0}_{13;24}}{D^{2,0}_{1234}}\right]^2 = \frac{2-Q}{2} \tag{4.23g}$$

$$\left[\frac{D^{4,0}_{13;24}}{D^{4,0}_{1234}}\right]^2 = -\frac{(Q^2-4Q+2)(Q^2-3Q-2)}{4}. \tag{4.23h}$$

In Table 4.2 we summarise these findings: it gives a picture of the extent of our current knowledge of the random Potts model[3].

3 We have not included in this table the most recent findings of [48].

(r,s) \ σ	1234	12;34	13;24	14;23
$(1,1)^D$	0	1	0	0
$(0,\frac{1}{2})$	$\sqrt{2}C^{(0,\frac{1}{2})}_{(0,\frac{1}{2}),(0,\frac{1}{2})}$	$-\sqrt{2}C^{(0,\frac{1}{2})}_{(0,\frac{1}{2}),(0,\frac{1}{2})}$	0	0
$(2,\frac{1}{2})$	0	0	(4.23e) $\frac{1}{2}C^{(0,\frac{1}{2})}_{(0,\frac{1}{2}),(0,\frac{1}{2})}$	$\pm iD^{(2,\frac{1}{2})}_{13;24}$
$(4,\frac{1}{2})$	(4.23a) $\frac{1}{2}D^{(0,\frac{1}{2})}_{1234}$	(4.23b) $\frac{1}{2}D^{(4,\frac{1}{2})}_{1234}$	(4.23f) $\frac{1}{2}D^{(2,\frac{1}{2})}_{13,24}$	$\pm D^{(4,\frac{1}{2})}_{13;24}$
$(2,0)$	B	(4.23c) $\frac{1}{2}D^{(2,0)}_{1234}$	(4.23g) $\frac{1}{2}D^{(2,0)}_{1234}$	$\pm D^{(2,0)}_{13;24}$
$(4,0)$	B	(4.23d) $\frac{1}{2}D^{(4,0)}_{1234}$	(4.23h) $\frac{1}{2}D^{(4,0)}_{1234}$	$\pm D^{(4,0)}_{13;24}$
$(4,\frac{1}{4})$	0	0	B	$\pm iD^{(4,\frac{1}{4})}_{13;24}$
$\vdots$	$\cdots$			

Table 4.2: Structure constants $D^{(r,s)}_{\sigma}$ entering the different connectivities indexed by σ, for the first labels $r \in 2\mathbb{Z}$. The letter B indicates that the corresponding constant has been determined by numerical bootstrap [47].

These structure constants are of the type $D^{(r,s)}_{(0,1/2),(0,1/2)}$. Solving the full CFT would amount to find also the structure constants of the type $D^{(r_3,s_3)}_{(r_1,s_1),(r_2,s_2)}$ which govern the OPEs of fields V_{r_1,s_1}, V_{r_2,s_2} with different dimensions. As discussed in Section 4.3 the structure constants $D^{(1,n)^{D,\text{quot}}}_{(0,s_1),(0,s_2)}$, $s_1 \neq s_2 \in \mathbb{Z}+1/2$ enter the expansions of the connectivities on the square torus. We do not know if all constants $D^{(r_3,s_3)}_{(r_1,s_1),(r_2,s_2)}$ enter the expansions of physical correlation functions.

4.3 CONNECTIVITIES ON THE TORUS

We now present our results on the torus.
Although the general case of a rectangular torus ($M \neq N$) contains interesting information which we discuss in Section 4.3.2, we have mainly worked on a square torus with modular parameter $\tau = i$ (cf. Section 2.2), parametrised by the coordinate w. Below we give our general result for the connectivities, and explain the different expansions involved. Technical details about the derivation are provided in Section 4.3.1. Our general prediction for the dominant topological corrections to the s-channel expansions are:

$$p_{12}\left(w_{12},N|\tau=i\right)=\frac{1}{\left|w_{12}\right|^{4\Delta_{0,\frac{1}{2}}}}\left[1+\sum_{n>1}a^{(2)}_{(\Delta^{D,\text{quot}}_{1,n})}(\tau)\left|\frac{w_{12}}{N}\right|^{2\Delta^{D,\text{quot}}_{1,n}}\right] \tag{4.24}$$

$$p_{123}\left(w_{12},w_{13},w_{23},N|\tau=i\right)=\frac{D^{(0,\frac{1}{2})}_{(0,\frac{1}{2}),(0,\frac{1}{2})}}{\left|w_{12}w_{13}w_{23}\right|^{2\Delta_{0,\frac{1}{2}}}}+\frac{1}{\left|w_{12}^2w_{23}\right|^{2\Delta_{0,\frac{1}{2}}}}\sum_{n>1}a^{(3)}_{(\Delta^{D,\text{quot}}_{1,n})}\left(\frac{w_{12}}{w_{23}}|\tau\right)\left|\frac{w_{23}}{N}\right|^{2\Delta^{D,\text{quot}}_{1,n}} \tag{4.25}$$

$$p_{1234}\left(w_{12},w_{34},w_{24},N|\tau=i\right)=\frac{1}{\left|w_{12}w_{34}\right|^{4\Delta_{0,\frac{1}{2}}}}\left[p_{1234}(w)+\sum_{n>1}a^{(4)}_{(\Delta^{D,\text{quot}}_{1,n})}\left(\frac{w_{12}}{w_{24}},\frac{w_{34}}{w_{24}}|\tau\right)\left|\frac{w_{24}}{N}\right|^{2\Delta^{D,\text{quot}}_{1,n}}\right] \tag{4.26}$$

We recall (cf. Chapter 2) that each term correspond to the contribution of a particular field in the CFT. Here there are several expansions involved, of which we compute the dominant terms:

1. the topological expansion in w_{ij}/N: we computed the leading and first sub-leading terms corresponding to the contributions of $V^{D,\text{quot}}_{(1,2)}$ and $V^{D,\text{quot}}_{(1,3)}$.

2. the expansions of the coefficients $a^{(i)}_{\Delta}$. They are given by (2.68,2.78,2.87):

$$a^{(2)}_{(\Delta^D_{1,n})}(\tau) = \langle V_{(1,n)^D}\rangle_\tau D^{(1,n)^D}_{(0,\frac12),(0,\frac12)} \tag{4.27}$$

$$a^{(3)}_{(\Delta^D_{1,n})}\left(\frac{w_{12}}{w_{23}}|\tau\right) = \langle V_{(1,n)^D}\rangle_\tau \sum_{\Delta_L} D^{(\Delta_L)}_{(0,\frac12),(0,\frac12)} D^{(1,n)^D}_{(\Delta_L),(0,\frac12)} \left|\left(\frac{w_{12}}{w_{23}}\right)^{\Delta_L}\right|^2 \tag{4.28}$$

$$a^{(4)}_{(\Delta^D_{1,n})}\left(\frac{w_{12}}{w_{24}},\frac{w_{34}}{w_{24}}|\tau\right) = \langle V_{(1,n)^D}\rangle_\tau \sum_{\Delta_L,\Delta_R} D^{(\Delta_L)}_{(0,\frac12),(0,\frac12)} D^{(\Delta_R)}_{(0,\frac12),(0,\frac12)} D^{(1,n)^D}_{(\Delta_L),(\Delta_R)} \left|\left(\frac{w_{12}}{w_{24}}\right)^{\Delta_L}\left(\frac{w_{34}}{w_{24}}\right)^{\Delta_R}\right|^2 \tag{4.29}$$

   where we used notation (0.1), and with the one-point function given by (2.20).

   i. The one-point functions are expansions over the elliptic nome $q = e^{2\pi i\tau}$ (see Section 2.3). They are given in Section 4.3.1.

   ii. The coefficients $a^{(3)}$ and $a^{(4)}$ are themselves expansions over all –primary and descendant fields V_L, V_R which satisfy the fusions at each node (see diagrams 4.5 below).

   - We computed the contributions of the dominant and subdominant primary fields.
   - In addition the contributions of the descendants of V_L and V_R were computed up to order 2 (ie taking into account the contributions of level 1 and level 2 descendants).

3. Finally the plane four-point function in 4.29 is given by expansion (4.17) in the cross-ratio w.

In (4.24-4.26) the structure constants $D^{(r_3,s_3)}_{(r_1,s_1),(r_2,s_2)}$ are taken to be the Liouville structure constants:

$$D^{(r_3,s_3)}_{(r_1,s_1),(r_2,s_2)} = \begin{cases} \sqrt{2}C^{(r_3,s_3)}_{(r_1,s_1),(r_2,s_2)} & \text{if } r_i, s_i = 0, \mathbb{Z}+\frac12,\ i=1,2,3 \\ C^{(r_3,s_3)}_{(r_1,s_1),(r_2,s_2)} & \text{otherwise.} \end{cases} \tag{4.30}$$

These structure constants can be conveniently computed for any Q from [100].
The agreement of (4.24-4.26) with the numerical data is excellent: not only it is good when computing the dominant terms of the different expansions above, but most importantly it improves when adding subleading contributions, as shown in Figure 4.3 for the topological expansion and in Figure 4.4 for the $a^{(i)}$'s expansion. Thus the spectra (4.1) and the Liouville structure constants are consistent not only one the plane but also on the torus. Another observation, which is not explained at the moment is that the topological contributions involve only the diagonal, degenerate sector $S^{D,\text{quot}}_{1,\mathbb{N}_*}$. In the full spectrum (4.2), these diagonal fields are not the ones with the smallest dimensions, as is visible in Figure 4.2. The fact that other fields with smaller dimension do not contribute can have two origins:

- either they do not appear in the corresponding fusion
- or their one-point function vanishes, so that $a^{(i)}_{(\Delta)} = 0$ (cf. (4.27-4.29)). This is the case of the fields in $S_{0,\mathbb{Z}+\frac{1}{2}}$ for integer values of Q.

We give avenues to explore this issue in Section 4.3.2.

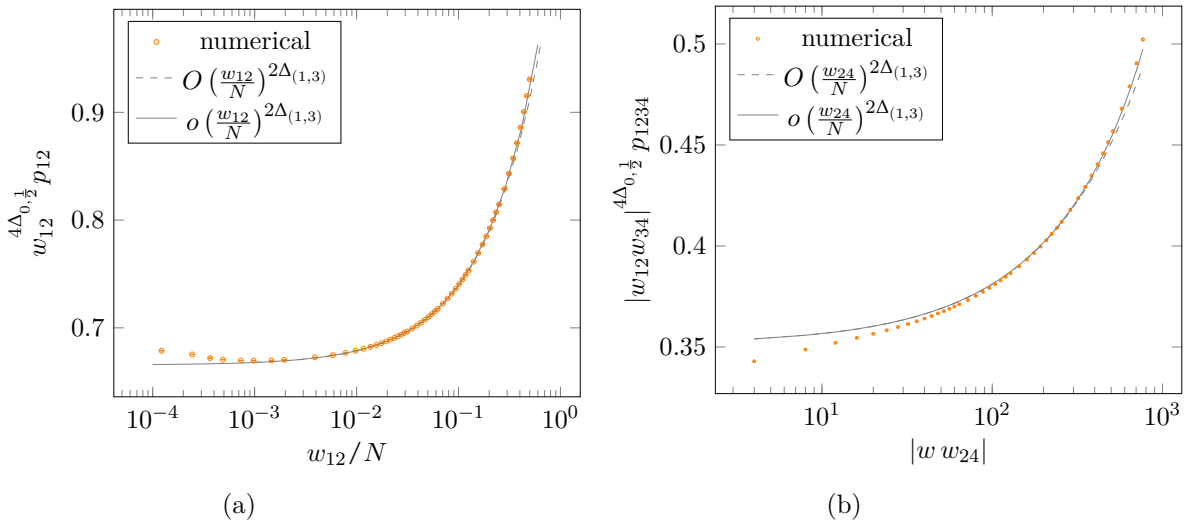

(a) (b)

Figure 4.3: Expansions (4.24) (a) and (4.26) (b) computed including only the dominant (dashed) and both dominant and subdominant topological corrections (solid), and the comparison with numerical data at $Q = 3.25$, where the dimension of the sub-dominant field $V^D_{(1,3)}$ is small (see Figure 4.2). Error bars are smaller that the marker size.

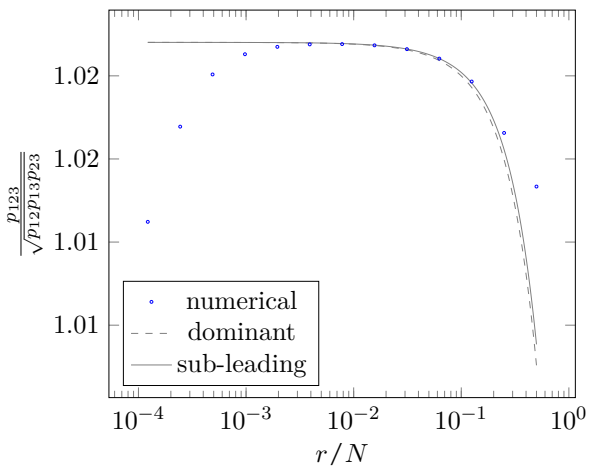

(a) Ratio of three- to two-point connectivities measured at $Q = 1$, with the points at the vertices of an isosceles triangle of side r.

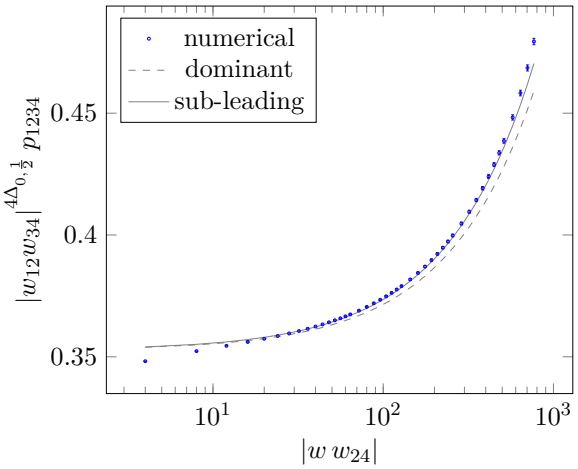

(b) Four-point connectivity measured at $Q = 2.75$.

Figure 4.4: Convergence of the level expansion of the three-point function (left) and convergence of the channel expansion of the four-point function (right). Dashed (resp. solid) correspond to computation of $a^{(i)}$ to the dominant (resp. subdominant) orders.

4.3.1 *Constraints from* $S^{D,\text{quot}}_{1,\mathbb{N}_*}$

The computation of the expansions (4.27-4.29) rely on the fact that the energy field is degenerate. As seen in Section 4.2, this fact has the important consequence that some structure constants are related by shift equations. In the topological expansions the degenerate fields $V^{D,\text{quot}}_{(1,n)}$ provide other types of constraints, which make some of the expansions (4.24-4.26) exact. These constraints originate from the fusion rules that a degenerate field imposes at the different nodes of a given diagram as shown in Figure 4.5:

- on which fields contribute to its one-point function
- on which fields appear in the intermediate channels V_L, V_R.

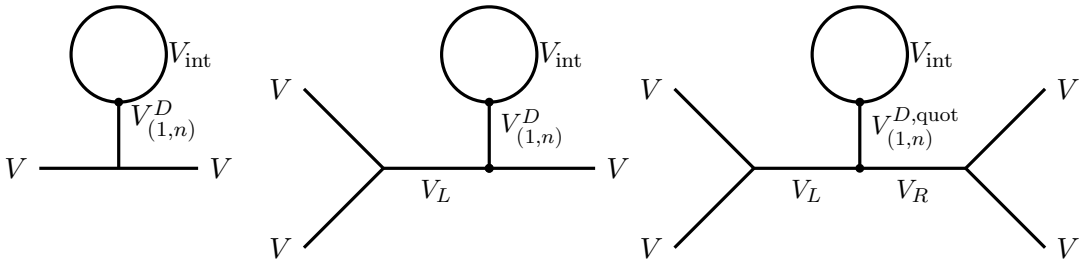

Figure 4.5: The degenerate field $V^{D,\text{quot}}_{(1,n)}$ imposes fusion rules at the marked nodes.

One-point functions of $\langle V^{D,\text{quot}}_{(1,2)}\rangle$ *and* $\langle V^{D,\text{quot}}_{(1,3)}\rangle$

In particular the level 2 degeneracy of $V^{D,\text{quot}}_{(1,2)}$ puts strong constraints on the fields which contribute to its one-point expansion (2.21). Indeed the fusion rules:

$$\mathcal{R}\times\mathcal{R}_{\text{int}}\to\mathcal{R}_{\text{int}} \quad \text{from (2.16)} \tag{4.31}$$
$$\mathcal{R}_{1,2}\times\mathcal{R}_{r,s}=\mathcal{R}_{r,s\pm1} \quad \text{from degeneracy} \tag{4.32}$$

imply

$$\begin{aligned}&\alpha_{r,s\pm1}=\alpha_{r,s} \quad \text{or}\\ &\alpha_{r,s\pm1}=Q-\alpha_{r,s}\end{aligned} \tag{4.33}$$

The only solution is $r,s=0,1/2$, so that only the connectivity field flows in the internal channel (see Figure 4.6). The expansion (2.21) then becomes exact:

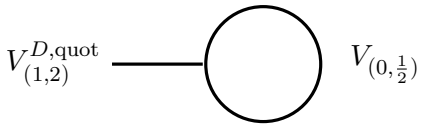

Figure 4.6

$$\langle V^{D,\text{quot}}_{(1,2)}\rangle_\tau=\frac{(2\pi)^{2\Delta_{(1,2)}}}{Z(q,\bar q)}\,(Q-1)\,C^{(0,\frac12)}_{(0,\frac12),(1,2)^D}q^{\Delta_{(0,\frac12)}-\frac{c}{24}}\bar q^{\Delta_{(0,\frac12)}-\frac{c}{24}}\left|\mathcal{F}^{(1)}_{\Delta_{(0,\frac12)}}(\Delta_{(1,2)}|q)\right|^2 \tag{4.34}$$

with the $Q-1$ factor coming from the multiplicity of the connectivity field. In practice, to compute this expansion we truncate the q series coming from the expansion of the partition function, as well as the expansion of the conformal block.
Such reduction does not happen for the subleading field $V^{D,\text{quot}}_{(1,3)}$: indeed from the fusion

$$\mathcal{R}_{1,3} \times \mathcal{R}_{r,s} = \mathcal{R}_{r,s-2} \oplus \mathcal{R}_{r,s} \oplus \mathcal{R}_{r,s+2} \tag{4.35}$$

any field can flow in the internal channel. The expansion (2.21) is therefore computed by including the contributions of all fields of lowest dimension in the spectrum, ie from 4.2:

$$\begin{aligned}\langle V^{D,\text{quot}}_{(1,3)} \rangle_\tau = \frac{(2\pi)^{2\Delta_{(1,3)}}}{|q|^{\frac{c}{12}} Z(q,\bar{q})} \Bigg[& 2C^{(0,\frac{1}{2})}_{(0,\frac{1}{2}),(1,3)^D} q^{\Delta_{(0,\frac{1}{2})}} \bar{q}^{\Delta_{(0,\frac{1}{2})}} \left| \mathcal{F}^{(1)}_{\Delta_{(0,\frac{1}{2})}}(\Delta_{(1,3)}|q) \right|^2 \\ & + C^{(1,2)}_{(1,2),(1,3)^D} q^{\Delta_{(1,2)}} \bar{q}^{\Delta_{(1,2)}} \left| \mathcal{F}^{(1)}_{\Delta_{(1,2)}}(\Delta_{(1,3)}|q) \right|^2 \\ & + C^{(0,\frac{3}{2})}_{(0,\frac{3}{2}),(1,3)^D} q^{\Delta_{(0,\frac{3}{2})}} \bar{q}^{\Delta_{(0,\frac{3}{2})}} \left| \mathcal{F}^{(1)}_{\Delta_{(0,\frac{3}{2})}}(\Delta_{(1,3)}|q) \right|^2 \Bigg].\end{aligned} \tag{4.36}$$

This is shown in Figure 4.7 for Q around 3, where the contribution of $V^{D,\text{quot}}_{(1,3)}$ in the topological expansions (4.24-4.26) is visible numerically. For smaller Q the dimension $\Delta_{1,3}$ becomes very large (cf. Figure 4.2) and the contribution of $V^{D,\text{quot}}_{(1,3)}$ can be neglected. Exactly at $Q=3$ we have (4.16):

$$\begin{aligned} V_{(0,\frac{1}{2})} &= V_{(3,3)} \\ V_{(0,\frac{3}{2})} &= V_{(3,1)} \\ V_{(1,3)} &= V_{(5,2)}. \end{aligned}$$

The extra fusion rules imposed by the last equality reduce the possible internal fields to $\left\{V_{(3,3)}, V_{(1,2)}, V_{(1,3)}\right\}$, so that in that case we obtain the exact expansion:

$$\begin{aligned}\langle V^{D,\text{quot}}_{(1,3)} \rangle_\tau \overset{Q=3}{=} \frac{(2\pi)^{2\Delta_{(1,3)}}}{|q|^{\frac{c}{12}} Z(q,\bar{q})} \Bigg[& 2C^{(3,3)^D}_{(3,3)^D,(1,3)^D} q^{\Delta_{(3,3)}} \bar{q}^{\Delta_{(3,3)}} \left| \mathcal{F}^{(1)}_{\Delta_{(3,3)}}(\Delta_{(1,3)}|q) \right|^2 \\ & + C^{(1,2)^D}_{(1,2)^D,(1,3)^D} q^{\Delta_{(1,2)}} \bar{q}^{\Delta_{(1,2)}} \left| \mathcal{F}^{(1)}_{\Delta_{(1,2)}}(\Delta_{(1,3)}|q) \right|^2 \\ & + C^{(1,3)^D}_{(1,3)^D,(1,3)^D} q^{\Delta_{(1,3)}} \bar{q}^{\Delta_{(1,3)}} \left| \mathcal{F}^{(1)}_{\Delta_{(1,3)}}(\Delta_{(1,3)}|q) \right|^2 \Bigg].\end{aligned} \tag{4.37}$$

The last term is extremely small

$$\frac{C^{(1,3)^D}_{(1,3)^D,(1,3)^D} q^{\Delta_{(1,3)}} \bar{q}^{\Delta_{(1,3)}} \left| \mathcal{F}^{(1)}_{\Delta_{(1,3)}}(\Delta_{(1,3)}|q) \right|^2}{C^{(1,2)^D}_{(1,2)^D,(1,3)^D} q^{\Delta_{(1,2)}} \bar{q}^{\Delta_{(1,2)}} \left| \mathcal{F}^{(1)}_{\Delta_{(1,2)}}(\Delta_{(1,3)}|q) \right|^2} \sim 10^{-10}. \tag{4.38}$$

We compare in Figure 4.7 the exact expansion (4.37) with (4.36), which shows that the truncation (4.36) gives a very good approximation at $Q=3$.

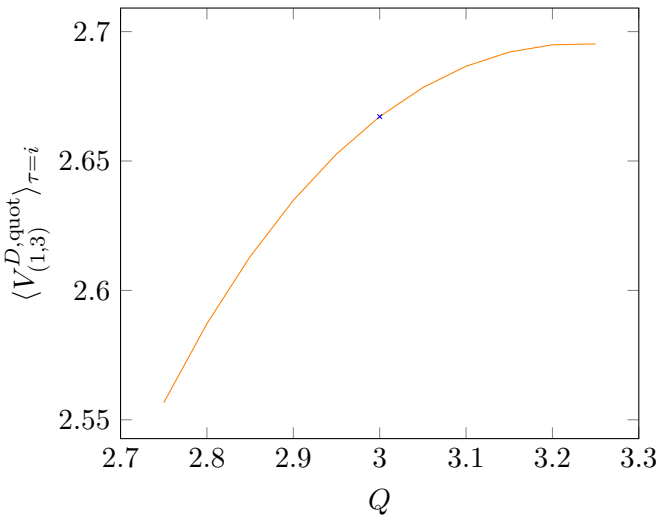

Figure 4.7: $\langle V^{D,\text{quot}}_{(1,3)} \rangle_{\tau=i}$ computed as expansion (4.36) (orange curve), and the exact value (4.37) at $Q = 3$ (blue cross).

Constraints on the three-point

The fusion rule imposed by $V^{D,\text{quot}}_{(1,2)}$ at the node in diagram 4.5 reads:

$$\mathcal{R}_{1,2} \times \mathcal{R}_{0,\frac{1}{2}} = \mathcal{R}_{0,\frac{1}{2}} \oplus \mathcal{R}_{0,\frac{3}{2}} \tag{4.39}$$

so that there only two possible intermediate channels:

$$\begin{aligned} V_L &= V_{(0,\frac{1}{2})} \\ V_L &= V_{(0,\frac{3}{2})}. \end{aligned} \tag{4.40}$$

The expansion of the coefficient $a^{(3)}_{(\Delta^D_{1,2})}$ (4.28) thus truncates to:

$$\begin{aligned} a^{(3)}_{(\Delta^D_{1,2})} = \langle V_{(1,2)^D} \rangle_\tau \Bigg[& \sqrt{2} C^{(0,\frac{1}{2})}_{(0,\frac{1}{2}),(0,\frac{1}{2})} C^{(1,2)^D}_{(0,\frac{1}{2}),(0,\frac{1}{2})} \left| \frac{w_{12}}{w_{23}} \right|^{2\Delta_{(0,\frac{1}{2})}} \left| \mathcal{F}^{(3)}_{\Delta_{(0,\frac{1}{2})}} \left(\Delta_{(1,2)}, \Delta_{(0,\frac{1}{2})} \middle| \frac{w_{12}}{w_{23}} \right) \right|^2 \\ & + \sqrt{2} C^{(0,\frac{3}{2})}_{(0,\frac{1}{2}),(0,\frac{1}{2})} C^{(1,2)^D}_{(0,\frac{3}{2}),(0,\frac{1}{2})} \left| \frac{w_{12}}{w_{23}} \right|^{2\Delta_{(0,\frac{3}{2})}} \left| \mathcal{F}^{(3)}_{\Delta_{(0,\frac{3}{2})}} \left(\Delta_{(1,2)}, \Delta_{(0,\frac{1}{2})} \middle| \frac{w_{12}}{w_{23}} \right) \right|^2 \Bigg] \end{aligned} \tag{4.41}$$

with the contribution of the descendants contained in the three-point blocks (2.79). The comparison with the numerical points is given in Figure 4.4a, with the conformal block expansion truncated to level one or to level 2.

Constraints on the four-point

Similarly for the four-point function the dimensions of V_L and V_R are constrained by $V^{D,\text{quot}}_{(1,2)}$:

$$\alpha_{r_R,s_R} = \alpha_{r_L,s_L \pm 1}. \tag{4.42}$$

From the fusion spectrum 4.1, Figure 4.2 and the constraint above, the dominant and first subdominant contributions are given respectively by

$$\begin{aligned} &\text{dominant} \quad V_L = V_R = V_{(0,\frac{1}{2})} \\ &\text{subdominant} \quad V_L = V_{(0,\frac{1}{2})} \quad V_R = V_{(0,\frac{3}{2})}. \end{aligned} \tag{4.43}$$

The convergence of the channel expansion of $a^{(4)}$ (4.29) is shown in Figure 4.4b. Notably, the agreement of this expansion, as well as (4.41) with the numerics[4] provided a test that $D^{(0,\frac{3}{2})}_{(0,\frac{1}{2}),(0,\frac{1}{2})}$ is indeed given by $\sqrt{2}C^{(0,\frac{3}{2})}_{(0,\frac{1}{2}),(0,\frac{1}{2})}$.

4.3.2 *Further developments*

In this section we point out an aspect which has not been investigated in the published articles. We noted above that only the degenerate diagonal fields contribute to topological corrections of the connectivities (4.24-4.26). The question is wether the other fields do not appear in the fusion spectrum or if their contribution is zero because their one-point functions vanish.
The analysis in Article II and Article III has been done mainly on the square torus $M = N$. In this case the one-point functions of non-scalar fields vanish by rotational invariance (see next chapter for more details), and therefore they would not contribute to the connectivities (4.24-4.26). However, on a non-square torus $M \neq N$ we get in principle contributions from non-scalar fields. As explained in details in the next chapter, we can directly probe such contributions by taking the difference of connectivities measured along two different axes. Let us consider for simplicity the two-point connectivity measured along two perpendicular axes w and $w^\perp$:

$$|w|^{4\Delta_{0,\frac{1}{2}}} \left(p_{12}(w) - p_{12}(w^\perp)\right) = 4\, d_0^{(2)} \left\{ a_T^{(2)}(\tau) \left|\frac{w}{N}\right|^2 + a_{(2,1)}^{(2)}(\tau) \left|\frac{w}{N}\right|^{\Delta_{2,1}+\bar{\Delta}_{2,1}} + \cdots \right\} \tag{4.44}$$

where the leading contribution comes from the two stress-energy tensors T and $\bar{T}$ which are the non-scalar fields with the smallest dimensions $\Delta + \bar{\Delta} = 2$. Looking at Figure 4.2, the next contribution should come from the primary field $V_{(2,1)}$. The coefficient $a_T^{(2)} = \frac{2\Delta_{0,1/2}}{c}\langle T \rangle_\tau$ can be computed for all Q (see Section 2.4.1 and next chapter). Prediction (4.44) has been tested in Article II for $Q = 1$. In this particular case the dimension and spin of $V_{(2,1)}$ become precisely equal to those of the stress-energy tensor (cf. Figure 4.2). We would like to repeat this analysis for $Q > 1$, where the contribution of $V_{(2,1)}$ should become numerically visible. Namely, we could measure:

$$a_{(2,1)}^{(2)}(\tau) = D^{(2,1)}_{(0,\frac{1}{2}),(0,\frac{1}{2})} \langle V_{(2,1)} \rangle_\tau. \tag{4.45}$$

It would be interesting to be able to extract the value of $D^{(2,1)}_{(0,\frac{1}{2}),(0,\frac{1}{2})}$, and see if it is given by one of the constants $D_\sigma^{(2,1)}$ of Table 4.2.

4 The agreement is even better seen for values of Q at which singularities arise, such as the case $Q = 2$ discussed in Section C.1 and D.1 of Article III.

4.4 CONCLUSION

The study of the connectivities of the random Potts model on the torus provided tests of conjectures on the underlying CFT, notably in what concerns the structure constants. These conjectures have been subsequently put on solid grounds by the (almost complete) determination of the four-point connectivities [47, 48]. The analysis on the square torus showed that for all connectivities the topological corrections are given by the diagonal, degenerate fields in the theory. Wether the connectivity fields do not fuse onto the other fields in the spectrum, or wether these latter do not appear in the expansions because their one-point functions vanish is an open question. This question can be partially answered by carrying the same analysis on general, rectangular torii, where non-scalar fields have generically non-zero one-point functions.
Importantly, the predictions of the torus effects provide a numerical test of the universality class for other percolation systems, which can be applied to a large class of models (notably, no knowledge of a lattice representation is required), and which goes beyond the determination of critical exponents by probing non-trivial CFT data. In this way, our prediction for the torus two-point connectivity of pure percolation will be of importance in the analysis of the random surface model in the next chapter.

As a concluding note, the Potts CFT saga is an illustrative example of a fruitful combination of bootstrap and lattice expertises. One can hope that all the pieces of the puzzle will fall in place in the near future, with more structure constants being determined by precise numerical bootstrap [48], and deeper study of the algebraic structure of the model [49].

Journal of Statistical Mechanics:
Theory and Experiment

SISSA

PAPER: QUANTUM STATISTICAL PHYSICS, CONDENSED MATTER, INTEGRABLE SYSTEMS

Two-point connectivity of two-dimensional critical *Q*-Potts random clusters on the torus

Journal of Statistical Mechanics: Theory and Experiment
An IOP and SISSA journal

PAPER: Quantum statistical physics, condensed matter, integrable systems

Two-point connectivity of two-dimensional critical Q-Potts random clusters on the torus

Nina Javerzat[1], Marco Picco[2] and Raoul Santachiara[1]

[1] LPTMS, CNRS (UMR 8626), Univ.Paris-Sud, Université Paris-Saclay, 91405 Orsay, France
[2] LPTHE, UMR 7589, Sorbonne Université and CNRS, France
E-mail: nina.javerzat@u-psud.fr, picco@lpthe.jussieu.fr and raoul.santachiara@u-psud.fr

Received 29 August 2019
Accepted for publication 28 November 2019
Published 4 February 2020

Online at stacks.iop.org/JSTAT/2020/023101
https://doi.org/10.1088/1742-5468/ab6331

Abstract. We consider the two dimensional Q-random-cluster Potts model on the torus and at the critical point. We study the probability for two points to be connected by a cluster for general values of $Q \in [1, 4]$. Using a conformal field theory (CFT) approach, we provide the leading topological corrections to the plane limit of this probability. These corrections have universal nature and include, as a special case, the universality class of two-dimensional critical percolation. We compare our predictions to Monte Carlo measurements. Finally, we take Monte Carlo measurements of the torus energy one-point function that we compare to CFT computations.

Keywords: conformal field theory, correlation functions

J. Stat. Mech. (2020) 023101

1742-5468/20/023101+23$33.00

Contents

1. Introduction

The critical point of a two-dimensional statistical model can be often characterised in terms of extended objects that, in the continuum limit, are described by conformal invariant fractal structures [1]. The study of these fractals provided new insights into the nature of critical phenomena paving the way to mathematically rigorous approaches [2]. On the one hand, many of the results found so far involve quantities related to two-point correlation functions of a conformal field theory (CFT). The only exceptions concern observables that satisfy some differential equation and whose definition requires the existence of a boundary, such as crossing probabilities [3] or SLE interfaces [4]. On the other hand, the (bootstrap) solution of a CFT requires the knowledge of three- and four-point correlation functions. Besides some special cases [5, 6], the only known bootstrap solutions known to describe statistical critical points are the minimal models. These CFTs have been successful in providing the behaviour of local observables of critical systems, such as the Ising spin correlation function, but they are too simple to capture the geometry of conformal fractals. The description of these fractals hints therefore at the existence of a CFT whose solution remains an open puzzle.

J. Stat. Mech. (2020) 023101

The random cluster Q-state Potts models [7] represent an ideal laboratory in this context. This is a one parameter family of models which includes as special cases the spanning forests ($Q \to 0$) [8], the (bond) percolation ($Q = 1$), the Ising ($Q = 2$) and the three-state Potts ($Q = 3$) spin models, as well as the permutation symmetric point of the Ashkin–Teller model ($Q = 4$). For $0 \leqslant Q \leqslant 4$, the Q-state Potts model has a critical point at which the clusters percolate and have a conformal invariant measure. Natural observables are the cluster connectivities, given by the probability that a number of lattice points belong to the same or different clusters [9–11]. The conjecture of Delfino and Viti on the three-point connectivities [12] has been at the origin of a series of papers [13–20] which unveiled important insights on the still unknown bootstrap solution.

In this paper we focus on the *two-point* connectivity *on a torus*. This study is motivated by two facts:

- In order to increase the number of samplings, Monte Carlo measurements are conveniently taken on doubly periodic lattices [19]: a precise knowledge of topological corrections is therefore needed to extract the scaling plane limit which is then compared to the CFT on the sphere predictions.
- The torus topological effects encode informations on the set of states and on the three-point functions, which are the basic ingredients to solve a CFT.

In section 2 we review notions of CFT on a torus and provide the general formulas we will need. In section 3 we define the lattice observables and we provide analytical results on their universal finite size behaviours. These results are then compared with the numerical results in section 5, where details of the simulations are also discussed. The final conclusions are found in section 6.

2. Conformal field theory on a torus

2.1. Virasoro algebra and its representation

Consider first a CFT on a plane $z \in (\mathbb{C} \bigcup \{\infty\})$ [21] with $T(z)$ and $\bar{T}(\bar{z})$ the holomorphic and anti-holomorphic component of the stress energy-tensor. The holomorphic stress-energy modes $L_n^{(z)}$, defined in (A.1) form the Virasoro algebra $\mathcal{V}_c$ with central charge c:

$$\left[L_n^{(z)}, L_m^{(z)}\right] = (n-m)L_{n+m}^{(z)} + \frac{c}{12} n(n^2-1)\delta_{n,m}. \tag{2.1}$$

The anti-holomorphic modes $\bar{L}_n^{(z)}$ are analogously defined and form a second Virasoro algebra $\overline{\mathcal{V}}_c$, with the same central charge, that commutes with (2.1).

A highest-weight representation of $\mathcal{V}_c$ is labelled by the conformal dimension Δ: it contains the primary field V_Δ, $L_n|V_\Delta\rangle = 0$ for $n > 0$, and its descendants, obtained by acting with the negative modes on the primary state. Given a Young diagram $Y = \{n_1, n_2 \cdots\}$, with $n_i \in \mathbb{N}, n_i \leqslant n_{i+1}$, the fields

$$V_\Delta^{(Y)} = L_{-Y}^{(z)} V_\Delta = L_{-n_1}^{(z)} L_{-n_2}^{(z)} \cdots V_\Delta \quad (V_\Delta^{(\{0\})} = V_\Delta) \tag{2.2}$$

J. Stat. Mech. (2020) 023101

form a complete basis of the Δ representation. The descendant $V_\Delta^{(Y)}$ has total dimension $\Delta + |Y|$, where $|Y| = \sum n_i$ is called the level of the descendant. For general Δ, the number of independent descendants is therefore the number of partitions of $|Y|$. The inner product $H_\Delta(Y, Y')$ between descendants is defined as:

$$H_\Delta(Y, Y') = \lim_{z\to\infty} z^{2\Delta} \left\langle V_\Delta(z) L_Y^{(0)} L_{-Y'}^{(0)} V_\Delta(0) \right\rangle, \tag{2.3}$$

and is completely defined by the algebra (2.1). For certain values of Δ, see (2.9), the representations are degenerate: they contain a descendant field, usually called the null state, which has vanishing norm. For unitary CFTs, the null state is set to zero. Otherwise, one can have CFTs where null states are not vanishing, like for instance in [22]. For the sake of simplicity, we will continue to denote the descendant states as $V_\Delta^{(Y)}$ even when the presence of a vanishing null state makes their number smaller than the number of partitions. In this case, the notation Y is meant to label the independent non-vanishing descendants.

The spectrum $\mathcal{S}$ of a CFT is formed by the representations of $\mathcal{V}_c \otimes \overline{\mathcal{V}}_c$ appearing in the theory and labelled by the holomorphic and anti-holomorphic dimensions $\Delta, \bar{\Delta}$. In order to simplify the formulas, we use the notations $(\Delta)_i = \Delta_i, \bar{\Delta}_i$ and $(\Delta, Y)_i = (\Delta_i, Y_i), (\bar{\Delta}_i, \bar{Y}_i)$. In these notations, a $\mathcal{V}_c \otimes \overline{\mathcal{V}}_c$ primary field and its descendants are

$$V_{(\Delta)}(z, \bar{z}) = V_\Delta(z) V_{\bar{\Delta}}(\bar{z}), \quad V_{(\Delta,Y)}(z, \bar{z}) = L_{-Y}^{(z)} \bar{L}_{-\bar{Y}}^{(\bar{z})} V_\Delta(z) V_{\bar{\Delta}}(\bar{z}). \tag{2.4}$$

The product of two primary fields (OPE) can be expanded in terms of the states appearing in the spectrum $\mathcal{S}$ [21]:

$$V_{(\Delta)_1}(z, \bar{z})\, V_{(\Delta)_2}(0) \to a_{(\Delta)_1,(\Delta)_2}^{(\Delta,Y)_3}(z, \bar{z})\, V_{(\Delta,Y)_3}(0), \tag{2.5}$$

where the coefficients are factorised as:

$$a_{(\Delta)_1,(\Delta)_2}^{(\Delta,Y)_3}(z, \bar{z}) = C_{(\Delta)_1,(\Delta)_2}^{(\Delta)_3}\, \beta_{\Delta_1,\Delta_2}^{(\Delta_3,Y_3)}(z)\, \beta_{\bar{\Delta}_1,\bar{\Delta}_2}^{(\bar{\Delta},\bar{Y}_3)}(\bar{z}). \tag{2.6}$$

One factor is the (model dependent) structure constant $C_{(\Delta)_1,(\Delta)_2}^{(\Delta)_3}$, the other factor is fixed by the algebra (2.1):

$$\beta_{\Delta_1,\Delta_2}^{(\Delta_3,Y_3)}(z) = z^{-\Delta_1-\Delta_2+\Delta_3+|Y|} \sum_{\substack{Y' \\ |Y'|=|Y|}} H_{\Delta_3}^{-1}(Y, Y')\, \Gamma_{(\Delta_2,\{0\}),(\Delta_1,\{0\}))}^{(\Delta_3,Y')}, \tag{2.7}$$

where:

$$\Gamma_{(\Delta_1,Y_1),(\Delta_2,Y_3)}^{(\Delta_3,Y_3)} = \frac{\left\langle L_{-Y_3}^{(\infty)}\, V_{\Delta_3}(\infty) L_{-Y_2}^{(1)} V_{\Delta_2}(1) L_{-Y_1}^{(0)} V_{\Delta_1}(0) \right\rangle}{\langle V_{\Delta_3}(\infty) V_{\Delta_2}(1) V_{\Delta_1}(0) \rangle}. \tag{2.8}$$

Under the replacement $\Delta_i \to \bar{\Delta}_i$, the above formulas define $\beta_{\bar{\Delta}_1,\bar{\Delta}_2}^{(\Delta_3,\bar{Y}_3)}(\bar{z})$ too. The three-point function (2.8) can be computed in an efficient way by the recursion formulas in [23].

In the study of the critical random Potts model, the following series of notations turns out to be very convenient. The conformal dimension can be parametrised as follows

J. Stat. Mech. (2020) 023101

$$\Delta = \Delta_{(r,s)} = \frac{c-1}{24} + \frac{1}{4}\left(r\beta - \frac{s}{\beta}\right)^2. \tag{2.9}$$

A representation is degenerate if $r, s \in \mathbb{N}^*$, and has a null state at level rs. The symbols

$$V_{\Delta_{(r,s)},\Delta_{(r,s)}} = V_{(r,s)^D}, \quad V_{\Delta_{(r,s)},\Delta_{(r,-s)}} = V_{(r,s)} \tag{2.10}$$

indicate the diagonal and non-diagonal primary fields and the notations

$$(r,s)^D, \quad (r,s) \tag{2.11}$$

denote the representations associated to $V_{(r,s)^D}$ and $V_{(r,s)}$ respectively. This allows us to use a lighter notations for the structure constants, for instance:

$$C^{(r,s)^D}_{(r_1,s_1),(r_2,s_2)} = C^{(\Delta_{r_3,s_3},\Delta_{r_3,s_3})}_{(\Delta_{r_1,s_1},\Delta_{r_1,-s_1}),(\Delta_{r_2,s_2},\Delta_{r_2,-s_2})}. \tag{2.12}$$

A set of these representations is denoted as

$$\mathcal{S}^D_X = \{(r,s)^D\}_{(r,s)\in X}, \quad \mathcal{S}_X = \{(r,s)\}_{(r,s)\in X}, \tag{2.13}$$

where X is a given set of pairs (r,s). A third set type is $\mathcal{S}^{\text{quot}}_X$ that contains the degenerate representations with vanishing null state.

2.2. Torus correlation functions

So far we have reviewed the properties of a CFT that do not depend on the topology of the surface. The theory of Virasoro algebra on general Riemann surfaces can be found in [24]. Let us consider now a CFT on a torus with periods ω_1 and ω_2. In the numerical simulations one usually considers doubly periodic rectangular lattices of size $M \times N$, where $M, N \in \mathbb{R}_{>0}$. We therefore set:

$$\omega_1 = \mathrm{i}M, \quad \omega_2 = N, \quad \tau = \frac{\omega_1}{\omega_2} = \mathrm{i}\frac{M}{N}, \quad q = \mathrm{e}^{2\pi\mathrm{i}\tau}. \tag{2.14}$$

The results we will obtain can be of course generalized to the case $\mathrm{Re}\,\tau \neq 0$. In the following, we represent the torus as a finite cylinder of size N with the ends, at distance $M = O(N)$, glued together. Accordingly, we use the map

$$w = -\mathrm{i}\,\frac{N}{2\pi}\ln z \tag{2.15}$$

sending the plane (z) to an infinite cylinder (w) of size N.

We define a general field $V^{\mathcal{C},N}_{(\Delta,Y)}$ on the cylinder of size N as:

$$V^{\mathcal{C},N}_{(\Delta,Y)}(w,\bar{w}) = L^{\mathcal{C},(w)}_{-Y}\bar{L}^{\mathcal{C},(\bar{w})}_{-\bar{Y}}\, V^{\mathcal{C},N}_{(\Delta)}(w,\bar{w}), \tag{2.16}$$

where $L^{\mathcal{C},(w)}_{-n}$, $\bar{L}^{\mathcal{C},(w)}_{-n}$ are the conformal generators on the cylinder. They are related to the fields on the cylinder of size $N = 1$ by a factor arising from their transformation under (2.15), see appendix :

$$V^{\mathcal{C},N}_{(\Delta,Y)}(w,\bar{w}) = \left(\frac{2\pi}{N}\right)^{\Delta+\bar{\Delta}+|Y|+|\bar{Y}|} V^{\mathcal{C},N=1}_{(\Delta,Y)}(w,\bar{w}). \tag{2.17}$$

Henceforth, we will often omit the symbol $\mathcal{C}, N$ when the field on the cylinder is a primary, i.e. $V^{\mathcal{C},N}_{(\Delta)}(w) \to V_{(\Delta)}(w)$. The relation between $L^{\mathcal{C},(w)}_{-n}$ and $L^{(z)}_{-n}$ is obtained using the transformation of T under the map (2.15) see appendix .

The torus function $\left\langle \prod_i V_{(\Delta_i)} \right\rangle_\tau$ corresponds to the trace of the ons. The one-point torus correlation function can be associated with the following diagram:

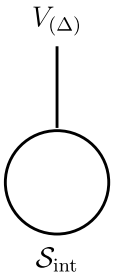

where $\mathcal{S}_{\rm int} \in \mathcal{S}$ is the set of representations that propagate along the M direction and whose fusion with themselves contains the representation (Δ). It takes the form:

$$\langle V_{(\Delta)} \rangle_\tau = \frac{1}{Z} \mathrm{Tr}_{\mathcal{S}_{\rm int}} \left(q^{L_0^{\mathcal{C},(\infty)}} \bar{q}^{\bar{L}_0^{\mathcal{C},(\infty)}} V_{(\Delta)}(0) \right) = \frac{1}{Z} \sum_{(\Delta_{\rm int}) \in \mathcal{S}_{\rm int}} C^{(\Delta)}_{(\Delta_{\rm int}),(\Delta_{\rm int})} \mathcal{F}^{\Delta_{\rm int}}_{\Delta}(q)\, \mathcal{F}^{\bar{\Delta}_{\rm int}}_{\bar{\Delta}}(\bar{q}), \tag{2.18}$$

where $L_0^{\mathcal{C},(\infty)} = L_0^{(0)} - \frac{c}{24}$ and $\mathcal{F}^{\Delta_{\rm int}}_{\Delta}(q)$ is the torus conformal block:

$$\begin{aligned} \mathcal{F}^{\Delta_{\rm int}}_{\Delta}(q) &= q^{\Delta_{\rm int} - \frac{c}{24}}\, \bar{q}^{\bar{\Delta}_{\rm int} - \frac{c}{24}} \sum_{\substack{Y,Y' \\ |Y|=|Y'|}} q^{|Y|} H^{-1}_{\Delta_{\rm int}}(Y,Y')\ \Gamma^{(\Delta_{\rm int},Y')}_{(\Delta_{\rm int},Y),(\Delta,\{\emptyset\})} \\ &= q^{\Delta_{\rm int} - \frac{c}{24}}\, \bar{q}^{\bar{\Delta}_{\rm int} - \frac{c}{24}} \left(1 + \frac{2\Delta_{\rm int} + \Delta(\Delta-1)}{2\Delta_{\rm int}} q + \cdots \right) \end{aligned} \tag{2.19}$$

see (2.3)–(2.8). The torus partition function Z can be related to the identity one-point function, for which $\mathcal{S}_{\rm int} = \mathcal{S}$,

$$Z = \mathrm{Tr}_{\mathcal{S}} \left(q^{L_0^{\mathcal{C},(\infty)}} \bar{q}^{\bar{L}_0^{\mathcal{C},(\infty)}} \right) = \sum_{(\Delta_{\rm int}) \in \mathcal{S}} \mathcal{F}^{\Delta_{\rm int}}_{0}(q)\, \mathcal{F}^{\bar{\Delta}_{\rm int}}_{0}(\bar{q}). \tag{2.20}$$

The computation of $\mathcal{F}^{\Delta_{\rm int}}_{0}(q)$ using recursion relations is discussed in [25].

The s-channel expansion of the torus two-point function $\left\langle V_{(\Delta)_1}(w) V_{(\Delta)_2}(0) \right\rangle_\tau$ is described by the diagram:

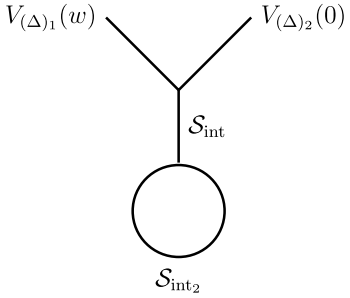

https://doi.org/10.1088/1742-5468/ab6331

J. Stat. Mech. (2020) 023101

where $\mathcal{S}_{\text{int}}$ contains the fields appearing in the fusion $V_{(\Delta)_1}V_{(\Delta)_2}$ and $\mathcal{S}_{\text{int}_2}$ is the spectrum of the one-point torus function of the fields in $\mathcal{S}_{\text{int}}$. One can show, see appendix, that the two-point torus function can be expanded as:

$$\langle V_{(\Delta)_1}(w)V_{(\Delta)_2}(0)\rangle_\tau = \left(\frac{N}{2\pi}\right)^{-\Delta_1-\Delta_2-\bar{\Delta}_1-\bar{\Delta}_2} \sum_{(\Delta,Y)_{\text{int}}\in\mathcal{S}_{\text{int}}} a^{(\Delta,Y)_{\text{int}}}_{(\Delta)_1,(\Delta)_2}\left(\frac{2\pi w}{N}\right)\left\langle V^{\mathcal{C}}_{(\Delta,Y)}\right\rangle_\tau . \tag{2.21}$$

3. Q-Potts random cluster model

Let us consider a rectangular lattice $N \times M$ with periodic boundary conditions in the two directions. The edges of the graph carry a bond with probability p, or no bond with probability $1-p$. According to these bonds, the lattice is split into a disjoint union of connected clusters. The random cluster Q-state Potts model [26] is defined by the partition function

$$\mathcal{Z}_Q = \sum_{\mathcal{G}} Q^{\#\text{ clusters}} p^{\#\text{ bonds}} (1-p)^{\#\text{ edges without bond}}. \tag{3.1}$$

At the critical value

$$p = p_c = \frac{\sqrt{Q}}{\sqrt{Q}+1}, \tag{3.2}$$

the probability that there exists a percolating cluster jumps from 0 to 1, in the limit of infinite lattice size. The model becomes conformally invariant in the scaling limit, and has central charge c:

$$c = 1 - 6\left(\beta - \beta^{-1}\right)^2, \qquad Q = 4\cos^2\pi\beta^2 \quad \text{with} \quad \frac{1}{2} \leqslant \beta^2 \leqslant 1\ . \tag{3.3}$$

The scaling limit Z_Q of the Potts partition function (3.1) at the critical point (3.2) was computed in [27]:

$$Z_Q = \text{equation (4.8) of [27]}, \quad \text{with } e_0 \to 2-2\beta^2, \quad g \to 4\beta^2, \quad h_{s,r} \to \Delta_{(-2r,\frac{s}{2})}. \tag{3.4}$$

The corresponding total spectrum is:

$$\mathcal{S}^{\text{Potts}} = \mathcal{S}^{D,\text{quot}}_{(1,\mathbb{N}^*)} \bigcup_{\substack{j\geqslant 2\\ M|j,p\wedge M=1}} \mathcal{S}_{(j,\mathbb{Z}+\frac{p}{M})} \bigcup \mathcal{S}_{(0,\mathbb{Z}+\frac{1}{2})}. \tag{3.5}$$

The multiplicities associated to the above sectors have also been computed [27] and, for general Q, assume general real values. We refer the reader to [18] for a derivation of (3.5) from the representations of Temperley–Lieb type algebras. $\mathcal{S}^{D,\text{quot}}_{(1,\mathbb{N}^*)}$ is the thermal sector [28] and contains the identity and the energy field:

$$\text{Identity field} = V_{(1,1)^D}, \quad \text{Energy field} = V_{(1,2)^D}.$$

The space of n-point cluster connectivities has been defined in [9]. Here we will focus only on the two-point connectivities:

J. Stat. Mech. (2020) 023101

$$p_{12} = \text{Probability}(w_1, w_2 \text{ are in the same cluster}). \tag{3.6}$$

At the critical point (3.2) and in the plane limit $N, M \to \infty$, the Coulomb gas approach [29] determines the scaling limit of the probability p_{12} :

$$\text{Plane scaling limit : } \; p_{12} = c_0 \, |w|^{-4\Delta_{(0,\frac{1}{2})}}, \quad w = w_1 - w_2, \tag{3.7}$$

where c_0 is a non-universal constant, see section 5. From the above equation one sees that, in the plane, the two-point connectivity is related to the plane two-point function of the

$$\text{Connectivity field} = V_{(0,\frac{1}{2})}, \tag{3.8}$$

belonging to the magnetic sector $\mathcal{S}_{(0,\mathbb{Z}+\frac{1}{2})}$ [30]. It is natural to assume that the relation between p_{12} and the $V_{(0,\frac{1}{2})}$ two-point function holds on the torus, i.e.:

$$\text{Torus scaling limit : } p_{12} = c_0 \, \left\langle V_{(0,\frac{1}{2})}(w) V_{(0,\frac{1}{2})}(0) \right\rangle_\tau, \quad w = w_1 - w_2. \tag{3.9}$$

Let us mention that a rigorous proof of (3.2) has been obtained recently in [31] where the behaviour of the probability (3.6) in the sub-critical regime $p < p_c$ and on the torus was also studied.

4. Two-point Potts torus connectivity

According to Monte Carlo simulations (see section 5) while $(0, \frac{1}{2})$ is the field in (3.5) with the smallest non-zero conformal dimension, the leading topological correction is given by the energy state $(1,2)^D$. The contribution from the second thermal operator $(1,3)^D$ is also visible at $Q \sim 3$. Based on these observations, we assume that $\left\langle V_{(0,\frac{1}{2})}(w) V_{(0,\frac{1}{2})}(0) \right\rangle_\tau$ is given by (2.21) with $\mathcal{S}_{\text{int}} = \mathcal{S}^{D,\text{quot}}_{(1,\mathbb{N}^*)}$. In particular we compute the contributions of the first three dominant channels:

$$\mathcal{S}_{\text{int}} = \{(1,1)^D, (1,2)^D, (1,3)^D\}. \tag{4.1}$$

The agreement between Monte Carlo and analytic results presented below confirms that this truncated spectrum (4.1) provides a good approximation to $\left\langle V_{(0,\frac{1}{2})}(w) V_{(0,\frac{1}{2})}(0) \right\rangle_\tau$. Some arguments going in this direction come also from the analysis in [18, 20] where the spectrum of all independent four-point connectivities has been determined. In particular, it was shown that the asymptotic of the probability $p_{12} \cap p_{34}$ (related to $P_0 + P_1$ in [20]), in the limit $z_2 - z_1 \to 0$ and $z_3 - z_2 \gg 1$, is dominated by the low lying states $(1,1)^D, (1,2)^D, (1,3)^D, (2,0), \cdots$. In this limit one expects that $p_{12} \cap p_{34} \sim \; p_{12} \, p_{34} +$ corrections, where the corrections are produced by the configurations which correlate the p_{12} and p_{13} probabilities and which are associated to the state $(2,0)$ [20].

J. Stat. Mech. (2020) 023101

Table 1. c_0 and c_1 from a fit of the numerical data to the form (5.1). The last column contains the analytical determination in (4.11*a*).

Q	c_0	c_1	$c_{(1,2)}$
1	0.747 19	0.356	0.357 07
1.25	0.733 23	0.392	0.393 023
$2+\cos\frac{3\pi}{5}$	0.726 93	0.414	0.411 442
1.5	0.721 78	0.4343	0.427 244
1.75	0.711 99	0.459	0.458 989
2.0	0.703 37	0.488	0.488 863
2.25	0.695 56	0.518	0.517 293
2.5	0.688 27	0.551	0.544 607
2.75	0.681 13	0.578	0.571 079
3.0	0.673 76 (2)	0.599	0.596 962
3.25	0.665 55 (5)	0.627	0.622 532
$2+\sqrt{2}$	0.659 02 (7)	0.642	0.639 326

In the limit:

$$N \to \infty, \quad \frac{M}{N} \to O(1), \quad 1 \ll w \ll N, \tag{4.2}$$

using the expression for the two-point function (2.21) with the internal spectrum (4.1) we obtain the following N^{-1} expansion

$$\begin{aligned}\left\langle V_{(0,\frac{1}{2})}(w)V_{(0,\frac{1}{2})}(0)\right\rangle_\tau &= |w|^{-4\Delta_{(0,\frac{1}{2})}} \sum_{X\in\{(1,1)^D,(1,2)^D,(1,3)^D\}} C^X_{(0,\frac{1}{2}),(0,\frac{1}{2})} \left|\frac{2\pi w}{N}\right|^{2\Delta_X} (\langle V_X\rangle_\tau \\ &+ \left(\frac{2\pi}{N}\right)^2 \beta_X^{\{2\}} \left(w^2 \left\langle L^{\mathcal{C},(0)}_{-2} V_X\right\rangle_\tau + \bar{w}^2 \left\langle \bar{L}^{\mathcal{C},(0)}_{-2} V_X\right\rangle_\tau\right) \\ &+ \left(\frac{2\pi}{N}\right)^3 \beta_X^{\{3\}} \left(w^3 \left\langle L^{\mathcal{C},(0)}_{-3} V_X\right\rangle_\tau + \bar{w}^3 \left\langle \bar{L}^{\mathcal{C},(0)}_{-3} V_X\right\rangle_\tau\right) + \cdots\Bigg),\end{aligned} \tag{4.3}$$

where we set $\beta_X^Y = \beta^{(\Delta_X,Y)}_{\Delta_{(0,\frac{1}{2})},\Delta_{(0,\frac{1}{2})}}$. Note that descendants of the type $L^{\mathcal{C}}_{-1}L^{\mathcal{C}}_{-Y}V_X$ are total derivatives and their torus one-point functions vanish.

The main message here is that the leading topological correction for the two-point connectivity is given, for $1 \leqslant Q \leqslant 4$ by the energy $(1,2)^D$ state. Given two-points w_1, w_2 on a torus (2.14) and at distance $r = |w_1 - w_2|$, the scaling limit of the probability (3.6) is:

$$\begin{aligned}p_{12} = \frac{c_0}{r^{4\Delta_{(0,\frac{1}{2})}}}\Bigg[1 + \left(\frac{r}{N}\right)^{2\Delta_{(1,2)}} \left(\frac{(2\pi)^{2\Delta_{(1,2)}}}{Z_Q(q)}(Q-1)\left[C^{(1,2)^D}_{(0,\frac{1}{2}),(0,\frac{1}{2})}\right]^2 q^{2\left(\Delta_{(0,\frac{1}{2})}-\frac{c}{24}\right)}(1+O(q))\right) \\ + O\left(\left(\frac{r}{N}\right)^2\right)\Bigg]\end{aligned} \tag{4.4}$$

where c_0 is a non-universal constant evaluated in table 1, and $C^{(1,2)^D}_{(0,1/2),(0,1/2)}$ is given in (4.16). At the critical percolation $Q = 1$ point, we have:

J. Stat. Mech. (2020) 023101

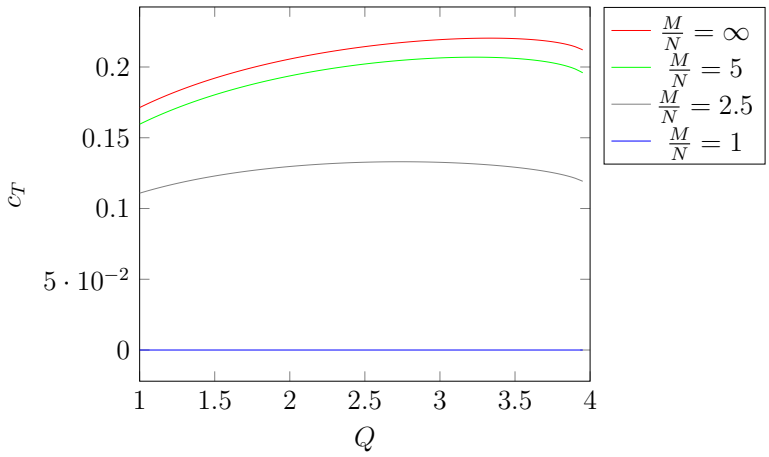

Figure 1. The contribution c_T of the stress-energy tensor, as a function of Q and for different values of the aspect ratio $\frac{M}{N}$.

$$p_{12} = \frac{c_0}{r^{\frac{5}{24}}}\left[1 + \left(\frac{r}{N}\right)^{\frac{5}{4}}\left((2\pi)^{\frac{5}{4}}\pi\sqrt{3}\left(\frac{4}{9}\frac{\Gamma(\frac{7}{4})}{\Gamma(\frac{1}{4})}\right)^2 e^{-\frac{5\pi}{24}\frac{M}{N}} + O\left(e^{-\frac{53}{24}\pi\frac{M}{N}}\right)\right) + O\left(\left(\frac{r}{N}\right)^2\right)\right]. \tag{4.5}$$

The formula (4.4) represents, at the best of our knowledge, a new analytic result on the universal properties of general Q random Potts critical clusters and, in particular, of the critical percolation clusters (4.5). The derivation of (4.4) and (4.5), of the next $\frac{r}{N}$ sub-leading topological terms and of the systematic computation of the q expansion, are given below.

4.1. Identity channel contributions

The leading contribution to (4.3) comes from the identity. In particular we have:

$$\text{Leading} \ : \ |w|^{-4\Delta_{(0,\frac{1}{2})}} \quad (\text{plane limit}), \tag{4.6a}$$

$$\text{Sub-leading} \ : \ |w|^{-4\Delta_{(0,\frac{1}{2})}}\left[\left(\frac{w}{N}\right)^2 c_T + \left(\frac{\bar{w}}{N}\right)^2 c_{\bar{T}}\right] \tag{4.6b}$$

$$\text{Next to sub-leading} : O\left(\frac{1}{N^4}\right). \tag{4.6c}$$

The dominant term corresponds to the plane limit while the sub-leading factors c_T and $c_{\bar{T}}$:

$$c_T = \frac{2\Delta_{(0,\frac{1}{2})}}{c}\left\langle T^{\mathcal{C}}\right\rangle_\tau, \quad c_{\bar{T}} = \frac{2\Delta_{(0,\frac{1}{2})}}{c}\left\langle \bar{T}^{\mathcal{C}}\right\rangle_\tau \tag{4.7}$$

are proportional to the stress energy one-point function, with

$$\left\langle T^{\mathcal{C}}\right\rangle_\tau = \mathrm{i}\pi\partial_\tau \log Z_Q. \tag{4.8}$$

J. Stat. Mech. (2020) 023101

In figure 1 we plot c_T as a function of Q and for different τ, i.e. for different ratios $\frac{M}{N}$: for a square torus, $M=N$ and $\langle T^{\mathcal{C}}\rangle_\tau = \langle \bar{T}^{\mathcal{C}}\rangle_\tau = 0$, for all Q. This is the reason the N^{-2} corrections were not visible in the fits in [20]. In the cylinder limit $M/N \to \infty$ one recovers the well known result $\langle T^{\mathcal{C}}\rangle_{i\infty} = (2\pi)^2 \frac{c}{24}$. It is interesting to stress that the $\lim_{c\to 0} \frac{2\Delta_{(0,\frac{1}{2})}}{c} \left\langle T^{\mathcal{C}} \right\rangle_\tau$ is finite and different from zero. No subtleties, arising from the existence at $c=0$ of a logarithmic partner of the stress energy tensor, seem to emerge. Indeed one can write

$$Z = 1 + O(Q-1) \tag{4.9}$$

which gives a finite limit for

$$c_T = -\frac{2\Delta_{(0,\frac{1}{2})}}{c} 2\pi^2 q\partial q Z. \tag{4.10}$$

The next corrections from the identity channel appear at order N^{-4} and are related to the propagation of the identity descendants $\langle T^{\mathcal{C}}\bar{T}^{\mathcal{C}}\rangle_\tau$, $\langle L^{\mathcal{C}}_{-4}\mathrm{Id}\rangle_\tau$ and $\langle \bar{L}^{\mathcal{C}}_{-4}\mathrm{Id}\rangle_\tau$.

4.2. Energy channel contributions

Besides the identity, the energy $V_{(1,2)^D}$ field has the lowest dimension in $\mathcal{S}^{D,\mathrm{quot}}_{(1,\mathbb{N}^*)}$. The $(1,\,2)^D$ contribution to (4.3) is given by

$$\text{Leading} : |w|^{-4\Delta_{(0,\frac{1}{2})}} \left(\frac{|w|}{N}\right)^{2\Delta_{(1,2)}} c_{(1,2)}, \tag{4.11a}$$

$$\text{Sub-leading} : O\left(\frac{1}{N^{2\Delta_{(1,2)}+4}}\right) \tag{4.11b}$$

where:

$$c_{(1,2)} = (2\pi)^{2\Delta_{(1,2)}}\ C^{(1,2)^D}_{(0,\frac{1}{2}),(0,\frac{1}{2})} \left\langle V_{(1,2)^D}\right\rangle_\tau . \tag{4.12}$$

We can compute the one-point function $\left\langle V_{(1,2)^D}\right\rangle_\tau$ by using the vanishing of the $(1,2)^D$ null state, which determines the OPE [21]:

$$V_{(1,2)} \times V_{(r,s)} \to V_{(r,s+1)} \oplus V_{(r,s-1)} \tag{4.13}$$

$(0,\frac{1}{2})$ is the only representation which satisfies both the above OPE and

$$V_{(1,2)} \times V_{(0,\frac{1}{2})} \to V_{(0,\frac{1}{2})}. \tag{4.14}$$

Therefore the one-point function $\left\langle V_{(1,2)^D}\right\rangle_\tau$ gets contribution only from the propagation of the $(0,\frac{1}{2})$ state, i.e. $\mathcal{S}_{\mathrm{int}} = \{(0,\frac{1}{2})\}$ in (2.18). This property was pointed out in [32] where the energy one-point function for minimal models was computed in terms of a Coulomb gas integral. Collecting all these facts, we obtain:

J. Stat. Mech. (2020) 023101

$$\langle V_{(1,2)^D}\rangle_\tau = \frac{Q-1}{Z_Q}\, C^{(1,2)^D}_{(0,\frac{1}{2}),(0,\frac{1}{2})} \left|\mathcal{F}^{\Delta_{(0,\frac{1}{2})}}_{\Delta_{(1,2)}}(q)\right|^2$$
$$= \frac{Q-1}{Z_Q}\, C^{(1,2)^D}_{(0,\frac{1}{2}),(0,\frac{1}{2})}\, |q|^{2\left(\Delta_{(0,\frac{1}{2})}-\frac{c}{24}\right)} \left|1+\frac{2\Delta_{(0,\frac{1}{2})}+\Delta_{(1,2)}(\Delta_{(1,2)}-1)}{2\Delta_{(0,\frac{1}{2})}}q+\cdots\right|^2 \tag{4.15}$$

where the factor $Q-1$ comes from the multiplicity of the $\mathcal{S}_{(0,\mathbb{Z}+\frac{1}{2})}$ sector computed in [27] and the structure constant is given by:

$$C^{(1,2)^D}_{(0,\frac{1}{2}),(0,\frac{1}{2})} = \beta^4 \frac{\gamma\left(-\frac{1}{2}\right)}{\gamma\left(-\frac{1}{2\beta^2}\right)}\sqrt{\gamma\left(\frac{1}{\beta^2}\right)\gamma\left(2-\frac{2}{\beta^2}\right)}, \quad \gamma(x)=\frac{\Gamma(x)}{\Gamma(1-x)}. \tag{4.16}$$

The next energy contributions come from the descendants $L^{\mathcal{C}}_{-2}V_{(1,2)^D}$ and $\bar{L}^{\mathcal{C}}_{-2}V_{(1,2)^D}$. The null state in the representation $(1,2)^D$ is

$$\chi = \left(-\beta^2(L^{(1)}_{-1})^2 + L^{(1)}_{-2}\right) V_{(1,2)^D}(1). \tag{4.17}$$

Using (A.4)

$$L^{\mathcal{C},(0)}_{-2} = \left(\frac{2\pi \mathrm{i}}{N}\right)^2 \left(L^{(1)}_{-2} - \frac{c}{24} - \frac{13}{12}L^{(1)}_0\right) \tag{4.18}$$

and setting the null vector to zero

$$L^{(1)}_{-2}V_{(1,2)^D}(1) = \beta^2 (L^{(1)}_{-1})^2\, V_{(1,2)^D}(1) \tag{4.19}$$

leads to

$$\left\langle L^{\mathcal{C},(0)}_{-2}V_{(1,2)^D}(0)\right\rangle_\tau = \left\langle \bar{L}^{\mathcal{C},(0)}_{-2}V_{(1,2)^D}(0)\right\rangle_\tau = 0, \tag{4.20}$$

which explains why the sub-leading corrections in (4.11*a*) are found in the fourth level descendants of the energy (the third level descendant is a total derivative). Using the expression of the one-point function (4.15) in (4.11*a*) with $r=|w|$, one obtains our result (4.4).

At the critical percolation point $Q=1$, the bond probabilities, associated to the energy field (see next section), are independent. The CFT energy one-point function (4.15), which actually probes the fluctuation induced corrections to the bulk constant value, vanishes at $Q=1$. On the other hand, the vanishing of the one-point function is exactly cancelled by the divergence in the structure constant (4.16), thus providing a non-zero contribution to $\lim_{Q\to 1} C^{(1,2)^D}_{(0,1/2),(0,1/2)}\langle V_{(1,2)^D}\rangle_\tau$. The result is given in (4.5).

When $M\neq N$, we have seen that we have a N^{-2} contribution of the energy tensor to the topological corrections. Even if this term is sub-leading in the parameter $\frac{r}{N}$, $r=|w|$, in finite size simulations it can interfere or even be dominant with respect to the energy contribution. In figure 2 we plot as function of Q, and for different ratios $\frac{M}{N}$, the regimes of $\frac{r}{N}$ dominated by the energy (below the curve) or by the stress-energy (above the curve) topological corrections:

J. Stat. Mech. (2020) 023101

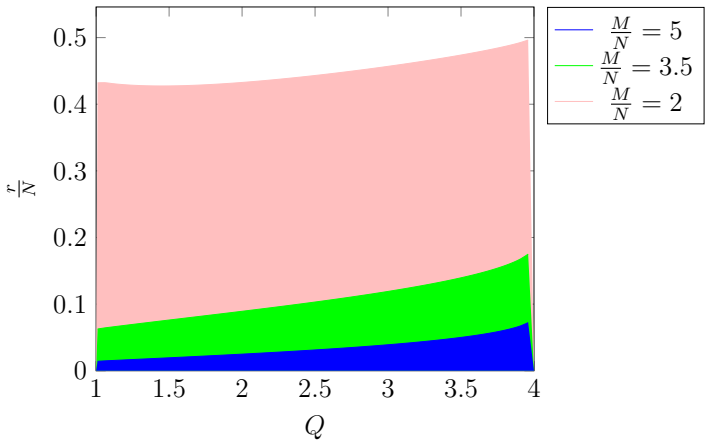

Figure 2. Regimes of $\frac{r}{N}$ dominated by the energy (resp. the stress-energy tensor) contribution below (resp. above) the curve, as a function of Q, and for different ratios $\frac{M}{N}$.

4.3. $(1, 3)^D$ channel contributions

$(1,3)^D$ has a dimension $4 \geqslant 2\Delta_{(1,3)} \geqslant 2$ for $1 \leqslant Q \leqslant 4$, decreasing with Q. Despite this relatively high dimension, the term

$$\text{Leading} : |w|^{-4\Delta_{(0,\frac{1}{2})}} \left(\frac{|w|}{N}\right)^{2\Delta_{(1,3)}} c_{(1,3)} \tag{4.21a}$$

$$\text{Sub-leading} : O\left(\frac{1}{N^{2\Delta_{(1,3)}+2}}\right) \tag{4.21b}$$

where:

$$c_{(1,3)} = (2\pi)^{2\Delta_{(1,3)}} \; C^{(1,3)^D}_{(0,\frac{1}{2}),(0,\frac{1}{2})} \left\langle V_{(1,3)^D}(0)\right\rangle_\tau \tag{4.22}$$

provides a visible contribution when $Q \geqslant 3$, see next section 5.4.

We consider then $\left\langle V_{(1,3)^D}\right\rangle_\tau$. Differently from the case of the energy field, the fusion rule imposed by the vanishing of the $(1,3)^D$ null state:

$$V_{\Delta_{(1,3)}} \times V_{\Delta_{(r,s)}} \to V_{\Delta_{(r,s+2)}} \oplus V_{\Delta_{(r,s)}} \oplus V_{\Delta_{(r,s-2)}}, \tag{4.23}$$

does not fix the representations contributing to its one-point function, since the fusion $V_{\Delta_{(1,3)}} \times V_{\Delta_{(r,s)}} \to V_{\Delta_{(r,s)}}$ is allowed for all r, s. This can be seen also from the fact that the structure constant $C^{(1,3)^D}_{(\Delta),(\Delta)}$ is different from zero for any Δ and c [21]. Parametrising Δ as in (2.9), one has, for three diagonal (spinless) fields [33]:

$$C^{(1,3)^D}_{(r,s)^D,(r,s)^D} = \sqrt{\frac{\gamma^3(\frac{1}{\beta^2})\gamma(2-\frac{2}{\beta^2})\gamma(2-\frac{3}{\beta^2})}{\gamma(\frac{2}{\beta^2})} \frac{\gamma^2(r+\frac{1-s}{\beta^2})}{\gamma^2(1+r-\frac{1+s}{\beta^2})}}. \tag{4.24}$$

The above value of the structure constant can be derived either from the vanishing of the third level null state of $(1,3)^D$ or from a Coulomb gas integral, as the three vertex fields satisfy the charge neutrality condition. One can expect on solid grounds

J. Stat. Mech. (2020) 023101

that $C^{(1,3)^D}_{(r,s)^D,(r,s)^D}$ describes certain three-point correlation functions in the Q-state Potts model. In [15] for instance, the structure constant $C^{(1,3)^D}_{(1,0),(1,0)}$ has been checked to correspond to the scaling limit of certain lattice transfer matrix amplitudes. In the case of two non-diagonal fields, $C^{(1,3)^D}_{(r,s),(r,s)}$ has been shown in [15, 34] to be given by $C^{(1,3)^D}_{(r,s),(r,s)} = \sqrt{C^{(1,3)^D}_{(r,s)^D,(r,s)^D} C^{(1,3)^D}_{(r,-s)^D,(r,-s)^D}}$.

One can expect that all the states X in the Potts spectrum (3.5), such that $C^{(1,3)^D}_{X,X} \neq 0$ contribute to $\left\langle V_{(1,3)^D} \right\rangle_\tau$. However, one has to pay special attention, in particular when using truncations in the s-channel spectrum: there can be highly non-trivial cancellations between states. This is known to be the case when the central charge takes rational values, and a finite number of states in the spectrum closes under OPE (see section 5 of [35] and references therein).

We obtain:

$$\left\langle V_{(1,3)^D} \right\rangle_\tau = \frac{1}{Z_Q}\Big((Q-1) C^{(1,3)^D}_{(0,\frac{1}{2}),(0,\frac{1}{2})} \left| \mathcal{F}^{\Delta_{(0,\frac{1}{2})}}_{\Delta_{(1,3)}}(q) \right|^2 + C^{(1,3)^D}_{(1,2)^D,(1,2)^D} \left| \mathcal{F}^{\Delta_{(1,2)}}_{\Delta_{(1,3)}}(q) \right|^2$$
$$+ (Q-1) C^{(1,3)^D}_{(0,\frac{3}{2}),(0,\frac{3}{2})} \left| \mathcal{F}^{\Delta_{(0,\frac{3}{2})}}_{\Delta_{(1,3)}}(q) \right|^2 + \frac{Q(Q-3)}{2} C^{(1,3)^D}_{(2,0),(2,0)} \left| \mathcal{F}^{\Delta_{(2,0)}}_{\Delta_{(1,3)}}(q) \right|^2 + \cdots \Big), \tag{4.25}$$

where $\cdots$ indicates next sub-leading contributions. In the above formula, the Q dependent prefactors come again from the multiplicity of the states propagating in the torus. In the following figure, the value $c_{(1,3)}$ in (4.22) for $M = N$ is plotted as a function of Q in the region of Q where the comparison with Monte Carlo results is possible:

In figure 3 we tagged the values of Q at which Monte Carlo data have been taken.

At $Q = 3$, only three channels ($\mathcal{S}_{\text{int}} = \{(0, \frac{1}{2}), (1,2)^D, (1,3)^D\}$) contribute to $\left\langle V^D_{(1,3)}(0) \right\rangle_\tau$, so we expect that, for $Q \sim 3$, $\{(0, \frac{1}{2}), (1,2)^D\}$ produce the main contributions, while all others are suppressed by some power of $Q - 3$.

5. Monte Carlo simulation and CFT comparisons

5.1. General results for the two-point correlation functions

We collected data on square lattices of size $N \times N$ with periodic boundary conditions on both directions, thus having the topology of a torus (2.14) with $M = N$ (for $M \neq N$ see next subsection). We considered various linear sizes N up to $N = 8192$. The probability (3.6) is computed by considering the lattice points (x, y) and $(x + r, y)$ or (x, y) and $(x, y + r)$ and next averaging over x and y. We took data for $Q = 1 + n/4$ for $n = 1, \cdots 9$ and $Q = 2 + 2\cos\frac{3\pi}{5}, 2 + \sqrt{2}$. For each value of Q, we averaged over 10^6 independent samples generated with the Chayes–Machta algorithm [36, 37]. This algorithm is a generalisation of the Swendsen–Wang algorithm for non integer values of Q.

In figure 4, we present the rescaled correlation function $r^{4\Delta_{(0,\frac{1}{2})}} p_{12}(r)$ as a function of r for various values of Q as shown in the caption. While we observe a plateau for a

J. Stat. Mech. (2020) 023101

value $\simeq 0.7$, we also see that there exist strong deviations for large r. This is due to the fact that we work on a torus, thus we expect topological corrections which have a maximum at $r = \frac{N}{2}$. We also need to take into account the small size corrections which, as can be observed in figure 4, will be present only for small sizes up to $r \simeq 10$. A general form of fit for the rescaled function $r^{4\Delta_{(0,\frac{1}{2})}} p_{12}(r)$ is given by :

$$f(N,r) = c_0 \left(1 + \sum_{j \geqslant 1} c_j \left(\frac{r}{N}\right)^{d_j}\right) \left(1 + g_1\, r^{-g_2}\right) \ . \tag{5.1}$$

The above form of fit is factorised into three factors. The first factor c_0 is the non-universal normalisation of the lattice two-point functions. The second part, with parameters c_j, $(j \geqslant 1)$ encodes the torus corrections: d_j and c_j are the universal quantities to be compared respectively to the dimensions and the factors computed in the previous sections using CFT, see (4.4). The third factor takes into account the small size corrections. In the case of the Ising model, an exact computation shows that this correction is described by this form with $g_2 = 2$ and a small coefficient $g_1 = \frac{1}{64}$ [38].

A first numerical result is that the dominant topological correction is of the form $\left(\frac{r}{N}\right)^{2\Delta_{(1,2)}}$, i.e. $d_1 \sim 2\Delta_{(1,2)}$. In figure 5, we show the behaviour of $r^{4\Delta_{(0,\frac{1}{2})}} p_{12}(r) - c_0$ with c_0 the constant part corresponding to the value of the plateau and this for various values of $Q = 1, \cdots 3$ as shown in the caption and for $N = 8192$. We observe that the correction is a power of r. We do a fit in the range $r \in [50\text{–}200]$ obtaining the powers $d_1 = \{1.251, 1.115, 0.997, 0.898, 0.793\}$ for $Q \in [1,3]$, which are very close to the corresponding set of values of $2\Delta_{(1,2)} = \{1.25, 1.1776, 1, 0.8982, 0.8\}$. The best fit is also shown in figure 5 as thin lines. Note that these fits agree with the numerical data also for much larger distances, $r > 200$. In the case of $Q = 2$, the exact result for the two-point function [27] is :

$$Q = 2, \quad r^2 \left\langle V_{(0,\frac{1}{2})}(r) V_{(0,\frac{1}{2})}(0) \right\rangle_{\tau = i} = 1 + 0.488\,863\, \frac{r}{N} + 0.211\,556\, \left(\frac{r}{N}\right)^4 + \cdots . \tag{5.2}$$

This explains that the leading correction alone gives already a very good fit as shown in figure 5. We observe that this is also true for other values of Q, in agreement with our results (4.4) for $N = M$.

In table 1, we give the numerical results for c_0 and c_1 obtained with a fit while keeping only the leading topological correction and fixing $d_1 = 2\Delta_{(1,2)}$. The fit is done with numerical data $r \in [6, 2048]$. With this range of data, we obtain a good fit (measured with the goodness of fit) for each value of Q. The numerical errors on c_0 and c_1 are indicated in the table either in parenthesis or smaller than one last digit. These fits also take into account small distance corrections. We obtained $g_1 \simeq 0.02$ and $g_2 \simeq 2$ for not too large values of Q. Further details on these fits are found in [20]. In table 1, we also show in the last column the values $c_{(1,2)}$ computed in section 4.2. The agreement is excellent with the numerical value c_1, in particular for small values of Q. For large values of Q, we expect that larger corrections have to be taken into account. In order to check the presence of larger corrections we can simply attempt a fit to the form (5.1) while adding a second correction $c_2 (r/N)^{d_2}$. We will come back to this point later.

J. Stat. Mech. (2020) 023101

5.2. Non-square torus

In this section we extend our results to non-square lattices. We checked the agreement between analytical and numerical results for various aspect ratios $\frac{M}{N}$ and for different Q's. Here we present results for $\frac{M}{N}=2$ and $Q=1$, which involves taking a non-trivial limit, see section 4.1. In this regime, the topological correction coming from the stress-energy tensor is non-zero and is given by (4.10). We consider the correlation measured in the vertical (v) (resp. horizontal (h)) directions. The coefficients $c_T^{(v)}$, $c_T^{(h)}$ of $\left(\frac{r}{N}\right)^2$ (resp. $\left(\frac{r}{M}\right)^2$) and $c_{(1,2)}^{(v)}$, $c_{(1,2)}^{(h)}$ of $\left(\frac{r}{N}\right)^{2\Delta_{(1,2)}}$ (resp. $\left(\frac{r}{M}\right)^{2\Delta_{(1,2)}}$) are,

$$c_T^{(v)} = 2\,c_T(\frac{M}{N}) = 0.175\,608 \quad c_T^{(h)} = 2\left(\frac{M}{N}\right)^{-2} c_T(\frac{N}{M}) = -0.175\,608$$
$$c_{(1,2)}^{(v)} = c_{(1,2)}(\frac{M}{N}) = 0.185\,569 \quad c_{(1,2)}^{(h)} = \left(\frac{M}{N}\right)^{-2\Delta_{(1,2)}} c_{(1,2)}(\frac{N}{M}) = 0.185\,557.$$

In figure 6 we show the numerical results and the best fits (dashed lines). We obtain

$$c_T^{(h)} = -0.165(2) \quad c_T^{(v)} = 0.192(2)$$
$$c_{(1,2)}^{(h)} = 0.183(1) \quad c_{(1,2)}^{(v)} = 0.180(4).$$

The agreement is good. We also show in the inset the difference between vertical and horizontal correlations. This measures directly the contribution of the stress-energy tensor since the contribution of the energy cancels. We obtain $c_T^{(v-h)} = 0.172(1)$.

5.3. Link with one-point correlation function

We compare now the value of c_1 and the theoretical prediction $c_{(1,2)}$ in (4.12) to the torus one-point function of the lattice energy field $\left\langle \varepsilon^{\text{latt}} \right\rangle_\tau$. The lattice energy field can be written in terms of the fields in the thermal series $\mathcal{S}^{D,\text{quot}}_{(1,\mathbb{N}^*)}$, see section 3, giving:

$$\left\langle \varepsilon^{\text{latt}} \right\rangle_\tau = e_0 + \frac{1}{N^{2\,\Delta_{(1,2)}}}\, e_1 + \cdots \tag{5.3}$$

where e_0 is the usual bulk energy density, associated to the identity $V_{(1,1)^D}$ field, and the sub-leading term e_1 is related to the energy $V_{(1,2)^D}$ field:

$$e_1 = (2\pi)^{2\Delta_{(0,\frac{1}{2})}}\, N_\varepsilon^{-1}\, \left\langle V_{(1,2)^D} \right\rangle_\tau . \tag{5.4}$$

In the above formula, N_ε is the normalisation relating the lattice to the scaling energy field and is computed by determining the energy-energy correlation $\left\langle \varepsilon^{\text{latt}}(x)\varepsilon^{\text{latt}}(0) \right\rangle_\tau$, in a similar way as we evaluate c_0 for the connectivity function.

In practice, we define the energy operator $\varepsilon^{\text{latt}}(x)$ as the probability that it contains a FK bond. For a given cluster configuration, $b_o(x)$ is the probability that the site $x=(x_1,x_2)$ is in the same FK cluster as the site (x_1+1,x_2) and $b_v(x)$ is the probability that the site x is in the same FK cluster as the site (x_1,x_2+1). Then the energy operator is defined as

$$\varepsilon^{\text{latt}}(x) = b_o(x) + b_v(x) - 1. \tag{5.5}$$

J. Stat. Mech. (2020) 023101

Table 2. Comparison of the dimensions of the fourh descendant of the energy, and of the field $V_{(1,3)}$, and thus of the sub-dominants $\frac{r}{N}$ corrections, for different values of Q.

Q	$2\Delta_{(1,2)}+4$	$2\Delta_{(1,3)}$
1	5.25	4
2	5	3.33
3	4.8	2.8

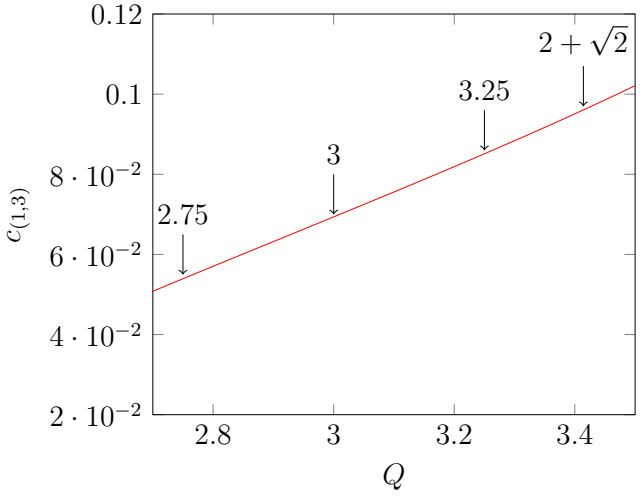

Figure 3. The coefficient $c_{(1,3)}$, computed for values of Q close to 3, where it produces a visible contribution. We tagged the values of Q at which Monte Carlo data has been taken.

This subtraction corresponds to imposing $e_0 = 0$ in (5.3). e_1 is obtained by measuring $\left\langle \varepsilon^{\text{latt}} \right\rangle_\tau$ and fitting to the form (5.3). The constant N_ε is fixed by measuring the two-point energy operator. The measurement for the one-point correlation function have been done on small lattices, up to $N = 256$ for the computation of e_1 and with 100 million samples for each size. We need to use many samples (and then not too big lattices), since $2\Delta_{(1,2)} = O(1)$ and then the deviation from the infinite size is very small. The same is also true for N_ε: it is determined from the two-point energy function which decreases very quickly as a function of the distance. The fits were done for distances $r = 8$–30 where we ignored small size and topological corrections. As a comparison, the measurements for c_1 from the two-point correlation function have been done on very large lattices, $N = 8192$. In figure 7, we compare the result $C^{(1,2)^D}_{(0,\frac{1}{2}),(0,\frac{1}{2})}\, N_\varepsilon\, e_1$ (shown in green) with c_1 computed numerically (shown as red circles) and with $c_{(1,2)}$ of (4.12) (shown as blue circles). The agreement between the two measured quantities and the analytical result is very good.

In the limit $Q \to 1$, we observe that $C^{(1,2)^D}_{(0,\frac{1}{2}),(0,\frac{1}{2})}\, N_\varepsilon\, e_1$ converges to the measured value c_1 and $c_{(1,2)}$. Indeed, we can check numerically that, for $Q \simeq 1$, one has $e_1 \simeq 0.25\ (Q-1)$ while $N_\epsilon \simeq 5.0\ (Q-1)^{-0.5}$.

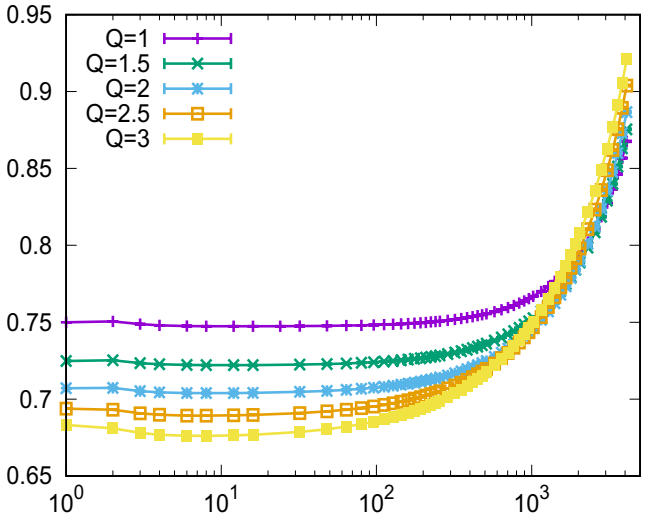

Figure 4. Rescaled two-point connectivity for the Q Potts models at $N = 8192$ for various values of Q as shown in the caption.

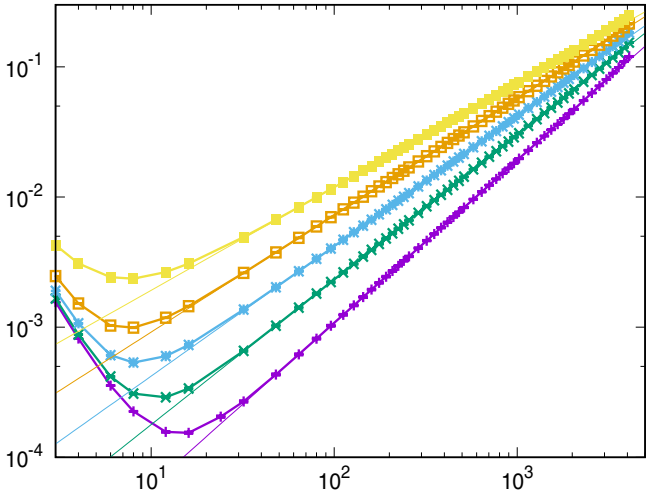

Figure 5. Same data as in figure 4 with the subtraction of the plateau. The thin lines corresponds to best fit as discussed in the text.

5.4. Further corrections

We want to check numerically the existence of further topological corrections. We expect that there exist corrections of order 4 from the descendants of the identity, see section 4.1 and of order $2\Delta_{(1,2)} + 4$ from the energy descendants, see section 4.2. There exist also the contribution of order $2\Delta_{(1,3)}$, see section 4.3. In table 2 we give a comparison of their respective dimensions.

For $Q < 3$ the coefficient $c_{(1,3)}$ becomes very small (see figure 3 in section 4.3), while the dimension $2\Delta_{(1,3)}$ is large and comparable to the dimensions of the descendant fields. Numerically it will then be difficult to distinguish the different contributions for small Q's.

We first compare our numerical data to a fit of the form

$$f(N, r) = c_0 \left(1 + c_1 \left(\frac{r}{N}\right)^{d_1} + c_2 \left(\frac{r}{N}\right)^{d_2}\right) (1 + g_1 r^{-g_2}) \,. \tag{5.6}$$

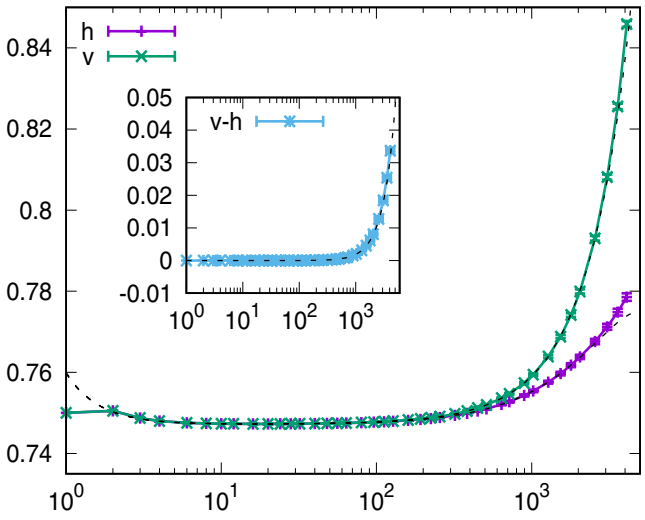

Figure 6. Rescaled two-point connectivity for $Q = 1$ and $\frac{M}{N} = 2$, at $N = 8192$. We show separately the vertical and horizontal connectivities. The inset contains the difference between these two connectivities.

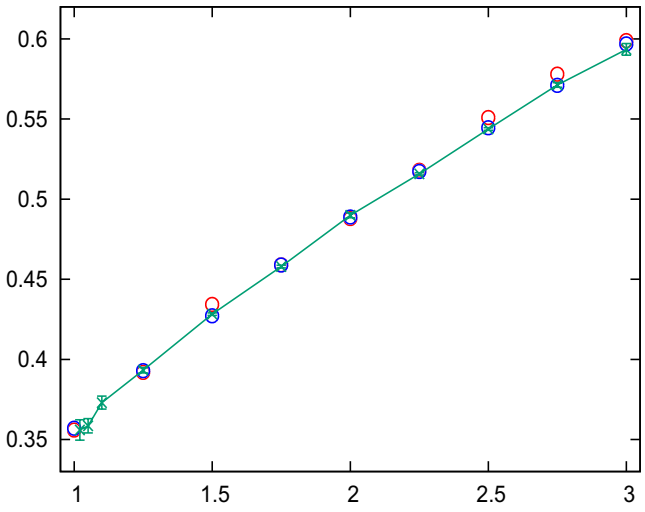

Figure 7. $C^{(1,2)^D}_{(0,\frac{1}{2}),(0,\frac{1}{2})} N_\varepsilon e_1$ versus Q compared to the numerical values c_1 shown as red circles and the analytical predictions $c_{(1,2)}$ shown as blue circles.

Here d_2 is an effective dimension which takes into account all possible higher corrections, while we assume the value $d_1 = 2\Delta_{(1,2)}$ and we take for $c_1 = c_{(1,2)}$, see (4.12). Even so, it is a difficult task since we are left with five parameters. One could try to ignore the small distance corrections by considering only data at large distances, say $r > r_{\min} = 50$. This is what we have done for determining the power corresponding to the dominant correction. We consider a fit in the range $r_{\min} \leqslant r \leqslant r_{\max}$, with $r_{\min} = 50$ and $r_{\max} = 4096$. For the second correction, the fit gives a much less clear image. We observe that the second correction is much larger than $d_1 = 2\Delta_{(1,2)}$ and its value decreases with Q. We measure $c_2 \simeq 0.44$ and $d_2 \simeq 5.3$ for $Q = 1$; $c_2 \simeq 0.35$ and $d_2 \simeq 4.4$ for $Q = 2$; $c_2 \simeq 0.29$ and $d_2 \simeq 3.6$ for $Q = 3$. We only quote approximate numbers for c_2 and d_2 since they depend on the range $r_{\min}$ and $r_{\max}$. Still we observe that only for

large values of Q, i.e. $Q \simeq 3$, we have a dimension $d_2 < 4$. This is in agreement with what we expect since it is only for Q close to 3 that the exponent $2\Delta_{(1,3)}$ is smaller than 4 and $c_{(1,3)}$ becomes non negligible. For smaller values of Q, our numerics are not able to give further information.

For $Q = 3$, we can improve by trying a fit to the form

$$f(N,r) = c_0 \left(1 + c_1 \left(\frac{r}{N}\right)^{d_1} + c_2 \left(\frac{r}{N}\right)^{d_2} + c_3 \left(\frac{r}{N}\right)^{d_3}\right) \left(1 + g_1\, r^{-g_2}\right) , \qquad (5.7)$$

while imposing the dimensions $d_1 = 2\Delta_{(1,2)}$, $d_2 = 2\Delta_{(1,3)}$ and $d_3 = 4$ or $2\Delta_{(1,2)} + 4$. In a fit with $r \geqslant 50$, we obtain a value of c_2 in the range $0.05 - 0.08$ (the smallest value is obtained for $d_3 = 4$ and the largest for $d_3 = 2\Delta_{(1,2)} + 4 = 4.8$), that is comparable with the prediction $c_{(1,3)} \simeq 0.07$ given by (4.22) for $Q = 3$ (see figure 3).

6. Conclusions

In this paper we considered the two-point connectivity p_{12} (3.6) of the critical Q-random cluster Potts model (3.1) on a torus of parameters (2.14). We focused on the universal corrections to the plane scaling limit of p_{12} originating from the torus topology for general values of $Q \in [1, 4]$. Combining CFT techniques with Monte Carlo insights, which suggested the ansatz (4.1), we have computed analytically the first dominant corrections to p_{12} in the limit (4.2). The theoretical results on p_{12}, summarised in (4.4), found a very good agreement with Monte Carlo measurements, as shown in figure 5 and in table 1. Moreover, we tested the CFT one-point torus energy function (4.15) against Monte Carlo measurements of the corresponding lattice observable, obtaining again a very good agreement, as shown in figure 7.

Our theoretical results probe non trivial features of the CFT describing the Q-state random Potts model, such as the multiplicities of the spectrum (3.5) or the validity of the three-point functions (4.16) and (4.24) for general values of the central charge. The topological corrections furnish a subtle characterisation of the Potts random clusters which goes beyond the computation of their fractal dimension. As a special case, we obtained the result (4.5) that represents a new universal behaviour of critical percolation. The study of the torus two-point connectivity represents, together with the plane three-point connectivity [39], a natural and powerful method to test various conjectures related to critical percolation.

Acknowledgments

We are grateful to Vladimir Dotsenko, Benoit Estienne, Christian Hagendorf, Yacine Ikhlef, Jesper Jacobsen, for helpful discussions and we thank in particular Sylvain Ribault with whom this project started.

Appendix. The *s*-channel expansion of the torus two-point function

The Virasoro generators are the modes of the stress-energy tensor. On the plane $z \in \mathbb{C} \bigcup \{\infty\}$, they are defined as:

J. Stat. Mech. (2020) 023101

$$L_n^{(z)} V_{(\Delta,Y)}(z,\bar{z}) = \frac{1}{2\pi \mathrm{i}} \oint_{\mathcal{C}_z} \mathrm{d}\, z'\, (z'-z)^{n+1}\, T(z') V_{(\Delta,Y)}(z,\bar{z}), \quad n \in \mathbb{Z}. \tag{A.1}$$

Under a conformal map $z' = f(z)$, a primary operator transforms:

$$V_{(\Delta)}(z,\bar{z}) = f'(z)^{\Delta} \bar{f}'(\bar{z})^{\bar{\Delta}}\, V_{(\Delta)}(f(z), \bar{f}(\bar{z})), \tag{A.2}$$

while the transformation of the Virasoro generators takes the form [24][3]:

$$\begin{aligned} L_n^{(z)} &= \frac{c}{12}\frac{1}{2\pi \mathrm{i}} \oint_z \mathrm{d}y (y-z)^{n+1} \{f, y\} + \frac{1}{2\pi \mathrm{i}} \oint_z \mathrm{d}y \sum_m \frac{L_m^{(f(z))} [f'(y)]^2}{(f(y)-f(z))^{m+2}} (y-z)^{n+1} \\ &= \frac{c}{12}\frac{1}{2\pi \mathrm{i}} \oint_z \mathrm{d}y (y-z)^{n+1} \{f, y\} + [f'(z)]^{-n} L_n^{(f(z))} + \frac{1-n}{2} f'' (f')^{-n-2} L_{n+1}^{(f(z))} \\ &\quad + \left(\frac{2-n}{6} f' f''' + \frac{1}{8}(n^2+n-4)(f'')^2\right)(f')^{-n-4} L_{n+2}^{(f(z))} + \cdots \end{aligned} \tag{A.3}$$

where $\{f, y\}$ is the Schwarzian derivative.

To compute torus correlation functions, one needs to know the transformation of (A.1) under the map (2.15). For finite w, one obtains for instance:

$$\begin{aligned} L_0^{(z)} &= L_0^{\mathcal{C},(w)} \\ L_{-1}^{(z)} &= z^{-1} \left(\frac{N}{2\pi \mathrm{i}}\right) \left(L_{-1}^{\mathcal{C},(w)} - \frac{2\pi \mathrm{i}}{N} L_0^{\mathcal{C},(w)}\right) \\ L_{-2}^{(z)} &= z^{-2} \left(\frac{N}{2\pi \mathrm{i}}\right)^2 \left(L_{-2}^{\mathcal{C},(w)} - \frac{3}{2}\frac{2\pi \mathrm{i}}{N} L_{-1}^{\mathcal{C},(w)} + \frac{13}{12}\left(\frac{2\pi \mathrm{i}}{N}\right)^2 L_0^{\mathcal{C},(w)} + \left(\frac{2\pi \mathrm{i}}{N}\right)^2 \frac{c}{24}\right) \\ &\cdots \end{aligned} \tag{A.4}$$

The modes with $L_n^{\mathcal{C},(w=\infty)}$, obtained from $L_n^{(0)}$ are instead related to contour integrals that are non-contractible on the cylinder. One finds for instance:

$$L_{-n}^{(0)} = L_{-n}^{\mathcal{C},(\infty)} + \frac{c}{24}\delta_{n,0}. \tag{A.5}$$

Using the above relation, one can easily verify that the one-point torus function of total derivative $\langle L_{-1}^{\mathcal{C},(0)} V_{(\Delta)} \rangle_\tau \propto \langle (L_{-1}^{(1)} + L_0^{(1)}) V_{(\Delta)} \rangle$ vanishes, as can be seen from the vanishing of the matrix elements (2.8):

$$\begin{aligned} &\left\langle L_{Y'}^{(\infty)} V_{(\Delta')} L_{-1}^{(1)} V_{(\Delta)} L_{-Y}^{(0)} V_{(\Delta')} \right\rangle + \left\langle L_{Y'}^{(\infty)} V_{(\Delta')} L_0^{(1)} V_{(\Delta)} L_{-Y}^{(0)} V_{(\Delta')} \right\rangle \\ &\qquad = (|Y| - |Y'| - \Delta + \Delta) \left\langle L_{Y'}^{(\infty)} V_{(\Delta')} V_{(\Delta)} L_{-Y}^{(0)} V_{(\Delta')} \right\rangle = 0. \end{aligned} \tag{A.6}$$

For the two-point function one obtains using (2.15):

$$\langle V_{(\Delta_1)}(w_1,\bar{w}_1) V_{(\Delta_2)}(w_2,\bar{w}_2) \rangle_\tau = \frac{1}{Z} \mathrm{Tr}_{\mathcal{S}_{\mathrm{int}}} \left(q^{L_0^{\mathcal{C},(\infty)}} \bar{q}^{\bar{L}_0^{\mathcal{C},(\infty)}} V_{(\Delta_1)}(w_1,\bar{w}_1) V_{(\Delta_2)}(w_2,\bar{w}_2) \right). \tag{A.7}$$

Using (A.2) under the map (2.15)[4] and the OPE (2.5), we find:

[3] Note that there is a misprint in [24] for the term $m = n+2$, as can be checked explicitly in the case $f(z) = z^2$.
[4] Note that the is drop since the dimensions of our fields satisfy $\Delta - \bar{\Delta} \in 2\mathbb{Z}$.

J. Stat. Mech. (2020) 023101

$$V_{(\Delta_1)}(w_1,\bar{w}_1)V_{(\Delta_2)}(w_2,\bar{w}_2) = \left(\frac{2\pi}{N}\right)^{\Delta_1+\Delta_2}\left(\frac{2\pi}{N}\right)^{\bar{\Delta}_1+\bar{\Delta}_2} z_1^{\Delta_1} z_2^{\Delta_2}\bar{z}_1^{\bar{\Delta}_1}\bar{z}_2^{\bar{\Delta}_2} V_{(\Delta_1)}(z_1,\bar{z}_1)V_{(\Delta_2)}(z_2,\bar{z}_2)$$
$$= \left(\frac{2\pi}{N}\right)^{\Delta_1+\Delta_2}\left(\frac{2\pi}{N}\right)^{\bar{\Delta}_1+\bar{\Delta}_2} z_1^{\Delta_1} z_2^{\Delta_2}\bar{z}_1^{\bar{\Delta}_1}\bar{z}_2^{\bar{\Delta}_2}$$
$$\times \sum_{(\Delta,Y)} C^{(\Delta)}_{(\Delta)_1,(\Delta)_2} z_{12}^{-\Delta_1-\Delta_2+\Delta+Y}\bar{z}_{12}^{-\bar{\Delta}_1-\bar{\Delta}_2+\bar{\Delta}+\bar{Y}}\tilde{\beta}^{(\Delta,Y)}_{\Delta_1,\Delta_2}\tilde{\beta}^{(\bar{\Delta},\bar{Y})}_{\bar{\Delta}_1,\bar{\Delta}_2} V_{(\Delta,Y)}(z_2,\bar{z}_2) \tag{A.8}$$

where we made explicit the z dependence of the coefficients (2.7): $\beta^{(\Delta,Y)}_{\Delta_1,\Delta_2}(z_{12}) = z_{12}^{-\Delta_1-\Delta_2+\Delta+Y}\tilde{\beta}^{(\Delta,Y)}_{\Delta_1,\Delta_2}$. Mapping $V_{(\Delta,Y)}(z_2,\bar{z}_2)$ back to the cylinder:

$$V_{(\Delta,Y)}(z_2,\bar{z}_2) = \left(\frac{2\pi\mathrm{i}}{N}\right)^{-\Delta-Y} z_2^{-\Delta-Y}\left(-\frac{2\pi\mathrm{i}}{N}\right)^{-\bar{\Delta}-\bar{Y}}\bar{z}_2^{-\bar{\Delta}-\bar{Y}}\left(L^{\mathcal{C},w_2}_{-Y}+\cdots\right)\left(\bar{L}^{\mathcal{C},\bar{w}_2}_{-\bar{Y}}+\cdots\right)V^{\mathcal{C}}_{(\Delta)}(w_2,\bar{w}_2)$$

where $\left(L^{\mathcal{C},w_2}_{-Y}+\cdots\right)$ is a linear combination of generators on the cylinder as in relations (A.4). We can now take the trace, and writing only the holomorphic part we get:

$$\langle V_{(\Delta_1)}(w_1)V_{(\Delta_2)}(w_2)\rangle_\tau = \left(\frac{2\pi}{N}\right)^{\Delta_1+\Delta_2}\left(\frac{z_2}{z_1}\right)^{\Delta_2}\left(1-\frac{z_2}{z_1}\right)^{-\Delta_1-\Delta_2}$$
$$\times \sum_{(\Delta,Y)\in\mathcal{S}_{\mathrm{int}}} C^{(\Delta)}_{(\Delta)_1,(\Delta)_2}\tilde{\beta}^{(\Delta,Y)}_{\Delta_1,\Delta_2}\left(\frac{2\pi\mathrm{i}}{N}\right)^{-\Delta-Y}\left(\frac{z_2}{z_1}\right)^{-\Delta-Y}\left(1-\frac{z_2}{z_1}\right)^{\Delta+Y}\langle\left(L^{\mathcal{C},w_2}_{-Y}+\cdots\right)V^{\mathcal{C}}_{(\Delta)}(w_2)\rangle_\tau. \tag{A.9}$$

Writing $\frac{z_2}{z_1} = \mathrm{e}^{-\frac{2\pi\mathrm{i}}{N}w_{12}}$ and expanding the exponentials, one has:

$$\begin{aligned}\langle V_{(\Delta_1)}(w_1)V_{(\Delta_2)}(w_2)\rangle_\tau &= w_{12}^{-\Delta_1-\Delta_2}\sum_{(\Delta)\in\mathcal{S}_{\mathrm{int}}} w_{12}^{\Delta} C^{(\Delta)}_{(\Delta)_1,(\Delta)_2}\Bigg(\langle V_{(\Delta)}(w_2)\rangle_\tau \\ &\quad + w_{12}\left\{\frac{2\pi\mathrm{i}}{N}\frac{\Delta_1-\Delta_2+\Delta}{2}+\tilde{\beta}^{(\Delta,1)}_{\Delta_1,\Delta_2}(L^{\mathcal{C},(w_2)}_{-1}-\frac{2\pi\mathrm{i}}{N}L^{\mathcal{C},(w_2)}_{0})\right\}\langle V_{(\Delta)}(w_2)\rangle_\tau + O(w_{12}^2)\Bigg) \\ &= w_{12}^{-\Delta_1-\Delta_2}\sum_{(\Delta)\in\mathcal{S}_{\mathrm{int}}} w_{12}^{\Delta} C^{(\Delta)}_{(\Delta)_1,(\Delta)_2}\Bigg(\langle V_{(\Delta)}(w_2)\rangle_\tau \\ &\quad + w_{12}\tilde{\beta}^{(\Delta,1)}_{\Delta_1,\Delta_2}\langle L^{\mathcal{C},(w_2)}_{-1}V_{(\Delta)}(w_2)\rangle_\tau + O(w_{12}^2)\Bigg).\end{aligned} \tag{A.10}$$

We assume that such cancellations occur at every order in w_{12}. Using the notation (2.16), we can finally arrive at equation (2.21). Notice that the coefficients $a^{(\Delta,Y)_{\mathrm{int}}}_{(\Delta)_1,(\Delta)_2}$ are evaluated using the generators on the plane, while the descendant fields $V^{\mathcal{C}}_{(\Delta,Y)}$ are obtained by acting with the cylinder generators.

References

[1] Duplantier B 2006 Conformal random geometry (arXiv:math-ph/0608053)
[2] Bauer M and Bernard D 2006 2D growth processes: SLE and Loewner chains *Phys. Rep.* **432** 115–221
[3] Cardy J L 1992 Critical percolation in finite geometries *J. Phys. A: Math. Gen.* **25** L201
[4] Cardy J 2005 SLE for theoretical physicists *Ann. Phys.* **318** 81–118
[5] Gaberdiel M R and Kausch H G 1999 A local logarithmic conformal field theory *Nuclear Phys.* B **538** 631–58

J. Stat. Mech. (2020) 023101

[6] Kausch H G 2000 Symplectic fermions *Nuclear Phys.* B **583** 513–41
[7] Wu F Y 1982 The Potts model *Rev. Mod. Phys.* **54** 235
[8] Caracciolo S, Jacobsen J L, Saleur H, Sokal A D and Sportiello A 2004 Fermionic field theory for trees and forests *Phys. Rev. Lett.* **93** 080601
[9] Delfino G and Viti J 2011 Potts q-color field theory and scaling random cluster model *Nuclear Phys.* B **852** 149–73
[10] Gori G and Viti J 2017 Exact logarithmic four-point functions in the critical two-dimensional Ising model *Phys. Rev. Lett.* **119** 191601
[11] Gori G and Viti J 2018 Four-point boundary connectivities in critical two-dimensional percolation from conformal invariance *J. High Energy Phys.* **2018** 131
[12] Delfino G and Viti J 2011 On three-point connectivity in two-dimensional percolation *J. Phys. A: Math. Theor.* **44** 032001
[13] Picco M, Santachiara R, Viti J and Delfino G 2013 Connectivities of Potts Fortuin–Kasteleyn clusters and time-like Liouville correlator *Nuclear Phys.* B **875** 719–37
[14] Delfino G, Picco M, Santachiara R and Viti J 2013 Spin clusters and conformal field theory *J. Stat. Mech.* P11011
[15] Estienne B and Ikhlef Y 2015 Correlation functions in loop models (arXiv:1505.00585)
[16] Ikhlef Y, Lykke Jacobsen J and Saleur H 2015 Three-point functions in $c \leqslant= 1$ Liouville theory and conformal loop ensembles *Phys. Rev. Lett.* **116** 130601
[17] LeClair A and Squires J 2018 Conformal bootstrap for percolation and polymers *J. Stat. Mech.* 123105
[18] Jacobsen J L and Saleur H 2018 Bootstrap approach to geometrical four-point functions in the two-dimensional critical Q-state Potts model: a study of the s-channel spectra (arXiv:1809.02191)
[19] Picco M, Ribault S and Santachiara R 2016 A conformal bootstrap approach to critical percolation in two dimensions *SciPost Phys.* **1** 009
[20] Picco M, Ribault S and Santachiara R 2019 On four-point connectivities in the critical 2d Potts model *SciPost Phys.* **7** 044
[21] Ribault S 2014 Conformal field theory on the plane (arXiv:1406.4290)
[22] Ribault S and Santachiara R 2015 Liouville theory with a central charge less than one *J. High Energy Phys.* 109
[23] Kanno S, Matsuo Y and Shiba S 2010 Analysis of correlation functions in Toda theory and AGT-W relation for SU(3) quiver *Phys. Rev.* D **82** 066009
[24] Eguchi T and Ooguri H 1987 Conformal and current algebras on a general Riemann surface *Nuclear Phys.* B **282** 308–28
[25] Javerzat N, Santachiara R and Foda O 2018 Notes on the solutions of Zamolodchikov-type recursion relations in Virasoro minimal models *J. High Energy Phys.* 109
[26] Fortuin C and Kasteleyn P 1972 On the random-cluster model: I. Introduction and relation to other models **57** 536–64
[27] Di Francesco P, Saleur H and Zuber J-B 1987 Relations between the Coulomb gas picture and conformal invariance of two-dimensional critical models *J. Stat. Phys.* **49** 57–79
[28] Dotsenko V and Fateev V 1985 Operator algebra of two-dimensional conformal theories with central charge $C \leqslant 1$ *Phys. Lett.* B **154** 291–5
[29] Jacobsen J 2012 Loop models and boundary CFT Henkel M and Karevski D *Conformal Invariance: an Introduction to Loops, Interfaces and Stochastic Loewner Evolution* (Berlin: Springer)
[30] Saleur H 1987 Conformal invariance for polymers and percolation *J. Phys. A: Math. Gen.* **20** 455
[31] Beffara V and Duminil-Copin H 2010 The self-dual point of the two-dimensional random-cluster model is critical for $q \geqslant 1$ (arXiv:1006.5073)
[32] Jayaraman T and Narain K 1990 Correlation functions for minimal models on the torus *Nuclear Phys.* B **331** 629–58
[33] Dotsenko V and Fateev V 1985 Four-point correlation functions and the operator algebra in 2D conformal invariant theories with central charge $C \leqslant 1$ *Nuclear Phys.* B **251** 691–734
[34] Migliaccio S and Ribault S 2017 The analytic bootstrap equations of non-diagonal two-dimensional CFT *J. High Energy Phys.* 169
[35] Santachiara R and Viti J 2014 Local logarithmic correlators as limits of Coulomb gas integrals *Nuclear Phys.* B **882** 229–62
[36] Chayes L and Machta J 1998 Graphical representations and cluster algorithms II *Physica* A **254** 477–516
[37] Deng Y, Garoni T M, Machta J, Ossola G, Polin M and Sokal A D 2007 Dynamic critical behavior of the Chayes–Machta algorithm for the random-cluster model, I. two dimensions *J. Stat. Phys.* **144** 459
[38] Wu T T, McCoy B M, Tracy C A and Barouch E 1976 Spin-spin correlation functions for the two-dimensional Ising model: exact theory in the scaling region *Phys. Rev.* B **13** 316
[39] Cao X, Rosso A and Santachiara R 2015 Conformal invariance of loop ensembles under Kardar–Parisi–Zhang dynamics *EPL* **111** 16001

J. Stat. Mech. (2020) 023101

Journal of Statistical Mechanics: Theory and Experiment
An IOP and SISSA journal

PAPER: Quantum statistical physics, condensed matter, integrable systems

Three- and four-point connectivities of two-dimensional critical Q-Potts random clusters on the torus

Nina Javerzat[1], Marco Picco[2] and Raoul Santachiara[1]

[1] LPTMS, CNRS (UMR 8626), Univ.Paris-Sud, Université Paris-Saclay, 91405 Orsay, France
[2] LPTHE, UMR 7589, Sorbonne Université and CNRS, France
E-mail: nina.javerzat@u-psud.fr, picco@lpthe.jussieu.fr and raoul.santachiara@u-psud.fr

Received 10 January 2020
Accepted for publication 17 February 2020
Published 27 May 2020

Online at stacks.iop.org/JSTAT/2020/053106
https://doi.org/10.1088/1742-5468/ab7c5e

Abstract. In a recent paper, we considered the effects of the torus lattice topology on the two-point connectivity of Q-Potts clusters. These effects are universal and probe non-trivial structure constants of the theory. We complete here this work by considering the torus corrections to the three- and four-point connectivities. These corrections, which depend on the scale invariant ratios of the triangle and quadrilateral formed by the three and four given points, test other non-trivial structure constants. We also present results of Monte Carlo simulations in good agreement with our predictions.

Keywords: conformal field theory, correlation functions

J. Stat. Mech. (2020) 053106

1742-5468/20/053106+30$33.00

Contents

1. Introduction

The two-dimensional Q-Potts model is a one-parameter family of models which describe random clusters on a lattice [1] and admit for $Q \leqslant 4$ a continuous transition between a percolating and a non-percolating cluster phase [2]. At the critical point the clusters form conformal invariant fractal structures whose description challenges our understanding of the fractal geometry in critical phenomena [3]. For more than thirty years, physicists have been trying to solve the conformal field theories (CFT) that capture, for general $Q \in \mathbb{R}, Q \leqslant 4$, the continuum limit of the critical Q-Potts models. Despite many important results, in particular the computation of the partition function [4], the derivation of exact formulas for many critical exponents [5] and the progress in the representation theory of the Temperley–Lieb type algebras underlying these models [6, 7], the problem of defining the correct CFT solution remains an open issue. In particular, the knowledge of the CFT structure constants, which determine the small-distance asymptotic behavior of the CFT many-point correlation functions, is missing. A remarkable proposal was done in [8], where the so-called $c \leqslant 1$ Liouville structure constants [9–11]—until then considered non-physical—were conjectured to describe the three-point connectivity, i.e. the probability that three given points belong to the same cluster. Inspired by this result, new crossing-symmetric solutions, based on the $c \leqslant 1$ Liouville-type constants, have been found [12–16], and some of them proposed to describe four-point cluster connectivities [13, 14]. In [17] it was argued, and numerically shown, that there are states which provide a non-vanishing contribution to the connectivities but that are not taken into account by these bootstrap solutions. These contributions are, for general values of Q, very small and the bootstrap solutions remain a very good approximation (within the Monte Carlo simulation precision) to the cluster connectivities.

In [18], we considered the effects of the torus lattice topology on the two-point Potts connectivity, which probe non-trivial structure constants of the theory. Putting together the exact analysis in [17] and the results in [13, 14], we were able to capture the dominant torus corrections to the infinite plane results. In this paper, we complete this work by considering the torus corrections of three- and four-point connectivities, which are expected to test much more non-trivial structure constants. Indeed these corrections contain structure constants which do not satisfy any differential equations, contrary to the two-point case.

In section 2 we give the framework within which our problem is stated. In section 3 we outline the CFT approach to study universal finite-size effects on the torus. In section 4 we define the Q-Potts model and the lattice observables we will consider and we review the relevant results about the CFT describing the critical Q-Potts model. In section 5 we give the new theoretical predictions about the three- and four-point connectivities. These predictions are compared to Monte Carlo simulations. In section 6 we summarise and discuss the results.

J. Stat. Mech. (2020) 053106

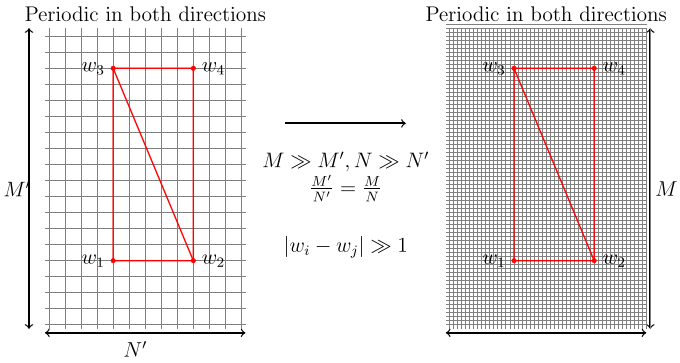

Figure 1. Scaling limit of multi-point observables on double-periodic lattices.

2. Scaling limit of multi-point observables on double-periodic lattices

Consider a lattice statistical model that undergoes a second-order phase transition, and define it on an $M \times N$ square lattice of mesh $a_0 = 1$ with double-periodic boundary conditions. The lattice has then the topology of a torus with nome q:

$$q = \mathrm{e}^{2\pi \mathrm{i} \tau}, \quad \tau = \mathrm{i}\frac{M}{N}. \tag{2.1}$$

To characterise the universality class, one defines a lattice observable $\mathcal{O}(w_1, \ldots, w_n)$, with $w_1, \ldots, w_n$ indicating points on the torus, and studies its scaling limit $P(w_1, \ldots, w_n)$ at the critical point, see figure 1. Supposing that $\mathcal{O}$ is multiplicatively renormalisable (see chapter 2 in [19]) one has:

$$P(w_1, w_2, \ldots, w_n) = \lim_{\substack{N\to\infty \\ \frac{M}{N}=O(1)}} N^{2n\Delta} \mathcal{O}(w_1, \ldots, w_n) \tag{2.2}$$

where 2Δ is the scaling dimension associated to the lattice observable. One may think for instance of the n-point Ising spin correlation function at the ferromagnetic–paramagnetic transition. In this case the scaling dimension is $2\Delta = \frac{1}{8}$, as rigorously proven in [20]. The basic assumptions we will work with are:

- the system is conformal invariant;
- when $w_i - w_j \gg 1$, $P(w_1, \ldots, w_n)$ is given by the torus n-point correlation function of spinless primary fields with scaling dimension 2Δ; and
- the corresponding CFT has a discrete spectrum.

The limit

$$\frac{|w_i - w_j|}{N} \to 0 \tag{2.3}$$

corresponds to the infinite plane limit. In the $n = 2, 3$ case, the conformal invariance fixes the spatial dependence:

$$P(w_1, w_2) \xrightarrow{\frac{w_{12}}{N}\to 0} \frac{c_0^{(2)}}{|w_{12}|^{4\Delta}}, \quad P(w_1, w_2, w_3) \xrightarrow{\frac{w_{ij}}{N}\to 0} c_0^{(3)} \frac{D}{|w_{12} w_{13} w_{23}|^{2\Delta}}, \tag{2.4}$$

J. Stat. Mech. (2020) 053106

where D is an universal constant. For $n = 4$:

$$P(w_1, w_2, w_3, w_4) \xrightarrow{\frac{w_{ij}}{N} \to 0} \frac{c_0^{(4)}}{|w_{12} w_{34}|^{4\Delta}} P(z), \quad z = \frac{w_{12} w_{34}}{w_{13} w_{24}}, \tag{2.5}$$

which means that the problem has been reduced to the computation of a function $P(z)$, with z the cross-ratio. The $c_0^{(n)}$ in the above expressions are non-universal constants. In this paper we will study the behavior of $P(w_1, \ldots, w_n)$ when the distances between points

$$0 < \frac{|w_i - w_j|}{N} \ll 1, \tag{2.6}$$

are small but different from zero. In this case we expect corrections to the infinite plane limit coming from the torus topology:

$$P(w_1, w_2) = \frac{c_0^{(2)}}{|w_{12}|^{4\Delta}} \left[1 + f_\tau^{(2)}\left(\frac{w_{12}}{N}\right)\right] \tag{2.7}$$

$$P(w_1, w_2, w_3) = \frac{c_0^{(3)}}{|w_{12}|^{4\Delta} |w_{23}|^{2\Delta}} \left[D \left|\frac{w_{12}}{w_{23}}\right|^{2\Delta} \left|\left(1 + \frac{w_{12}}{w_{23}}\right)\right|^{-2\Delta} + f_\tau^{(3)}\left(\frac{w_{12}}{w_{23}}, \frac{w_{23}}{N}\right)\right] \tag{2.8}$$

$$P(w_1, w_2, w_3, w_4) = \frac{c_0^{(4)}}{|w_{12}|^{4\Delta} |w_{34}|^{4\Delta}} \left[P\left(\frac{w_{12} w_{34}}{w_{13} w_{24}}\right) + f_\tau^{(4)}\left(\frac{w_{12} w_{34}}{w_{13} w_{24}}, \frac{w_{24}}{N}\right)\right]. \tag{2.9}$$

The functions f_τ, symmetric under the replacements $N \leftrightarrow M, \tau \leftrightarrow -\tau^{-1}$, encode the corrections to the infinite plane limit. The assumption that $P(w_1, \ldots, w_n)$ is given by a correlator of local fields in some CFT can be considered quite optimistic if it is applied to non-local observables, such as the geometric properties of critical fractals. Actually we will study these types of observables, namely the n-point connectivities of critical Potts clusters. However, we will show that the CFT approach not only well describes the plane limit of the cluster connectivities [13, 14] but also captures the very non-trivial effects of the lattice topology. The functions f_τ are known only in a few cases, namely when the CFT is the compactified free boson [21, 22], as in the case of the Ising energy and spin correlation functions, or when a Coulomb gas description is available [23, 24]. However, as we will show below, these functions can always be expressed as multiple series expansions. This approach is useful for lattice sizes $N \gg 1$ and location of points $\{w_i\}$ for which the series converge quickly.

J. Stat. Mech. (2020) 053106

3. Conformal field theory approach

We outline here how to compute the large N expansion of the functions f_τ in (2.7)–(2.9). Let us consider a CFT with:

$$\text{central charge: } c, \text{ and spectrum: } \mathcal{S} \tag{3.1}$$

defined on the torus (2.1). The central charge c is the parameter that defines the algebra of the conformal generators, the Virasoro algebra (A.1). The set of the Virasoro representations entering a CFT forms its spectrum $\mathcal{S}$. We refer the reader to [25] for an introduction to CFT. Henceforth we indicate $V_{(\Delta)}$ a primary field with $(\Delta) = \Delta, \bar{\Delta}$ its left and right dimensions. The notation (Δ) will refer either to the highest weight state associated to $V_{(\Delta)}$ or to the entire representation formed by the set of descendants states. The symbol $(\Delta, Y) = \Delta, Y, \bar{\Delta}, \bar{Y}$ denotes one of the descendant states with dimensions $\Delta + |Y|$ and $\bar{\Delta} + |\bar{Y}|$, where $|Y|$, $|\bar{Y}| \in \mathbb{N}$ are the levels of the descendant: as reviewed in appendix A, this notation comes from the fact that the descendant states forming a basis of an irreducible representation are labeled by the Young tableaux Y, $\bar{Y}$ with number of boxes $|Y|$ and $|\bar{Y}|$.

A CFT is solved when, in addition to the central charge and the spectrum, the structure constants $D^{(\Delta_3)}_{(\Delta_1),(\Delta_2)}$, defined in (A.5) and in (A.8), are known.

Suppose we consider a case where the CFT is solved. In particular we are interested in the functions:

$$\langle V_{(\Delta_1)}(w_1) \cdots V_{(\Delta_n)}(w_n) \rangle, \quad n = 2, 3, 4 \tag{3.2}$$

where $\langle \cdots \rangle$ denotes the CFT correlation on the torus (2.1). Notice that $V_{(\Delta)}$ may not be uniquely defined by its scaling dimensions. This is the case, for instance, when the CFT has an additional symmetry with multiplicities in the representations.

3.1. CFT partition function

The CFT partition function Z takes the form:

$$Z = \sum_{(\Delta)\in\mathcal{S}} q^{\Delta - c/24} \bar{q}^{\bar{\Delta} - c/24} \left[1 + O(q, \bar{q})\right], \tag{3.3}$$

where q is the nome given in (2.1) and the terms in the square brackets correspond to all the contributions of order $O(q^{|Y|}\bar{q}^{|\bar{Y}|})$, coming from the descendants states (Δ, Y).

3.2. One-point function

The one-point function $\langle V_{(\Delta,Y)} \rangle$ on a torus of size N has the expression [26]:

J. Stat. Mech. (2020) 053106

$$\left\langle V_{(\Delta,Y)}\right\rangle = \frac{1}{Z}\frac{(2\pi)^{\Delta+|Y|+\bar{\Delta}+|\bar{Y}|}}{N^{\Delta+\bar{\Delta}+|Y|+|\bar{Y}|}}\sum_{(\Delta')\in\mathcal{S}} D^{(\Delta')}_{(\Delta),(\Delta')} q^{\Delta'-c/24}\bar{q}^{\Delta'-c/24}\left[1+O(q,\bar{q})\right]$$
$$= \frac{1}{N^{\Delta+\bar{\Delta}+|Y|+|\bar{Y}|}}\left\langle V_{(\Delta,Y)}\right\rangle_{(N=1)}, \tag{3.4}$$

where in order to make the dependence on N more explicit, we introduced, as in [18], the notation $\langle\cdots\rangle_{(N=1)}$ to indicate a CFT correlation computed on the torus (2.1) with $N=1$.

The representations (Δ') contributing to the one-point $V_{(\Delta,Y)}$ torus function are the ones for which the structure constant $D^{(\Delta')}_{(\Delta),(\Delta')}$ does not vanish, and which satisfy the fusion rule $(\Delta')\times(\Delta')\to(\Delta)$. Each term appearing in the sum (3.4) is given in (A.10) and can be represented in figure 2:

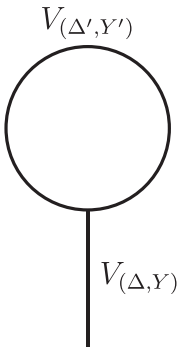

$$= D^{(\Delta,Y)}_{(\Delta',Y'),(\Delta',Y')} q^{\Delta'+|Y'|-c/24}\bar{q}^{\bar{\Delta}'+|\bar{Y}'|-c/24}$$

Figure 2. Diagrammatic representation of the torus one-point function.

where we denote $D^{(\Delta_3,Y_3)}_{(\Delta_1,Y_1),(\Delta_2,Y_2)}$ the constant associated to the three-point function of descendant fields, which is directly proportional to $D^{(\Delta_3)}_{(\Delta_1),(\Delta_2)}$, see (A.6).

3.3. Two-point function

The two-point function $\langle V_{(\Delta_1)}(w_1)V_{(\Delta_2)}(w_2)\rangle$ can be represented in the form:

$$\left\langle V_{(\Delta_1)}(w_1)V_{(\Delta_2)}(w_2)\right\rangle = \frac{1}{|w_{12}|^{2\Delta_1+2\Delta_2}}\sum_{(\Delta_{\rm top})\in\mathcal{S}} D^{(\Delta_{\rm top})}_{(\Delta_1),(\Delta_2)}\left(\frac{w_{12}}{N}\right)^{\Delta_{\rm top}}\left(\frac{\bar{w}_{12}}{N}\right)^{\bar{\Delta}_{\rm top}}$$
$$\times\left[\left\langle V_{(\Delta_{\rm top})}\right\rangle_{(N=1)} + O\left(\frac{w_{12}}{N},\frac{\bar{w}_{12}}{N}\right)\right]. \tag{3.5}$$

The contributions in the square bracket come from the descendants $V_{(\Delta_{\rm top},Y_{\rm top})}$. The $1/N$ scaling of the topological corrections is then determined by the fields $V_{(\Delta_{\rm top},Y_{\rm top})}$. Each of these terms is given in appendix A.3 and is associated to figure 3:

J. Stat. Mech. (2020) 053106

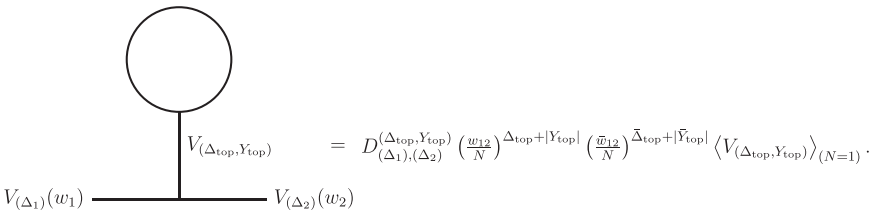

Figure 3. Diagrammatic representation of the torus two-point function.

When the field $V_{(\Delta_{\rm top},Y_{\rm top})} = {\rm Id}$ is the identity field, i.e. $\Delta_{\rm top} = \bar{\Delta}_{\rm top} = 0, |Y_{\rm top}| = |\bar{Y}_{\rm top}| = 0$ and with $\langle {\rm Id}\rangle = 1$, one recovers the plane limit (the primary fields are normalised such that $D^{\rm Id}_{(\Delta_1),(\Delta_2)} = 1$). Setting $(\Delta_1) = (\Delta_2) = (\Delta)$, we find the expansion of $f^{(2)}_\tau\left(\frac{w_{12}}{N}\right)$ in (2.7):

$$f^{(2)}_\tau\left(\frac{w_{12}}{N}\right) = D^{(\Delta)_{\rm min}}_{(\Delta),(\Delta)}\left(\frac{w_{12}}{N}\right)^{\Delta_{\rm min}}\left(\frac{\bar{w}_{12}}{N}\right)^{\bar{\Delta}_{\rm min}}\left\langle V_{(\Delta)_{\rm min}}\right\rangle_{(N=1)} + o\left(\frac{1}{N^{\Delta_{\rm min}+\bar{\Delta}_{\rm min}}}\right), \tag{3.6}$$

where $V_{(\Delta)_{\rm min}}$ is the state among the $V_{(\Delta_{\rm top})}$ appearing in the $(\Delta)\otimes(\Delta)$ fusion with lowest dimensions $\Delta_{\rm min}, \bar{\Delta}_{\rm min}$. Note that the assumption made in section 2 of the discreteness of the spectrum $\mathcal{S}$ implies that the dimensions of the fields are discretely spaced. A more detailed treatment of the two-point function can be found in [18].

3.4. Three-point function

In the channel expansion where $w_1 \to w_2$, $\langle V_{(\Delta_1)}(w_1)V_{(\Delta_2)}(w_2)V_{(\Delta_3)}(w_3)\rangle$ can be expressed as:

$$\begin{aligned}\left\langle V_{(\Delta_1)}(w_1)V_{(\Delta_2)}(w_2)V_{(\Delta_3)}(w_3)\right\rangle = |w_{12}|^{-2\Delta_1-2\Delta_2}\sum_{(\Delta_{\rm L})\in\mathcal{S}} D^{(\Delta_{\rm L})}_{(\Delta_1),(\Delta_2)} w_{12}^{\Delta_{\rm L}}\bar{w}_{12}^{\bar{\Delta}_{\rm L}} \\ \times\left[\left\langle V_{(\Delta_{\rm L})}(w_2)V_{(\Delta_3)}(w_3)\right\rangle + O\left(w_{12},\bar{w}_{12}\right)\right].\end{aligned} \tag{3.7}$$

The contributions in the square brackets come from the descendants of $V_{(\Delta)_{\rm L}}$ and are given in appendix C. Expanding the two-point function, similarly to what has been done above, one finds that each of these corrections can be associated to figure 4:

J. Stat. Mech. (2020) 053106

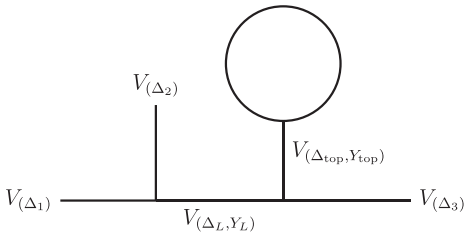

$$= D^{(\Delta_L,Y_L)}_{(\Delta_1),(\Delta_2)} D^{(\Delta_{\rm top})}_{(\Delta_L,Y_L),(\Delta_3)} \left(\tfrac{w_{12}}{w_{23}}\right)^{\Delta_L+|Y_L|} \left(\tfrac{\bar{w}_{12}}{\bar{w}_{23}}\right)^{\bar{\Delta}_L+|\bar{Y}_L|} \left(\tfrac{w_{23}}{N}\right)^{\Delta_{\rm top}+|Y_{\rm top}|} \left(\tfrac{\bar{w}_{23}}{N}\right)^{\bar{\Delta}_{\rm top}+|\bar{Y}_{\rm top}|} \left\langle V_{(\Delta_{\rm top},Y_{\rm top})}\right\rangle$$

Figure 4. Diagrammatic representation of the torus three-point function.

The terms with $\Delta_{\rm top} = \bar{\Delta}_{\rm top} = 0, |Y_{\rm top}| = |\bar{Y}_{\rm top}| = 0$ add up to give the plane limit. We can specify now to the case $(\Delta_1) = (\Delta_2) = (\Delta_3) = (\Delta)$ and give the form of the double expansion of $f^{(3)}_\tau$ in (2.8):

$$f^{(3)}_\tau\left(\frac{w_{12}}{w_{23}}, \frac{w_{23}}{N}\right) = c^{(3)}_{\rm min}\left(\frac{w_{12}}{w_{23}}, \tau\right)\left(\frac{w_{23}}{N}\right)^{\Delta_{\rm min}}\left(\frac{\bar{w}_{23}}{N}\right)^{\bar{\Delta}_{\rm min}} + o\left(\frac{1}{N^{\Delta_{\rm min}+\bar{\Delta}_{\rm min}}}\right). \tag{3.8}$$

The coefficient $c^{(3)}_{\rm min}$ is given by:

$$c^{(3)}_{\rm min}\left(\frac{w_{12}}{w_{23}}, \tau\right) = \left\langle V_{(\Delta_{\rm min})}\right\rangle \sum_{(\Delta_{\rm L},Y_{\rm L})\in\mathcal{S}} D^{(\Delta_{\rm L},Y_{\rm L})}_{(\Delta),(\Delta)} D^{(\Delta_{\rm min})}_{(\Delta_{\rm L},Y_{\rm L}),(\Delta)} \left(\frac{w_{12}}{w_{23}}\right)^{\Delta_{\rm L}+|Y_{\rm L}|}\left(\frac{\bar{w}_{12}}{\bar{w}_{23}}\right)^{\bar{\Delta}_{\rm L}+|\bar{Y}_{\rm L}|}. \tag{3.9}$$

The field $V_{(\Delta_{\rm min})}$ corresponds to the state with lowest dimensions $\Delta_{\rm min}, \bar{\Delta}_{\rm min}$ appearing in the $(\Delta_{\rm L}) \otimes (\Delta)$ fusion, and therefore it can be different from the one appearing in (3.6).

3.5. Four-point function

In the s- channel, the four-point function admits the following expansion:

$$\begin{aligned}\left\langle V_{(\Delta_1)}(w_1)V_{(\Delta_2)}(w_2)V_{(\Delta_3)}(w_3)V_{(\Delta_4)}(w_4)\right\rangle \\ = \sum_{(\Delta_{\rm L}),(\Delta_{\rm R})\in\mathcal{S}} D^{(\Delta_{\rm L})}_{(\Delta_1),(\Delta_2)} D^{(\Delta_{\rm R})}_{(\Delta_3),(\Delta_4)} w_{12}^{\Delta_l-\Delta_1-\Delta_2}\bar{w}_{12}^{\bar{\Delta}_{\rm L}-\bar{\Delta}_1-\bar{\Delta}_2} w_{34}^{\Delta_{\rm R}-\Delta_3-\Delta_4}\bar{w}_{34}^{\bar{\Delta}_{\rm R}-\bar{\Delta}_3-\bar{\Delta}_4} \\ \times\left[\left\langle V_{(\Delta_{\rm L})}(w_2)V_{(\Delta_{\rm R})}(w_4)\right\rangle + O\left(w_{12},\bar{w}_{12},w_{34},\bar{w}_{34}\right)\right].\end{aligned} \tag{3.10}$$

As explained in appendix D, each term of the above sum is represented in figure 5:

J. Stat. Mech. (2020) 053106

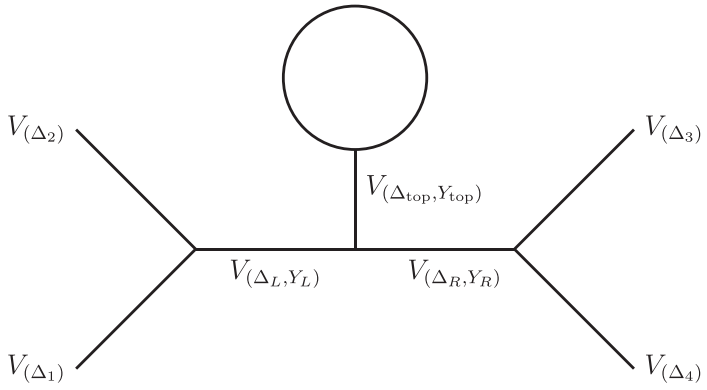

$$= D^{(\Delta_L,Y_L)}_{(\Delta_1),(\Delta_2)} D^{(\Delta_R,Y_R)}_{(\Delta_3),(\Delta_4)} D^{(\Delta_{\rm top})}_{(\Delta_L,Y_L),(\Delta_R,Y_R)} \left(\tfrac{w_{12}}{w_{24}}\right)^{\Delta_L+|Y_L|} \left(\tfrac{\bar{w}_{12}}{\bar{w}_{24}}\right)^{\bar{\Delta}_l+|\bar{Y}_L|} \left(\tfrac{w_{34}}{w_{24}}\right)^{\Delta_L+|Y_L|} \left(\tfrac{\bar{w}_{34}}{\bar{w}_{24}}\right)^{\bar{\Delta}_R+|\bar{Y}_R|} \times \left(\tfrac{w_{24}}{N}\right)^{\Delta_{\rm top}+|Y_{\rm top}|} \left(\tfrac{\bar{w}_{24}}{N}\right)^{\bar{\Delta}_{\rm top}+|\bar{Y}_{\rm top}|} \left\langle V_{(\Delta_{\rm top},Y_{\rm top})} \right\rangle$$

Figure 5. Diagrammatic representation of the torus four-point function.

The sum over the diagrams with $\Delta_{\rm top} = \bar{\Delta}_{\rm top} = 0, |Y_{\rm top}| = |\bar{Y}_{\rm top}| = 0$ coincides with the s- channel expansion of the plane four-point correlation function [25]. Setting $(\Delta_i) = (\Delta)$, $i = 1, \ldots, 4$, the multi-series expansion of $f^{(4)}_\tau$ in (2.9) takes the form:

$$f^{(4)}_\tau \left(\frac{w_{12}}{w_{24}}, \frac{w_{34}}{w_{24}}, \frac{w_{24}}{N}\right) = c^{(4)}_{\rm min} \left(\frac{w_{12}}{w_{24}}, \frac{w_{34}}{w_{24}}, \tau\right) \left(\frac{w_{24}}{N}\right)^{\Delta_{\rm min}} \left(\frac{\bar{w}_{24}}{N}\right)^{\bar{\Delta}_{\rm min}} + o\left(\frac{1}{N^{\Delta_{\rm min}+\bar{\Delta}_{\rm min}}}\right), \tag{3.11}$$

where:

$$c^{(4)}_{\rm min} \left(\frac{w_{12}}{w_{24}}, \frac{w_{34}}{w_{24}}, \tau\right) = \left\langle V_{(\Delta_{\rm min})} \right\rangle \sum_{\substack{(\Delta_{\rm L},Y_{\rm L}),\\ (\Delta_{\rm R},Y_{\rm R})\in\mathcal{S}}} D^{(\Delta_{\rm L},Y_{\rm L})}_{(\Delta),(\Delta)} D^{(\Delta_{\rm R},Y_{\rm R})}_{(\Delta),(\Delta)} D^{(\Delta_{\rm min})}_{(\Delta_{\rm L},Y_{\rm L}),(\Delta_{\rm R},Y_{\rm R})} \times \left(\frac{w_{12}}{w_{24}}\right)^{\Delta_{\rm L}+|Y_{\rm L}|} \left(\frac{\bar{w}_{12}}{\bar{w}_{24}}\right)^{\bar{\Delta}_{\rm L}+|\bar{Y}_{\rm L}|} \left(\frac{w_{34}}{w_{24}}\right)^{\Delta_{\rm R}+|Y_{\rm R}|} \times \left(\frac{\bar{w}_{34}}{\bar{w}_{24}}\right)^{\bar{\Delta}_{\rm R}+|\bar{Y}_{\rm R}|}. \tag{3.12}$$

4. $Q-$Potts random cluster model: CFT versus Monte Carlo results

We want to apply the above formulas to the study of the connectivities of the Q-Potts clusters.

J. Stat. Mech. (2020) 053106

4.1. Lattice model and multi-point connectivities

Let us consider a double-periodic square lattice with parameters (2.1) whose edges can carry a bond or not. The random cluster Q-state Potts model [27] on such a lattice is defined by the partition function

$$\mathcal{Z}_Q = \sum_{\mathcal{G}} Q^{\#\text{clusters}} p^{\#\text{bonds}} (1-p)^{\#\text{edges without bond}}, \tag{4.1}$$

where $\mathcal{G}$ denotes one of the possible bond configurations and $p \in [0,1]$. The clusters percolate at the critical value

$$p = p_c = \frac{\sqrt{Q}}{\sqrt{Q}+1}, \tag{4.2}$$

The lattice multi-point observables $\mathcal{O}$ at $p = p_c$ we consider is:

$$\mathcal{O}(w_1, \dots, w_n) = \text{Probability}(w_1, w_2, \dots, w_n \text{ are in the same cluster}). \tag{4.3}$$

For $n = 2, 3$ the above probabilities scan the space of all possible connectivities, while, for $n = 4$, the space of connectivities is four dimensional [28], see also [9, 12–14, 17, 18, 24, 29, 30]. Here we will focus only on the above type of connectivity.

4.2. The CFT describing the critical Potts cluster model: state of the art

We parametrise the central charge c and the conformal dimension Δ as follows:

$$c = 1 - 6\big(\beta - \beta^{-1}\big)^2, \quad \Delta = \Delta_{(r,s)} = \frac{c-1}{24} + \frac{1}{4}\left(r\beta - \frac{s}{\beta}\right)^2. \tag{4.4}$$

A representation is degenerate if $r, s \in \mathbb{N}^*$, and has a null state at level rs. The symbols

$$V_{\Delta_{(r,s)},\Delta_{(r,s)}} = V_{(r,s)^D}, \quad V_{\Delta_{(r,s)},\Delta_{(r,-s)}} = V_{(r,s)} \tag{4.5}$$

indicate the diagonal and non-diagonal primary fields. The notations

$$(r,s)^D, \quad (r,s) \tag{4.6}$$

denote the representations associated to $V_{(r,s)^D}$ and $V_{(r,s)}$ respectively. This allows us to use a lighter notation for the structure constants, for instance:

$$D^{(r,s)^D}_{(r_1,s_1),(r_2,s_2)} = D^{(\Delta_{r_3,s_3},\Delta_{r_3,s_3})}_{\big(\Delta_{r_1,s_1},\Delta_{r_1,-s_1}\big),\big(\Delta_{r_2,s_2},\Delta_{r_2,-s_2}\big)}. \tag{4.7}$$

A set of these representations is denoted as

$$\mathcal{S}^D_X = \{(r,s)^D\}_{(r,s)\in X}, \quad \mathcal{S}_X = \{(r,s)\}_{(r,s)\in X}, \tag{4.8}$$

where X is a given set of pairs (r,s). A third set type is $\mathcal{S}^{\text{quot}}_X$ that contains the degenerate representations with vanishing null state.

What do we know about the CFT describing the critical Potts clusters? We know

J. Stat. Mech. (2020) 053106

- the central charge $c(\beta)$. In the β parametrisation (4.4), the critical Q-Potts model is related to a CFT with:

$$Q = 4\cos^2\pi\,\beta^2 \quad \text{with } \frac{1}{2} \leqslant \beta^2 \leqslant 1. \tag{4.9}$$

- the spectrum $\mathcal{S} = \mathcal{S}^{\text{Potts}}$ [4]

$$\mathcal{S}^{\text{Potts}} = \mathcal{S}^{D,\text{quot}}_{(1,\mathbb{N}^*)} \bigcup_{\substack{j\geqslant 2\\ M|j, p\wedge M=1}} \mathcal{S}_{\left(j,\mathbb{Z}+\frac{p}{M}\right)} \bigcup \mathcal{S}_{\left(0,\mathbb{Z}+\frac{1}{2}\right)}. \tag{4.10}$$

The multiplicities associated to the above sectors have also been computed [4] and, for general Q, assume general real values. We refer the reader to [17] and references therein for a detailed discussion of (4.10).

We do not know:

- the CFT Potts model structure constants. In other words, for general Q, a complete bootstrap solution of the Potts CFT has not been found yet.

The informations on the central charge and on the spectrum allow the computation of certain probabilities on the torus, such as the cluster wrapping probability [30–32], as well as the determination of different critical exponents or equivalently of the plane two-point functions. Using a Coulomb gas technique [33], the scaling limit $p_{12}(w_1, w_2)$ of $\mathcal{O}(w_1, w_2)$ is obtained as

$$p_{12}(w_1, w_2) = \lim_{\substack{N\to\infty\\ N/M=O(1)}} N^{4\Delta_{\left(0,\frac{1}{2}\right)}} \mathcal{O}(w_1, w_2), \tag{4.11}$$

and the plane limit

$$p_{12}(w_1, w_2) \xrightarrow{\frac{w_{12}}{N}\to 0} = \frac{c_0}{|w_1 - w_2|^{4\Delta_{\left(0,\frac{1}{2}\right)}}}, \tag{4.12}$$

is given by the two-point function of fields $V_{\left(0,\frac{1}{2}\right)}$, for this reason called the connectivity fields. This result implies also that the cluster fractal dimension is $2 - 2\Delta_{\left(0,\frac{1}{2}\right)}$. In (4.12), c_0 corresponds to the non-universal constant $c_0^{(2)}$ appearing in (2.7) and has been computed numerically in [13, 14, 18]. In [18], we set:

$$p_{12}(w_1, w_2) = c_0 \left\langle V_{\left(0,\frac{1}{2}\right)}(w_1) V_{\left(0,\frac{1}{2}\right)}(w_2) \right\rangle, \tag{4.13}$$

and we made the assumption that the connectivity fields entering the two-point function admit the following fusion

$$V_{\left(0,\frac{1}{2}\right)} \otimes V_{\left(0,\frac{1}{2}\right)} = V_{(1,1)^D} \oplus V_{(1,2)^D} \oplus V_{(1,3)^D} + \cdots \tag{4.14}$$

The representations in $\mathcal{S}^{D,\text{quot}}_{(1,\mathbb{N}^*)}$ have vanishing null-states, and this fixes their fusion rules [25]. For instance, for the field $(1,2)^D$ one has:

$$V_{(1,2)^D} \times V_{(r,s)} = V_{(r,s+1)} \oplus V_{(r,s-1)}. \tag{4.15}$$

J. Stat. Mech. (2020) 053106

Moreover, the structure constants $D^{(1,s)^D}_{(\Delta_1)(\Delta_2)}$ can be exactly computed and expressed in terms of Γ functions [25]. In [18] we showed that using (4.14), we obtained very good predictions for p_{12}. Following (4.11), we define the scaling limits:

$$p_{12\cdots n}(w_1, w_2, \ldots, w_n) = \lim_{\substack{N\to\infty \\ N/M=O(1)}} N^{2n\Delta_{\left(0,\frac{1}{2}\right)}} \mathcal{O}(w_1, w_2, \ldots, w_n). \tag{4.16}$$

The plane limits of p_{123} and p_{1234} have been at the center of an intense research activity in the last few years as they may directly probe the CFT structure constants. Let us consider the plane limit of p_{123} first. As explained in [34], if the plane p_{12} can be rewritten in terms of an equivalent local model [33], this is no more true for p_{123} which keeps its non-local nature. Despite this, an important progress was done in [8] where the plane limit of p_{123} was conjectured to be given by a CFT three-point correlator of fields $V_{\left(0,\frac{1}{2}\right)}$:

$$p_{123}(w_1, w_2, w_3) \xrightarrow{\frac{w_{12}}{N}\to 0} c_0^{(3)} \frac{D^{\left(0,\frac{1}{2}\right)}_{\left(0,\frac{1}{2}\right),\left(0,\frac{1}{2}\right)}}{|w_{12}w_{13}w_{24}|^{2\Delta_{\left(0,\frac{1}{2}\right)}}}. \tag{4.17}$$

The conjecture in [8] is even stronger, as it proposes a value for the structure constant:

$$D^{\left(0,\frac{1}{2}\right)}_{\left(0,\frac{1}{2}\right),\left(0,\frac{1}{2}\right)} = \sqrt{2} C^{\left(0,\frac{1}{2}\right)}_{\left(0,\frac{1}{2}\right),\left(0,\frac{1}{2}\right)}, \tag{4.18}$$

where the $C^{(\Delta_3)}_{(\Delta_1),(\Delta_2)}$ are the $c \leqslant 1$ Liouville structure constants [9–11, 15], defined in appendix B. The factor $\sqrt{2}$ in (4.17) originates from a two-fold multiplicity of the theory [8, 34]. Equation (4.17) has been numerically checked in [34–37]. Finally, the non-universal constant $c_0^{(3)}$ was verified, for a square lattice, to be strictly related to $c_0^{(2)}$ [36]:

$$c_0^{(3)} = (c_0^{(2)})^{\frac{3}{2}} = c_0^{\frac{3}{2}}. \tag{4.19}$$

The above result is consistent with the fact that one can associate a non-universal normalisation $c_0^{\frac{1}{2}}$ to each field $V_{\left(0,\frac{1}{2}\right)}$.In [17] the full space of $n = 4$ connectivities has been considered and the set of representations entering the corresponding s- channel, i.e. small z see (2.5), determined. For p_{1234} the result is:

$$\begin{aligned} p_{1234}(w_1, w_2, w_3, w_4) &\xrightarrow{\frac{w_{ij}}{N}\to 0} c_0^2 |w_{12}w_{34}|^{-4\Delta_{\left(0,\frac{1}{2}\right)}} P_0(z) \\ P_0(z) &= \sum_{\substack{(0,s) \\ s\in\frac{2\mathbb{N}+1}{2}}} \left(D^{(0,s)}_{\left(0\frac{1}{2}\right),\left(0,\frac{1}{2}\right)}\right)^2 |z|^{2\Delta_{(0,s)}} (1 + O(z,\bar{z})) \\ &+ \sum_{\substack{(r,s) \\ r\in 2\mathbb{Z}*, s\in\mathbb{Q}, rs\in 2\mathbb{Z}}} \left(D^{(r,s)}_{\left(0\frac{1}{2}\right),\left(0,\frac{1}{2}\right)}\right)^2 z^{\Delta_{(r,s)}} \bar{z}^{\Delta_{(r,-s)}} (1 + O(z,\bar{z})) \end{aligned} \tag{4.20}$$

J. Stat. Mech. (2020) 053106

In [13, 14] it has been shown that using—whenever they are well defined—the $c \leqslant 1$ Liouville structure constants provides an extremely good approximation to the plane $n = 4$ connectivities. The dominant terms for $P_0(z)$ are:

$$P_0(z) = 2\left(C^{\left(0,\frac{1}{2}\right)}_{\left(0,\frac{1}{2}\right)\left(0,\frac{1}{2}\right)}\right)^2 |z|^{2\Delta_{\left(0,\frac{1}{2}\right)}} (1 + O(z)) + \left(D^{(2,0)}_{\left(0,\frac{1}{2}\right),\left(0,\frac{1}{2}\right)}\right)^2 \times |z|^{2\Delta_{(2,0)}} (1 + O(z)) + 2\left(C^{\left(0,\frac{3}{2}\right)}_{\left(0,\frac{1}{2}\right),\left(0,\frac{1}{2}\right)}\right)^2 |z|^{2\Delta_{\left(0,\frac{3}{2}\right)}} (1 + O(z)) + \cdots \quad (4.21)$$

The value of $\left(D^{(2,0)}_{\left(0,\frac{1}{2}\right),\left(0,\frac{1}{2}\right)}\right)^2$ has been determined numerically in [14] when $Q = 1$.

5. The dominant torus corrections to p_{123} and p_{1234}

We present here the new results concerning the dominant torus correction of p_{123} and p_{1234}, defined in (4.16). Analogously to what we have done for p_{12} [18], see (4.13), we assume that

$$\begin{aligned} p_{123} &= c_0^{\frac{3}{2}} \left\langle V_{\left(0,\frac{1}{2}\right)}(w_1) V_{\left(0,\frac{1}{2}\right)}(w_2) V_{\left(0,\frac{1}{2}\right)}(w_3) \right\rangle \\ p_{1234} &= c_0^2 \left\langle V_{\left(0,\frac{1}{2}\right)}(w_1) V_{\left(0,\frac{1}{2}\right)}(w_2) V_{\left(0,\frac{1}{2}\right)}(w_3) V_{\left(0,\frac{1}{2}\right)}(w_4) \right\rangle, \end{aligned} \quad (5.1)$$

and we apply the CFT approach outlined in section 3 by using the fusions (4.14) and (4.15) and the following one:

$$V_{\left(0,\frac{1}{2}\right)} \otimes V_{\left(0,\frac{1}{2}\right)} = \bigoplus_{s \in \frac{2\mathbb{N}+1}{2}} V_{(0,s)} \bigoplus_{\substack{(r,s) \\ r \in 2\mathbb{Z}*, s \in \mathbb{Q}, rs \in 2\mathbb{Z}}} V_{(r,s)} \quad (5.2)$$

This fusion comes from (4.17) and (4.20). We will use the Liouville constants $C^{(0,2\mathbb{N}+1)}_{\left(0,\frac{1}{2}\right),\left(0,\frac{1}{2}\right)}$ for the connectivity sector. There are no predictions for the other structure constants. Luckily we will in general not need them as they produce sub-dominant diagrams for the values of Q, $1 \leqslant Q \leqslant 4$ considered here. The only exception is the channel $(2, 0)$ which produces a small but visible contribution at $Q = 1$. In this case we will use the value for $D^{(2,0)}_{\left(0,\frac{1}{2}\right),\left(0,\frac{1}{2}\right)}$ found numerically in [14]. The fusion (5.2) is not in principle contradictory with (4.14). Indeed, there may exist different fields $V_{\left(0,\frac{1}{2}\right)}$ with the same dimension but with different fusion rules. This fact can be well understood for $Q = 3$ where the primary fields carry a Z_3 charge. In this case there are two fields, $V^{\pm 1}_{\left(0,\frac{1}{2}\right)}$ with Z_3 charge ± 1. The fields $V^{+}_{\left(0,\frac{1}{2}\right)} V^{-}_{\left(0,\frac{1}{2}\right)} \to V_{(1,1)} \oplus V_{(1,2)} \cdots$ fuse into the Z_3 neutral sector, where one finds the identity $V_{(1,1)}$, while the two fields $V^{+}_{\left(0,\frac{1}{2}\right)} V^{+}_{\left(0,\frac{1}{2}\right)} \to V^{-}_{\left(0,\frac{1}{2}\right)} \oplus V^{-}_{\left(0,\frac{1}{2}\right)} \oplus \cdots$ fuse into the sector of charge -1. For general Q however, we do not fully understand how to characterise the primary fields $V_{\left(0,\frac{1}{2}\right)}$ to describe the space of connectivity (see also the

J. Stat. Mech. (2020) 053106

discussion in appendix C.3 of [14]). Analogously to the $n=2$ case [18], we find using (4.14), (4.15) and (5.2), that the dominant topological corrections to p_{123} and p_{1234} are associated to the energy one-point function $\left\langle V_{(1,2)^D}\right\rangle$. Comparing with (3.8) and (3.11) we have that $\Delta_{\min}=\Delta_{(1,2)^D}$. We stress the fact that the fusions (4.14) and (5.2) produce diagrams proportional to $\left\langle V_{\left(0,\frac{1}{2}\right)}\right\rangle$ and which would be dominant, as $\Delta_{\left(0,\frac{1}{2}\right)}<\Delta_{(1,2)}\,\forall Q$. However we conjecture that the one-point function of the connectivity field vanishes for any Q. If this is easy to show by symmetry argument for $Q=2,3,4$, we could not prove it for general Q. The agreement of our results with the Monte Carlo measurements supports this conjecture. The computation of the functions $f_\tau^{(3)}$ and $f_\tau^{(4)}$ in (2.8) and (2.9) is based on two approximations.

- We compute only the diagrams that contribute to the dominant torus correction, which is sufficient in general for comparison with the numerical data. The only exception are the diagrams proportional to $\left\langle V_{(1,3)^D}\right\rangle$ which produce a sub-dominant contribution that is visible numerically near $Q=3$. Higher $1/N$ corrections coming from descendant fields could in principle be computed but are expected to give very sub-dominant contributions.
- For any dominant diagram, we compute the contributions of the descendants at levels one and two. As explained in the next subsection, we expect the contribution of level three to be negligible.

5.1. Three-point connectivity p_{123}

Using the fusion (4.15), the only contributions of order $O\left(\left(\frac{w_{23}}{N}\right)^{2\Delta_{(1,2)}}\right)$ come from the fusion channels $V_{\left(0,\frac{1}{2}\right)}\times V_{\left(0,\frac{1}{2}\right)}\to V_{\left(0,\frac{1}{2}\right)}$ and $V_{\left(0,\frac{1}{2}\right)}\times V_{\left(0,\frac{1}{2}\right)}\to V_{\left(0,\frac{3}{2}\right)}$, represented respectively by figures 6(a) and (b).

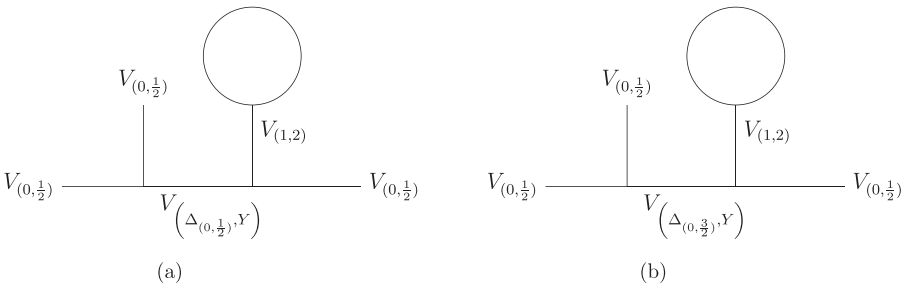

Figure 6. Diagrammatic representation of the two channels contributing to the topological corrections of the three-point connectivity.

As detailed in appendix C we can compute the coefficient $c^{(3)}_{(1,2)}\left(\frac{w_{12}}{w_{23}},\tau\right)$ defined as:

$$p_{123}=\frac{c_0^{\frac{3}{2}}}{\left|w_{12}w_{23}w_{13}\right|^{2\Delta_{\left(0,\frac{1}{2}\right)}}}\left[D+\left|\frac{w_{13}}{w_{12}}\right|^{2\Delta_{\left(0,\frac{1}{2}\right)}}c^{(3)}_{(1,2)}\left(\frac{w_{12}}{w_{23}},\tau\right)\left|\frac{w_{23}}{N}\right|^{2\Delta_{(1,2)}}+\text{subleading}\right]. \quad (5.3)$$

J. Stat. Mech. (2020) 053106

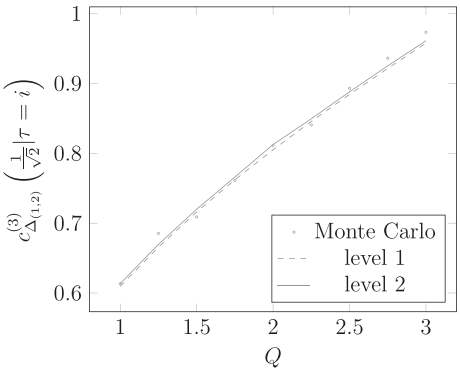

Q	$c^{(3)\,an}_{(1,2)}$	$c^{(3),MC}_{(1,2)}$
1	0.613397	0.613208
1.25	0.669589	0.685314
1.5	0.719907	0.708886
1.75	0.766007	0.761209
2	0.812445	0.811437
2.25	0.849444	0.840513
2.5	0.88805	0.892975
2.75	0.92519	0.93614
3	0.961232	0.973289

Figure 7. Comparison of the analytic $c^{(3)}_{(1,2)}$ with the corresponding numerical coefficient, for different values of Q, for the isosceles geometry. In the figure we compare the coefficients computed to order $\frac{w_{12}}{w_{23}}$ (dashed) and $\left(\frac{w_{12}}{w_{23}}\right)^2$ (solid).

In particular, to compare with the Monte Carlo numerical data we set $\tau = i$ (i.e. $M = N$), and we fix the three points w_1, w_2, w_3 at the vertices of isosceles triangles. First we consider the configuration $(w_1, w_2, w_3) = (0, r, ir)$, also considered in [36] and compute the coefficient $c^{(3),\mathrm{an}}_{(1,2)} = c^{(3)}_{(1,2)}\left(\frac{1}{\sqrt{2}}, \tau = i\right)$ at level 2, see equation (C.7) in the appendix. The comparison with the Monte Carlo results $c^{(3),\mathrm{MC}}_{(1,2)}$, for different values of Q, is given in figure 7. In the figure we show the convergence of our expansion, computed to order $\frac{w_{12}}{w_{23}}$ ie to level one (dashed) and $\left(\frac{w_{12}}{w_{23}}\right)^2$ i.e. to level two (solid). The contribution of order $\left(\frac{w_{12}}{w_{23}}\right)^3$ is expected to be negligible, below the precision of the numerical measurements.

We test also the CFT predictions for triangles of different shapes. We took new Monte Carlo measurements by setting the points at: $(w_1, w_2, w_3) = ((k-i)r, (k+i)r, 0)$. We refer the reader to [13, 14, 36] for the details on the measurement of the three-point correlations. We compute the coefficient $c^{(3),\mathrm{an}}_{(1,2)} = c^{(3)}_{(1,2)}\left(\frac{2}{\sqrt{k^2+1}}, \tau = i\right)$ which now depends on k. The comparison with the Monte Carlo measurements, taken at $Q = 1$ and for different values of k is shown in figure 8(a). For large k we expect our $\frac{w_{12}}{w_{23}}$ expansion to converge better, however the numerical measurements get less precise for large k, which explains the deviation between analytical and numerical points in figure 8(a). Still, the agreement is good.

In figure 8(b), we plotted the ratio

$$R(w_1, w_2, w_3) = \frac{p_{123}(w_1, w_2, w_3)}{\sqrt{p_{12}(w_1, w_2)p_{23}(w_2, w_3)p_{13}(w_1, w_3)}} \tag{5.4}$$

at $Q = 1$. This ratio was considered in [8, 37]. Using our expression (5.3) for p_{123} and the result in [18] for p_{12},

J. Stat. Mech. (2020) 053106

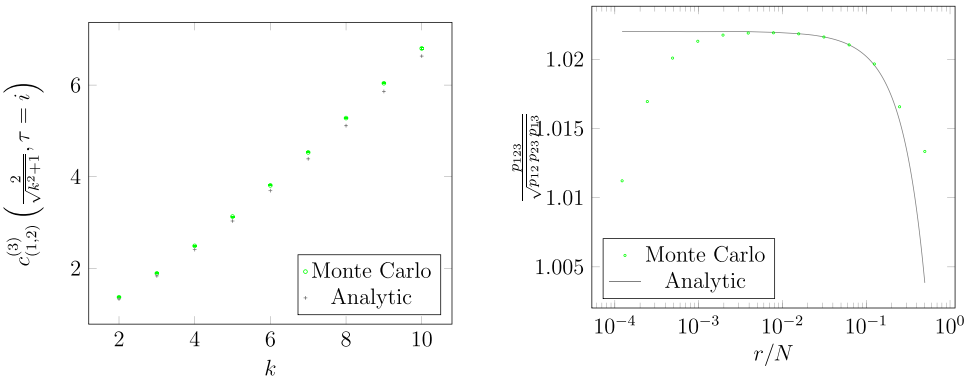

Figure 8. (a)Comparison of the analytic $c^{(3)}_{(1,2)}$ with the corresponding numerical coefficient, for different values of the geometric parameter k. (b) Comparison of the ratio (5.5) with the Monte Carlo data. At short distances the numerical point deviate significantly since this regime is not captured by the CFT description.

$$R = \frac{D^{\left(0,\frac{1}{2}\right)}_{\left(0,\frac{1}{2}\right),\left(0,\frac{1}{2}\right)}\left(1 + c^{(3)}_{1,2}\left|\frac{w_{23}}{N}\right|^{2\Delta_{(1,2)}} + \cdots\right)}{\prod_{i<j}\left(1 + c^{(2)}_{1,2}\left|\frac{w_{ij}}{N}\right|^{2\Delta_{(1,2)}} + \cdots\right)^{\frac{1}{2}}}$$
$$= D^{\left(0,\frac{1}{2}\right)}_{\left(0,\frac{1}{2}\right),\left(0,\frac{1}{2}\right)}\left[1 + \left(\left|\frac{w_{23}}{r}\right|^{2\Delta_{(1,2)}} c^{(3)}_{1,2} - \frac{1}{2}c^{(2)}_{1,2}\sum_{i<j}\left|\frac{w_{ij}}{r}\right|^{2\Delta_{(1,2)}}\right) \times \left(\frac{r}{N}\right)^{2\Delta_{(1,2)}} + \cdots\right]. \tag{5.5}$$

In particular in [37] the quantity $\ln\left(D^{\left(0,\frac{1}{2}\right)}_{\left(0,\frac{1}{2}\right),\left(0,\frac{1}{2}\right)} - R\right)$ was studied numerically for percolation, as a function of the log of the distance between the points. From (5.5), the behavior is,

$$\ln\left(D^{\left(0,\frac{1}{2}\right)}_{\left(0,\frac{1}{2}\right),\left(0,\frac{1}{2}\right)} - R\right) = \ln\left[\frac{D^{\left(0,\frac{1}{2}\right)}_{\left(0,\frac{1}{2}\right),\left(0,\frac{1}{2}\right)}\left(\frac{1}{2}c^{(2)}_{1,2}\sum_{i<j}\left|\frac{w_{ij}}{r}\right|^{2\Delta_{(1,2)}} - \left|\frac{w_{23}}{r}\right|^{2\Delta_{(1,2)}} c^{(3)}_{1,2}\right)}{N^{2\Delta_{(1,2)}}}\right]$$
$$+ 2\Delta_{(1,2)}\,\ln r. \tag{5.6}$$

Then for any configuration of points the slope equals $2\Delta_{(1,2)} = 1.25$ for percolation. With the points at the vertices of an equilateral triangle, this slope was measured in [37] to be ~ 1.3 in the regime where the distance between points is large, which is in fair agreement with our prediction. Note that for equilateral as well as isosceles triangles parametrised with k, the coefficient $\left(\left|\frac{w_{23}}{r}\right|^{2\Delta_{(1,2)}} c^{(3)}_{1,2} - \frac{1}{2}c^{(2)}_{1,2}\sum_{i<j}\left|\frac{w_{ij}}{r}\right|^{2\Delta_{(1,2)}}\right)$ is negative, resulting in a decrease of the ratio R when r approaches $N/2$.

J. Stat. Mech. (2020) 053106

5.2. Four-point connectivity p_{1234}

According to the s- channel fusion for $p_{1234}(w_1, w_2, w_3, w_4)$, see [14, 17], the main topological corrections are of order $O\left(\left(\frac{w_{24}}{N}\right)^{2\Delta_{(1,2)}}\right)$. We define the associated coefficient $c^{(4)}_{(1,2)}\left(\frac{w_{12}}{w_{24}}, \frac{w_{34}}{w_{24}}, \tau\right)$ as:

$$p_{1234} = \frac{c_0^2}{|w_{12}w_{34}|^{4\Delta_{\left(0,\frac{1}{2}\right)}}}\left[P_0(z) + c^{(4)}_{(1,2)}\left(\frac{w_{12}}{w_{24}}, \frac{w_{34}}{w_{24}}, \tau\right)\left(\frac{w_{24}}{N}\right)^{2\Delta_{(1,2)}} + \text{subleading}\right], \tag{5.7}$$

We compute the dominant contributions to the coefficient $c^{(4)}_{(1,2)}$ which, for all values of Q, come from the terms associated to figures 9 and 10. Each contribution is of order $z^{\Delta_L+\Delta_R}$.

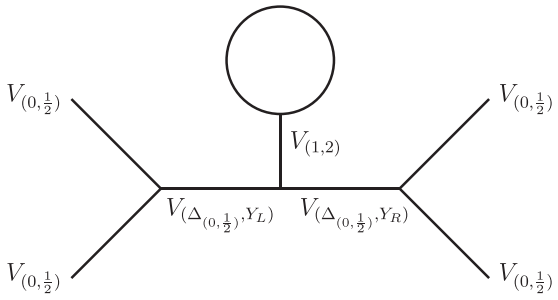

Figure 9. Diagrammatic representation of the leading contribution to the topological corrections of the four-point connectivity.

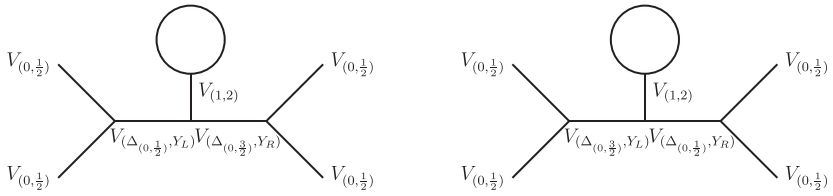

Figure 10. Diagrammatic representation of the sub-leading contribution to the topological corrections of the four-point connectivity.

The next contribution would come from figure 11, for which the structure constants are unknown. However this contribution would be of order[3] $z^{\Delta_{(2,0)}+\Delta_{(2,1)}+1}$, which is very sub-dominant.

[3] $V_{(2,1)}$ is not a diagonal field (see appendix D).

J. Stat. Mech. (2020) 053106

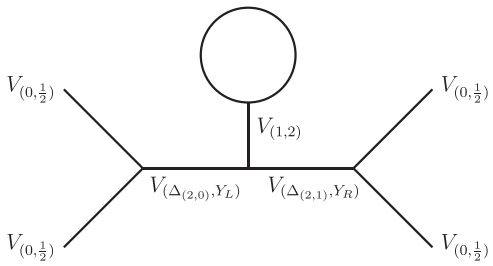

Figure 11. Diagrammatic representation of the next to sub-leading contribution to the topological corrections of the four-point connectivity. This contribution is not visible numerically.

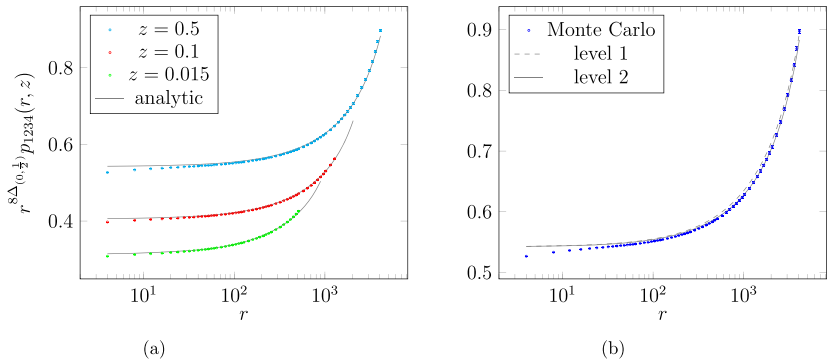

Figure 12. Numerical and analytic rescaled four-point connectivity at $Q = 2.75$, for different values of the cross-ratio z (a) and for $z = 0.5$ (b) where we show the convergence of the level expansion.

To compare our expansion of (5.7) with the numerical simulations we take again $\tau = i$ and we fix the four points w_1, w_2, w_3, w_4 at the vertices of a rectangle, i.e. $(w_1, w_2, w_3, w_4) = (ir, 0, \lambda r, (\lambda + i)r)$. The cross ratio is

$$z = \frac{w_{12}w_{34}}{w_{13}w_{24}} = \frac{1}{\lambda^2 + 1}.$$

In figure 12(a) we plot the function $r^{8\Delta_{(0,\frac{1}{2})}} p_{1234}(r, z)$ at $Q = 2.75$ and for different values of the cross-ratio z. For $z = 0.5$, we show in figure 12(b) the convergence of the level expansion (see appendix D). Taking $\lambda \geqslant 5$ ensures that we can truncate the expansion at level 2 and still obtain good agreement with the numerical data. In the following we will take $\lambda = 5$ corresponding to $z = 0.038\,4615$.

In figure 13(a), we compute the connectivity including the contributions of the dominant figure 9 and first sub-dominant figure 10 in $c^{(4)}_{(1,2)}$. Note that the value $Q = 2.75$ chosen for these plots is arbitrary.

J. Stat. Mech. (2020) 053106

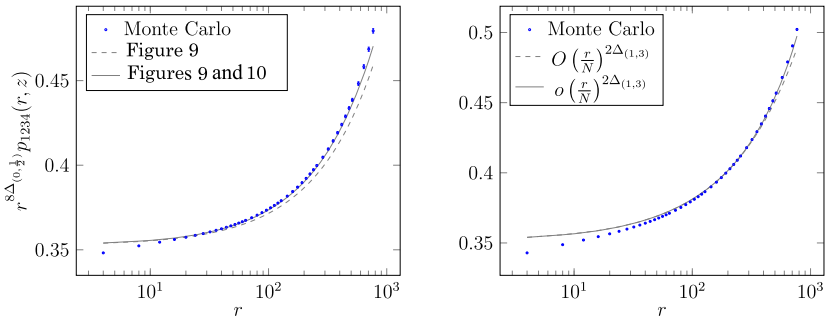

(a) $Q = 2.75$ (b) $Q = 3.25$

Figure 13. Numerical and analytic rescaled four-point connectivity. In (a) we show the convergence of the diagrammatic expansion of $c^{(4)}_{(1,2)}$. In (b) we show the effect of the contribution of the sub-dominant field $V_{(1,3)}$ when Q is close to 3.

5.2.1. $Q > 2$. When $Q > 2$ the topological correction coming from the field $V_{(1,3)^D}$, while being still sub dominant, produces a visible effect. We illustrate this for $Q = 3.25$ on figure 13(b), where the term $c^{(4)}_{(1,3)}\left(\frac{w_{12}}{w_{24}}, \frac{w_{34}}{w_{24}}, \tau\right)\left(\frac{w_{24}}{N}\right)^{2\Delta_{(1,3)}}$ is included (solid line) or not (dashed line) in the expansion of the connectivity.

5.2.2. $Q = 2$. As explained in appendices B and D, some structure constants entering the computation of both the plane limit and the first topological correction diverge at $Q = 2$. In particular the contribution of the $\left(0, \frac{3}{2}\right)$ channel to the plane limit is divergent. As explained in sections 2.2 and 3.3 of [14], for rational central charge the diverging contributions of channels with the same dimension (here $\left(0, \frac{3}{2}\right)$ and $(2, 0)$) cancel each other in (4.20) to give a finite limit.

However, as detailed in appendix D.1 the contribution of the same channel $\left(0, \frac{3}{2}\right)$ to the topological correction (figure 10) has a finite limit. Below we show the connectivity computed including (solid) or not (dashed) this contribution in $c^{(4)}_{(1,2)}$. The comparison with the numerical data seems to indicate that this channel must be included in the topological corrections (figure 14(a)).

5.2.3. $Q < 2$. In this section we will only consider the case $Q = 1$. For other values of Q the computation of the connectivity is similar to what we showed before. Note however that for $1 \leqslant Q \leqslant 2$, considering that $2\Delta_{(2,0)} < 2\Delta_{\left(0,\frac{3}{2}\right)}$ the contribution of $(2, 0)$ to the plane limit (4.21) is dominant over $\left(0, \frac{3}{2}\right)$. This contribution cannot be computed using our approach since the structure constant $D^{(2,0)}_{\left(0,\frac{1}{2}\right),\left(0,\frac{1}{2}\right)}$ is unknown for arbitrary Q. Nonetheless, the contribution of this field is very small ($\sim 5.10^{-5}$ at $Q = 1$) and simply neglecting it gives a good agreement with the numerical data, for all $Q \in [1, 4]$. We plot in figure 14 the connectivity at $Q = 1$, whose expression involves non-trivial limits of the structure constants, detailed in appendices B and D. We include the contribution of $V_{(2,0)}$ in the plane four-point function (4.21) using the structure constant computed numerically in [14], though this contribution is very small.

J. Stat. Mech. (2020) 053106

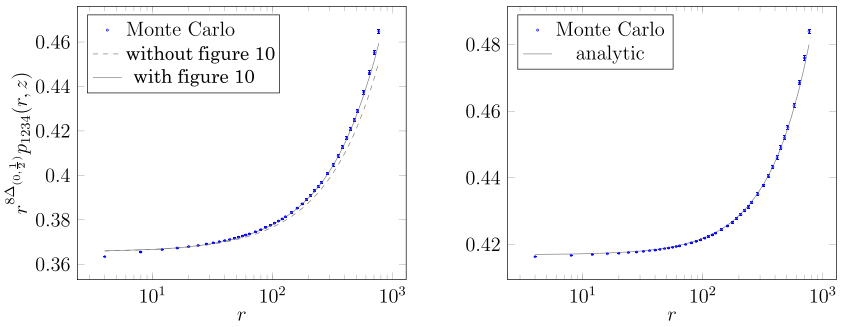

(a) $Q = 2$ (b) $Q = 1$

Figure 14. Numerical and analytic rescaled four-point connectivity in the special limits $Q = 2$ and $Q = 1$. In (a) we show that one must include the finite $Q \to 2$ limit of the contribution of the $\left(0, \frac{3}{2}\right)$ channel. In (b) the expression involves the non-trivial $Q \to 1$ limits of the structure constants, and include the contribution of $V_{(2,0)}$ in the plane four-point function.

6. Conclusions

In this paper we completed the work initiated in [18] where the two-point connectivity of critical Potts clusters living on a torus had been considered. We focused on the three-point and four-point connectivities p_{123} and p_{1234} defined in (4.11). Motivated by the understanding of the CFT which describes the critical Potts clusters, the study of these higher-point connectivities is particularly interesting as it probes more fusion rules than the two-point connectivity. Moreover, contrary to the two-point connectivity, the three- and four-point connectivities cannot be written in terms of local correlation functions. In the CFT approach, explained in section 3, we used the informations coming from the works [14, 17]. In particular we used the fusion rules (4.14), (4.15) and (5.2) and the $c \leqslant 1$ Liouville structure constants. We computed the dominant figures 6(a) and (b) for p_{123} and figures 9–11 for p_{1234}. A very satisfying agreement with the corresponding Monte Carlo measurements was found.

We showed that the leading topological corrections for p_{123} and p_{1234} are expected to scale with the size as N^{-x}, where $x = 2\Delta_{(1,2)^D}$, i.e. with an exponent which is the energy scaling dimension. Note that we worked with square tori, for which the correction coming from the stress-energy tensor vanishes. For non-square tori, depending on the aspect ratio M/N this latter contribution can become dominant [18].

The results presented here further support the fact that the use of $c \leqslant 1$ Liouville-type constants provides a very good description of Potts clusters, even when they live on a non-trivial topology. For $Q = 1$ (percolation) and $Q = 2$ (Ising) we showed in sections 5.2.2, 5.2.3 and in appendices C and D subtle cancellations of the singularities appearing in the Liouville constants. More generally, although the CFT approach uses correlations of local fields, it remains valid for describing these geometrical objects.

We stress the fact that, although our results are based on functions (the Liouville-type constants in this case) which are very singular in Q, they turn out to have a

J. Stat. Mech. (2020) 053106

smooth dependence on Q as required by statistical physics applications, due to the aforementioned cancellations. An interesting open question is studying more systematically these fine-tuned cancellations. In particular, one can expect these cancellations to be put in relation, in the spirit of [38], with the logarithmic features arising from the study of the integrable structures of the lattice model. Finally, the universal results we obtained for pure percolation can be used for testing models that are conjectured to be in the same universality class, such as, for instance, the long-range percolation appearing in the study of quantum chaos [39].

Acknowledgments

We thank Sylvain Ribault and Vladimir Dotsenko for discussion, as well as Yacine Ikhlef, Benoit Estienne and Jesper Jacobsen. R S thanks the International Institute of Physics of Natal for its hospitality during the period where this work was completed.

Appendix A. CFT definitions and notations

A.1. Kinematic data

We first recall that for a CFT on a plane $z \in (\mathbb{C} \bigcup \{\infty\})$ [25] with $T(z)$ and $\bar{T}(\bar{z})$ the holomorphic and anti-holomorphic component of the stress energy-tensor, the holomorphic stress-energy modes L_n form the Virasoro algebra $\mathcal{V}_c$ with central charge c:

$$[L_n, L_m] = (n-m)L_{n+m} + \frac{c}{12} n(n^2-1)\delta_{n,m}. \tag{A.1}$$

The anti-holomorphic modes $\bar{L}_n$ are analogously defined and form a second Virasoro algebra $\overline{\mathcal{V}}_c$, with the same central charge, that commutes with (A.1). A highest-weight representation of $\mathcal{V}_c$ is labeled by the conformal dimension Δ: it contains the primary field V_Δ, $L_n|V_\Delta\rangle = 0$ for $n > 0$, and its descendants, obtained by acting with the negative modes on the primary state. Given a Young diagram $Y = \{n_1, n_2 \cdots\}$, with $n_i \in \mathbb{N}, n_i \leqslant n_{i+1}$, the fields

$$V_\Delta^{(Y)} = L_{-Y} V_\Delta = L_{-n_1} L_{-n_2} \cdots V_\Delta (V_\Delta^{(\{0\})} = V_\Delta) \tag{A.2}$$

form a complete basis of the Δ representation. The descendant $V_\Delta^{(Y)}$ has total dimension $\Delta + |Y|$, where $|Y| = \sum n_i$ is called the level of the descendant. For general Δ, the number of independent descendants is therefore the number of partitions of $|Y|$. The inner product $H_\Delta(Y, Y')$ between descendants is defined as:

$$H_\Delta(Y, Y') = \lim_{z\to\infty} z^{2\Delta} \langle V_\Delta(z) L_Y L_{-Y'} V_\Delta(0) \rangle , \tag{A.3}$$

and is completely determined by the algebra (A.1). The spectrum $\mathcal{S}$ of a CFT is formed by the representations of $\mathcal{V}_c \otimes \overline{\mathcal{V}}_c$ appearing in the theory and labeled by the

J. Stat. Mech. (2020) 053106

holomorphic and anti-holomorphic dimensions $\Delta, \bar{\Delta}$. In order to simplify the formulas, we use the notations $(\Delta_i) = \Delta_i, \bar{\Delta}_i$ and $(\Delta_i, Y_i) = (\Delta_i, Y_i), (\bar{\Delta}_i, \bar{Y}_i)$. The s- channel expansion of the four-point conformal block is also completely determined by the algebra (A.1):

$$\mathcal{F}_{\Delta}^{(s)}(\Delta_i|z) = z^{\Delta}\left(1 + \frac{(\Delta+\Delta_1-\Delta_2)(\Delta+\Delta_4-\Delta_3)}{2\Delta}z + O(z^2)\right) \tag{A.4}$$

A.2. Dynamic data

The product of two fields (OPE) can be expanded in terms of the states appearing in the spectrum $\mathcal{S}$ [25]:

$$V_{(\Delta_1,Y_1)}(z,\bar{z})V_{(\Delta_2,Y_2)}(0) \to z^{-\Delta_1-|Y_1|-\Delta_2-|Y_2|+\Delta_3+|Y_3|} D^{(\Delta_3,Y_3)}_{(\Delta_1,Y_1),(\Delta_2,Y_2)} V_{(\Delta_3,Y_3)}(0), \tag{A.5}$$

where the coefficients are factorised as:

$$D^{(\Delta_3,Y_3)}_{(\Delta_1,Y_1),(\Delta_2,Y_2)} = D^{(\Delta_3)}_{(\Delta_1),(\Delta_2)} \beta^{(\Delta_3,Y)}_{(\Delta_1,Y_1),(\Delta_2,Y_2)} \beta^{(\bar{\Delta}_3,\bar{Y}_3)}_{(\bar{\Delta}_1,\bar{Y}_1),(\bar{\Delta}_2,\bar{Y}_2)}. \tag{A.6}$$

One factor is fixed by the algebra (A.1):

$$\beta^{(\Delta_3,Y_3)}_{(\Delta_1,Y_1),(\Delta_2,Y_2)} = \sum_{Y,|Y|=|Y_3|} H^{-1}_{\Delta_3}(Y,Y_3)\, \Gamma^{(\Delta_3,Y)}_{(\Delta_2,Y_2),(\Delta_1,Y_1))}, \tag{A.7}$$

where the Virasoro matrix elements $\Gamma^{(\Delta_3,Y)}_{(\Delta_2,Y_2),(\Delta_1,Y_1)}$ relate three states (i.e. are associated to the knots of the conformal block diagrams) and are completely determined by the commutation relation (A.1). They can be computed using the recursion relations in [29]. The other factor is the (model dependent) structure constant $D^{(\Delta_3)}_{(\Delta_1),(\Delta_2)}$. These constants can be defined as:

$$D^{(\Delta_3)}_{(\Delta_1),(\Delta_2)} = \left\langle V_{(\Delta_1)}(\infty)V_{(\Delta_2)}(1)V_{(\Delta_2)}(0)\right\rangle_{\text{Plane}}, \tag{A.8}$$

where $\langle\cdots\rangle_{\text{Plane}}$ is the CFT correlator on the infinite plane. The three-point functions determine the fusions between the different representations appearing in the spectrum. Note that, as also recently pointed out in [40], a more solid definition of structure constants is based on the four-point function. There can be indeed subtleties as the ones discussed in section 5.3 of [38]. In the case under consideration here, we can safely define the structure constants as in (A.8).

A.3. One- and two- point functions on the torus

We recall here the topological expansion of the two-point function of primary or descendant (spin-less) fields:

J. Stat. Mech. (2020) 053106

$$\begin{aligned}
&\frac{\langle V_{(\Delta_1,Y_1)}(w_1)V_{(\Delta_2,Y_2)}(w_2)\rangle}{|w_{12}|^{-2\Delta_1-2\Delta_2}w_{12}^{-|Y_1|-|Y_2|}\bar{w}_{12}^{-|\bar{Y}_1|-|\bar{Y}_2|}}\\
&\quad=\sum_{(\Delta_{\rm top},Y)}D^{(\Delta_{\rm top},Y)}_{(\Delta_1,Y_1),(\Delta_2,Y_2)}\left(\frac{w_{12}}{N}\right)^{\Delta_{\rm top}+|Y|}\left(\frac{\bar{w}_{12}}{N}\right)^{\bar{\Delta}_{\rm top}+|\bar{Y}|}\langle V_{(\Delta_{\rm top},Y)}\rangle_{(N=1)}\\
&\quad=\sum_{(\Delta_{\rm top})}D^{(\Delta_{\rm top})}_{(\Delta_1),(\Delta_2)}\left(\frac{w_{12}}{N}\right)^{\Delta_{\rm top}}\left(\frac{\bar{w}_{12}}{N}\right)^{\bar{\Delta}_{\rm top}}\Big[\beta^{(\Delta_{\rm top})}_{(\Delta_1,Y_1),(\Delta_2,Y_2)}\beta^{(\bar{\Delta}_{\rm top})}_{(\Delta_1,\bar{Y}_1),(\Delta_2,\bar{Y}_2)}\langle V_{(\Delta_{\rm top})}\rangle_{(N=1)}\\
&\qquad+\beta^{(\Delta_{\rm top},-1)}_{(\Delta_1,Y_1),(\Delta_2,Y_2)}\beta^{(\bar{\Delta}_{\rm top})}_{(\Delta_1,\bar{Y}_1),(\Delta_2,\bar{Y}_2)}\langle L_{-1}V_{(\Delta_{\rm top})}\rangle_{(N=1)}\frac{w_{12}}{N}\\
&\qquad+\beta^{(\Delta_{\rm top})}_{(\Delta_1,Y_1),(\Delta_2,Y_2)}\beta^{(\bar{\Delta}_{\rm top},-1)}_{(\Delta_1,\bar{Y}_1),(\Delta_2,\bar{Y}_2)}\langle \bar{L}_{-1}V_{(\Delta_{\rm top})}\rangle_{(N=1)}\frac{\bar{w}_{12}}{N}+O\left(\frac{w_{12}}{N}\frac{\bar{w}_{12}}{N}\right)\Big].
\end{aligned}\tag{A.9}$$

The torus one-point function can be expanded in the elliptic nome q as [26]:

$$\begin{aligned}
\langle V_{(\Delta,Y)}\rangle_{N=1}&=\frac{(2\pi)^{\Delta+|Y|+\bar{\Delta}+|\bar{Y}|}}{Z}\sum_{(\Delta',Y')}D^{(\Delta',Y')}_{(\Delta,Y),(\Delta',Y')}q^{\Delta'-c/24+|Y'|}\bar{q}^{\bar{\Delta}'-c/24+|\bar{Y}'|}\\
&=\frac{(2\pi)^{\Delta+|Y|+\bar{\Delta}+|\bar{Y}|}}{Z}\sum_{(\Delta')}D^{(\Delta')}_{(\Delta),(\Delta')}q^{\Delta'-c/24}\bar{q}^{\bar{\Delta}'-c/24}\Big|1+\beta^{(\Delta',-1)}_{(\Delta,Y),(\Delta',-1)}\,q\\
&\quad+\left(\beta^{(\Delta',\{-1,-1\})}_{(\Delta,Y),(\Delta',\{-1,-1\})}+\beta^{(\Delta',-2)}_{(\Delta,Y),(\Delta',-2)}\right)q^2+\cdots\Big|^2.
\end{aligned}\tag{A.10}$$

Appendix B. $c\leqslant 1$ Liouville structure constants

The Liouville structure constants are the unique solutions of certain bootstrap equations for central charge $c\leqslant 1$ [15]. The structure constant of fields with dimensions $\Delta_1,\Delta_2,\Delta_3$ is given by [9–11]:

$$C^{(\Delta_3)}_{(\Delta_1),(\Delta_2)}=-A(\beta)\frac{\Upsilon_\beta(\alpha_1+\alpha_2+\alpha_3+2\beta-1/\beta)\prod_{\sigma\in\mathcal{S}_3}\Upsilon_\beta(\alpha_{\sigma(1)}+\alpha_{\sigma(2)}-\alpha_{\sigma(3)}+\beta)}{\sqrt{\prod_{j=1}^3\Upsilon_\beta(2\alpha_j+\beta)\Upsilon_\beta(2\alpha_j+2\beta-1/\beta)}}\tag{B.1}$$

where the charges α are related to the dimensions Δ by $\Delta=\mathrm{i}\alpha\left(\frac{c-1}{24}-\mathrm{i}\alpha\right)$, and,

$$A(\beta)=\frac{\beta^{\beta^{-2}-\beta^2-1}}{\Upsilon_\beta(\beta)}\sqrt{\gamma(\beta^2)\gamma(\beta^{-2}-1)},\quad \gamma(x)=\frac{\Gamma(x)}{\Gamma(1-x)}.\tag{B.2}$$

The special function Υ_β obeys the shift equations,

$$\Upsilon_\beta(x+\beta)=\Upsilon_\beta(x)\beta^{1-2\beta x}\,\gamma(\beta x)\tag{B.3a}$$

$$\Upsilon_\beta\left(x+\frac{1}{\beta}\right)=\Upsilon_\beta(x)\beta^{2\frac{x}{\beta}-1}\gamma\left(\frac{x}{\beta}\right)\tag{B.3b}$$

J. Stat. Mech. (2020) 053106

$$\Upsilon_\beta\left(\beta+\frac{1}{\beta}-x\right)=\Upsilon_\beta(x). \tag{B.3c}$$

Υ_β has simple zeroes for $x\in\left(-\beta\mathbb{N}-\frac{1}{\beta}\mathbb{N}\right)\cup\left(\beta\mathbb{N}_*+\frac{1}{\beta}\mathbb{N}_*\right)$. When one of the fields is degenerate, (B.1) can be written in terms of gamma functions. Some constants entering the computation of the connectivities of the Q-Potts model become singular for special values of Q:

$$\begin{aligned}C^{(1,2)^D}_{(0,\frac{1}{2}),(0,\frac{1}{2})}&=-4\beta^4\frac{\Gamma\left(1+\frac{1}{2}\beta^{-2}\right)}{\Gamma\left(-\frac{1}{2}\beta^{-2}\right)}\sqrt{\frac{2^{3-4\beta^{-2}}\Gamma\left(\frac{3}{2}-\beta^{-2}\right)}{\Gamma\left(-\frac{1}{2}+\beta^{-2}\right)}}\\&=\frac{4}{9}\frac{\Gamma\left(\frac{7}{4}\right)}{\Gamma\left(\frac{1}{4}\right)}\sqrt{\frac{\pi\sqrt{3}}{Q-1}},\quad Q\to 1\end{aligned} \tag{B.4a}$$

$$\begin{aligned}C^{(1,2)^D}_{(0,\frac{1}{2}),(0,\frac{3}{2})}&=\beta^2\left[-\frac{\Gamma(2-2\beta^{-2})\Gamma\left(-\frac{1}{2}\beta^{-2}\right)\Gamma(\beta^{-2})\Gamma\left(\frac{3}{2}\beta^{-2}\right)}{\Gamma\left(1-\frac{3}{2}\beta^{-2}\right)\Gamma\left(1+\frac{1}{2}\beta^{-2}\right)\Gamma(-1+2\beta^{-2})\Gamma(-\beta^{-2})}\right]^{1/2}\\&=-\frac{1}{3}\sqrt{\frac{\pi\sqrt{3}}{Q-1}\frac{\Gamma\left(-\frac{3}{4}\right)\Gamma\left(\frac{9}{4}\right)}{\Gamma\left(-\frac{5}{4}\right)\Gamma\left(\frac{7}{4}\right)}},\quad Q\to 1\\&\propto 1/\sqrt{\Gamma\left(1-\frac{3}{2}\beta^{-2}\right)}\sim\sqrt{Q-2},\quad Q\to 2\end{aligned} \tag{B.4b}$$

$$C^{(0,\frac{3}{2})}_{(0,\frac{1}{2}),(0,\frac{1}{2})}\propto\sqrt{\Gamma\left(1-\frac{3}{2}\beta^{-2}\right)}\sim\frac{1}{\sqrt{Q-2}}. \tag{B.4c}$$

Appendix C. Derivation of the three-point corrections

We write the s-channel expansion of the three-point function $\langle V_{(\Delta_1)}(w_1)V_{(\Delta_2)}(w_2)V_{(\Delta_3)}(w_3)\rangle$ of spin-less fields[4] by inserting the OPE $V_{(\Delta_1)}(w_1)V_{(\Delta_2)}(w_2)$:

$$\frac{\langle V_{(\Delta_1)}(w_1)V_{(\Delta_2)}(w_2)V_{(\Delta_3)}(w_3)\rangle}{|w_{12}|^{-2\Delta_1-2\Delta_2}}=\sum_{\substack{(\Delta_{\rm L})\in\mathcal{S}\\(Y_{\rm L})}}D^{(\Delta_{\rm L},Y_{\rm L})}_{(\Delta_1),(\Delta_2)}w_{12}^{\Delta_{\rm L}+|Y_{\rm L}|}\bar{w}_{12}^{\bar{\Delta}_{\rm L}+|\bar{Y}_{\rm L}|}\left\langle V_{(\Delta_{\rm L},Y_{\rm L})}(w_2)V_{(\Delta_3)}(w_3)\right\rangle. \tag{C.1}$$

The plane limit is given by the term $\Delta_{\rm L}=\Delta_3$ corresponding to figures C.1(a) while the topological corrections are associated to figures C.1(b).

[4] For simplicity of notation we derive the result for spin-less fields; it is straightforward to extend it to fields with spin.

J. Stat. Mech. (2020) 053106

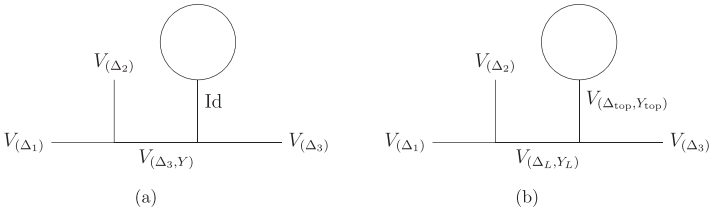

Figure C.1. Diagrammatic representation of the plane limit (a) and the topological corrections (b) of the torus three-point function.

Accordingly we write (C.1) as,

$$\frac{\langle V_{(\Delta_1)}(w_1)V_{(\Delta_2)}(w_2)V_{(\Delta_3)}(w_3)\rangle}{|w_{12}|^{-2\Delta_1-2\Delta_2}|w_{23}|^{2\Delta_3}} = \left|\frac{w_{12}}{w_{23}}\right|^{2\Delta_3}\sum_{(Y)} D^{(\Delta_3,Y)}_{(\Delta_1),(\Delta_2)} D^{\rm Id}_{(\Delta_3,Y),(\Delta_3)}\left(\frac{w_{12}}{w_{23}}\right)^{|Y|}\left(\frac{\bar w_{12}}{\bar w_{23}}\right)^{|\bar Y|}$$
$$+ \sum_{\substack{(\Delta_{\rm L},Y_{\rm L})\\(\Delta_{\rm top},Y_{\rm top})}} D^{(\Delta_{\rm L},Y_{\rm L})}_{(\Delta_1),(\Delta_2)} D^{(\Delta_{\rm top},Y_{\rm top})}_{(\Delta_{\rm L},Y_{\rm L}),(\Delta_3)}\left(\frac{w_{12}}{w_{23}}\right)^{\Delta_{\rm L}+|Y_{\rm L}|}\left(\frac{\bar w_{12}}{\bar w_{23}}\right)^{\bar\Delta_{\rm L}+|\bar Y_{\rm L}|}$$
$$\times \left(\frac{w_{23}}{N}\right)^{\Delta_{\rm top}+|Y_{\rm top}|}\left(\frac{\bar w_{23}}{N}\right)^{\bar\Delta_{\rm top}+|\bar Y_{\rm top}|}\left\langle V_{(\Delta_{\rm top},Y_{\rm top})}\right\rangle_{N=1}. \qquad \text{(C.2)}$$

Let us detail how to recover the plane limit from the first sum. We compute,

$$\sum_Y \beta^{(\Delta_3,Y)}_{\Delta_1,\Delta_2}\beta^{(\Delta_3,\bar Y)}_{\Delta_1,\Delta_2}\beta^{\rm Id}_{(\Delta_3,Y),\Delta_3}\beta^{\rm Id}_{(\Delta_3,\bar Y),\Delta_3}\left(\frac{w_{12}}{w_{23}}\right)^{|Y|}\left(\frac{\bar w_{12}}{\bar w_{23}}\right)^{|\bar Y|}$$
$$= \left|1+\beta^{(\Delta_3,-1)}_{\Delta_1,\Delta_2}\beta^{\rm Id}_{(\Delta_3,-1),\Delta_3}\frac{w_{12}}{w_{23}} + \left(\beta^{(\Delta_3,\{-1,-1\})}_{\Delta_1,\Delta_2}\beta^{\rm Id}_{(\Delta_3,\{-1,-1\}),\Delta_3}\right.\right.$$
$$\left.\left. + \beta^{(\Delta_3,-2)}_{\Delta_1,\Delta_2}\beta^{\rm Id}_{(\Delta_3,-2),\Delta_3}\right)\frac{w_{12}^2}{w_{23}^2}+\cdots\right|^2. \qquad \text{(C.3)}$$

Computing the coefficients using (A.7) and the relations in [29] we find

$$\left|1-(\Delta_1-\Delta_2+\Delta_3)\frac{w_{12}}{w_{23}}+\frac{1}{2}(\Delta_1-\Delta_2+\Delta_3)(1+\Delta_1-\Delta_2+\Delta_3)\frac{w_{12}^2}{w_{23}^2}+\cdots\right|^2$$
$$= \left|1+\frac{w_{12}}{w_{23}}\right|^{-2\Delta_1+2\Delta_2-2\Delta_3} = \left|\frac{w_{23}}{w_{13}}\right|^{2\Delta_1-2\Delta_2+2\Delta_3} \qquad \text{(C.4)}$$

and therefore

J. Stat. Mech. (2020) 053106

$$\langle V_{(\Delta_1)}(w_1)V_{(\Delta_2)}(w_2)V_{(\Delta_3)}(w_3)\rangle = \frac{1}{|w_{12}|^{2\Delta_1+2\Delta_2}|w_{23}|^{2\Delta_3}}\left[\frac{D^{(\Delta_3)}_{(\Delta_1),(\Delta_2)}}{|w_{12}|^{-2\Delta_3}|w_{23}|^{-2\Delta_1+2\Delta_2}|w_{13}|^{2\Delta_1-2\Delta_2+2\Delta_3}} + f_\tau^{(3)}\left(\frac{w_{12}}{w_{23}},\frac{w_{23}}{N}\right)\right] \tag{C.5}$$

with the function $f_\tau^{(3)}$ defined in (2.8):

$$f_\tau^{(3)}\left(\frac{w_{12}}{w_{23}},\frac{w_{23}}{N}\right) = \sum_{(\Delta_{\rm top},Y_{\rm top})} c^{(3)}_{(\Delta_{\rm top},Y_{\rm top})}\left(\frac{w_{12}}{w_{23}}\right)\left(\frac{w_{23}}{N}\right)^{\Delta_{\rm top}+|Y_{\rm top}|}\left(\frac{\bar w_{23}}{N}\right)^{\bar\Delta_{\rm top}+|\bar Y_{\rm top}|} \tag{C.6}$$

and $c^{(3)}_{(\Delta_{\rm top},Y_{\rm top})}\left(\frac{w_{12}}{w_{23}}\right)$ given in (3.9). Specialising to the Q-Potts model, we took $\Delta_1=\Delta_2=\Delta_3=\Delta_{\left(0,\frac12\right)}$ and we computed the most dominant $1/N$ correction to the plane three-point function, corresponding to $\Delta_{\rm top}=\Delta_{\rm min}=\Delta_{(1,2)}$. As explained in section 5.1, the fusion (4.15) of $V_{(1,2)}$ imposes that either $\Delta_{\rm L}=\Delta_{\left(0,\frac12\right)}$ or $\Delta_{\rm L}=\Delta_{\left(0,\frac32\right)}$ corresponding to figures 6(a) and (b). The level expansion of $c^{(3)}_{(1,2)}$ is similar to (C.3) and was also carried out to level 2 i.e. $|Y_{\rm L}|=2$ in (3.9), which showed sufficient precision for comparison with the numerical results:

$$\begin{aligned} c^{(3)}_{(1,2)}\left(\frac{w_{12}}{w_{23}}\right) =& \langle V_{(1,2)}\rangle_{(N=1)}\left\{D^{\left(0,\frac12\right)}_{\left(0,\frac12\right),\left(0,\frac12\right)}D^{(1,2)}_{\left(0,\frac12\right),\left(0,\frac12\right)}\left|\frac{w_{12}}{w_{23}}\right|^{2\Delta_{\left(0,\frac12\right)}}\right. \\ &\times\left|1+\beta^{\left(0,\frac12,-1\right)}_{\left(0,\frac12\right),\left(0,\frac12\right)}\beta^{(1,2)}_{\left(0,\frac12,-1\right),\left(0,\frac12\right)}\frac{w_{12}}{w_{23}}+O\left(\frac{w_{12}^2}{w_{23}^2}\right)\right|^2 \\ &+D^{\left(0,\frac32\right)}_{\left(0,\frac12\right),\left(0,\frac12\right)}D^{(1,2)}_{\left(0,\frac32\right),\left(0,\frac12\right)}\left|\frac{w_{12}}{w_{23}}\right|^{2\Delta_{\left(0,\frac32\right)}} \\ &\left.\times\left|1+\beta^{\left(0,\frac32,-1\right)}_{\left(0,\frac12\right),\left(0,\frac12\right)}\beta^{(1,2)}_{\left(0,\frac32,-1\right),\left(0,\frac12\right)}\frac{w_{12}}{w_{23}}+O\left(\frac{w_{12}^2}{w_{23}^2}\right)\right|^2\right\} \end{aligned} \tag{C.7}$$

C.1. Special cases: $Q=1$ and $Q=2$

- When $Q=1$, the $\frac{1}{\sqrt{Q-1}}$ singularities in $D^{(1,2)^D}_{\left(0,\frac12\right),\left(0,\frac12\right)}$ and in $D^{(1,2)^D}_{\left(0,\frac12\right),\left(0,\frac32\right)}$ (resp. figures 6(a) and (b)) are canceled in (C.7) by the factor $\sqrt{Q-1}$ in the energy one-point function

$$\langle V_{(1,2)^D}\rangle_{N=1} = \frac{Q-1}{Z_Q}D^{(1,2)^D}_{\left(0,\frac12\right),\left(0,\frac12\right)}|q|^{2\left(\Delta_{\left(0,\frac12\right)}-\frac{c}{24}\right)}|1+O(q)|^2, \tag{C.8}$$

  yielding a finite, non-zero limit for $c^{(3)}_{(1,2)}$.

J. Stat. Mech. (2020) 053106

- When $Q=2$, the zero and the pole in (B.4b) and (B.4c) cancel in the product $C^{\left(0,\frac{3}{2}\right)}_{\left(0,\frac{1}{2}\right),\left(0,\frac{1}{2}\right)} C^{(1,2)^D}_{\left(0,\frac{3}{2}\right),\left(0,\frac{1}{2}\right)}$, giving a finite contribution of the $\left(0,\frac{3}{2}\right)$ channel 6(b) to $c^{(3)}_{(1,2)}$.

Appendix D. Derivation of the four-point corrections

We write the s-channel expansion of the four-point function $\langle V_{(\Delta_1)}(w_1)V_{(\Delta_2)}(w_2)V_{(\Delta_3)}(w_3)V_{(\Delta_4)}(w_4)\rangle$ of four (primary, spin-less) fields by inserting the OPEs of $V_{(\Delta_1)}(w_1)V_{(\Delta_2)}(w_2)$ and $V_{(\Delta_3)}(w_3)V_{(\Delta_4)}(w_4)$:

$$\begin{aligned}&\frac{V_{(\Delta_1)}(w_1)V_{(\Delta_2)}(w_2)V_{(\Delta_3)}(w_3)V_{(\Delta_4)}(w_4)}{|w_{12}|^{-2\Delta_1-2\Delta_2}|w_{34}|^{-2\Delta_3-2\Delta_4}}\\&= \sum_{(\Delta_\mathrm{L},Y_\mathrm{L})} D^{(\Delta_\mathrm{L},Y_\mathrm{L})}_{(\Delta_1),(\Delta_2)} w_{12}^{\Delta_\mathrm{L}+|Y_\mathrm{L}|}\bar{w}_{12}^{\bar{\Delta}_\mathrm{L}+|\bar{Y}_\mathrm{L}|} V_{(\Delta_\mathrm{L},Y_\mathrm{L})}(w_2) \sum_{(\Delta_\mathrm{R},Y_\mathrm{R})} D^{(\Delta_\mathrm{R},Y_\mathrm{R})}_{(\Delta_3),(\Delta_4)} w_{34}^{\Delta_\mathrm{R}+|Y_\mathrm{R}|}\bar{w}_{34}^{\bar{\Delta}_\mathrm{R}+|\bar{Y}_\mathrm{R}|} V_{(\Delta_\mathrm{R},Y_\mathrm{R})}(w_4).\end{aligned} \tag{D.1}$$

Inserting the expansion (A.9) of $\langle V_{(\Delta_\mathrm{L},Y_\mathrm{L})}(w_2)V_{(\Delta_\mathrm{R},Y_\mathrm{R})}(w_4)\rangle$,

$$\begin{aligned}&\frac{\langle V_{(\Delta_1)}(w_1)V_{(\Delta_2)}(w_2)V_{(\Delta_3)}(w_3)V_{(\Delta_4)}(w_4)\rangle}{|w_{12}|^{-2\Delta_1-2\Delta_2}|w_{34}|^{-2\Delta_3-2\Delta_4}}\\&= \sum_{\substack{(\Delta_\mathrm{L},Y_\mathrm{L})\\(\Delta_\mathrm{R},Y_\mathrm{R})}} D^{(\Delta_\mathrm{L},Y_\mathrm{L})}_{(\Delta_1),(\Delta_2)} D^{(\Delta_\mathrm{R},Y_\mathrm{R})}_{(\Delta_3),(\Delta_4)} D^{(\Delta,Y)}_{(\Delta_\mathrm{L},Y_\mathrm{L}),(\Delta_\mathrm{R},Y_\mathrm{R})} \left(\frac{w_{12}}{w_{24}}\right)^{\Delta_\mathrm{L}+|Y_\mathrm{L}|}\\&\quad\times\left(\frac{\bar{w}_{12}}{\bar{w}_{24}}\right)^{\bar{\Delta}_\mathrm{L}+|\bar{Y}_\mathrm{L}|}\left(\frac{w_{34}}{w_{24}}\right)^{\Delta_\mathrm{R}+|Y_\mathrm{R}|}\left(\frac{\bar{w}_{34}}{\bar{w}_{24}}\right)^{\bar{\Delta}_\mathrm{R}+|\bar{Y}_\mathrm{R}|}\\&\quad\times\sum_{(\Delta_\mathrm{top},Y_\mathrm{top})}\left(\frac{w_{24}}{N}\right)^{\Delta_\mathrm{top}+|Y_\mathrm{top}|}\left(\frac{\bar{w}_{24}}{N}\right)^{\bar{\Delta}_\mathrm{top}+|\bar{Y}_\mathrm{top}|}\langle V_{(\Delta_\mathrm{top},Y_\mathrm{top})}\rangle.\end{aligned} \tag{D.2}$$

The plane limit P_0 is given by the terms with $\Delta_\mathrm{top}=0$ and $\Delta_\mathrm{L}=\Delta_\mathrm{R}$, corresponding to figure D.1.
and can be written as a function of the cross-ratio z:

$$P_0(z)=\sum_{(\Delta)} D^{(\Delta)}_{(\Delta_1),(\Delta_2)} D^{(\Delta)}_{(\Delta_3),(\Delta_4)} \left|\mathcal{F}^{(s)}_{(\Delta)}(\Delta_i|z)\right|^2 \tag{D.3}$$

where $\mathcal{F}^{(s)}_{(\Delta)}(\Delta_i|z)$ is the s- channel four-point conformal block (A.4). Then,

$$\begin{aligned}&\langle V_{(\Delta_1)}(w_1)V_{(\Delta_2)}(w_2)V_{(\Delta_3)}(w_3)V_{(\Delta_4)}(w_4)\rangle\\&\quad=\frac{1}{|w_{12}|^{2\Delta_1+2\Delta_2}|w_{34}|^{2\Delta_3+2\Delta_4}}\left[P_0(z)+f^{(4)}_\tau\left(\frac{w_{12}}{w_{24}},\frac{w_{34}}{w_{24}},\frac{w_{24}}{N}\right)\right]\end{aligned} \tag{D.4}$$

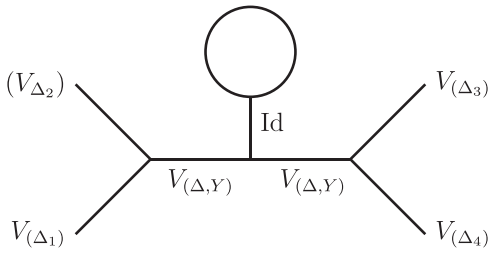

Figure D.1. Diagrammatic representation of the plane limit of the torus four-point function.

with

$$f_\tau^{(4)}\left(\frac{w_{12}}{w_{24}},\frac{w_{34}}{w_{24}},\frac{w_{24}}{N}\right)=\sum_{(\Delta_{\rm top},Y_{\rm top})} c^{(4)}_{(\Delta_{\rm top},Y_{\rm top})}\left(\frac{w_{12}}{w_{24}},\frac{w_{34}}{w_{24}},\tau\right)\left(\frac{w_{24}}{N}\right)^{\Delta_{\rm top}+|Y_{\rm top}|}\left(\frac{\bar{w}_{24}}{N}\right)^{\bar{\Delta}_{\rm top}+|\bar{Y}_{\rm top}|}, \tag{D.5}$$

where $c^{(4)}_{(\Delta_{\rm top},Y_{\rm top})}\left(\frac{w_{12}}{w_{24}},\frac{w_{34}}{w_{24}},\tau\right)$ is given by (3.12). The contribution of each diagram of the type in figure 5 to $c^{(4)}$ is of order $z^{\frac{1}{2}(\Delta_{\rm L}+\bar{\Delta}_{\rm L}+\Delta_{\rm R}+\bar{\Delta}_{\rm R})}=z^{\Delta_{\rm L}+\Delta_r-\frac{1}{2}(s_{\rm L}+s_{\rm R})}$. The non-diagonal fields in the spectrum of the Q-Potts model have spins $S_{(r,s)}=-rs$: those with non-zero spin give therefore very sub-dominant contributions to the four-point connectivity.

D.1. Special cases: $Q=1$ and $Q=2$

- When $Q=1$, the $\frac{1}{\sqrt{Q-1}}$ singularities in $D^{(1,2)^D}_{\left(0,\frac{1}{2}\right),\left(0,\frac{1}{2}\right)}$ and in $D^{(1,2)^D}_{\left(0,\frac{1}{2}\right),\left(0,\frac{3}{2}\right)}$ (resp. figures 9 and 10) are canceled by the factor $\sqrt{Q-1}$ in the energy one-point function, exactly as in the three-point case.
- When $Q=2$, again as in the three-point case, the zero and the pole in (B.4b) and (B.4c) coming from the contribution of figure 10 cancel in the product $C^{\left(0,\frac{3}{2}\right)}_{\left(0,\frac{1}{2}\right),\left(0,\frac{1}{2}\right)}C^{(1,2)^D}_{\left(0,\frac{3}{2}\right),\left(0,\frac{1}{2}\right)}$. The contribution of the $\left(0,\frac{3}{2}\right)$ channel to $c^{(4)}_{(1,2)}$ is therefore finite, contrary to the contribution of the same channel to the plane four-point function. In that latter case, the divergences of the different channels with the same dimension cancel each other.

References

[1] Wu F Y 1982 The potts model *Rev. Mod. Phys.* **54** 235–68
[2] Beffara V and Duminil-Copin H 2010 The self-dual point of the two-dimensional random-cluster model is critical for $q\geqslant 1$ (arXiv:1006.5073)
[3] Bertrand D 1989 Two-dimensional fractal geometry, critical phenomena and conformal invariance *Phys. Rep.* **184** 229–57
[4] di Francesco P, Saleur H and Zuber J B 1987 Relations between the coulomb gas picture and conformal invariance of two-dimensional critical models *J. Stat. Phys.* **49** 57–79
[5] Saleur H 1987 Conformal invariance for polymers and percolation *J. Phys. A: Math. Gen.* **20** 455

J. Stat. Mech. (2020) 053106

[6] Gainutdinov A M, Jacobsen J L, Saleur H and Vasseur R 2013 A physical approach to the classification of indecomposable virasoro representations from the blob algebra *Nucl. Phys.* B **873** 614–81

[7] Read N and Saleur H 2007 Associative-algebraic approach to logarithmic conformal field theories *Nucl. Phys.* B **777** 316–51

[8] Delfino G and Viti J 2011 On three-point connectivity in two-dimensional percolation *J. Phys. A: Math. Theor.* **44** 032001

[9] Kostov I K and Petkova V B 2006 Bulk correlation functions in 2-D quantum gravity *Theor. Math. Phys.* **146** 108–18

[10] Schomerus V 2006 Non-compact string backgrounds and non-rational CFT *Phys. Rep.* **431** 39–86

[11] Zamolodchikov A B 2005 Three-point function in the minimal liouville gravity *Theor. Math. Phys.* **142** 183

[12] Santiago M and Ribault S 2018 The analytic bootstrap equations of non-diagonal two-dimensional CFT *J. High Energ. Phys.* JHEP05(2018)169

[13] Picco M, Ribault S and Santachiara R 2016 A conformal bootstrap approach to critical percolation in two dimensions *SciPost Phys.* **1** 009

[14] Picco M, Ribault S and Santachiara R 2019 On four-point connectivities in the critical 2d Potts model *SciPost Phys.* **7** 44

[15] Ribault S and Santachiara R 2015 Liouville theory with a central charge less than one *J. High Energy Phys.* JHEP8(2015)109

[16] Ribault S 2019 The non-rational limit of d-series minimal models (arXiv:1909.10784)

[17] Jacobsen J L and Saleur H 2018 Bootstrap approach to geometrical four-point functions in the two-dimensional critical Q-state Potts model: a study of the s-channel spectra (arXiv:1809.02191)

[18] Javerzat N, Picco M and Santachiara R 2020 Two-point connectivity of two-dimensional critical q- potts random clusters on the torus *J. Stat. Mech.: Theory Exp.* 023101

[19] Cardy J 2008 Conformal field theory and statistical mechanics (arXiv:0807.3472)

[20] Chelkak D, Hongler C and Izyurov K 2012 Conformal invariance of spin correlations in the planar Ising model (arXiv:1202.2838)

[21] di Francesco P, Saleur H and Zuber J B 1987 Critical Ising correlation functions in the plane and on the torus *Nucl. Phys.* B **290** 527

[22] Saleur H 1988 Correlation functions of the critical ashkin-teller model on a torus *J. Stat. Phys.* **50** 475–508

[23] Bagger J, Nemeschansky D and Zuber J-B 1989 Minimal model correlation functions on the torus *Phys. Lett.* B **216** 320–4

[24] Jayaraman T and Narain K S 1990 Correlation functions for minimal models on the torus *Nucl. Phys.* B **331** 629–58

[25] Ribault S 2014 Conformal field theory on the plane (arXiv:1406.4290)

[26] Fateev V A and Litvinov A V 2010 On AGT conjecture *J. High Energy Phys.* JHEP02(2010)014

[27] Fortuin C M and Kasteleyn P W 1972 On the random-cluster model *Physica* **57** 536–64

[28] Delfino G and Viti J 2011 Potts q-color field theory and scaling random cluster model *Nucl. Phys.* B **852** 149–73

[29] Kanno S, Matsuo Y and Shiba S 2010 Analysis of correlation functions in Toda theory and AGT-W relation for SU(3) quiver *Phys. Rev.* D **82** 066009

[30] Langlands R P, Pichet C, Pouliot P and Saint-Aubin Y 1992 On the universality of crossing probabilities in two-dimensional percolation *J. Stat. Phys.* **67** 553–74

[31] Blanchard T 2014 Wrapping probabilities for Potts spin clusters on a torus *J. Phys. A: Math. Theor.* **47** 342002

[32] Haru T P 1994 Critical percolation on the torus *J. Stat. Phys.* **75** 1167–77

[33] Jacobsen J 2012 Loop models and boundary cft *Conformal Invariance: An Introduction to Loops, Interfaces and Stochastic Loewner Evolution* ed M Henkel and D Karevski vol 853 (Berlin: Springer) ch 4 pp 141–81

[34] Ikhlef Y, Jacobsen J L and Saleur H 2016 Three-point functions in $c\leqslant 1$ Liouville theory and conformal loop ensembles *Phys. Rev. Lett.* **116** 130601

[35] Benoit E and Ikhlef Y 2015 Correlation functions in loop models (arXiv:1505.00585)

[36] Picco M, Santachiara R, Viti J and Delfino G 2013 Connectivities of Potts Fortuin-Kasteleyn clusters and time-like Liouville correlator *Nucl.Phys.* B **875** 719–37

[37] Ziff R M, Simmons J J H and Kleban P 2011 Factorization of correlations in two-dimensional percolation on the plane and torus *J. Phys. Math. Gen.* **44** 065002

[38] Santachiara R and Viti J 2014 Local logarithmic correlators as limits of Coulomb gas integrals *Nucl. Phys.* B **882** 229–62

[39] Bogomolny E and Schmit C 2007 Random wavefunctions and percolation *J. Phys. A: Math. Theor.* **40** 14033–43

[40] Dotsenko V S 2019 Four spins correlation function of the q states potts model, for general values of q. Its percolation model limit $q \to 1$ *Nucl. Phys.* B **953** 114973

J. Stat. Mech. (2020) 053106

5

PERCOLATION OF RANDOM SURFACES

In this chapter we study another continuous family of models, parametrised by the strength of the asymptotic decay of the site-site correlation. Namely, denoting the site occupation by θ:

$$\theta(\mathbf{r}) = \begin{cases} 1 \text{ if the site at position } \mathbf{r} \text{ is occupied} \\ 0 \text{ otherwise} \end{cases} \tag{5.1}$$

the probability that two sites at distance r are occupied decays algebraically:

$$\mathbb{E}\left[\theta(\mathbf{r})\theta(0)\right] - \mathbb{E}\left[\theta(\mathbf{r})\right]\mathbb{E}\left[\theta(0)\right] \overset{r\gg 1}{\approx} r^{2H}, \quad H < 0. \tag{5.2}$$

H is a negative real number, called Hurst exponent. We will indeed show in the next sections that the decay above can be obtained by considering the excursion sets (sites where the height is higher than some level) of a random surface characterised by its Hurst exponent (or roughness) H. For each value of H there exist a critical occupation probability at which the level clusters percolate. When the site occupation is spatially uncorrelated, pure percolation is recovered. This line of models therefore coincides with the $Q-$Potts line at the pure percolation point, as sketched in Figure 5.1 below. However, the way correlations are introduced differ in the two models, leading to different universal properties of the random clusters. While the Potts CFT is on the way to being solved, the level clusters of random surfaces are much less understood.

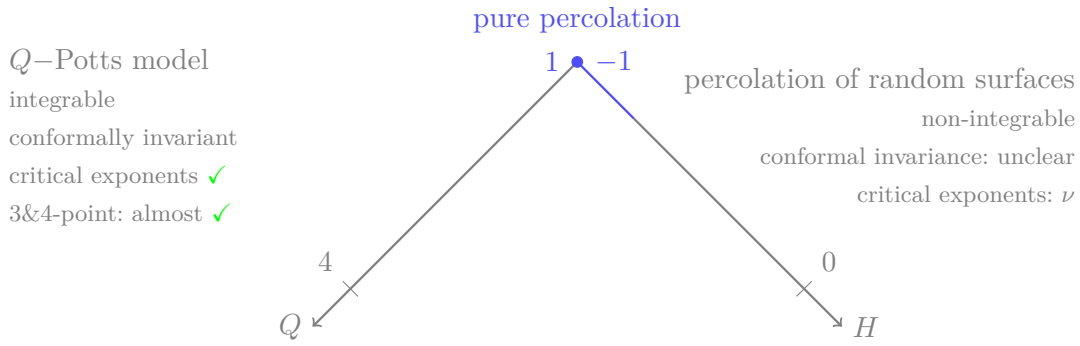

Figure 5.1

Indeed, only the behaviour of the thermal exponent ν with H is conjectured, while the magnetic exponent β has been estimated numerically. We recall that for the Potts model, all critical exponents were determined exactly from the Coulomb-gas CFT. Here, not only do we ignore what CFT gives the critical exponents, but even the question of conformal invariance of the percolation clusters had not been clearly answered so far.

The aim of the work Article IV was primarily to investigate the presence of conformal invariance in this model. We developed a new method of analysis of percolation-type systems, which exploits the information contained in the two-point torus connectivity. By probing the existence of a traceless stress-energy tensor, it is a direct method to establish the conformal invariance of the

measure of the random clusters. Further features of the potential underlying CFT can also be investigated. The strategy is to make the following assumptions:

1. The clusters are conformally invariant.
2. There exist a (unkown) CFT whose correlators describe the cluster connectivities. In particular the two-point torus connectivity is given by a torus two-point function.
3. As for pure percolation, the spectrum is discrete and the energy field gives the dominant torus correction to the two-point connectivity.

If the above is satisfied, then the behaviour of the connectivity with the geometry of the torus is (rather strongly) constrained by conformal invariance. This is clear from the results of Chapter 2, which we exploit in a precise way. Comparison with numerical measurements then allows to confirm or not the inital assumptions and in particular settle on the question of conformal invariance.
Throughout this chapter we show that for the model of percolation of random surfaces this method allowed us to:

1. Establish firmly the conformal invariance of the clusters.
2. Show that the torus two-point connectivity is well described by the torus two-point function of a field in a CFT.
3. Probe the first terms in the torus partition function of this CFT.
4. Show that the energy field is not degenerate.
5. Estimate numerically quantities involving crucial data of a CFT: the central charge, structure constants and multiplicities.

In Section 5.1 we define precisely the model of percolation of random surfaces. In Section 5.2 we review the state of the art: we discuss the relevance of correlations and what is known of the universality class of the new critical points. We also comment on previous works which studied the potential conformal invariance of the system. In Section 5.3 we explain in details our protocol to test conformal invariance of a percolation-type critical point. In Section 5.4 we explain how the two-point torus connectivity allows to obtain important information on the underlying CFT, notably ragarding points 3-5 above. We discuss the results obtained for the particular model we consider. This method is however general and can very well be applied to other models for which conformal invariance and/or the nature of the CFT are questioned. Finally in Section 5.5 we discuss how to similarly exploit the three-point connectivity to complete our results on the CFT of percolation of random surfaces.

5.1 PERCOLATION OF RANDOM SURFACES

A correlated percolation system can be obtained by cutting a two-dimensional random surface $u(\mathbf{x})$ at some height –or level, h. Namely we define the site occupation $\theta(\mathbf{x})$ as:

$$\theta(\mathbf{x}) = \begin{cases} 1 & u(\mathbf{x}) \geq h \\ 0 & u(\mathbf{x}) < h. \end{cases} \tag{5.3}$$

The set of occupied sites is called excursion set and its connected components at a given level, the level clusters. To have a more relaxing and pleasant image in mind, one can imagine the random surface as a landscape of hills flooded with water up to some height, as in the picture below (inspired from [103]). At low height, lakes are disconnected. Increasing the height, these isolated lakes connect and a waterway (or percolating cluster) eventually emerges[1].

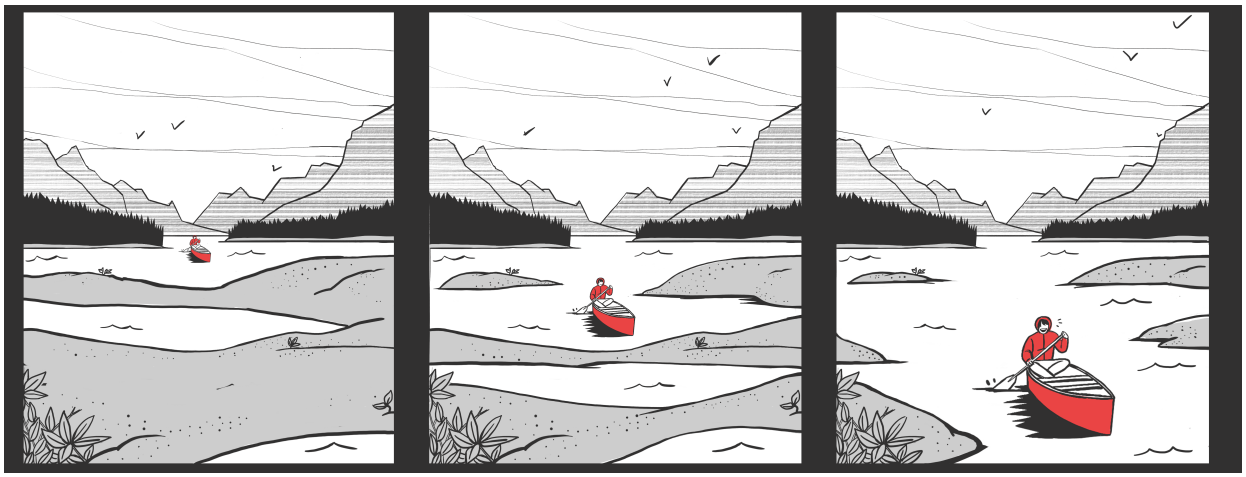

A central point is that the long-distance site-site correlation $\mathbb{E}\left[\theta(\mathbf{x})\theta(\mathbf{y})\right]$ inherits its behaviour from the long-distance covariance of the random surface $\mathbb{E}\left[u(\mathbf{x})u(\mathbf{y})\right]$. We are thus interested in surfaces u such that the covariance decays algebraically:

$$\mathbb{E}\left[u(\mathbf{x})u(\mathbf{y})\right] - \mathbb{E}\left[u(\mathbf{x})\right]\mathbb{E}\left[u(\mathbf{y})\right] \sim |\mathbf{x}-\mathbf{y}|^{2H}, \quad |\mathbf{x}-\mathbf{y}| \gg 1 \tag{5.4}$$

so that the site-site correlation is given by (5.2):

$$\mathbb{E}\left[\theta(\mathbf{r})\theta(0)\right] - \mathbb{E}\left[\theta(\mathbf{r})\right]\mathbb{E}\left[\theta(0)\right] = \mathbb{E}\left[\theta(\mathbf{x})\theta(\mathbf{y})\right] - p^2(h) \sim |\mathbf{x}-\mathbf{y}|^{2H}, \quad |\mathbf{x}-\mathbf{y}| \gg 1. \tag{5.5}$$

The mean occupation is translation invariant, $\mathbb{E}\left[\theta(\mathbf{x})\right] = \mathbb{E}\left[\theta(0)\right] = p(h)$. We consider real $H < 0$, where for each value of H there exist a level $h = f(H)$ corresponding to a critical phase transition (see introduction of Article IV).

5.1.1 *Why study such a model ?*

There are several motivations for studying such long-range correlated percolation surfaces. First, many physical phenomena can be described with a correlated percolation model (see for instance the review [104]). Algebraic decay of the correlation is moreover found in many cases, such as: a fluid flow in a porous medium [105, 106], the turbulent motion of a fluid [107], the growth of cities [108] ....
Secondly, the properties of the percolation surface allow to access properties of the random function itself, as pointed out in [109] where the quantum eigenfunctions of chaotic systems are studied through their level clusters.
Of particular interest to us, from a bootstrap point of view, is that it provides a new line of critical points where scale invariance enlarges to conformal invariance. While this holds for

1 Note that this corresponds to taking the altitude as $-u$.

models defined from local, unitary Hamiltonians [110, 111], it is not so evident for non-unitary models. In particular, the model under consideration here is highly non-local in its definition. It has indeed been shown to be equivalent to a random cluster $Q-$Potts model with quenched, long-range correlated disorder, in the $Q \to 1$ limit [53]. While the partition function of the non-disordered random cluster Potts model can be rewritten in terms of local (albeit complex) Boltzmann weights [91], it is not known wether this is possible in the presence of disorder. We will see below that the potential CFT describing this new line of critical points does not correspond to any known CFT, and might represent therefore a new bootstrap solution.

5.1.2 *Discrete fractional Gaussian surface*

There is a certain freedom in choosing the random function u, since the important property is the long-distance behaviour of its covariance (5.4), which is independent of microscopic details. The full details on how the function is generated are given in Appendix A of Article IV and we only report here the necessary equations.
The random function is a discrete fractional Gaussian surface. It is a real function, defined on a discrete $M \times N$ lattice: $\mathbf{x} = (x_1, x_2) \in [0, 1, \cdots, N-1] \times [0, 1, \cdots, M-1]$ by:

$$u(\mathbf{x}) = \frac{1}{\text{norm}} \sum_{\mathbf{k}} \lambda_{\mathbf{k}}^{-\frac{H+1}{2}} \hat{w}(\mathbf{k}) e^{i\mathbf{k}\mathbf{x}}, \quad H \in [-1, 0]. \tag{5.6}$$

The randomness is contained in $\hat{w}(\mathbf{k})$: it is the Fourier transform of a random surface $w(\mathbf{x})$ whose heights at each point are completely uncorrelated. Namely:

$$\mathbb{E}\left[w(\mathbf{x})w(\mathbf{y})\right] - \mathbb{E}\left[w(\mathbf{x})\right]\mathbb{E}\left[w(\mathbf{y})\right] \propto \delta_{x_1,y_1}\delta_{x_2,y_2}. \tag{5.7}$$

Correlations are induced by the factor $\lambda_{\mathbf{k}}^{-\frac{H+1}{2}}$, whose definitions[2] are given in Appendix A of Article IV.
When $H = -1$, $\lambda_{\mathbf{k}}^{-\frac{H+1}{2}} = 1$ and $u = w$. Cutting the function (cf. (5.3)) produces a surface of uncorrelated, aka pure, percolation. When $H \in]1, 0[$, we have instead:

$$\mathbb{E}\left[|u(\mathbf{x}) - u(\mathbf{y})|^2\right] \sim |\mathbf{x} - \mathbf{y}|^{2H}, \quad |\mathbf{x} - \mathbf{y}| \gg 1 \tag{5.8}$$

and at $H = 0$ the correlation shows logarithmic decay: the scaling limit of u behaves as a Gaussian free field[3].
In Section 5.2 we discuss what happens then to the long-distance properties of the corresponding percolation surface.

5.1.3 *An aside: who was Mr. Hurst ?*

Originally the Hurst exponent describes the behaviour of the autocorrelation of a process evolving with time: for positive $H \in [0, 1]$ the profile of our function u (5.8), parametrised by t describes a fractional Brownian motion $W_H(t)$:

$$\mathbb{E}\left[|W_H(t_1) - W_H(t_2)|^2\right] \sim |t_2 - t_1|^{2H}, \quad |t_2 - t_1| \gg 1. \tag{5.9}$$

2 We use two different types of factors. We show that this, as well as the distribution of w, does not affect the long-distance properties of the percolation clusters.
3 See also the choice of λ in Article IV such that u coincides with the Gaussian free field at $H = 0$, with its covariance satisfying the (discrete) Laplace equation.

For $H = 1/2$ this is the usual Brownian motion, which has independent increments. When $H > 1/2$ ($H < 1/2$) the increments are positively (negatively) correlated.
The denomination comes from the name of British physicist Harold Edwin Hurst (1880-1978). Hurst worked in Egypt and studied the fluctuations of the water level of the Nile. The huge river, subject to both drought and flood, needed to be controlled with strategically built reservoirs, for crop irrigation as well as to prevent the floods, which caused massive people displacements. As Hurst noted [112], a consistent policy cannot be laid down from the sole knowledge of the past year behaviour, as "the past is never exactly repeated". A more involved model must be sought since in particular, the behaviour of the water level within a year is not observed to be independent from the past years ($H \neq 1/2$). Interestingly, by studying the river statistics as well as other phenomena (the growth of tree rings in Canada, the wheat prices,...) Hurst noticed that the time behaviour seems to be described by the same value of $H \sim 0.75$, pointing at some universality... Eventually, Hurst plan was selected for the building of the Aswan High Dam in the 50's (although geopolitical considerations took over, so that the actual dam was not built according to Hurst recommendations [113]).

5.2 STATE OF THE ART

As seen in Section 5.1.2, the case $H = -1$ corresponds to uncorrelated sites, namely:

$$\mathbb{E}\left[\theta(\mathbf{x})\theta(\mathbf{y})\right] - p^2(h) \sim \delta\left(|\mathbf{x}-\mathbf{y}|\right). \tag{5.10}$$

Therefore, the long-distance properties of the clusters at the critical level are given by the universality class of pure percolation. Now we turn on the correlations, $H > -1$. We expect that for H close to -1, correlations decay fast enough so as to preserve the pure long-distance properties: in other words, correlations are not relevant and the clusters remain in the pure percolation universality class. The question is then: does there exist a value of $H \in]-1, 0]$ such that correlations become relevant, and the universality class changes ?
This question has been answered by Weinrib [53]. With the site-site correlation decaying as (5.5), one can ask for which range of H a consistent phase transition characterised by ν^{pure} exist. Namely, for which values of H do the correlation lengths ξ_V in different regions of size V diverge at the same value p_c of the site occupation: $\xi_V \sim (p_V - p_c)^{-\nu^{\text{pure}}}$. For this to occur, fluctuations in the average site occupation p_V of the region of size V must be small when p approaches p_c. Taking the region to have typical size ξ, one finds that these fluctuations behave at long distances as [53]:

$$\frac{\mathbb{E}[p_\xi^2] - \mathbb{E}[p_\xi]^2}{(p_c - p)^2} \sim \frac{1}{(p_c - p)^{2H\nu^{\text{pure}}+2}}, \quad H > -1. \tag{5.11}$$

This goes to zero if $H\,\nu^{\text{pure}} + 1 < 0$, so that such transition is inconsistent when:

$$H\,\nu^{\text{pure}} + 1 > 0 \Leftrightarrow H > -\frac{3}{4} \tag{5.12}$$

and new critical behaviour emerges[4]. The use of this extended Harris criterion allows also to predict the new values of the thermal exponent for $H \in [-3/4, 0]$:

$$\nu = -\frac{1}{H} \tag{5.13}$$

4 Rigorous arguments can be found in Section 3.1 of the introduction of [114] as well as in [115].

sketched in Figure 5.2.

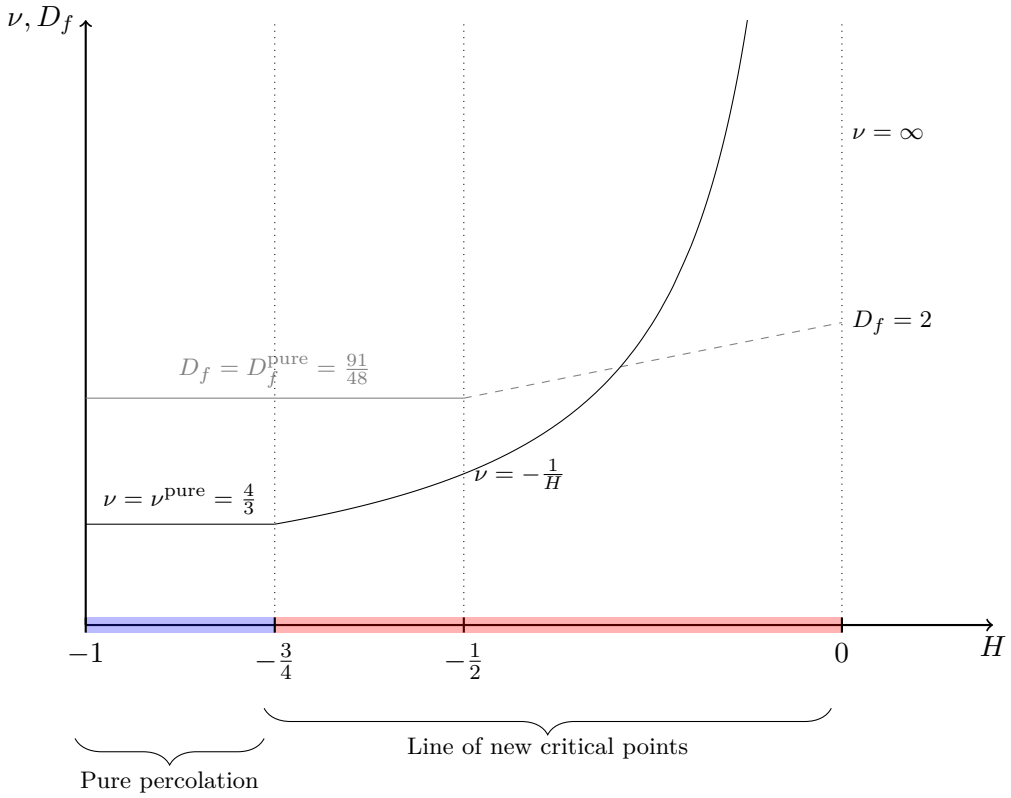

Figure 5.2: Summary of the state of the art. The black curve gives the theoretical prediction [53] for the thermal exponent ν, while the gray lines sketch the behaviour of the fractal dimension observed in numerical studies [54, 116, 117].

Prediction (5.13) has been subsequently confirmed in numerous numerical works [54, 116–119]. There is no theoretical prediction concerning the other main exponent which characterise the transition, the magnetic exponent β. In [54, 116, 117] the fractal dimension of the clusters, $D_f = 2 - \beta/\nu$ [42] is measured (see for instance Appendix B of Article IV). We report in Figure 5.2 its observed behaviour with H. For $H \in [-1, -3/4]$ the numerical values of [54, 116, 117] are in agreement with the pure percolation value $D_f = D_f^{\text{pure}}$, consistently with the prediction [53] that the universality class is pure percolation. For $H > -3/4$, while ν starts varying continuously, the the fractal dimension seems to remain constant $D_f \overset{\text{within error bars}}{=} D_f^{\text{pure}}$ up to some value of H estimated to be $H \sim -1/2$ [54, 117]. For $H > -1/2$, D_f increases to reach the value $D_f = 2$ of the free Gaussian field [120–122] at $H = 0$. Such behaviour is not understood. In particular, perturbative renormalisation group analysis [53] fails to predict it, and it is not determined at present whether the fractal dimension varies very slowly with H, or is truly "superuniversal" and remains fixed to the pure value. In the latter case, this behaviour would contrast with most continuous families of models, where all critical exponents vary continuously. For instance in the $Q-$Potts model every scaling dimension is a continuous function of the central charge, as seen from the torus partition function (4.3). There exist nonetheless models where the dimensions of one or several fields are superuniversal. This is the case of the self-dual critical line of the Ashkin-Teller model, along which the dimensions of the spin and disorder fields are fixed [69,

123]. It has also been conjectured that the thermal exponent of the disordered $Q-$state Potts model keeps the same value for all $Q \geq 2$ [124, 125].

Besides the determination of critical exponents, an important question is the presence of conformal invariance in this model. We know that the random clusters of pure percolation are conformally invariant [33], but what about those of the new critical points $H \in [-3/4, 0]$? If they are conformally invariant as well, does there exist a consistent CFT describing them, and what is this CFT ?

The question of conformal invariance in these correlated percolation systems has been investigated through study of the boundaries of the level clusters, and their potential equivalence with Schramm Loewner Evolution (SLE) traces [107, 126, 127]. In this approach the boundaries of the percolating clusters are considered as a growing curve, starting from the boundary of the system. If the measure of this curve is conformally invariant, then its evolution in the scaling limit can be described by a Brownian motion (see [32] for a review of SLE). By checking wether the clusters boundaries obey the SLE statistics, one can in principle test their conformal invariance. In [107] the percolating clusters boundaries are studied for $H = -2/3$ and conformal invariance is ruled out. In [126, 127] the complete (also called hull) and accessible (also called external) perimeters of the percolating clusters are studied, and are found to obey the SLE statistics. Their conformal invariance is therefore conjectured, for all $H \in [-1, 0]$. The diffusion constants κ and $\tilde{\kappa}$ of the Brownian motion associated to both perimeters are estimated. They satisfy the duality relation $\kappa = 16/\tilde{\kappa}$ [41, 128]. In addition, the fractal dimensions d_f^{complete} and $d_f^{\text{accessible}}$ of both perimeters are estimated numerically, see also [116]. They both show significant variation for $-3/4 \leq H \leq 0$, contrary to the fractal dimension of clusters which is observed to stay constant for $-1 \leq H \leq -1/2$ (cf. Figure 5.2). Actually from the results in [116, 126, 127] one can wonder wether the fractal dimensions of the boundaries remain equal to their pure percolation values for $H \in [-1, -3/4]$ (when the system is conjectured to be in the pure percolation universality class). For all H the numerical values are found to agree with the relation $(d_f^{\text{complete}} - 1)(d_f^{\text{accessible}} - 1) = 1$, satisfied by the perimeters of the Potts clusters [41]. Nevertheless these clusters are not the Potts clusters, as is visible from the behaviour of the fractal dimension D_f with H in Figure 5.2, and as we further argue in Section 5.4.2.

The results of the next sections are based on a completely different approach, which probes directly statistical properties of the clusters, and not of their boundary. This provides first a direct test of the conformal invariance of their measure, and shows further that the CFTs describing the Potts and random surface clusters are different. The relation between the statistical properties of the bulk and boundaries of these latter remains notheless mysterious.

5.3 CONFORMAL INVARIANCE OF PERCOLATING RANDOM SURFACES

Our exploration tool is the scaling limit p_{12} of the torus two-point connectivity. As explained in the introduction ii, assumptions 1 and 2 translate into the following assumption:

$$p_{12}(\mathbf{x}_1, \mathbf{x}_2)_{\text{torus}} = d_0^{(2)} \langle V_{\Delta_\sigma}(\mathbf{x}_1) V_{\Delta_\sigma}(\mathbf{x}_2) \rangle_\tau, \tag{5.14}$$

with $d_0^{(2)}$ a non-universal constant. The connectivity field is denoted V_{Δ_σ}, in analogy with the Potts model where it is identified with the spin field(s). It has dimensions $\Delta_\sigma = \bar{\Delta}_\sigma = \frac{2-D_f}{2}$ so that the two-point connectivity is given in the plane limit by:

$$p_{12}(\mathbf{x}_1, \mathbf{x}_2) \sim \frac{1}{|\mathbf{x}_1 - \mathbf{x}_2|^{4-2D_f}} \tag{5.15}$$

where we have used that the decay is given by the exponent η (cf. (iv)) and the scaling relation $\eta = 4 - 2D_f$ (see for instance Section 3.3 of [42]).
We take complex coordinate w on the $M \times N$ torus, such that the real (resp. imaginary) axis $w \in \mathbb{R}$ (resp.$i\mathbb{R}$) is parallel to the N (resp. M) direction. The two-point function $\langle V_{\Delta_\sigma}(w) V_{\Delta_\sigma}(0)\rangle$ can be written as the s-expansion (2.66) derived in Chapter 2:

$$\langle V_{\Delta_\sigma}(w) V_{\Delta_\sigma}(0)\rangle_\tau = \frac{1}{|w|^{4\Delta_\sigma}} \sum_{\Delta,\bar{\Delta}\in S} D^{(\Delta)}_{\sigma,\sigma} \left(\frac{w}{N}\right)^{\Delta} \left(\frac{\bar{w}}{N}\right)^{\bar{\Delta}} \langle V_{\Delta,\bar{\Delta}}\rangle_\tau \tag{5.16}$$

where the sum is over primary and descendant fields in the fusion spectrum S of the two spin fields. This spectrum is a priori unknown. Separating the contributions of scalar fields and fields with spin $s = \Delta - \bar{\Delta}$ we get:

$$\begin{aligned}\langle V_{\Delta_\sigma}(w) V_{\Delta_\sigma}(0)\rangle_\tau =& \frac{1}{|w|^{4\Delta_\sigma}} \Bigg\{ \sum_{\Delta=\bar{\Delta}} D^{(\Delta)}_{\sigma,\sigma} \left|\frac{w}{N}\right|^{2\Delta} \langle V_{\Delta,\Delta}\rangle_\tau \\ &+ \sum_{\Delta-\bar{\Delta}>0} D^{(\Delta)}_{\sigma,\sigma} \left(\left(\frac{w}{N}\right)^{\Delta} \left(\frac{\bar{w}}{N}\right)^{\bar{\Delta}} \langle V_{\Delta,\bar{\Delta}}\rangle + \left(\frac{w}{N}\right)^{\bar{\Delta}} \left(\frac{\bar{w}}{N}\right)^{\Delta} \langle V_{\bar{\Delta},\Delta}\rangle_\tau \right) \Bigg\}.\end{aligned} \tag{5.17}$$

Writing the complex coordinate $w = r\, e^{i\theta}$ and using that $\langle V_{\Delta,\bar{\Delta}}\rangle = \langle V_{\bar{\Delta},\Delta}\rangle$:

$$\begin{aligned}\langle V_{\Delta_\sigma}(w) V_{\Delta_\sigma}(0)\rangle_\tau =& \frac{1}{r^{4\Delta_\sigma}} \Bigg\{ \sum_{\Delta=\bar{\Delta}} D^{(\Delta)}_{\sigma,\sigma} \langle V_{\Delta,\Delta}\rangle_\tau \left(\frac{r}{N}\right)^{2\Delta} \\ &+ \sum_{\Delta-\bar{\Delta}>0} D^{(\Delta)}_{\sigma,\sigma} 2\cos\left(\theta[\Delta-\bar{\Delta}]\right) \langle V_{\Delta,\bar{\Delta}}\rangle_\tau \left(\frac{r}{N}\right)^{\Delta+\bar{\Delta}} \Bigg\}\end{aligned} \tag{5.18}$$

so we can write:

$$p_{12}(w) = \frac{d_0^{(2)}}{r^{4\Delta_\sigma}} \sum_{\Delta-\bar{\Delta}\geq 0} D^{(\Delta)}_{\sigma,\sigma} \left(2 - \delta_{\Delta,\bar{\Delta}}\right) \cos\left(\theta[\Delta-\bar{\Delta}]\right) \langle V_{\Delta,\bar{\Delta}}\rangle_\tau \left(\frac{r}{N}\right)^{\Delta+\bar{\Delta}}. \tag{5.19}$$

The behaviour of the two-point connectivity depends therefore on two geometrical parameters: the aspect ratio through the dependence of the one-point functions on the modular parameter q: $\langle V_{\Delta,\bar{\Delta}}\rangle = \langle V_{\Delta,\bar{\Delta}}\rangle_{q=e^{-2\pi M/N}}$ (see Section 2.3), and the angle θ at which the connectivity is measured. When $M = N$, the system is isotropic. Every direction being equivalent, the connectivity does not depend on θ. Indeed on the square torus the non-scalar contributions vanish since:

$$\langle V_{\Delta,\bar{\Delta}}\rangle_{q=e^{-2\pi}} \overset{\Delta\neq\bar{\Delta}}{=} 0 \tag{5.20}$$

by rotational invariance. Taking $M \neq N$ amounts to introduce anisotropy: how much is measured by the contributions of the fields with spin. This is clearly seen by considering the connectivity measured in a direction perpendicular to w ie $w^\perp = iw = re^{i(\theta+\pi/2)}$. The difference of the two connectivities is:

$$\begin{aligned}p_{12}(w) - p_{12}(w^\perp) = \frac{d_0^{(2)}}{r^{4\Delta_\sigma}} \sum_{\Delta-\bar{\Delta}>0} D^{(\Delta)}_{\sigma,\sigma} 2\Big(&\cos\left(\theta[\Delta-\bar{\Delta}]\right) \\ &- \cos\left([\theta+\pi/2][\Delta-\bar{\Delta}]\right)\Big) \langle V_{(\Delta)}\rangle \left(\frac{r}{N}\right)^{\Delta+\bar{\Delta}}\end{aligned} \tag{5.21}$$

in which the contributions of scalar fields cancel out. Note that, for all aspect ratios this difference must also vanish when $\theta = \pi/4$, since in that case the two perpendicular directions are equivalent: $p_{12}\left(\frac{r}{\sqrt{2}}(i+1)\right) = p_{12}\left(\frac{r}{\sqrt{2}}(i-1)\right) \quad \forall r$. From (5.21) this implies that only fields with $\Delta - \bar{\Delta} = 2k$, $k \in \mathbb{Z}$ give a non-zero contribution to p_{12}. Hence we have:

$$p_{12}(w) = \frac{d_0^{(2)}}{r^{4\Delta_\sigma}} \sum_{\substack{\Delta-\bar{\Delta}=2k \\ k\geq 0}} D_{\sigma,\sigma}^{(\Delta)} \left(2 - \delta_{\Delta,\bar{\Delta}}\right) \cos\left(\theta[\Delta - \bar{\Delta}]\right) \langle V_{(\Delta)} \rangle \left(\frac{r}{N}\right)^{\Delta+\bar{\Delta}} \tag{5.22a}$$

$$p_{12}(w^\perp) = \frac{d_0^{(2)}}{r^{4\Delta_\sigma}} \sum_{\substack{\Delta-\bar{\Delta}=2k \\ k\geq 0}} D_{\sigma,\sigma}^{(\Delta)} \left(2 - \delta_{\Delta,\bar{\Delta}}\right)(-1)^{\frac{\Delta-\bar{\Delta}}{2}} \cos\left(\theta[\Delta - \bar{\Delta}]\right) \langle V_{(\Delta)} \rangle \left(\frac{r}{N}\right)^{\Delta+\bar{\Delta}} \tag{5.22b}$$

and

$$p_{12}(w) - p_{12}(w^\perp) = \frac{d_0^{(2)}}{r^{4\Delta_\sigma}} \sum_{\substack{\Delta-\bar{\Delta} \\ =2\mathrm{mod}4}} D_{\sigma,\sigma}^{(\Delta)} 4 \cos(\theta[\Delta - \bar{\Delta}]) \langle V_{(\Delta)} \rangle \left(\frac{r}{N}\right)^{\Delta+\bar{\Delta}}. \tag{5.23}$$

We know that the first dominant field contributing to (5.22a) must be the identity, in order to get back the plane limit (5.15). From assumption 3 the next dominant primary field in the fusion spectrum S with non-zero one-point function[5] is the energy field:

$$p_{12}(w) = \frac{d_0^{(2)}}{r^{4\Delta_\sigma}} \left(1 + D_{\sigma,\sigma}^{\varepsilon} \langle V_\varepsilon \rangle \left(\frac{r}{N}\right)^{2\Delta_\varepsilon} + \cdots\right). \tag{5.24}$$

This assumption is motivated by what has been observed in [46, 51] for the $Q-$state Potts model, and in particular in the pure percolation limit $Q \to 1$.
The numerical results obtained for the exponent of the first topological correction confirm this assumption for $H \lesssim -1/2$ as shown in Figure 3.5 of the article. This is a non-trivial piece of information: which fields enter the connectivity fusion is not an easy question, as we discussed in the case of the Potts model in Chapter 4. For greater H, as discussed in the article, strong non-universal effects prevent an accurate numerical analysis of the connectivity (5.22a).
But first and foremost, measuring (5.23) allows to test conformal invariance. Indeed, if the identity belongs to S, then also its descendants must appear in the expansion (5.22a). Two very important descendants of the identity are the level 2 descendants $L_{-2}\mathrm{Id}$ and $\bar{L}_{-2}\mathrm{Id}$: the stress-energy tensor fields T and $\bar{T}$. By their very definition they represent the most direct manifestation of conformal invariance. They also probe the anisotropy of the system, since they are the (non-scalar) fields with the lowest possible dimension $\Delta + \bar{\Delta} = 2$, and provide the dominant term in (5.23):

$$p_{12}(w) - p_{12}(w^\perp) = \frac{d_0^{(2)}}{r^{4\Delta_\sigma}} 4 \frac{2\Delta_\sigma}{c} \cos(2\theta) \langle T \rangle_\tau \left(\frac{r}{N}\right)^2 + \cdots \tag{5.25}$$

where we have replaced $D_{\sigma,\sigma}^{T} = \frac{2\Delta_\sigma}{c}$. The above equation tells us that we can check numerically both the dimension and the spin of the first contribution, by determining the exponent and coefficient of the first r/N term, and the behaviour of the latter with θ. Of course, even if the

5 Fields whose one-point function vanishes for symmetry reasons could indeed belong to S but not contribute to the connectivity, cf. Chapter 4.

stress tensors are present, numerical fits of the connectivity difference to the form (5.25) might give an effective exponent different from 2 if the higher order terms $\cdots$ are not negligible. We assume that the higher order corrections come from the next descendants of the identity, as is the case for pure percolation. To contribute they must have spin $\Delta - \bar{\Delta} = 2 \,\mathrm{mod} 4 = 2, 6, \cdots$. As shown in the Table below, the only such descendants up to order 6 are $L_{-6}\mathrm{Id}$, $L_{-4}L_{-2}\mathrm{Id}$ and $L_{-4}\bar{L}_{-2}\mathrm{Id}$, $L_{-2}^2\bar{L}_{-2}\mathrm{Id}$ as well as their antiholomorphic partners.

Y	$\bar{Y}$	$Y+\bar{Y}$	$Y-\bar{Y}$
2	2	4	0
4	0		4
6	0	6	6
4	2		2
3	3		0

Table 5.1: Descendants of the identity are of the type $L_{-k_1}\cdots L_{-k_n}\bar{L}_{-\bar{k}_1}\cdots\bar{L}_{-\bar{k}_n}\mathrm{Id}$ with $\sum_{k_i} = Y$ and $\sum_{\bar{k}_i} = \bar{Y}$. The ones which can contribute to (5.25) have spin $Y - \bar{Y} = 2, 6$ (we exclude $Y, \bar{Y} = 1$ since the identity is degenerate at level 1 and $Y, \bar{Y} = 3$ since $L_{-3}\mathrm{Id} \propto L_{-1}L_{-2}\mathrm{Id}$ whose one-point function vanishes, see (2.36,2.37).)

From (5.23) we then get:

$$p_{12}(w) - p_{12}(w^\perp) = \frac{d_0^{(2)}}{r^{4\Delta_\sigma}} 4 \left\{ \frac{2\Delta_\sigma}{c} \cos(2\theta) \langle T \rangle_\tau \left(\frac{r}{N}\right)^2 + (a_6 \cos(6\theta) + a_2 \cos(2\theta)) \left(\frac{r}{N}\right)^6 \right\} \tag{5.26}$$

with

$$a_6 = D_{\sigma,\sigma}^{L_{-6}\mathrm{Id}} \langle L_{-6}\mathrm{Id} \rangle + D_{\sigma,\sigma}^{L_{-4}L_{-2}\mathrm{Id}} \langle L_{-4}L_{-2}\mathrm{Id} \rangle \tag{5.27a}$$

$$a_2 = D_{\sigma,\sigma}^{L_{-4}\bar{L}_{-2}\mathrm{Id}} \langle L_{-4}\bar{L}_{-2}\mathrm{Id} \rangle + D_{\sigma,\sigma}^{L_{-2}^2\bar{L}_{-2}\mathrm{Id}} \langle L_{-2}^2\bar{L}_{-2}\mathrm{Id} \rangle. \tag{5.27b}$$

Taking into account these higher order term in the numerical fits, the results obtained confirm beautifully the $\cos(2\theta)$ dependence of the order 2 term, as shown in Figure 3.7 in the article. The order 6 term fairly agrees with the predicted θ dependence (5.26), though numerical precision is difficult to achieve for these subleading corrections (see Figure 3.8). Moreover, although numerical study of the connectivity (5.22a) is difficult for $H > -1/2$ as mentioned above, the non-universal effects cancel out in the difference (5.23), making the above analysis possible on the whole range of H[6]. Our assumptions, the CFT prediction and the numerical results are thereby self-consistent and establish the conformal invariance of the line $H \in [-1, 0[$.

5.4 THE CFT OF PERCOLATION OF RANDOM SURFACES

Exploiting the θ dependence of the torus connectivity allowed to establish conformal invariance. Further information can be extracted from its M/N dependence, through the behaviours of the

6 When H becomes very close to zero however it becomes difficult to evaluate precisely the percolation threshold.

stress-energy tensor and the energy field one-point functions. In Section 5.4.1 we show that from the former we can access the low-lying spectrum of the theory. In Section 5.4.2 we show that the energy field is not degenerate. In Section 5.4.3 we discuss the numerical estimates obtained for quantities involving the central charge and the energy structure constant. Finally in Section 5.4.4 we show that for $H \in [-1, -3/4]$ the numerical data for the two-point connectivity agrees perfectly with the predictions of pure percolation. This strengthens the conjecture [53] that the system is described by the pure percolation universality class for this range of H.

5.4.1 *The spectrum*

From (5.26), the behaviour of the quantity $d_0^{(2)} \frac{2\Delta_\sigma}{c} \langle T \rangle_\tau$ with τ can be obtained by measuring the connectivity difference on torii of different aspect ratios, at fixed value of θ (taken to be zero for convenience, see Section 3.3 of the article for the numerical details). From general conformal field theory on the torus we know that the stress-energy tensor one-point function, viewed as a function of the elliptic nome q, is related to the torus partition function (cf. (2.56)). It is thereby related to the spectrum of the theory. If this latter is discrete, $\langle T \rangle_\tau$ can be expanded as in equation (5.28):

$$\langle T \rangle_\tau = (2\pi)^2 \frac{\frac{c}{24} + n_{\Delta,\bar{\Delta}} \left(\frac{c}{24} - \Delta\right) q^\Delta \bar{q}^{\bar{\Delta}} + \cdots}{1 + n_{\Delta,\bar{\Delta}} q^\Delta \bar{q}^{\bar{\Delta}} + \cdots} = (2\pi)^2 \left(\frac{c}{24} - n_{\Delta,\bar{\Delta}} \Delta q^\Delta \bar{q}^{\bar{\Delta}} + \cdots \right) \tag{5.28}$$

$\Delta, \bar{\Delta}$ are the dimensions of the lowest-lying field $V_{\Delta,\bar{\Delta}}$ (besides the Identity), which has general multiplicity $n_{\Delta,\bar{\Delta}} \in \mathbb{R}$. Measuring directly this one-point function on a thin torus $q \to 0$ (namely, a cylinder) would give an estimate of the central charge. This is possible for instance when a lattice representation of the stress-energy tensor is available, which is not the case here. The quantity we access through the connectivity (5.26) is

$$d_0^{(2)} \frac{2\Delta_\sigma}{c} \langle T \rangle_\tau = d_0^{(2)} \frac{(2 - D_f)\pi^2}{6} \left(1 - 24\Delta \frac{n_{\Delta,\bar{\Delta}}}{c} q^\Delta \bar{q}^{\bar{\Delta}} + \cdots \right) \tag{5.29}$$

and unfortunately the central charge drops from the dominant term. The numerical fits of this quantity as a function of q show that the first low-lying state has dimension $\Delta = \Delta_\sigma$ (Figure 3.16 of the article), at least in the range of H where the fractal dimension is $D_f = D_f^{\text{pure}}$ (cf. Figure 5.2). In the range of H where this dimension changes, the numerics are not accurate enough to give a prediction. This is actually to be expected if the dominant contribution in (5.29) is indeed given by V_σ for all H: when H approaches zero, the fractal dimension approaches 2, and $\Delta_\sigma = \frac{2 - D_f}{2}$ goes to zero.
Note that this result is consistent with assumption 3 that the spectrum is the one of pure percolation, while relying only on assumptions 1 and 2.

5.4.2 *Non-degeneracy of the energy field*

In the CFT of pure percolation, the energy field is degenerate: $V_\varepsilon = V_{(1,2)}^{\text{quot}}$ (cf. previous chapter). In this section we argue that our numerical results for the correlated percolation problem are incompatible with such degeneracy. Indeed let us suppose that the energy field is degener-

ate: $V_\varepsilon = V^{\text{quot}}_{(1,2)}$. Then the only contribution to its one-point function is given by a field with dimension $\Delta_{0,1/2}$ (cf. Section 4.3.1 in the previous chapter):

$$\langle V^{\text{quot}}_{(1,2)}\rangle_\tau = (2\pi)^{2\Delta_{(1,2)}} n_{\Delta_{0,\frac12}} D^{(0,\frac12)}_{(0,\frac12),(1,2)^{\text{quot}}} q^{\Delta_{0,\frac12}} \bar q^{\Delta_{0,\frac12}} + o\left(q^{\Delta_{0,\frac12}} \bar q^{\Delta_{0,\frac12}}\right) \tag{5.30}$$

with the higher order terms coming from the q expansion of $1/Z(q,\bar q)$ in (4.34). Taking $q = \bar q = e^{-2\pi M/N}$ this one-point function behaves as:

$$\log\langle V^{\text{quot}}_{(1,2)}\rangle_\tau \sim \log\left[(2\pi)^{2\Delta_{(1,2)}} n_{\Delta_{0,\frac12}} D^{(0,\frac12)}_{(0,\frac12),(1,2)^{\text{quot}}}\right] + 2\Delta_{0,\frac12}\log q. \tag{5.31}$$

Namely in a log-log plot it should have slope $2\Delta_{0,\frac12}$. Now, if $\Delta_\varepsilon = \Delta_{(1,2)}$, using that:

$$\Delta_\varepsilon = 1 - \frac{1}{2\nu} = 1 + \frac{H}{2}, \qquad \text{(prediction [53])} \tag{5.32}$$

$$\Delta_{(1,2)} = -\frac12 + \frac34\beta^{-2}, \qquad \text{(degenerate dimension (0.8c))} \tag{5.33}$$

we can directly solve for β and relate the central charge to H as:

$$c = -\frac{6 + 11H + 4H^2}{3+H}. \tag{5.34}$$

Then the central charge would vary continuously for $H \in [-3/4, 0]$ as shown in Figure 5.3.

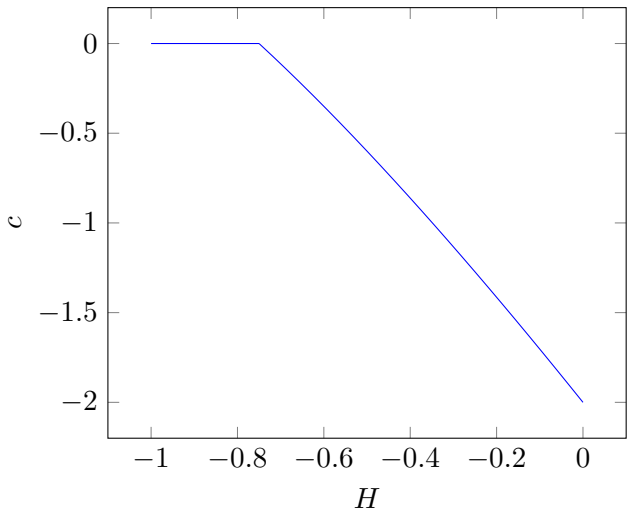

Figure 5.3: Behaviour of the central charge with H, under the assumption that $\Delta_\varepsilon = \Delta_{1,2}$ for all H.

This implies that $\Delta_{0,1/2}$, being a continuously varying function of the central charge:

$$\Delta_{0,\frac12} = \frac12\left(1 - \frac38\beta^{-2} - \frac12\beta^2\right) \tag{5.35}$$

should change continuously with $H > -3/4$, so that the slope in (5.31) should change upon increasing H. This is not what we observe numerically. Indeed, by measuring (5.24) on torii of different aspect ratios, we obtain the behaviour of $\langle V_\varepsilon\rangle_\tau$ with q. It follows the CFT prediction for a generic one-point function (2.20), namely:

$$\log\langle V_\varepsilon\rangle_\tau \sim a + 2\Delta\log q \tag{5.36}$$

as shown in Figure 3.10 of Article IV, where Δ is the most dominant dimension in the expansion (2.20). For the range of H accessible to numerical analysis of the connectivity, $H \in [-1, -1/2]$, we find that the slope 2Δ is given by $2\Delta = 2 - D_f = 2\Delta_\sigma$ (Table 3.11 of Article IV) and is in particular constant for $-3/4 < H \lesssim -1/2$, consistently with Figure 5.2. This result is incompatible with $\langle V_\varepsilon \rangle_\tau$ being given by (5.30) and hence the energy field is not degenerate.
This is an important result: we have seen in Chapter 4 that the presence of the degenerate field $V^{\text{quot}}_{(1,2)}$ in the spectrum of the Potts model leads to shift relations between the structure constants. Having in mind that these two families of models originate from the pure percolation point by introducing long-range correlations (Figure 5.1), it would be interesting to understand what preserves the degeneracy in one case, and destroys it in the other. In particular, is degeneracy of the energy field related to the integrability of the model ?

5.4.3 *More numerical results and how to go further*

In the preceeding sections we analysed the behaviours of $\langle T \rangle_\tau$ and $\langle V_\varepsilon \rangle_\tau$ with q, through the exponent of the dominant term in the q expansion. A byproduct of this analysis is the obtention of the associated coefficients: from the stress-tensor contribution we obtain the ratio n_σ/c (cf. (5.29)), and from the energy contribution we obtain $n_\sigma \left[D^\sigma_{\sigma,\varepsilon}\right]^2$ (cf. equation (2.14) of Article IV). The values for the accessible range of H are given in Tables 3.18 and 3.12 of Article IV.
In Figure 5.4a we report the numerical values of c/n_σ for different Hs. It is intriguing that, despite the numerical errors this ratio seems to stay fairly constant with H in that interval. For comparison we plot in Figure 5.4b the same ratio for the $Q-$Potts model. It seems that both central charge and spin multiplicity n_σ vary in a way that their ratio has a small dependence on H, at least in the range which has been analysed. In any case, this asks for a more thorough and accurate investigation, and especially for a direct estimation of the central charge, in the whole range of H.

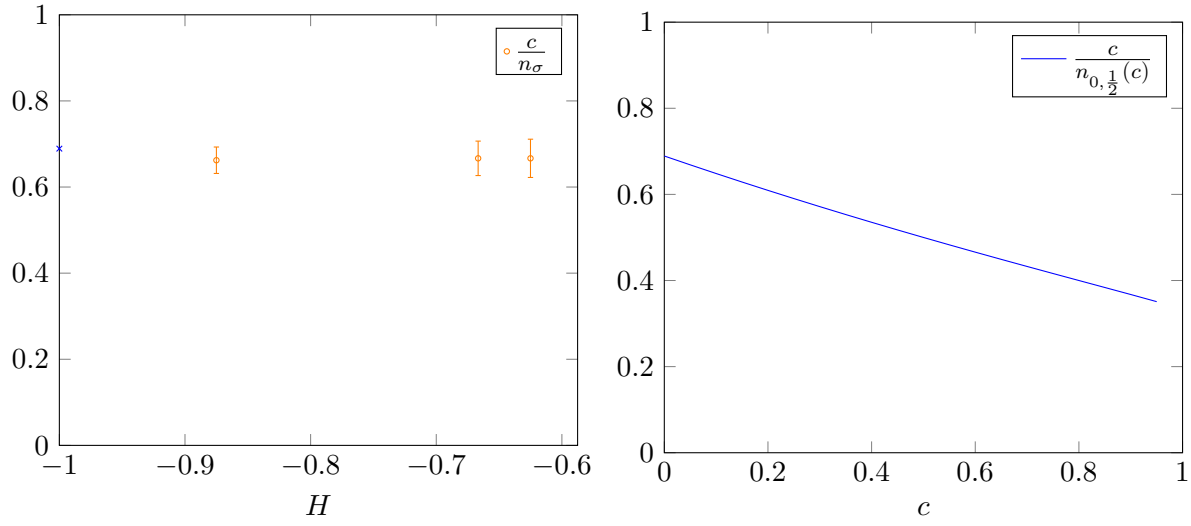

(a) (b)

Figure 5.4: Left: numerical estimates of the ratio c/n_σ. The blue cross corresponds to the exact value for pure percolation obtained as the limit $Q \to 1$ of the Potts model in Article II. Right: the same ratio in the Potts model, where the multiplicity $n_{0,1/2} = Q - 1$ (cf. Section 4.1.1).

In Figure 5.5 we report the numerical values of Table 3.12 for the quantity $\left[D^{\varepsilon}_{\sigma,\sigma}\right]^2 n_\sigma$. They are obtained from the behaviour of the coefficient of the dominant correction in (5.24) with q:

$$D^{\varepsilon}_{\sigma,\sigma}\langle V_\varepsilon\rangle_\tau = (2\pi)^{2\Delta_\varepsilon} n_\sigma \left[D^{\varepsilon}_{\sigma,\sigma}\right]^2 q^{2\Delta_\sigma} + o\left(q^{2\Delta_\sigma}\right) \tag{5.37}$$

The structure constant $D^{\varepsilon}_{\sigma,\sigma}$ and the multiplicity n_σ appear as a product in this coefficient, so that we cannot estimate them separately from measurements of $D^{\varepsilon}_{\sigma,\sigma}\langle V_\varepsilon\rangle_\tau$. However, in principle one can measure directly the one-point function $\langle V_\varepsilon\rangle_\tau$, which has an interpretation in terms of occupation probability (see for instance Section 5.3 in Article II). Taking the ratio $\left[D^{\varepsilon}_{\sigma,\sigma}\langle V_\varepsilon\rangle_\tau\right]_{\text{from } p_{12}} / \left[\langle V_\varepsilon\rangle_\tau\right]_{\text{direct}}$, one obtains $D^{\varepsilon}_{\sigma,\sigma}$. This allows then to estimate n_σ from the values in Table 3.12. Importantly, from the values of n_σ/c in Table 3.18 one can obtain a rough estimate of the central charge for different Hs.

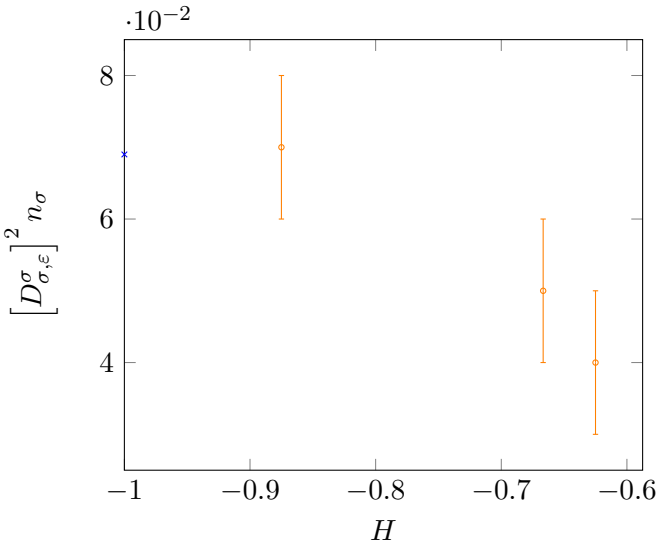

Figure 5.5: Numerical values from Table 3.12 of Article IV. The blue cross is the pure percolation value obtained as the $Q \to 1$ limit of the exact formula for the Potts model, (4.5) in Article II.

5.4.4 *Regime of irrelevant correlations*

The fact that for $H \in [-1, -3/4]$ the system is described by the pure percolation universality class has been tested at the level of critical exponents, by numerical estimation of ν and D_f [54, 116–119, 129]. Nevertheless, although the numerical results for these two exponents show convincingly that they stay equal to their pure value (see for instance Figure 4 in [118], Figure 4 (a) in [116] and Figure 8 in [129]), it is less clear of other critical exponents such as the fractal dimensions of the boundaries [116, 126]. In [126] it is even conjectured, on the basis of the numerical results, that the fractal dimension of the complete perimeter of the percolating cluster varies continuously for $H \in [-1, 0]$.

On the other hand the results on the two-point torus connectivity give strong evidence that the random clusters belong to the pure percolation universality class. They represent a test at the level of highly non-trivial data of the CFT. In particular, the first term in the s-channel

expansion (5.24) is known exactly from the limit $Q \to 1$ of the connectivity in the $Q-$Potts model [51]:

$$p_{12}(r, M = N) = \frac{d_0^{(2)}}{r^{\frac{5}{24}}} \left(1 + (2\pi)^{\frac{5}{4}} \pi \sqrt{3} \left(\frac{4}{9} \frac{\Gamma(\frac{7}{4})}{\Gamma(\frac{1}{4})} \right)^2 e^{-\frac{5\pi}{24}} \left(\frac{r}{N} \right)^{\frac{5}{4}} + \cdots \right). \tag{5.38}$$

This expression involves notably the limit $Q \to 1$ of the quantity $n_\sigma \left[D^\varepsilon_{\sigma,\sigma} \right]^2$. In Figure 5.6a we show the numerical data of the connectivity for Hurst exponent $-1 < H < -3/4$. The agreement with the prediction (5.38) is excellent[7]. By comparison, when $H > -3/4$ a significant deviation from (5.38) is found, as shown in Figure 5.6b. The behaviour is consistent with the fact that the exponent of r/N increases.

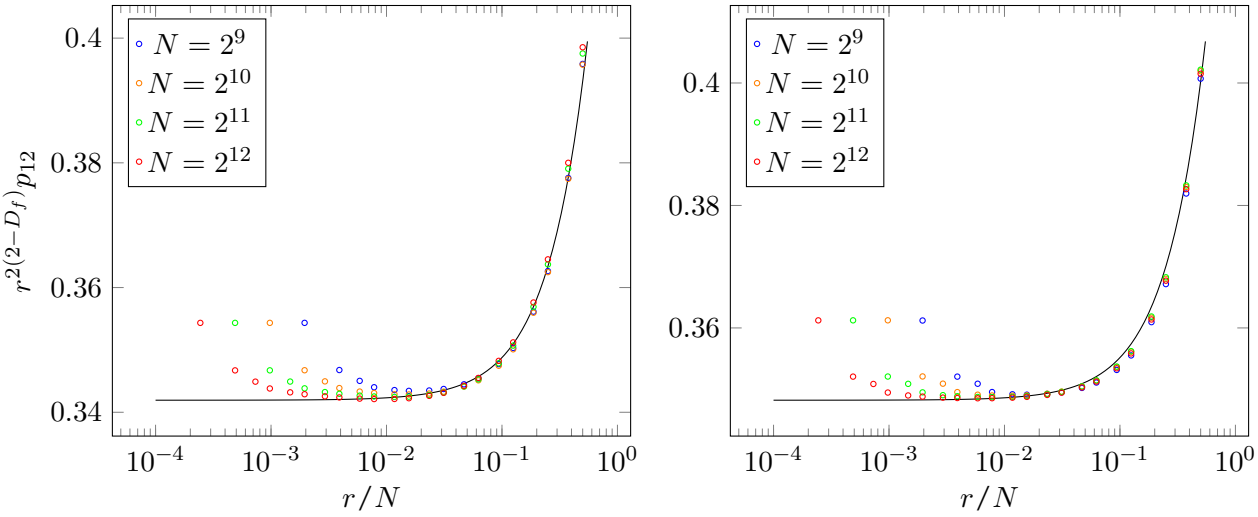

Figure 5.6: Left: numerical data for Hurst exponent $H = -7/8 \in]-1, -3/4]$. Right: numerical data for Hurst exponent $H = -2/3 > -3/4$, where the first topological correction is of order $(r/N)^{\frac{4}{3}}$. In both figures the black curve gives the prediction (5.38) from the CFT of pure percolation.

5.5 THE THREE-POINT CONNECTIVITY

The results of the previous sections are based on full exploitation of the information contained in the torus two-point connectivity. The three-point function on the plane is also an important quantity since it is constrained by *global* conformal invariance to the form (1.59). It follows that the ratio:

$$R(w_1, w_2, w_3) = \frac{p_{123}(w_1, w_2, w_3)}{\sqrt{p_{12}(w_1, w_2) p_{23}(w_2, w_3) p_{13}(w_1, w_3)}} \tag{5.39}$$

7 Further agreement could be found for the rightmost point by computing expansion (5.38) to the next order, ie order 6.

becomes constant in the plane limit and is proportional to the structure constant of three connectivity fields $D^{\sigma}_{\sigma,\sigma}$:

$$R(w_1, w_2, w_3) \overset{\text{plane limit}}{\to} \frac{d_0^{(3)}}{\left[d_0^{(2)}\right]^{3/2}} D^{\sigma}_{\sigma,\sigma}. \tag{5.40}$$

This ratio was studied for instance to determine the constant $D^{\sigma}_{\sigma,\sigma}$ of the Potts model [75] (cf. Introduction of Chapter 4). This was made possible by the fact that for the Potts model [76]:

$$d_0^{(3)} = \left[d_0^{(2)}\right]^{3/2}. \tag{5.41}$$

The ratio (5.39) was also studied in [130] to show numerically the global conformal invariance of a loop ensemble defined on rough surfaces driven by KPZ dynamics. The constant was shown numerically to coincide with the pure percolation one: $d_0^{(3)} / \left[d_0^{(2)}\right]^{3/2} D^{\sigma}_{\sigma,\sigma} = \sqrt{2} C^{\sigma}_{\sigma,\sigma}$ (cf. Section 4.2). Hence in that case too (5.41) seems to be verified. Therefore, in these two models the ratio (5.39) is an universal quantity.

It turns out that (5.41) does not hold for the percolation of random surfaces, as shown in Figure 5.7a. This implies that unfortunately one cannot measure $D^{\sigma}_{\sigma,\sigma}$ in this way. The ratio (5.39) is nonetheless an interesting object. Indeed, because of the strong non-universal effects in the two-point connectivity, less results were obtained in the regime of H where the fractal dimension changes ($H \gtrsim -1/2$). These effects are also present in the three-point connectivity, but cancel in the ratio (5.39) as is visible in Figure 5.7b. This ratio can then be used to carry out a similar analysis as the one described in Section 5.4.

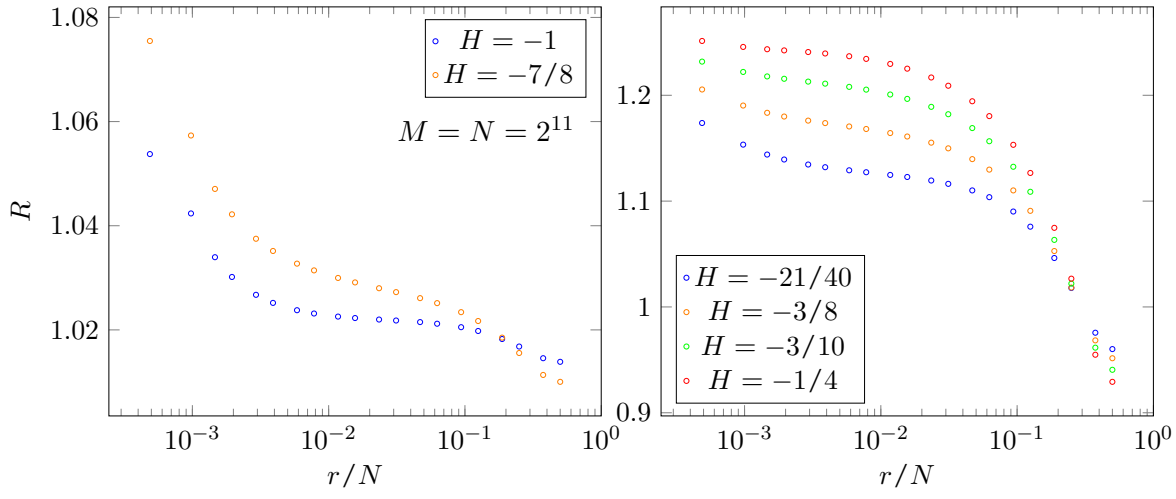

Figure 5.7: Ratio (5.39) measured for w_1, w_2, w_3 at the vertices of an isosceles triangle with $w_{12} = w_{13} = r$. Left: R is measured for two values of $H < -3/4$ where the system should be in the pure percolation universality class. There is a significant increase when $H \neq -1$. Right: the Hurst exponents are greater than $-1/2$, where non-universal effects in the two- and three-point connectivities are strong.

Indeed from the analysis of the topological corrections of the ratio R, one can obtain the same information as from the two-point connectivity. The points are taken to be at the vertices of an isosceles triangle:

$$w_1 = 0 \qquad w_{12} = -r\, e^{i\theta}$$
$$w_2 = r\, e^{i\theta} \qquad w_{13} = -r\, e^{i(\theta+\frac{\pi}{2})}$$
$$w_3 = ir\, e^{i\theta} \qquad w_{23} = r\sqrt{2}\, e^{i(\theta-\frac{\pi}{4})}$$

From the general expressions (2.66) and (2.81) and proceeding as in Section 5.3, we get:

$$p_{12}(r,\theta) = \frac{d_0^{(2)}}{r^{4\Delta_\sigma}}\left(1 + a_\varepsilon^{(2)}\left(\frac{r}{N}\right)^{2\Delta_\varepsilon} + 2\cos(2\theta)a_T^{(2)}\left(\frac{r}{N}\right)^2 + \cdots\right) \tag{5.42a}$$

$$p_{13}(r,\theta) = \frac{d_0^{(2)}}{r^{4\Delta_\sigma}}\left(1 + a_\varepsilon^{(2)}\left(\frac{r}{N}\right)^{2\Delta_\varepsilon} - 2\cos(2\theta)a_T^{(2)}\left(\frac{r}{N}\right)^2 + \cdots\right) \tag{5.42b}$$

$$p_{23}(r,\theta) = \frac{d_0^{(2)}}{(\sqrt{2}\,r)^{4\Delta_\sigma}}\left(1 + a_\varepsilon^{(2)}\left(\frac{\sqrt{2}\,r}{N}\right)^{2\Delta_\varepsilon} + 2\sin(2\theta)a_T^{(2)}\left(\frac{\sqrt{2}\,r}{N}\right)^2 + \cdots\right) \tag{5.42c}$$

$$p_{123}(r,\theta) = \frac{d_0^{(3)}}{(\sqrt{2}\,r^3)^{2\Delta_\sigma}}\left(D^\sigma_{\sigma,\sigma} + a_\varepsilon^{(3)}\left(\frac{\sqrt{2}\,r}{N}\right)^{2\Delta_\varepsilon} + 2\sin(2\theta)a_T^{(3)}\left(\frac{\sqrt{2}\,r}{N}\right)^2 + \cdots\right). \tag{5.42d}$$

The coefficients $a^{(2)}$, $a^{(3)}$ are given by (2.68, 2.78):

$$a_V^{(2)} = D^V_{\sigma,\sigma}\langle V\rangle_\tau \tag{5.43a}$$

$$a_V^{(3)} \sim D^\sigma_{\sigma,\sigma}\, D^V_{\sigma,\sigma} 2^{-\Delta_\sigma}\langle V\rangle_\tau, \tag{5.43b}$$

where we took into account only the dominant contribution in (5.43b). Note that the contribution of the stress-tensor (and of any non-scalar field) drops from p_{23} and p_{123} when $\theta = 0 \bmod \frac{\pi}{2}$, consistentely with the arguments given in Section5.3. Taking the ratio (5.39) and expanding in r/N we obtain at dominant orders:

$$R(r,\theta) = \frac{d_0^{(3)}}{\left[d_0^{(2)}\right]^{3/2}} D^\sigma_{\sigma,\sigma}\left(1 + D^\varepsilon_{\sigma,\sigma}\langle V_\varepsilon\rangle_\tau\left(2^{\Delta_\varepsilon-\Delta_\sigma} - 1 - 2^{\Delta_\varepsilon-1}\right)\left(\frac{r}{N}\right)^{2\Delta_\varepsilon}\right.$$
$$\left. + 2\sin(2\theta)\,\frac{2-D_f}{c}\langle T\rangle_\tau\left(2^{1-\Delta_\sigma} - 1\right)\left(\frac{r}{N}\right)^2 + \cdots\right). \tag{5.44}$$

At $\theta = 0$ one should be able to determine $D^\varepsilon_{\sigma,\sigma}\langle V_\varepsilon\rangle_\tau$ with good precision, since the contribution of T vanishes so that the next correction is of order higher than 2. Conversely, taking:

$$R(r,\theta) - R(r,\theta+\frac{\pi}{2}) = \frac{d_0^{(3)}}{\left[d_0^{(2)}\right]^{3/2}} D^\sigma_{\sigma,\sigma} \times 4\frac{2-D_f}{c}\langle T\rangle_\tau\left(2^{1-\Delta_\sigma} - 1\right)\sin(2\theta) \tag{5.45}$$

at say, $\theta = \pi/4$ one obtains $\langle T\rangle_\tau$. Measuring these quantities as functions of the aspect ratio one can follow the same analysis as in Section 5.4.3. and thereby explore the line $-1/2 \le H < 0$. It would be especially interesting to see wether n_σ/c shows variation in this range of H.

5.6 CONCLUSION

We have developed a new method to analyse a percolation-type transition, based on the exploitation of the topological corrections to the two-point connectivity. This method allows to directly test conformal invariance of the random clusters measure. In addition we obtain information on the underlying CFT. Applying this method to the percolation of random surfaces we showed that the clusters are conformally invariant. We obtained the first features of the (almost completely unknown) underlying CFT, beyond the critical exponents.
In the range $H \in [-1, -3/4]$, the numerical measurements of the connectivity show excellent agreement with the predictions of the CFT of pure percolation. This gives strong support to the conjecture that the system is described by the pure percolation universality class for these values of H. Indeed it is not only true concerning the thermal and magnetic exponents, but also at the level of finer CFT data, through quantities involving the spin multiplicity and the energy structure constant.
The main results in the range of H where correlations become relevant are that the low-lying states in the spectrum stay the same as in pure percolation, and that the energy field becomes non-degenerate. Further work, based on direct measurement of the energy one-point function, could permit to evaluate the central charge, the spin multiplicity and the energy structure constant separately. Obtaining estimates of the central charge for different values of H is especially crucial. It would allow notably a comparison with the values of the central charge that one can compute from the values of the diffusion coefficient κ obtained in [126, 127].

Solving completely this new CFT appears as an extremely difficult task, given that the CFT of pure percolation is still not fully solved today. In particular, the non-degeneracy of the energy field let us foresee that the relations between the structure constants, which proved crucial in understanding the pure percolation CFT (cf. previous chapter), are absent here. Nevertheless, there are a number of interesting aspects which can be explored without the need of a complete CFT solution.
First the model offers another example of a statistical system where a non-local quantity – the connectivity– is given by a correlator of local fields in a (conformal) quantum field theory. Understanding what features of a system make this relation hold is a vast open question. We learn from this model that integrability is not a necessary condition.
It also offers an example where the ratio of three- to two-point connectivities is not universal. This is quite unexpected from what has been observed in other models, belonging to the Potts universality class.
Of particular importance is the intriguing property that the bulk fractal dimension D_f seems to be superuniversal, ie. remains the same in different universality classes, up to some threshold value $H \sim -1/2$. Understanding if this is really the case and how such behaviour arises are open problems in their own right. Even more puzzling are the facts, indicated by the previous numerical results [116, 126, 127], that the fractal dimensions of the boundaries of the percolating cluster seem to vary continuously as soon as correlations are turned on ($H > -1$), and that their values seem to coincide with the fractal dimensions of the Potts clusters boundaries [41]. In this chapter we have given arguments that the statistical properties of the interior of the clusters are not given by the Potts universality class, and one can wonder wether the same CFT describes both the interior and the boundaries of these clusters.

At a more general level it remains to be understood what features make models with the same asymptotic decay of correlations fall into disctinct universality classes. As an example, the nodal clusters (level clusters at level zero) of the vorticity field of a turbulent fluid [107], or the ones of random wavefunctions of chaotic systems [109, 131] belong to the pure percolation universality class, although the decay of correlations in these models correspond to values of $H > -3/4$.

SciPost Phys. 9, 050 (2020)

Topological effects and conformal invariance in long-range correlated random surfaces

Nina Javerzat[⋆], **Sebastian Grijalva, Alberto Rosso and Raoul Santachiara**

Université Paris-Saclay, CNRS, LPTMS, 91405, Orsay, France

⋆ nina.javerzat@u-psud.fr

Abstract

We consider discrete random fractal surfaces with negative Hurst exponent $H < 0$. A random colouring of the lattice is provided by activating the sites at which the surface height is greater than a given level h. The set of activated sites is usually denoted as the excursion set. The connected components of this set, the level clusters, define a one-parameter (H) family of percolation models with long-range correlation in the site occupation. The level clusters percolate at a finite value $h = h_c$ and for $H \leq -\frac{3}{4}$ the phase transition is expected to remain in the same universality class of the pure (i.e. uncorrelated) percolation. For $-\frac{3}{4} < H < 0$ instead, there is a line of critical points with continously varying exponents. The universality class of these points, in particular concerning the conformal invariance of the level clusters, is poorly understood. By combining the Conformal Field Theory and the numerical approach, we provide new insights on these phases. We focus on the connectivity function, defined as the probability that two sites belong to the same level cluster. In our simulations, the surfaces are defined on a lattice torus of size $M \times N$. We show that the topological effects on the connectivity function make manifest the conformal invariance for all the critical line $H < 0$. In particular, exploiting the anisotropy of the rectangular torus ($M \neq N$), we directly test the presence of the two components of the traceless stress-energy tensor. Moreover, we probe the spectrum and the structure constants of the underlying Conformal Field Theory. Finally, we observed that the corrections to the scaling clearly point out a breaking of integrability moving from the pure percolation point to the long-range correlated one.

Received 03-06-2020
Accepted 17-09-2020
Published 12-10-2020
doi:10.21468/SciPostPhys.9.4.050

Check for updates

Contents

1 Introduction

The percolative properties of random fractal surfaces have been studied for a long time [1–4]. The universality class of their critical points remains a very active subject of research in the mathematical [5–7] and in the theoretical physics [8] communities, mainly because they challenge our understanding of both the emergence of conformal symmetry and of the way this symmetry is implemented.
Let us consider a random stationary function $u(\mathbf{x})$ on a lattice $u(\mathbf{x}) : \mathbb{Z}^2 \to \mathbb{R}$ which satisfies:

$$\mathbb{E}[u(\mathbf{x})] = 0, \quad \mathbb{E}\left[(u(\mathbf{x}) - u(\mathbf{y}))^2\right] \sim C(H)\,|\mathbf{x}-\mathbf{y}|^{2H} \quad (|\mathbf{x}-\mathbf{y}| >> 1), \tag{1}$$

where $\mathbb{E}[\cdots]$ is the average over the instances of $u(\mathbf{x})$, the symbol $\sim$ stands for asymptotically equivalent and $C(H)$ is some constant depending on H. The number H, $H \in \mathbb{R}$, is the surface roughness exponent [9], also known as Hurst exponent. The fractional Gaussian surfaces [7] that we consider here, see (4) below, is a class of random surfaces which satisfy the above properties. For positive $H > 0$, the function $u(\mathbf{x})$ is a fractional Brownian surface with unbounded height fluctuations, $\mathbb{E}\left[u(\mathbf{x})^2\right] = \infty$. The fluctuations remain unbounded also for $H = 0$ in which case the covariance decreases logarithmically, $\mathbb{E}[u(\mathbf{x})u(\mathbf{0})] \sim -\log|\mathbf{x}|$. For negative exponent $H < 0$, $u(\mathbf{x})$ is a long-ranged correlated surface with bounded fluctuations, $\mathbb{E}\left[u(\mathbf{x})^2\right] < \infty$.
A random partition of the lattice is obtained by setting a level h, $h \in \mathbb{R}$, and by declaring that a site $\mathbf{x}$ is activated (not activated) if $\theta_h(\mathbf{x}) = 1$ ($\theta_h(\mathbf{x}) = 0$), where $\theta_h(\mathbf{x}) : \mathbb{Z}^2 \to \{0, 1\}$:

$$\theta_h(\mathbf{x}) = \begin{cases} 0, & u(\mathbf{x}) < h \\ 1, & u(\mathbf{x}) \geq h. \end{cases} \tag{2}$$

A site is therefore activated with probability $p(h)$:

$$p(h) = \mathbb{E}[\theta_h(\mathbf{x})], \tag{3}$$

where we use the translational invariance in law. The set of activated points is usually known as the excursion set [10]. The study of the connected components of the excursion set, hereafter referred to as level clusters, defines a site percolation model [8, 11]. For general values of H there is a finite value of $h = h_c > -\infty$ below which a level cluster of infinite size is found with probability one [12]. This is the percolation critical point. Note that the characterisation of the class of random fields which permit percolation has been given in [2, 13, 14]. Close to the critical point, the main scaling behaviours are described by two critical exponents, the correlation length ν and the order parameter β exponents [11]. In particular, they determine the scaling of the h_c width distribution with the size of the system, see (56), and the Hausdorff dimension D_f of the level cluster, $D_f = 2 - \beta/\nu$. For $H > 0$, due to unbounded fluctuations of $u(\mathbf{x})$ and to the strong correlations, the level clusters are compact (i.e. without holes) regions with fractal dimension $D_f = 2$. The exponent ν is infinite $\nu = \infty$, as one can see from the fact that the h_c width distribution remains finite in the thermodynamic limit (self-averaging is broken) [12]. At $H > 0$ the transition is not critical. At the point $H = 0$, the fluctuations of the surface remain unbounded and the fractal dimension remains $D_f = 2$, as argued in [15] and recently proven in [16, 17] for the Gaussian free field. For negative roughness exponent instead, the surface fluctuations are bounded, the correlation length exponent ν is finite ($\nu < \infty$) and a genuine continous transition of percolation type occurs. Correspondingly, the level clusters have a richer fractal structure with $D_f < 2$.

In this paper we consider random surfaces with negative roughness exponent. If not stated otherwise, we take $H < 0$ henceforth. We generate a fractional Gaussian process on a flat torus of dimension $M \times N$. The surface $u(\mathbf{x})$ takes the form

$$u(\mathbf{x}) \propto \sum_{\mathbf{k}} \lambda_{\mathbf{k}}^{-\frac{H+1}{2}} \, \hat{w}(\mathbf{k}) \, e^{i\,\mathbf{k}\,\mathbf{x}}. \tag{4}$$

In the above equation $\lambda_{\mathbf{k}}$ and $e^{i\,\mathbf{k}\,\mathbf{x}}$ are respectively the eigenvalues and the eigenvectors of the discrete Laplacian operator $\Delta_{\mathbf{x}} u(\mathbf{x}) = \sum_{\mathbf{y},|\mathbf{y}-\mathbf{x}|=1} (u(\mathbf{y}) - u(\mathbf{x}))$ on the flat torus, and the $\hat{w}(\mathbf{k})$ are independent normally distributed random variables. The basic idea is to obtain correlated variables by convoluting uncorrelated ones. For $H = 0$ the function $u(\mathbf{x})$ is the discrete two-dimensional Gaussian free field on the torus. The role of open boundary conditions in one-dimensional fractional Gaussian processes is discussed in [18–20]. We generate also a second type of long range correlated random surface where the $\hat{w}(\mathbf{k})$ are drawn by a different distribution. Full details on how we generate the surfaces are given in Appendix A.

The probability of activating two distant sites inherits the long-range correlation of the random surfaces:

$$\mathbb{E}[\theta_h(\mathbf{x})\theta_h(\mathbf{y})] - p(h)^2 \sim C'(H)|\mathbf{x}-\mathbf{y}|^{2H} \quad (|\mathbf{x}-\mathbf{y}| \to \infty), \tag{5}$$

where $C'(H)$ is some constant depending on H and on the chosen distribution. For $H = -1$ the surfaces we generate are an instance of the two-dimensional white noise where the probabilities of activating two different sites are uncorrelated ($C'(-1) = 0$ in the above equation). The point $H = -1$ corresponds therefore to the pure percolation point. In Figure 1 we show instances of the surfaces (4) and the corresponding excursion set and level clusters at the critical point.

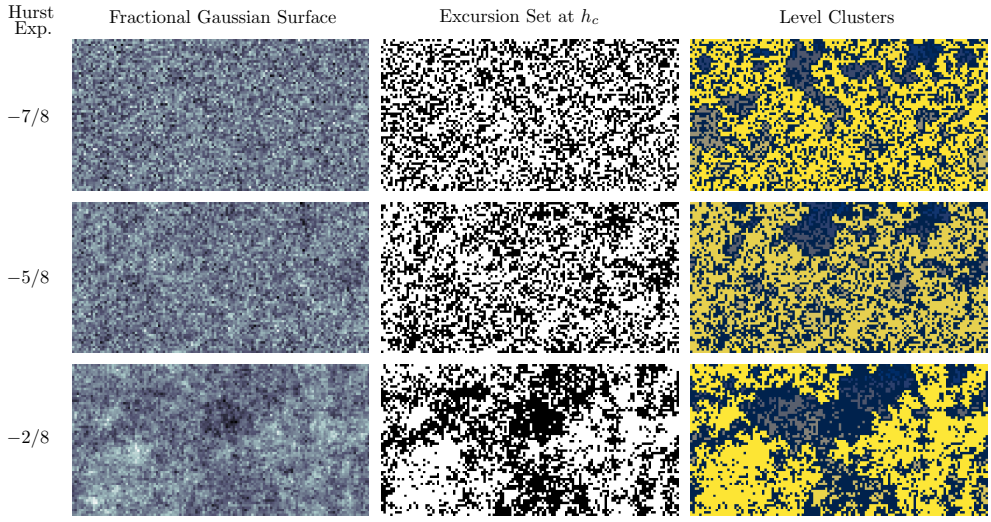

Figure 1: Instances of the fractional Gaussian surfaces (4) for $H \in \{-7/8, -5/8, -2/8\}$, generated on a $M \times N$ square lattice with $M = 2N$, $N = 2^6$. The excursion sets (white points) corresponding to level $h = h_c$ from Table 10 are shown in the second column, while the third column shows the level clusters. The yellow points in the third column are the points belonging to the percolating level cluster. Note that by increasing H, i.e. the correlation, the level clusters have less holes. This is consistent with the prediction that the fractal dimension $D_f \to 2$ for $H \to 0^-$.

The common understanding is that the percolating universal properties only depend on the asympotic behaviour of the covariance (1) and therefore on H. In [21] an extended Harris criterion was proposed, according to which the universality class remains the one of pure percolation for $H < -3/4$. Recent new arguments, based on the fractal dimension of the pivotal points support this prediction [22, 23]. The exponents ν and D_f are expected to be

$$\nu = \nu^{\text{pure}} = \frac{4}{3}, \quad D_f = D_f^{\text{pure}} = \frac{91}{48}, \quad \text{for } H \leq -\frac{3}{4}, \tag{6}$$

where ν^{pure} and D_f^{pure} are the pure percolation ($H = -1$) exponents. The fact that the system behaves as pure percolation for $H < -2$ was put on more rigorous grounds by [5, 24]. For $-3/4 < H < 0$ instead, the slower decay allows the correlation to change the large distance behaviour of the system, as was also argued in [3]. In particular, it was shown in [21] that there is a new line of critical points with an exponent $\nu = \nu^{\text{long}}$ which varies continuously with H:

$$\nu = \nu^{\text{long}} = -\frac{1}{H}, \quad -\frac{3}{4} < H < 0. \tag{7}$$

The above prediction was supported by many numerical works, see for instance [3, 4, 12, 25, 26]. There are no theoretical predition for D_f in the range $-3/4 < H < 0$. In Figure 1 the level clusters become visibly more compact by increasing the value of H. One can expect then D_f to increase when $H \to 0^-$. Even if the numerical results are not conclusive about the value of D_f^{long}, there are strong evidences that [12, 25–27]:

$$D_f = D_f^{\text{pure}} \quad \text{for } H \leq -\frac{1}{2}, \quad \text{and} \quad D_f^{\text{pure}} < D_f < 2 \quad \text{for } -\frac{1}{2} < H < 0. \tag{8}$$

In Appendix B, we numerically compute D_f. The results, summarised in Table 12, support the above scenario. The following diagram summarises the actual state of the art:

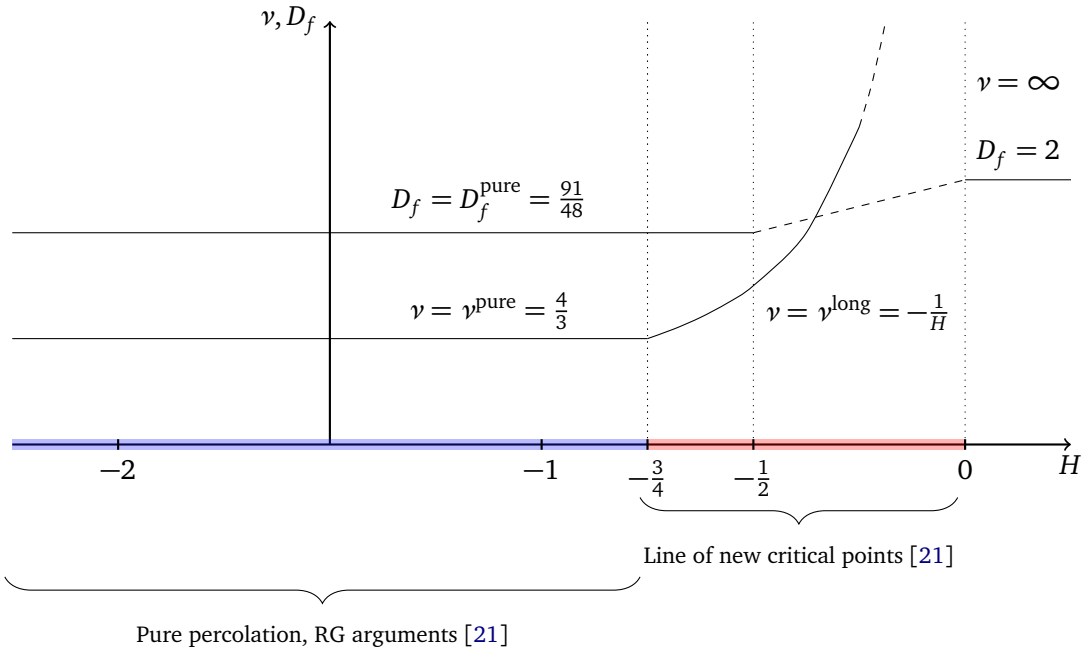

Figure 2

We stress the fact that the results mentioned above are based on the assumption that the kernel has a definite sign at large distances. For other important classes of random functions, this is not true anymore. This is the case for instance of the random plane wave [28]: this random function has an oscillating kernel which decays with an exponent $H = -1/4$, and the universality class of its percolation transition is conjectured to be the one of pure percolation [29].

Most of the results on critical pure percolation have been discovered by using conformal invariance [30]whose emergence has been rigourously proven in [31]. The values (6) have been predicted by the conformal field theory (CFT) approach [32,33], which allowed also the computation of the full partition function [34] and the derivation of exact formulas for cluster crossing probabilities [35]. Contrary to statistical models with local and positive Boltzmann weights, whose critical points are described by the unitary minimal models [36], the critical point of pure percolation is described by a non-unitary and logarithmic CFT [37,38]. This CFT is not fully known, but very recent results have paved the way to its complete solution [37–43]. The line of new critical points shown in Figure 2 remains by far less understood. As we will discuss below, even the emergence of conformal invariance is debated. Moreover, if these points are conformal invariant we expect that the corresponding CFT does not coincide with any of the known solutions, due to the highly non-local nature of the lattice model. This will be indeed confirmed by the results presented in this paper.

Recent numerical results have shown the emergence of conformal invariance [44], while in [45], where a random surface with $H = -2/3$ was considered, conformal symmetry has been ruled out. These papers check if the boundary of the percolation level cluster is described by a Stochastic Loewner Evolution (SLE) process [46]. The SLE numerical tests are in general very subtle and, in some cases not conclusive, as argued for instance in [47]. Moreover we observe that, in case of a positive SLE test as in [44], one expects the boundaries of the level clusters to be described by the loops of the $O(n)$ models either in their dense or critical phases [48]. In these models, the fractal dimensions of the loops D_b and of their interior D_f vary with n [49]. For instance, in the $O(n)$ dense phase, they are related by $D_f = D_b(2-3D_b)/(4(1-D_b))$. This

scenario is not consistent with the numerical findings for the level clusters of long-range correlated random surfaces, as can be directly seen from the fact that D_f does not show significant variation for $-3/4 < H < -1/2$ while D_b does [44]. Moreover, we provide further evidences that the line $-3/4 < H < 0$ is not the one of the $O(n)$ models. This point illustrates the fact that many fundamental questions remain open.

Our objective is to test conformal invariance and to extract new information about these critical points. We use a completely different protocol based on the study of the level clusters and their connectivity function. This is the probability that two sites belong to the same level cluster, see (10). Because the random surfaces have double periodicity, the level clusters live on a torus. For pure percolation, signatures of conformal invariance were shown to be encoded in toric boundary conditions effects in the connectivity function [50]. These effects depend on a non trivial combination of the two exponents ν and D_f, fixed by conformal invariance. Moreover, when the lattice is rectangular, $M \neq N$, a soft breaking of rotational symmetry is introduced. Using this anisotropy, we show that the connectivity function directly probes the existence of the two components of a traceless stress-energy tensor. The existence of this pair of fields is the most basic manifestation of conformal symmetry. Finally, we provide the first numerical measurements of quantities related to the conformal spectrum and structure constants of this new conformal critical points.

In Section 2 we define the connectivity function and we give the theoretical predictions for the toric effects. We discuss the main ideas behind the CFT approach on which these predictions are based. In Section 3 we provide the numerical evidences on the connectivity function. In Appendix A we provide full details on how we generate the random surfaces and in Appendix B, on how we locate the critical percolation point and compute the exponents ν and D_f.

2 Critical two-point connectivity of level clusters

In this section we consider the two-point connectivity $p_{12}(\mathbf{x_1}, \mathbf{x_2})$, referred to as simply correlation function in [11]. Defining the event:

$$\text{Conn}(\mathbf{x_1}, \mathbf{x_2}) = \mathbf{x_1} \text{ and } \mathbf{x_2} \text{ belong to the same level cluster,} \tag{9}$$

we define:

$$p_{12}(\mathbf{x_1} - \mathbf{x_2}) = \mathbb{E}\left[\text{Conn}(\mathbf{x_1}, \mathbf{x_2})\right], \tag{10}$$

where translational invariance in law has been taken into account. A study of two-point connectivity for general Gaussian random surfaces can be found in [51] where the large h asymptotic behaviour of (10) has been considered. Here we are interested in the behaviour of this probability at the critical point $h = h_c$.

2.1 Scaling limit in the infinite plane $M, N = \infty$

Let us consider first the regime in which toric size effects are negligeable. It corresponds to $M, N = \infty$, i.e. the infinite plane limit.
At the critical point, $h = h_c$, we have $p_{12}(\mathbf{x}) \sim |\mathbf{x}|^{-\eta}$, where η is the standard notation for the anomalous dimension of the two-point function [11]. Percolation theory tells us that η is directly related to the level cluster dimension D_f via the scaling relation $\eta = 4 - 2D_f$ [52]. One has therefore:

$$p_{12}(\mathbf{x_1} - \mathbf{x_2}) = \frac{d_0}{|\mathbf{x_1} - \mathbf{x_2}|^{2(2-D_f)}} \quad (|\mathbf{x_1} - \mathbf{x_2}| >> 1,\ M, N = \infty), \tag{11}$$

where d_0 is a non-universal constant which we evaluate numerically, see Table 1. We can use (11) to determine D_f. The corresponding values are denoted as $D_f^{(2)}$ in Table 12. The good agreement with the values $D_f^{(1)}$, obtained using the scaling of the average mass of the percolating level cluster (see Appendix B), confirms that we are sitting sufficiently close to the critical value h_c.
In Figure 3 we show the behaviour of $p_{12}(\mathbf{x_1}-\mathbf{x_2})$ for $H=-5/8$. One can easily notice a region $|\mathbf{x_1}-\mathbf{x_2}|\in[10,100]$ where the form (11) is well satisfied.

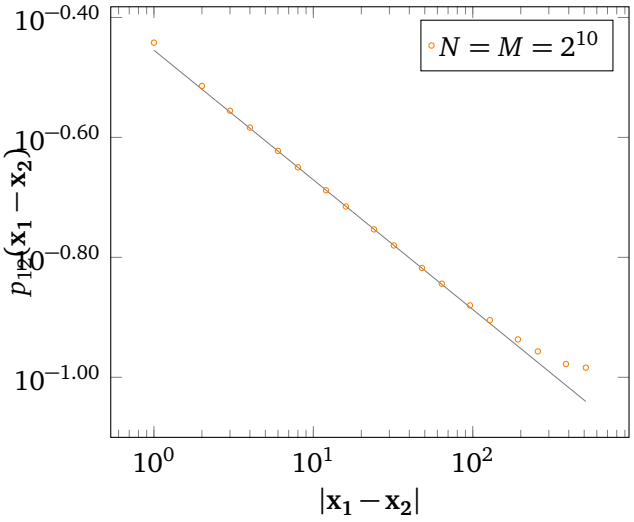

Figure 3: Two-point connectivity (10) for $H=-5/8$ and $N=M=2^{10}$. The data points were obtained by averaging over 10^5 instances of the surface and over the N^2 locations of point $\mathbf{x_1}$ (cf. Section 3). According to Table 10, the level h has been set to $h_c=-0.1985$. The continuous line shows the prediction (11) with $D_f=D_f^{(2)}=1.892$, see Table 12. For distances $6<|\mathbf{x_1}-\mathbf{x_2}|<100$ the data matches very well with the infinite plane prediction. For larger distances, the effect of the toric boundary conditions becomes visible.

2.2 Scaling limit in the torus: $M,N<\infty$.

As can be seen in Figure 3, when the distance between points approaches $N/2$, the data points start to deviate from the power-law behaviour: the contributions of the paths connecting the two points on the other side of the torus become non negligeable. We say that the topological corrections become visible. We expect these corrections to provide sub-leading $|\mathbf{x}|/N$ terms in (11) of universal nature. These effects have been studied in [50] for pure percolation ($H=-1$).
In the scaling limit, our system lives on a flat torus $\mathbb{T}_q$ of periods M and N and nome q:

$$\mathbb{T}_q: \quad q=e^{-2\pi\frac{M}{N}}. \tag{12}$$

As the connectivity between two points always depend on the vector connecting them, it is convenient to introduce the vector $\mathbf{x},\mathbf{x}^\perp\in\mathbb{T}_q$ that have polar coordinates $|\mathbf{x}|$ and θ:

$$\mathbf{x}\in\mathbb{T}_q, \quad \mathbf{x}=|\mathbf{x}|(\cos(\theta),\sin(\theta)), \quad \mathbf{x}^\perp=|\mathbf{x}|(-\sin(\theta),\cos(\theta)). \tag{13}$$

We propose the following form for the scaling limit of p_{12} on a torus:

$$p_{12}(\mathbf{x})=\frac{d_0}{|\mathbf{x}|^{2(2-D_f)}}\left(1+c_\nu(q)\left(\frac{|\mathbf{x}|}{N}\right)^{2-\frac{1}{\nu}}+2c_T(q)\cos(2\theta)\left(\frac{|\mathbf{x}|}{N}\right)^2+o\left(\left(\frac{|\mathbf{x}|}{N}\right)^2\right)\right), \tag{14}$$

which has been established in [50] for pure percolation and for the more general random cluster Q—Potts model. The coefficients $c_\nu(q)$, and $c_T(q)$, given in (19), are universal coefficients which depend only on the geometry of the torus. To explain the origin of (14) and the information we can extract from this formula, we need to recall some basic definitions and notions on CFT.

2.3 Basic notions of CFT

A CFT is a massless quantum field theory in which each (quantum) field $V_{\Delta,\bar\Delta}(\mathbf{x})$ is characterised by a pair of numbers $(\Delta,\bar\Delta)$, called left and right conformal dimensions, which give the scaling dimension ($\Delta^{\rm phys}=\Delta+\bar\Delta$) and the spin ($s=\Delta-\bar\Delta$) of the field. The set of fields entering a CFT is called the spectrum $\mathcal{S}$ of the theory, $\mathcal{S}=\oplus_{(\Delta,\bar\Delta)}V_{(\Delta,\bar\Delta)}$. The most important landmark of conformal invariance is the existence of two fields, commonly denoted as T and $\bar T$, with left-right dimensions $(\Delta,\bar\Delta)=(2,0)$ and $(\Delta,\bar\Delta)=(0,2)$. These fields are the conserved (chiral) Noether current associated to the conformal symmetry, and they correspond to the components of the traceless stress-energy tensor field.
In the CFT approach to statistical models, there is a correspondence between lattice operators and fields $V_{\Delta,\bar\Delta}(\mathbf{x})$. In particular, the long distance behaviour of lattice observables is described by the correlation functions of the fields $V_{\Delta,\bar\Delta}(\mathbf{x})$. Scale invariance fixes the infinite plane limit of the two-point functions. For a spinless field $V_{\Delta,\Delta}$ we have:

$$\left\langle V_{\Delta,\Delta}(\mathbf{x})V_{\Delta,\Delta}(0)\right\rangle_q = |\mathbf{x}|^{-4\Delta} \quad \left(\frac{|\mathbf{x}|}{N}\to 0\right), \tag{15}$$

where $\langle\cdots\rangle_q$ denotes the torus CFT correlation function on $\mathbb{T}_q$. A quantum field theory is completely solved if we can compute all its correlation functions. For a CFT, one needs two basic inputs: the spectrum $\mathcal{S}$ and the structure constants $C^{V_3}_{V_1,V_2}$. The latter are real constants associated to the amplitude with which two fields V_1 and V_2 fuse into a third one V_3. Said in other words, the constants $C^{V_3}_{V_1,V_2}$ determine the short-distance behaviour of the CFT correlation functions which is encoded, in the CFT jargon, in the Operator Product Expansion (OPE).
Among all the fields in a CFT, a major role is played by the density energy field $\varepsilon=V_{\Delta_\varepsilon,\Delta_\varepsilon}$ and the magnetic (order parameter) field $\sigma=V_{\Delta_\sigma,\Delta_\sigma}$, which are the (spinless) fields with the lowest scaling dimension in the thermal and magnetic sector. Their names come from the fact that, in a ferromagnetic/paramagnetic type transition, these are the fields which couple respectively to the temperature and to the magnetic field. Their dimensions Δ_ε and Δ_σ give the exponents ν and β of a critical point [53, Chapter 3]. In terms of ν and $D_f=(4-\eta)/2=2-\beta/\nu$ [11, Section 3.3] we have:

$$\Delta_\varepsilon=1-\frac{1}{2\nu},\quad \Delta_\sigma=1-\frac{D_f}{2}. \tag{16}$$

2.4 Three main assumptions

Our prediction (14) is based on three assumptions which have been verified for pure percolation [50, 54]. The first two assumptions are more general and concern the fact that the connectivity, which is non-local in nature, can be studied by correlations of local fields in a CFT.

- **1:** The system is conformally invariant in the scaling limit.
- **2:** The scaling limit of the connectivity (10) is described by the two spin field torus correlator:

$$p_{12}(\mathbf{x})=d_0\ \langle\sigma(\mathbf{x})\sigma(0)\rangle_q\,. \tag{17}$$

The two-point function $\langle\sigma\sigma\rangle_q$ can be expressed as an (s-channel) expansion:

$$p_{12}(\mathbf{x}) = d_0 \langle\sigma(\mathbf{x})\sigma(0)\rangle_q = \frac{d_0}{|\mathbf{x}|^{4\Delta_\sigma}} \sum_{\substack{V_{\Delta,\bar\Delta}\in\mathcal{S} \\ \Delta\geq\bar\Delta}} (2-\delta_{\Delta,\bar\Delta})\, C_{\sigma,\sigma}^{V_{\Delta,\bar\Delta}} \langle V_{\Delta,\bar\Delta}\rangle_q \cos\big((\Delta-\bar\Delta)\,\theta\big)\left(\frac{|\mathbf{x}|}{N}\right)^{\Delta+\bar\Delta}, \tag{18}$$

with $\mathbf{x} = |\mathbf{x}|(\cos(\theta),\sin(\theta))$, see (13). In general, p_{12} does not get contributions from all the fields in the spectrum $\mathcal{S}$, since structure constants $C_{\sigma,\sigma}^{V_{\Delta,\bar\Delta}}$ and/or one-point functions $\langle V_{\Delta,\bar\Delta}\rangle_q$ may vanish. We refer the reader to [50] for a detailed derivation of the above formula which is a direct consequence of the existence of an operator algebra and of the symmetry between the holomorphic and anti-holomorphic sectors. This latter symmetry is very natural for CFTs without boundaries and implies that if a field with spin $s > 0$ enters in the spectrum, then also its anti-holomorphic partner does, with the same physical dimension and with spin with opposite sign $-s$. The expansion (18) is then valid for almost all the CFTs. The information which characterise a specific CFT is encoded in the spectrum $\mathcal{S}$ and in the structure constants $C_{\sigma,\sigma}^{V_{\Delta,\bar\Delta}}$. In the case of pure percolation, for instance, the spectrum is known but not the structure constants, even if very recent progresses have paved the way to their determination [43]. The plane limit $M,N=\infty$ is recovered by noting that all the one-point functions $\langle V_{\Delta,\bar\Delta}\rangle_q$ vanish but the identity one $\langle\mathrm{Id}\rangle_q = \langle V_{0,0}\rangle_q = 1$. One obtains $p_{12}(\mathbf{x}) = d_0|\mathbf{x}|^{-4\Delta_\sigma}$ ($M,N=\infty$). Note that, in the infinite plane limit, one can prove for pure percolation (or more generally for the $O(n)$ models in their dense or critical phases) that p_{12} is given by the correlator of two spin fields σ, see for instance [49,55]. The exponent η is therefore $\eta = 4\Delta_\sigma$ which, by (16) gives equation (11).

It has been shown in [50] that the first dominant terms in the above series can be computed for pure percolation. Our third assumption is motivated by a generalisation of these results to the case of long-range percolation:

- **3:** The identity field ($\Delta=\bar\Delta=0$), the density energy density field ε and the stress-energy tensor fields T ($\Delta=2,\bar\Delta=0$), $\bar T$ ($\Delta=0,\bar\Delta=2$) are the fields with the lowest conformal dimension that appear in the fusion of two fields σ and whose torus one-point function does not vanish.

Using the above assumption in the expansion (18), one obtains expression (14) with the coefficients $c_\nu(q)$ and $c_T(q)$ given by:

$$c_\nu(q) = C_{\sigma,\sigma}^{\varepsilon}\langle\varepsilon\rangle_q, \quad c_T(q) = C_{\sigma,\sigma}^{T}\langle T\rangle_q = \frac{2\Delta_\sigma}{c}\langle T\rangle_q, \tag{19}$$

where c is the CFT central charge (which provides for instance the universal Casimir amplitude [56]). We refer the reader to [50,54] for a detailed explication of the CFT techniques used to study the topological effects.

Let us detail further the information one can extract from $c_\nu(q)$ and $c_T(q)$. The spectrum $\mathcal{S}$ and some structure constants $C_{V_1,V_2}^{V_3}$ enter in the determination of these coefficients. For a general CFT, the spectrum defines the torus partition function [57]:

$$Z(q) = q^{-\frac{c}{12}} \sum_{V_{\Delta,\bar\Delta}\in\mathcal{S}} n_{V_{\Delta,\bar\Delta}}\, q^{\Delta+\bar\Delta}, \tag{20}$$

where $n_{V_{\Delta,\bar\Delta}}$ is the multiplicity of the field $V_{\Delta,\bar\Delta}$. For small values of q, the leading contributions to the partition function are given by the representations with the smallest physical dimensions. The Identity field $V_{0,0}$ has the lowest physical dimension 0, with $n_{\mathrm{Id}}=1$. We will assume that

the sub-leading contribution to the partition function is given by a spinless field $V_{\Delta,\Delta}$ with multiplicity $n_{V_{\Delta,\Delta}}$. For non unitary CFTs, the number $n_{V_{\Delta,\bar{\Delta}}}$ can take general real values. This is the case of the $Q-$ state Potts model [34], in which the sub-dominant contribution is given by the spin field σ with multiplicity $n_\sigma = Q-1$.
In a general CFT, one-point torus functions can be expressed in the variable q, in a way similar to the partition function (20). As detailed in [50], the three assumptions of Section 2.4 lead to the following form for the energy density one-point torus function:

$$\langle \varepsilon \rangle_q = \frac{(2\pi)^{2\Delta_\varepsilon}}{Z(q)} C^{\varepsilon}_{\sigma,\sigma}\, n_\sigma q^{2\Delta_\sigma - \frac{c}{12}} (1 + O(q)). \tag{21}$$

The coefficient $c_v(q)$, given by (19), can therefore be expanded in q as:

$$c_v(q) = (2\pi)^{2\Delta_\varepsilon} \left[C^{\varepsilon}_{\sigma,\sigma}\right]^2 n_\sigma q^{2\Delta_\sigma} + o(q^{2\Delta_\sigma}). \tag{22}$$

In a similar way, using the formula [57]:

$$\langle T \rangle_q = -(2\pi)^2 q\, \partial_q \ln Z(q), \tag{23}$$

and expression (20) of the partition function, the coefficient $c_T(q)$ (given by (19)) admits the following small q expansion:

$$c_T(q) = \frac{(2-D_f)\pi^2}{6}\left(1 - 24\Delta \frac{n_{V_{\Delta,\Delta}}}{c} q^{2\Delta} + \cdots\right). \tag{24}$$

The above three assumptions do not put any constraint on the dimension Δ and multiplicity $n_{V_{\Delta,\Delta}}$ of the field giving the leading contribution to (24). For pure percolation, for which the partition function (20) is known exactly, this leading contribution is given by the spin field σ:

$$c_T(q) = \frac{(2-D_f)\pi^2}{6}\left(1 - 12(2-D_f)\frac{n_\sigma}{c} q^{2-D_f} + \cdots\right). \tag{25}$$

In that case the ratio n_σ/c can be obtained as the limit $Q \to 1$ of the analogous expression for the $Q-$ Potts model. Using the fact that in this limit the central charge $c_Q \sim Q-1$ ($|Q-1| \ll 1$), the limit $c \to 0$ of n_σ/c yields a finite non-zero limit, $n_\sigma/c = 4\pi/(5\sqrt{3})$.

2.5 Numerical protocols for testing CFT predictions

We have seen that, by using a CFT approach, the topological effects on p_{12} encode in principle highly non-trivial information about the critical point. We discuss now how to efficiently extract this information from a numerical study of p_{12} and how to interpret these results.
The torus shape can be exploited to disentangle the contributions of sub-leading and sub-sub leading terms in (14). This can be done by comparing the connectivities $p_{12}(\mathbf{x_2}-\mathbf{x_1})$ and $p_{12}(\mathbf{x_3}-\mathbf{x_1})$ between pairs of points $\mathbf{x_2}$ and $\mathbf{x_1}$ and $\mathbf{x_3}$ and $\mathbf{x_1}$ that are aligned on orthogonal axes, as illustrated in Figure 4. Note that similar ideas were used in [50].
Let us consider first the square torus, $M = N$ or $q = e^{-2\pi}$ and the case where $\mathbf{x_2}-\mathbf{x_1} = \mathbf{x}^h$ and $\mathbf{x_3}-\mathbf{x_1} = \mathbf{x}^v$ with $\mathbf{x}^h = |\mathbf{x}|(1,0)$ and $\mathbf{x}^v = |\mathbf{x}|(0,1)$. As the two cycles are equivalent, one has $p_{12}(\mathbf{x}^h) = p_{12}(\mathbf{x}^v)$. From (14) and (18), $p_{12}(\mathbf{x}^h) - p_{12}(\mathbf{x}^v) \sim 4\sum_{\Delta-\bar{\Delta}\neq 0} C^{V_{\Delta,\bar{\Delta}}}_{\sigma,\sigma} \langle V_{\Delta,\bar{\Delta}} \rangle_{q=e^{-2\pi}} N^{-\Delta-\bar{\Delta}}$, which implies $\langle V_{\Delta,\bar{\Delta}} \rangle_{q=e^{-2\pi}} = 0$ if $\Delta - \bar{\Delta} \neq 0$. In particular $\langle T \rangle_{q=e^{-2\pi}} = 0$ and therefore:

$$c_T(e^{-2\pi}) = 0. \tag{26}$$

The connectivity (14) therefore reduces to:

$$p_{12}(\mathbf{x}) = \frac{d_0}{|\mathbf{x}|^{2(2-D_f)}}\left(1 + c_v(q)\left(\frac{|\mathbf{x}|}{N}\right)^{2-\frac{1}{\nu}} + o\left(\left(\frac{|\mathbf{x}|}{N}\right)^2\right)\right), \quad \text{for } M = N. \tag{27}$$

Let us consider now the rectangular torus $M > N$ with again $\mathbf{x_2} - \mathbf{x_1} = \mathbf{x}^h$ and $\mathbf{x_3} - \mathbf{x_1} = \mathbf{x}^v$. In Figure 5 we show the corresponding measurements of $p_{12}(\mathbf{x}^h)$ and $p_{12}(\mathbf{x}^v)$ when $M = 2N$. The two connectivities are now different, which is explained by the simple fact that the paths closing on the other side of the small cycle (N) start to contribute for smaller distances than the ones closing on the largest one (M). From (14) and for general $\mathbf{x}$ we have:

$$p_{12}(\mathbf{x}) - p_{12}(\mathbf{x}^\perp) = \frac{d_0}{|\mathbf{x}|^{2(2-D_f)}}\left(4\cos(2\theta)\frac{2\Delta_\sigma}{c}\langle T\rangle_q\left(\frac{|\mathbf{x}|}{N}\right)^2 + o\left(\left(\frac{|\mathbf{x}|}{N}\right)^2\right)\right), \tag{28}$$

where $\mathbf{x}$ and $\mathbf{x}^\perp$ are parametrised as in (13), and $c_T(q)$ has been replaced by its expression (19).

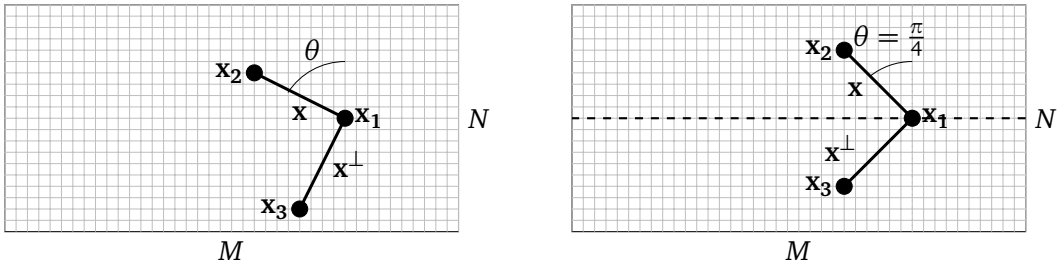

Figure 4: Left: We take three points $\mathbf{x_1}, \mathbf{x_2}, \mathbf{x_3}$ on the torus lattice $\mathbb{Z}^2/(N\mathbb{Z} \times M\mathbb{Z})$ such that $\mathbf{x_2} - \mathbf{x_1} = \mathbf{x}$ and $\mathbf{x_3} - \mathbf{x_1} = \mathbf{x}^\perp$, see (13). We measure $p_{12}(\mathbf{x})$ and $p_{12}(\mathbf{x}^\perp)$, defined in (10). Right: When $\theta = \pi/4$, $\mathbf{x}$ and $\mathbf{x}^\perp$ are symmetric by reflection with respect to the axis parallel to the M axis and passing through $\mathbf{x_1}$(dashed line). This implies $p_{12}(\mathbf{x}) = p_{12}(\mathbf{x}^\perp)$ for $\theta = \pi/4$.

Equation (28) is a clear consequence of the fact that, whenever an anisotropy is introduced, the response of the system is bound to be determined by the stress-energy tensor components T and $\bar{T}$ (see for instance Section 11.3 in [53]). It is interesting to note that Monte Carlo algorithms, based on the properties of rectangular torii [58, 59], have been proposed to measure the central charge and the leading fields in the partition function [60]. However, these methods can be applied to statistical models for which a direct lattice representation of the stress-energy tensor is available, such as the Ising model or the RSOS models [61]. In our case we do not know the stress-energy lattice representation. Actually, away from the pure percolation point $H = -1$, we do not even know the energy density lattice representation. This is also the reason why the connectivity functions are the most natural observables to study universal critical amplitudes of non-local models. Note that other non-scalar observables have been defined and discussed in [62, 63], where the angular dependence of their two-point function has been measured by Monte-Carlo simulations.

From the expansion (18) of the connectivity, the difference (28) gets in general contributions only from fields with a non-zero spin. By lattice symmetry arguments, this difference vanishes for $\theta = \pi/4$, as shown in Figure 4. One can directly see from (18) that the only fields which may contribute to (28) are fields with spin $\Delta - \bar{\Delta} = 2 \bmod 4$. For instance one expects in (28) a contribution from fields with $(\Delta, \bar{\Delta}) = (6, 0)$ and $(\Delta, \bar{\Delta}) = (4, 2)$. These fields exist in any CFT as, said in CFT jargon, they correspond to the higher level descendants of the identity: $L_{-6}V_{0,0}$, $L_{-4}L_{-2}V_{0,0}$ and $L_{-4}\bar{L}_{-2}$, $L_{-2}^2\bar{L}_{-2}V_{0,0}$. In pure percolation there are no fields in the

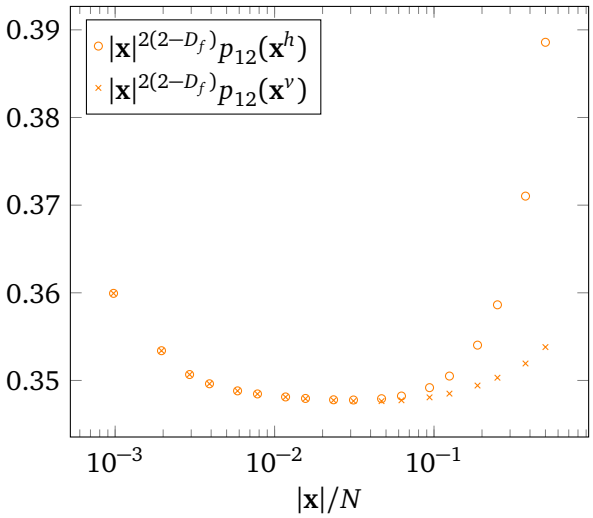

Figure 5: The connectivity measured for $H=-2/3$, along the small cycle (circles) and the long cycle (crosses) of a torus with $M/N=2, \quad N=2^{10}$. The data points were obtained by averaging over 10^5 instances of the surface and over the $N\times M$ locations of $\mathbf{x}$ (cf. Section 3. The connectivity measured along the long cycle of the torus is always smaller than the connectivity measured along the small cycle.

spectrum with spin greater than 2 and physical dimension $\Delta+\bar{\Delta}<6$. If we assume this is true also for correlated percolation $H>-1$, then we have:

$$p_{12}(\mathbf{x})-p_{12}(\mathbf{x}^\perp)=\frac{d_0}{|\mathbf{x}|^{2(2-D_f)}}\Bigg(4\cos(2\theta)c_T(q)\left(\frac{|\mathbf{x}|}{N}\right)^2 \\ +4\Big[\cos(2\theta)c_{6,2}(q)+\cos(6\theta)c_{6,6}(q)\Big]\left(\frac{|\mathbf{x}|}{N}\right)^6+o\left(\left(\frac{\mathbf{x}}{N}\right)^6\right)\Bigg). \tag{29}$$

Assuming that the identity descendants are the only fields contributing to $c_{6,2}$ and $c_{6,6}$, these coefficients can be fixed by computing the inner products and the matrix elements between the 11 identity descendants existing at level 6. We refer the reader to [50, 54] and references therein for the details of the general procedure. However, the numerical determination of these coefficients is not accurate enough for this cumbersome computation to be worth it. As a matter of fact we use this order 6 term as a fitting parameter to obtain better estimations of the order 2 coefficient.

2.6 Numerical evidences

We summarise here the main numerical results for p_{12} and the conclusions we can draw by comparing these results with the CFT predictions.

2.6.1 Conformal invariance

The quantity (14) is, first of all, a powerful test of conformal invariance. Via the numerical simulation of the connectivity we test two predictions:

- The dominant topological correction shows a precise interplay between the exponents ν and D_f. In particular the leading correction behaves as $|\mathbf{x}|^{2(2D_f-2)}(|\mathbf{x}|/N)^{2-1/\nu}$. This effect is more clearly seen on the square torus, see (27). Figure 9 shows that the numerical results for the values $H<-1/2$ agree with this prediction.

- The sub-leading term is $\propto |\mathbf{x}|^{2(2D_f-2)}\cos(2\theta)(|\mathbf{x}|/N)^2$. As explained above, the presence of such term implies the existence of a pair of fields with scaling dimension $\Delta+\bar{\Delta}=2$, which corresponds to the power 2 in the $(|\mathbf{x}|/N)^2$ decay, and with spin $\Delta-\bar{\Delta}=\pm 2$, which fixes the θ dependence. If such fields exist, they correspond by definition to the stress-energy tensor components T and $\bar{T}$. The presence of T and $\bar{T}$ is the most basic and direct consequence of conformal invariance. In numerical simulations, the sub-leading term is seen by considering a rectangular torus. Figures 10 and 11 show clearly the $(|\mathbf{x}|/N)^2$ decay and the $\cos(2\theta)$ dependence. Figure 12 shows further that the data is well described by the form (29).

2.6.2 Spectrum and structure constants

- The values of $c_\nu(q)$ for different values of q have been measured for $-1<H<-1/2$ and reported in Table 2. The results support the fact that for $H\leq -3/4$ the universality class is the one of pure percolation. Note that this a highly non-trivial verification, as it not only based on the values of critical exponents, but on the values of constants which depend on the spectrum and fusion coefficients of the theory. For $H>-3/4$, the data are quite well consistent with the CFT prediction (21), as shown in Figure 13. This is also consistent with the fact that the fusion between two spin field produces an energy field.

- We could measure with good precision the dependence of the coefficient $c_T(q)$ with q. Figure 15 shows that (25) is satisfied, and that the dimension of the most dominant field coincides with the dimension of the spin field.

3 Numerical results on two point connectivity

We generate the random surfaces (48, 52) and we measure the connectivity (10) of its level clusters, for the following set of values of H:

$$H=-\frac{7}{8},-\frac{2}{3},-\frac{5}{8},-\frac{21}{40},-\frac{19}{40},-\frac{3}{8},-\frac{1}{4} \tag{30}$$

which are representative for the line $-1\leq H<0$. Due to the periodicity properties (55), we have a site percolation model on a doubly-periodic lattice of size $M\times N$, i.e. the toric lattice $\mathbb{Z}^2/(N\mathbb{Z}+M\mathbb{Z})$. In the square torus case ($M=N$), $p_{12}(\mathbf{x})=p_{12}(|\mathbf{x}|)$. Without losing generality we measure p_{12} between pairs of points $\mathbf{x_1}$ and $\mathbf{x_2}$, aligned on the vertical or horizontal axes. For each H in (30), the data are taken for distances $|\mathbf{x_1}-\mathbf{x_2}|=|\mathbf{x}|=1,2,4,\cdots,N/2$, $|\mathbf{x}|=3,6,12,\cdots,3N/8$. For the rectangular torus, $M\neq N$, we measure the connectivity between the points $\mathbf{x_1}$ and $\mathbf{x_2}$, and between $\mathbf{x_1}$ and $\mathbf{x_3}$, $\mathbf{x_3}-\mathbf{x_1}=(\mathbf{x_2}-\mathbf{x_1})^\perp=\mathbf{x}^\perp$, see Figure 4. When $\mathbf{x}$ and $\mathbf{x}^\perp$ are aligned with the cycles of the torus ($\theta=0$), measurements are taken for aspect ratios $M/N=1,2\cdots 5$, and for distances $|\mathbf{x}|=1,2,4,\cdots,N/2$, and $|\mathbf{x}|=3,6,12,\cdots,3N/8$. Fixing the aspect ratio, we measured $p_{12}(\mathbf{x})$ for non-zero angles θ. On the lattice, angles are of the form $\theta=\arctan\left(\frac{a_2}{a_1}\right)$, with a_2 (resp.a_1) a given number of lattice sites in the M (resp.N) direction. Distances are then taken to be $|\mathbf{x}|=\sqrt{a_1^2+a_2^2}(1,2,4,\cdots)$, $|\mathbf{x}|=\sqrt{a_1^2+a_2^2}(3,6,12,\cdots)$, such that $|\mathbf{x}|\leq N/2$. We chose angles $\theta=0,\arctan(1/4)$, $\arctan(1/3),\arctan(1/2),\arctan(2/3)$, for fixed aspect ratio $M/N=3$.
Exploiting the translational invariance of the surface distribution, we average over the position $\mathbf{x_1}$ for each instance of $u(\mathbf{x})$, and then over 10^5 instances. In the scaling limit, the dependence of $p_{12}(\mathbf{x})$ with respect to the lattice size N is expected to be of the form $|\mathbf{x}|/N$. Plotting the

connectivity as a function of $|\mathbf{x}|/N$, we observe that the corrections to the scaling are still visible as the data points for different sizes do not collapse at large distances. In Figure 6a we show the data for $H = -5/8$ and for lattice sizes $M = N = 2^9 - 2^{12}$. One can see that the scaling limit is still not attained. These non-universal effects become even more important for larger H. As shown in Figure 6b for $H = -3/8$, even the infinite plane scaling limit is not clearly attained at the sizes of our simulations. Of course these non-universal effects make the analysis of the universal topological effects less precise, in particular for studying the contributions of the spinless fields. On the other hand, we observed that the non-universal effects are less important for the surface (52) generated by the kernel $\hat{S}_2(\mathbf{k})$, at least for values of $H < -1/2$. This is shown in 7b. For values of $H < -1/2$ and for the two surfaces (48) and (52) we could determine the non-universal constant d_0, as well as the dimension of the leading spinless contribution. For this latter, the consistency of the results obtained from the two surfaces makes the verification of the CFT predictions more solid. The coefficient c_ν and its dependence on the aspect ratio, on the other hand, could only be determined with sufficient precision for the surface (52).

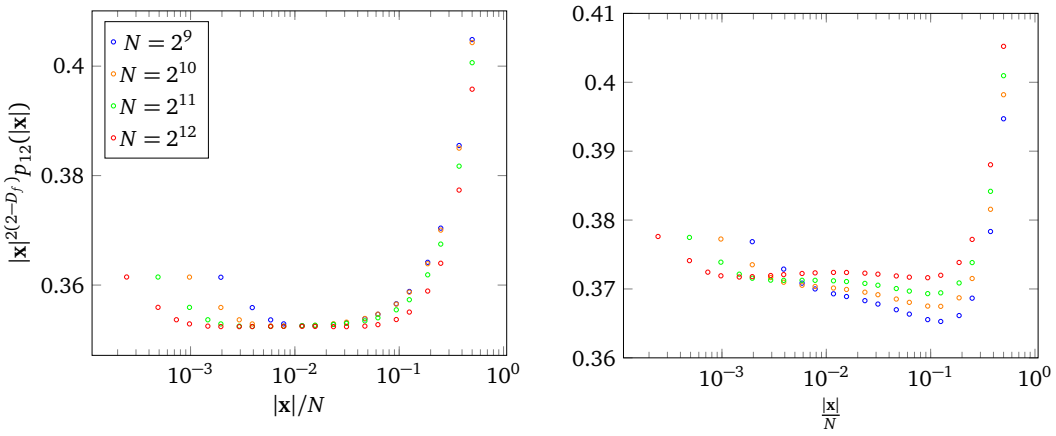

(a) $H = -5/8$

(b) $H = -3/8$

Figure 6: Convergence of the data points generated with surface (48), on the square torus of different sizes, for $H = -5/8$ (a) and $H = -3/8$ (b). Error bars are smaller than the marker size and we do not display them.

A very remarkable fact is that, for both surfaces, these corrections to the scaling terms cancel when one takes the differences between connectivities. This is shown in Figure 8 for the same values of H. The corrections may originate, for instance, from the fact that we are not sufficiently close to the critical point. More generally, any perturbation that drives the system out of the critical point and that does not break rotational invariance is related to a spinless field, whose contributions to the connectivity are isotropic. This explains why they disappear by taking the difference $p_{12}(\mathbf{x}) - p_{12}(\mathbf{x}^\perp)$. This mechanism allows to test the contribution of the fields with spin, and therefore of the stress-energy tensor, with a very good precision. For $H < -1/2$, our determination of the constants d_0 allowed moreover to acces the value of the universal coefficient $c_T(q)$. For $H > -1/2$, we could only determine the behaviour of $d_0\, c_T(q)$ with q.

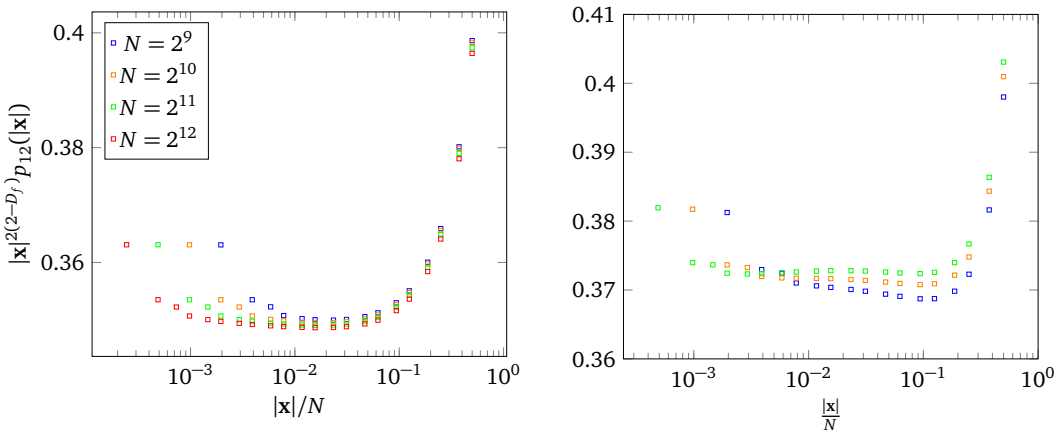

(a) $H = -5/8$ (b) $H = -3/8$

Figure 7: Convergence of the data points generated using the surface (52), on the square torus of different sizes, for $H < -5/8$ (a) and $H = -3/8$ (b).

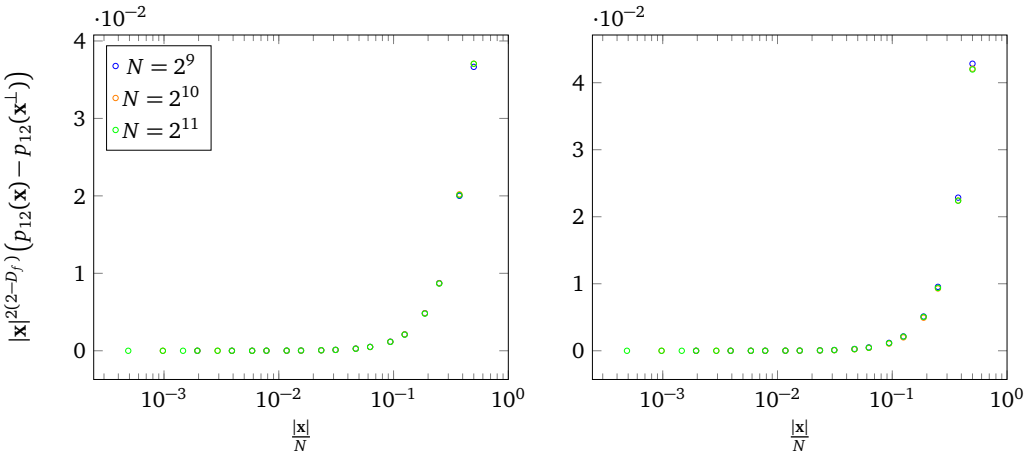

(a) $H = -5/8$ (b) $H = -3/8$

Figure 8: Convergence of the data points for the difference of connectivities (28) on rectangular torus $M = 2N$, for $H = -5/8$ (a) and $H = -3/8$ (b).

3.1 Plane limit

For $N = M = 2^{12}$, we fit the data points for $|\mathbf{x}| \in [4, 128]$, expected to be well described by the infinite plane limit (11) (see Figure 3), to the form

$$p_{12}(\mathbf{x}) \sim |\mathbf{x}|^{-2(2-D_f^{(2)})}. \tag{31}$$

The values $D_f^{(2)}$ of the fractal dimension are given in Table 12. To extract the topological corrections (27), we fit our numerical data to the form:

$$|\mathbf{x}|^{2(2-D_f^{(2)})} p_{12}(r) = d_0 \left(1 + \frac{d_1}{|\mathbf{x}|^{b_1}}\right)\left(1 + c_\nu \left(\frac{|\mathbf{x}|}{N}\right)^{2-1/\nu}\right). \tag{32}$$

The first factor takes into account the non-universal, small distance effects due to the lattice. We refer the reader to [39, 41] for a more detailed discussion of these ultraviolet corrections. The values of d_0 are reported in Table 1. The numerical values for the universal coefficient c_ν

are given in Table 2. They were obtained from the data generated using kernel (50), which converge faster to the scaling limit, and for which the agreement with (32) is excellent. This is shown in Figure 9.

Table 1: Non universal constant d_0 determined from the fit (32), for surfaces generated (1) with kernel (46) and (2) with kernel (50).

H	$d_0^{(1)}$	$d_0^{(2)}$
-7/8	0.3438(1)	0.3433(2)
-2/3	0.3490(1)	0.3482(1)
-5/8	0.3521(5)	0.3495(1)
-21/40	0.357(1)	0.355(9)

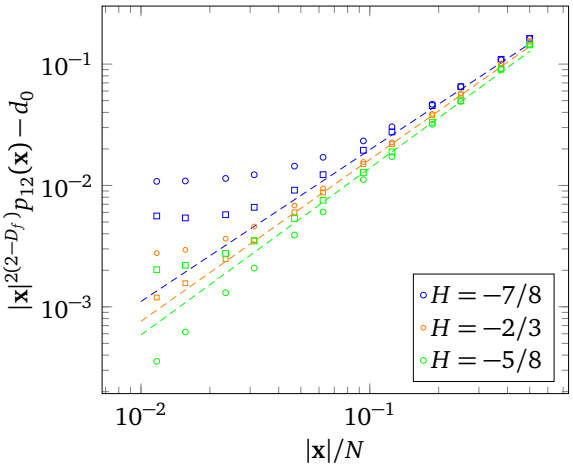

Figure 9: Numerical data for $|\mathbf{x}|^{2(2-D_f)}p_{12}(\mathbf{x})-d_0$ for $H=-7/8,-2/3,-21/40$, from surfaces (48) (circles) and (52) (squares). The lines show the prediction (27) with the exponent $2-1/\nu(H)$ given by (7).

3.2 Evidences of conformal invariance

With $M \neq N$, and following prediction (28), the quantity $\log\left[|\mathbf{x}|^{2(2-D_f^{(2)})}\left(p_{12}(\mathbf{x})-p_{12}(\mathbf{x}^\perp)\right)\right]$ should follow a line of slope 2. This is very clear for $H<-1/2$, as shown in Figure 10. When $H>-1/2$, the slope increases significantly: either there is no order 2 term (conformal invariance is broken), or this term is still present, with higher-order corrections making the effective slope significantly greater than 2. Assuming the latter and that the difference of connectivities is described by (29) on the whole line $H<0$, we fit our data for different angles θ to the form:

$$|\mathbf{x}|^{2(2-D_f^{(2)})}\left(p_{12}(\mathbf{x})-p_{12}(\mathbf{x}^\perp)\right)=c_2(\theta)\left(\frac{|\mathbf{x}|}{N}\right)^2+c_6(\theta)\left(\frac{|\mathbf{x}|}{N}\right)^6. \tag{33}$$

This fit shows good consistency with the data for all values of H, and allows to determine $c_2(\theta)$ with good precision. In Figure 11 we show that $c_2(\theta)$ has the expected behaviour (18): $c_2(\theta)\propto\cos(2\theta)$. This makes manifest the presence of a field with conformal dimension 2 and spin 2, and therefore of conformal invariance for all $H<0$.

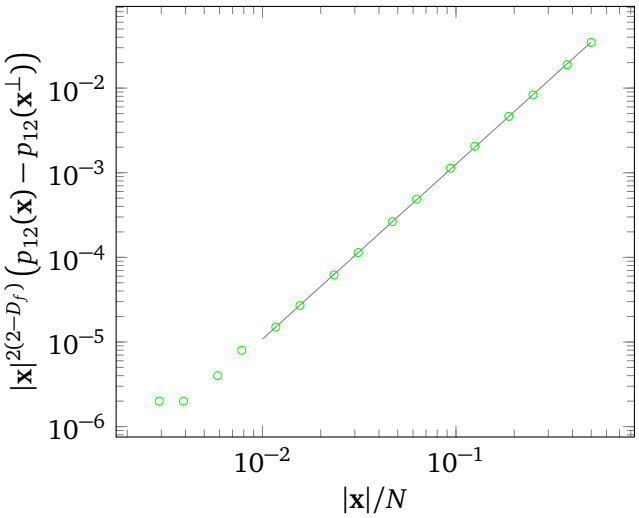

Figure 10: Difference of connectivities (28) for $H = -2/3$, measured for $M/N = 2, N = 2^{11}$ and $\theta = 0$. The best fit line has slope ~ 2.07, indicating the presence of the stress-energy tensor.

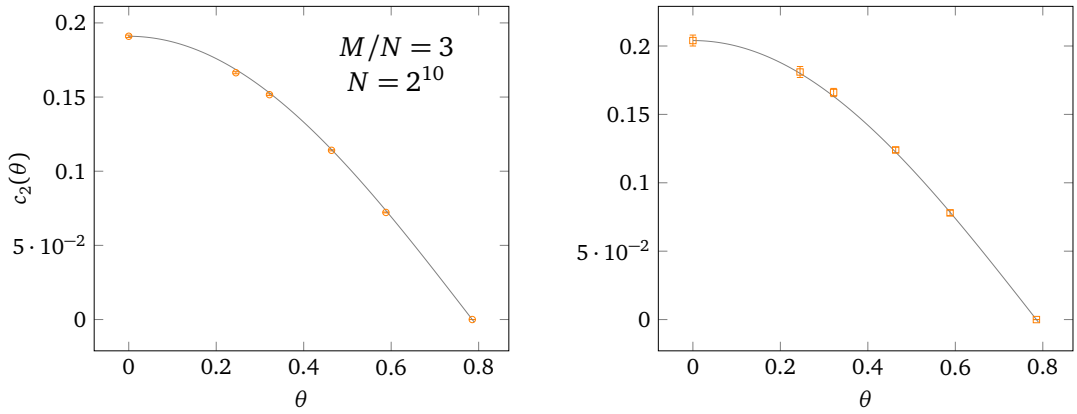

(a) $H = -2/3$ (b) $H = -3/10$

Figure 11: Values of $c_2(\theta)$ from fit (33), for different angles θ, for $H < -1/2$ (a) and $H > -1/2$ (b). The curves show the prediction $c_2(\theta) = c_2(0)\cos(2\theta)$.

The behaviour of the order 6 coefficient is also in fair agreement with prediction (29), as shown in Figure 12.

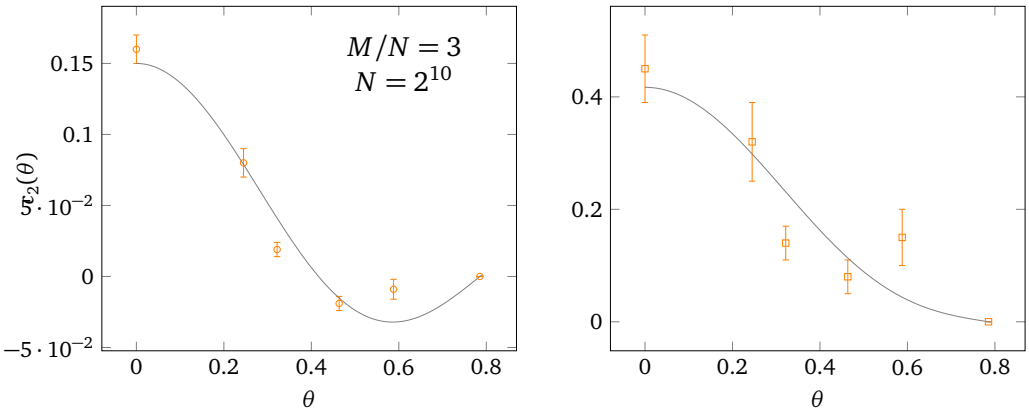

(a) $H = -2/3$ (b) $H = -3/10$

Figure 12: Values of $c_6(\theta)$ from fit (33), for different angles θ, for $H < -1/2$ (a) and $H > -1/2$ (b). The curves are fits to the form (29): $c_6(\theta) = c_{6,2}\cos(2\theta) + c_{6,6}\cos(6\theta)$.

3.3 Spectrum and structure constants

Setting θ to zero, we varied the aspect ratio and obtained c_v and c_T as functions of M/N, given in Tables 2 and 5.

The coefficient c_v is obtained by fitting the sum of connectivities $\frac{1}{2}|\mathbf{x}|^{2(2-D_f^{(2)})}\left(p_{12}(\mathbf{x}) + p_{12}(\mathbf{x}^\perp)\right)$ to the form (32). Taking the sum allows to remove the order 2 contributions of the stress-tensor fields.

Table 2: Best fit parameter $c_v(M/N)$, for different aspect ratios M/N. These values were obtained with the surface (52), which showed better convergence. When $H > -1/2$, the non-universal effects are too strong and are not described by the fit (32).

H \ M/N	1	2	3	4
percolation	0.355402	0.185569	0.0964413	0.0501208
-7/8	0.371(5)	0.170(5)	0.13(1)	0.040(5)
-2/3	0.352(4)	0.22(2)	0.135(5)	0.090(5)
-5/8	0.327(3)	0.15(1)	0.130(5)	0.075(5)

Figure 13 shows that the behaviour of $c_v(q)$ is in fair agreement with prediction (21):

$$c_v(q) \sim q^x, \tag{34}$$

with the slope x given by the dimension of the spin field $x = 2\Delta_\sigma = 2 - D_f$, see Table 3. We point out that this behaviour is incompatible with the fact that the energy field is degenerate at level 2. Indeed, if it was degenerate the slope $x = 2\Delta_\sigma$ would be a continuously varying function of the central charge [50] and would be expected to show significant variation with H. In general, the presence of degenerate fields is a crucial feature of a CFT [64], which in some cases allow to solve the theory [65–68]. For pure percolation, the energy field is degenerate, which leads to relations between the different structure constants of the theory [43, 68, 69].

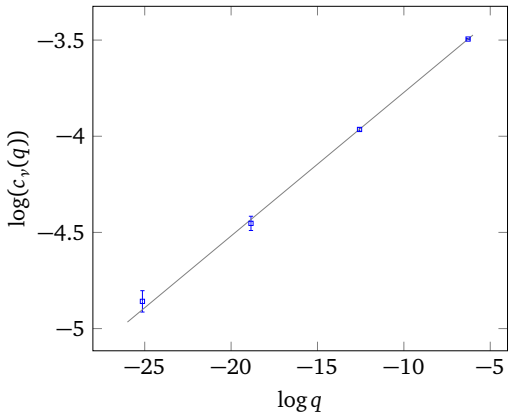

Figure 13: c_ν as a function of q and the best fit line, for $H = -2/3$.

Table 3: Exponent x determining the behaviour of $c_\nu(q)$ with q (34), obtained from fitting $\log c_\nu(q)$. These values are to be compared to the value of the spin dimension, which remains equal to the pure percolation value $2-D_f^{\text{pure}} \sim 0.104$ when $H < -1/2$.

H	x
-7/8	0.10(1)
-2/3	0.08(2)
-5/8	0.08(1)

Setting x to $2-D_f$, a fit of $c_\nu(q)$ as a function of q^{2-D_f} gives an estimation of the quantity $\left[C^{\varepsilon}_{\sigma,\sigma}\right]^2 n_\sigma$ (see 22), given in Table 4.

Table 4: Estimation of the coefficient $\left[C^{\varepsilon}_{\sigma,\sigma}\right]^2 n_\sigma$. The percolation prediction was computed in [50].

H	$\left[C^{\varepsilon}_{\sigma,\sigma}\right]^2 n_\sigma$
pure percolation	$\pi\sqrt{3}\left(\frac{4}{9}\frac{\Gamma(7/4)}{\Gamma(1/4)}\right)^2 \sim 0.069$
-7/8	0.07(1)
-2/3	0.05(1)
-5/8	0.04(1)

Conversely, to obtain $c_T(q)$ we fit the difference $|\mathbf{x}|^{2(2-D_f^{(2)})}\left(p_{12}(\mathbf{x})-p_{12}(\mathbf{x}^\perp)\right)$ to the form:

$$|\mathbf{x}|^{2(2-D_f^{(2)})}\left(p_{12}(\mathbf{x})-p_{12}(\mathbf{x}^\perp)\right) = c_2(q)\left(\frac{|\mathbf{x}|}{N}\right)^2 + c_6(q)\left(\frac{|\mathbf{x}|}{N}\right)^6, \tag{35}$$

where

$$c_2(q) = 4d_0\, c_T(q). \tag{36}$$

The values we obtained for $c_T(q)$, for both types of surfaces, are given in Tables 5, 6. Figure 14 shows the consistency betwwen the two sets of values, as expected from universality.

Table 5: Best fit parameter $c_2(M/N)/d_0$ for different aspect ratios M/N, for surfaces (48). The first line gives the numerical value of prediction (25) for pure percolation.

H \ M/N	1	2	3	4	5
pure percolation	0	0.3496	0.5109	0.5947	0.6383
-7/8	0	0.376(5)	0.531(5)	0.610(5)	0.645(5)
-2/3	0	0.383(5)	0.547(5)	0.607(5)	0.640(5)
-5/8	0	0.395(5)	0.555(5)	0.619(5)	0.641(5)

Table 6: Best fit parameter $c_2(M/N)/d_0$ for different aspect ratios M/N, for surfaces (52).

H \ M/N	1	2	3	4	5
-7/8	0	0.355(5)	0.493(5)	0.596(5)	0.602(5)
-2/3	0	0.340(5)	0.494(5)	0.574(5)	0.600(5)
-5/8	0	0.363(5)	0.494(5)	0.581(5)	0.613(5)

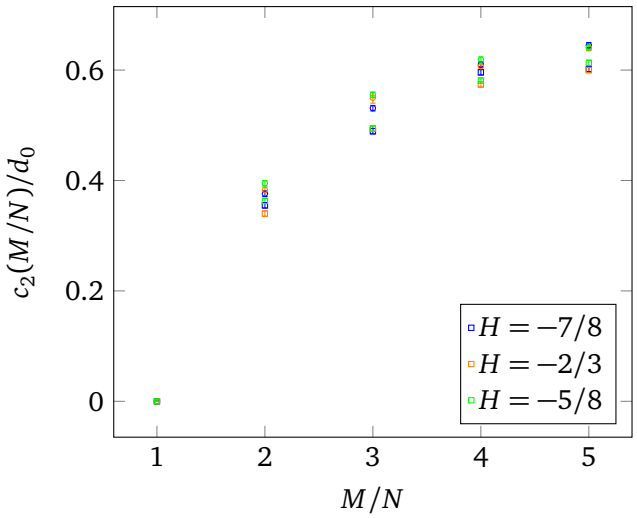

Figure 14: Comparison of the numerical values obtained for the universal quantity $c_2(M/N)/d_0$, for different Hurst exponents, for surfaces (48) (circles) and (52) (squares).

Following prediction (24), we fit the quantity $\log\left(2\frac{2-D_f}{3}\pi^2 - \frac{c_2(q)}{d_0}\right)$ as a function of $\log q$ to a line. This is shown in Figure 15, and we obtain values for the dominant dimension Δ close to the dimension of the spin field, see Table 7.

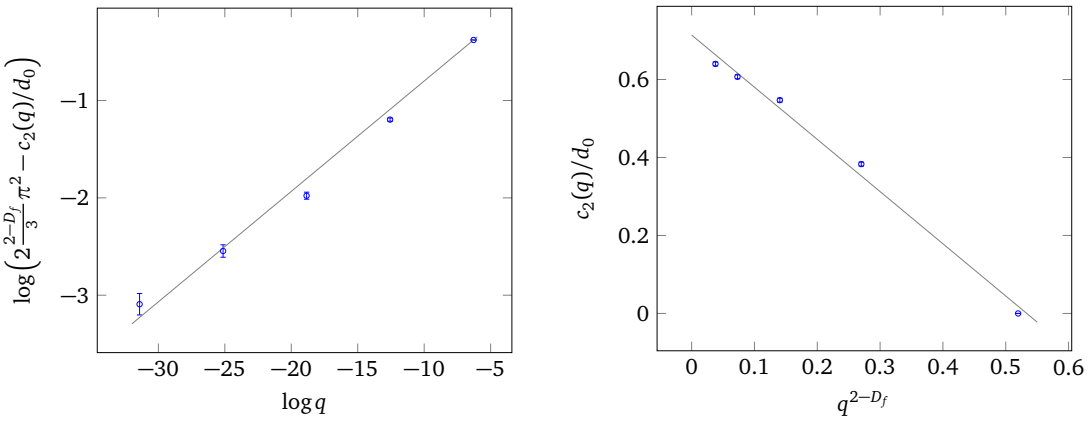

Figure 15: Numerical values at $H = -2/3$, for the quantities $\log\left(2\frac{2-D_f}{3}\pi^2 - c_2(q)/d_0\right)$ (left) and $c_2(q)/d_0$ (right), together with the corresponding best fit lines.

Table 7: Values of the dimension 2Δ of the most dominant field obtained from fitting $\log\left(2\frac{2-D_f}{3}\pi^2 - \frac{c_2(q)}{d_0}\right)$, (1) for surfaces (48) and (2) for surfaces (52).

H	$2\Delta^{(1)}$	$2\Delta^{(2)}$
-7/8	0.12(1)	0.10(1)
-2/3	0.11(1)	0.09(1)
-5/8	0.12(1)	0.10(1)

Assuming that this dimension is indeed the one of the spin field, $2\Delta = 2\Delta_\sigma = 2 - D_f$, we fit $c_2(q)/d_0$ as a function of q^{2-D_f}:

$$c_2(q)/d_0 = c_2(0)/d_0 + a\,y, \quad y = q^{2-D_f}, \tag{37}$$

see Figure 15. In particular, from (24):

$$\frac{1}{12(2-D_f)}\frac{a}{c_2(0)/d_0} = \frac{n_\sigma}{c}. \tag{38}$$

The values of the cylinder ($q \to 0$) limit and of the ratio n_σ/c obtained are given in Tables 8 and 9.

Table 8: Cylinder limit $c_2(0)/d_0$ and ratio of the spin field multiplicity n_σ to the central charge c, obtained from fit (37), for surfaces (48).

H	$c_2(0)/d_0$	n_σ/c
pure percolation	$\frac{2(2-D_f)\pi^2}{3} \sim 0.6854$	$\frac{4\pi}{5\sqrt{3}} \sim 1.4510$
-7/8	0.71(2)	1.51(7)
-2/3	0.71(2)	1.50(9)
-5/8	0.72(2)	1.5(1)

Table 9: Cylinder limit $c_2(0)/d_0$ and ratio of the spin field multiplicity n_σ to the central charge c, obtained from fit (37), for surfaces (52).

H	$c_2(0)/d_0$	n/c
-7/8	0.67(2)	1.51(8)
-2/3	0.66(2)	1.52(5)
-5/8	0.68(2)	1.51(7)

When $H > -1/2$, we could not determine the value of the plateau d_0, so we cannot determine the leading dimension in the expansion (24) as above. In Figure 16 we show the behaviour of $c_2(q)$ with $q^{2-D_f(H)}$, with $D_f(H)$ from Table 12. The points corresponding to large M/N deviate significantly from a line. This could be explained by the fact that, when $H \to 0$, the fractal dimension $D_f \to 2$, so that the coefficient of the q^{2-D_f} term in (24) becomes small and subleading terms in this expansion become non-negligeable.

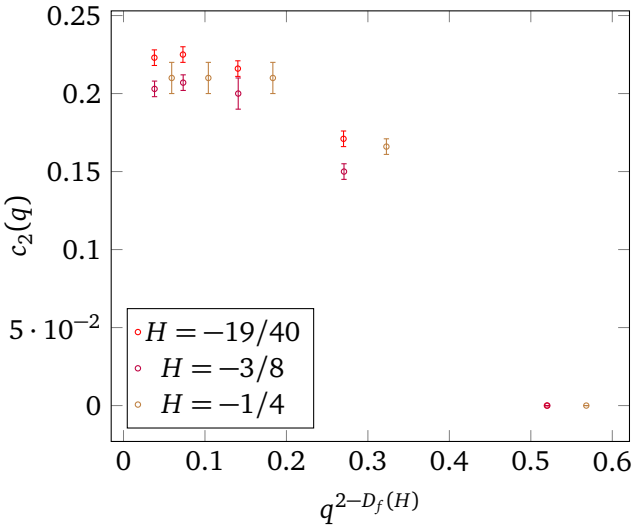

Figure 16: Behaviour of the coefficient $c_2(q)$ in the range $H > -1/2$.

4 Conclusion

In this paper we have studied the percolative properties of fractional random surfaces with negative Hurst exponent H. Via the connected components of their excursion sets, the level clusters, this problem is reformulated in terms of a long-range correlated two-dimensional site percolation model. The main motivation here was to better understand the universality of their percolation critical points, in particular in the region $-3/4 < H < 0$ where the correlation effects drive the system into universality classes different from the one of pure percolation. When the problem is defined on a rectangular domain of size $M \times N$ with toric boundary conditions, we argued that the two-point connectivity (10) represents an excellent observable to test conformal invariance. On the basis of three main assumptions, explained in Section 2.4, we predicted the leading contributions to the toric corrections, see (14) and (29). We tested these predictions by generating two types of fractional random surfaces (48) and (52), expected to have the same long distances behaviour. The comparison between the theory and the numerical simulations is summarised in Section 2.6. The main result is shown in Figure 10 and in Figure 11 and points out, for the first time, the existence of the two components of a traceless stress-energy tensor for all $H < 0$. Furthermore, the two point connectivity

on rectangular torus lattices gives access to the spectrum and to some fundamental structure constants of the underlying CFT, still unknown for any $H < 0$. Importantly, we find that the energy field in this CFT cannot be degenerate, whereas this is the case for pure percolation. We show that the leading contribution to the conformal partition function is the magnetic field σ with scaling dimension $2-D_f$, as shown in Figure 15 and in Table 7. The ratio n_σ/c of the multiplicity of the magnetic field to the central charge has also been determined numerically with quite good precision, and it is reported in Table 8. Finally, we succeeded in evaluating the product $\left[C^{\varepsilon}_{\sigma,\sigma}\right]^2 n_\sigma$, directly proportional to the fusion between the thermal and magnetic field. The results are given in Table 4. We conclude by noting that the fact that, for $H < -3/4$, the long-range correlation is irrelevant is a very established one. Nevertheless, the results in Table 4 verify this conjecture at the level of the structure constants of the theory, which encode much more information than the critical exponents. At the best of our knowledge, this is the first time such verification has been done. A last noteworthy observation concerns the corrections to the scaling of the critical level, when using the Binder method to locate the critical point (see Appendix B). From the values of the corresponding exponent ω given in Table 11, we argue that the long-range correlations break the integrability of the model.

Acknowledgements

We thank Marco Picco for explaining us many crucial aspects on the numerical analysis of critical percolation points, and Hugo Vanneuville for sharing his insights and guiding us through the mathematical literature. We thank also Sylvain Ribault and Hans Herrmann for useful discussions. SG acknowledges support from a SENESCYT fellowship from the Government of Ecuador as well as from CNRS in the last part of the project.

A Fractional Gaussian surfaces

To generate a random function $u(\mathbf{x})$ satisfying the properties (1), we use a method based on the Fourier Filtering Method [9]. The principle is to create correlated random variables by linearly combining uncorrelated ones. Let us first briefly sketch the method. Given a set of uncorrelated random variable $w(\mathbf{x})$, $\mathbb{E}[w(\mathbf{x})w(\mathbf{y})] = \delta_{\mathbf{x},\mathbf{y}}$, one can define, via a convolution, a new set of random variables $u(\mathbf{x})$:

$$u(\mathbf{x}) = \sum_{\mathbf{y}} S(\mathbf{x}-\mathbf{y})w(\mathbf{y}). \tag{39}$$

The convolution kernel $S(\mathbf{x})$ is a non-random function which determines the $u(\mathbf{x})$ covariance function:

$$\mathbb{E}[u(\mathbf{x})u(\mathbf{y})] = \sum_{\mathbf{z}} S(\mathbf{x}-\mathbf{z})S(\mathbf{y}-\mathbf{z}). \tag{40}$$

By Fourier transforming both sides of the above equation, one can see that the large distance asymptotics (1) is determined by the small $\mathbf{k}$ asymptotics of $\hat{S}(\mathbf{k})^2$, where $\hat{S}(\mathbf{k})$ is the Fourier transform of $S(\mathbf{x})$. In particular, $\hat{S}(\mathbf{k}) \sim |\mathbf{k}|^{-H-1}$(for $|\mathbf{k}| << 1$).

We apply this procedure to generate random long-range correlated surfaces. We consider a domain $[0,\cdots,N-1]\times[0,\cdots,M-1] \subset \mathbb{Z}^2$ where $\mathbf{x} = (x_1, x_2)$ denotes a lattice site:

$$\mathbf{x} = (x_1, x_2), \quad x_1 = 0, \cdots N-1$$

and

$$x_2 = 0, \cdots, M-1. \tag{41}$$

A random function $w(\mathbf{x})$ is generated by drawing its values independently at each point by an initial Gaussian distribution $P(w) = \mathcal{N}(0,1)$. The probability distribution function $P[w(\mathbf{x})]$ is therefore:

$$P[w(\mathbf{x})] = \prod_{\mathbf{x}} \frac{e^{-\frac{w(\mathbf{x})^2}{2}}}{\sqrt{2\pi}}. \tag{42}$$

The discrete Fourier transform of $w(\mathbf{x})$ is defined as:

$$\hat{w}(\mathbf{k}) = \frac{1}{N\,M} \sum_{\mathbf{x}} w(\mathbf{x}) e^{-i\,\mathbf{k}\,\mathbf{x}} = \frac{1}{N\,M} \sum_{x_1=0}^{N-1} \sum_{x_2=0}^{M-1} w(x_1,x_2) e^{-2\pi i \left(x_1 \frac{k_1}{N} + x_2 \frac{k_2}{M}\right)}, \tag{43}$$

where

$$\mathbf{k} = 2\pi \left(\frac{k_1}{N}, \frac{k_2}{M}\right), \quad k_1 = 0, \cdots, N-1,\ k_2 = 0, \cdots, M-1. \tag{44}$$

From (42) one has:

$$\mathbb{E}[\hat{w}(\mathbf{k})] = 0, \quad \mathbb{E}[\hat{w}(\mathbf{k})\hat{w}(\mathbf{p})] = \delta_{k_1,N-p_1}\delta_{k_2,M-p_2}. \tag{45}$$

We use the convolution kernel:

$$\hat{S}(\mathbf{k}) = \begin{cases} = \lambda_{\mathbf{k}}^{-\frac{H+1}{2}}, & \text{for } k_1, k_2 \neq 0 \\ = 1 \quad \text{for } k_1 = k_2 = 0, \end{cases} \tag{46}$$

where:

$$\lambda_{\mathbf{k}} = \left(2\cos\left(\frac{2\pi}{N}\,k_1\right) + 2\cos\left(\frac{2\pi}{M}\,k_2\right) - 4\right). \tag{47}$$

We generate the random surface $u(\mathbf{x})$ by doing the following inverse Fourier transform:

$$u(\mathbf{x}) = \frac{1}{\text{norm}} \sum_{\mathbf{k}} \hat{S}(\mathbf{k})\,\hat{w}(\mathbf{k})\,e^{i\,\mathbf{k}\,\mathbf{x}}, \quad \text{norm} = \sum_{\mathbf{k}} \hat{S}^2(\mathbf{k}). \tag{48}$$

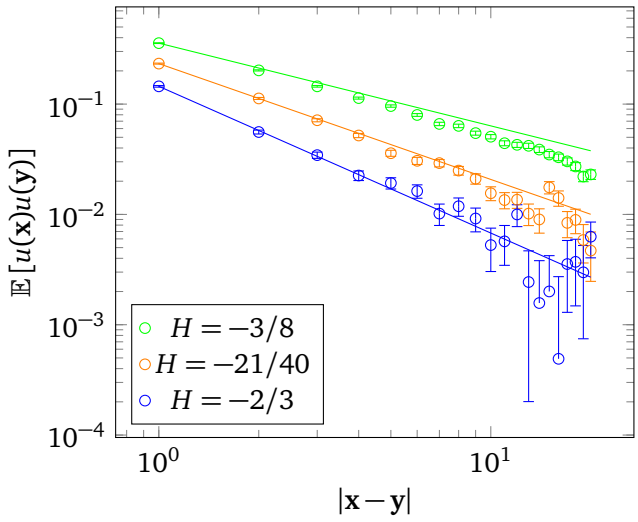

Figure 17: Numerical measurement of $\mathbb{E}[u(\mathbf{x})u(\mathbf{y})]$ for different values of the Hurst exponent, on square lattices of size $M = N = 2^8$. The lines have slopes $-2H$.

The universal properties do not depend on the initial distribution $P[w(\mathbf{x})]$ distribution nor on the precise form of the kernel as long as $\hat{S}(\mathbf{k})$ has the same small $\mathbf{k}$ asymptotic behaviour

[70]. As we explain in Section 3, we find useful to generate long-range correlated random surfaces by using another distribution $P_2[w(\mathbf{x})]$ for $w(\mathbf{x})$ and a different kernel. In particular, the $P_2[w(\mathbf{x})]$ is determined by the uniform distribution:

$$P_2[w(\mathbf{x})] = \prod_{\mathbf{x}} P(w(\mathbf{x})), \quad P(w(\mathbf{x})) = \begin{cases} 1, & |w(\mathbf{x})| < \frac{\sqrt{3}}{N} \\ 0, & |w(\mathbf{x})| > \frac{\sqrt{3}}{N} \end{cases} \tag{49}$$

and the kernel:

$$\hat{S}_2(\mathbf{k}) = \begin{cases} |\mathbf{k}|^{-H-1} & \text{for } \mathbf{k} \neq (0,0), \\ 1 & \text{for } \mathbf{k} = (0,0) \end{cases}, \tag{50}$$

where:

$$|\mathbf{k}| = \frac{2\pi}{N}\sqrt{k_1^2 + k_2^2}, \quad k_1, k_2 = -N/2, \cdots N/2 - 1. \tag{51}$$

The second kind of surfaces we generate are

$$u(\mathbf{x}) = \frac{1}{\text{norm}} \sum_{\mathbf{k}} \hat{S}_2(\mathbf{k})\, \hat{w}_2(\mathbf{k})\, e^{i\,\mathbf{k}\,\mathbf{x}}, \quad \text{norm} = \sum_{\mathbf{k}} \hat{S}_2^2(\mathbf{k}), \tag{52}$$

where we indicated as $\hat{w}_2(\mathbf{k})$ the Fourier transforms of the random function $w(\mathbf{x})$ of law (49). In the above equations we assumed $M = N$, but the generalization to $M \neq N$ is straightforward. Note that, due to the (Lyupanov) central limit theorem, $\hat{w}_2(\mathbf{k})$ is described in the large N limit by a Gaussian distribution and the function $u(\mathbf{x})$ can be considered an instance of a fractional Gaussian surface. For $H < 0$, the surface $u(\mathbf{x})$, generated by (48) or by (52):

- is real, $u(\mathbf{x}) \in \mathbb{R}$, from the property (45) and the symmetry of the kernel (46)
- satisfies (1). In Figure 17 we show the numerical measurements of $\mathbb{E}[u(\mathbf{x})u(\mathbf{y})]$ for the surface (48)and for different values of the roughness exponent. The data points are compared to the power law decay $|\mathbf{x}-\mathbf{y}|^{2H}$.
- has a zero mode which vanishes in law:

$$\mathbb{E}[\hat{u}(\mathbf{0})] = 0. \tag{53}$$

- is normalised such that:

$$\mathbb{E}\left[u(\mathbf{x})^2\right] = 1. \tag{54}$$

  Note that, in the thermodynamic limit, the normalisation constant in (48) is finite for negative H, as norm $\sim N^{2H} + O(1)$ ($N >> 1, M/N = O(1)$). The surface fluctuations are thus bounded.

- satisfies periodic boundary conditions in both directions

$$u(\mathbf{x} + \mathbf{t}) = u(\mathbf{x}), \quad \text{for } \mathbf{t} = (n\,N, m\,M),\ n, m \in \mathbb{N}. \tag{55}$$

B Percolation phase transition: critical level h_c and the critical exponents ν and D_f

We study here the critical percolative properties of the level clusters of the surface (48) and (52). In particular we determine numerically the critical level h_c and the exponents ν and D_f.

B.1 Critical level and correlation length exponent ν

For a sign-symmetric random function $u(\mathbf{x})$ on the Euclidean space, $\mathbf{x} \in \mathbb{R}^2$, the critical level is $h_c = 0$ by symmetry argument [13]. Our function $u(\mathbf{x})$ is defined on a lattice and h_c is expected to be negative. We determine the critical level h_c by the standard procedure of percolation theory [11]. We consider square domains of different sizes $N \times N$. We determine the average $\mathbb{E}[h_c(N)]$ of the level $h_c(N)$ at which a level cluster connecting the top and the bottom of the lattice appears. This quantity scales with the size of the lattice as:

$$\mathbb{E}[h_c(N)] - h_c \sim N^{-\frac{1}{\nu}}. \tag{56}$$

The data point for $\mathbb{E}[h_c(N)]$, shown in Figure 18 as a function of N^H for different values of H, are very well described by a linear interpolation, thus confirming the predition (7). Fitting the data to the form (56) with $\nu = \nu^{\text{long}}$, we obtain the values of h_c reported in Table 10.

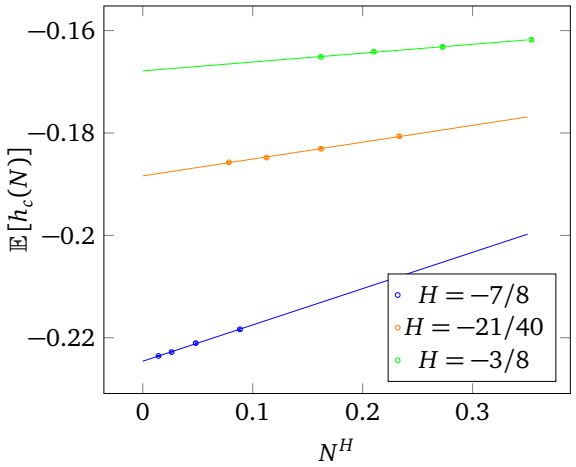

Figure 18: $\mathbb{E}[h_c(N)]$ for $N = 2^4, \cdots 2^7$ as a function of N^H. The lines are the best fits to the form (56) with $\nu = -1/H$ for different Hs. The intercepts with the vertical $N^H = 0$ axis ($N \to \infty$ limit), give the estimation for h_c.

Table 10: Critical level obtained from scaling (56), for the surfaces (48).

H	h_c
-7/8	-0.2238(1)
-2/3	-0.2034(1)
-5/8	-0.1985(1)
-21/40	-0.1860(2)
-19/40	-0.1775(3)
-3/8	-0.1670(5)
-3/10	-0.1570(5)

Another way to determine the critical point is based on the Binder method. We apply this method to study the surface (52). Defining the moments M_m as:

$$M_m = \sum_{i=0}^{\infty} i^m n_i, \tag{57}$$

with n_i the number of level clusters composed of i sites, one computes the ratio $r_N^{\text{Bin}}(h)$

$$r_N^{\text{Bin}}(h) = \frac{\mathbb{E}\left[M_4\right]}{\mathbb{E}\left[M_2\right]^2}, \tag{58}$$

where the average $\mathbb{E}[\cdots]$ is weighted by the distribution (49). The ratio $r_N^{\text{Bin}}(h)$ depends on the level h and on the system size N through a scaling relation of the type:

$$r_N^{\text{Bin}}(h) = f\left((h-h_c)N^{\frac{1}{\nu}}\right) + a\, N^{-\omega}, \tag{59}$$

where the function f is some scaling function, and the term $a\, N^{-\omega}$, with a a non-universal prefactor, is a correction to the scaling term. The interpretation of ω is discussed below. From (59), one can find the point $h_c(N)$ where the curves $r_N^{\text{Bin}}(h)$ and $r_{2N}^{\text{Bin}}(h)$ intersect [71] and use the fitting form:

$$h_c(N) = h_c + \frac{a}{N^x}, \tag{60}$$

to determine h_c, with x a free parameter. For each value in (30), we compute (58) for sizes $N = 2^s$, $s = 4, \cdots, 9$ and $N = 3 \times 2^s$, $s = 3, \cdots, 7$ averaged over 10^5 instances. We interpolate the curves and find their intersections. The Binder method shows less precision for H approaching 0. Indeed the correlation length exponent $\nu = -1/H$ increases fast, making the size effects much smaller. The curves $r_N^{\text{Bin}}(h)$ and $r_N^{\text{Bin}}(h)$ tend to be parallel, and localising their crossing point becomes difficult. In Figure 19 we show the scaling of the crossing points $h_c(N)$ for some values of H. Once the critical point is located, the thermal exponent ν can be estimated by using that:

$$\frac{d}{dh} r_N^{\text{Bin}}(h)|_{h=h_c} \sim N^{1/\nu}. \tag{61}$$

In Table 11 we give the values of h_c obtained from (60), and the values of ν obtained from (61). These latter are in fair agreement with the prediction (6, 7). Setting ν to (7) we estimate the values of ω as $\omega = x - 1/\nu$.

Table 11: Values of the critical level h_c obtained with the Binder method. The ν exponent is obtained from equation (61), and the value of the exponent w is obtained from scaling (60), with ν set to (7). The measurements have been taken for the surface (52).

H	h_c	ν	ω
-1	-0.3210(9)	1.33(2)	2.00(5)
-7/8	-0.3075(5)	1.46(8)	1.00(5)
-2/3	-0.2793(5)	1.67(5)	0.8(1)
-5/8	-0.2722(5)	1.9(1)	1.0(1)

It is quite interesting to comment on the exponent ω, which determines the correction to the scaling. The exponent ω is expected to be the conformal dimension of the first irrelevant thermal field. In [72] is was observed that, when the model is integrable, the corrections to the scaling are always associated to irrelevant fields that appear in the fusion between relevant ones. To be more specific, the authors of [72] considered those statistical models that are described by rational CFTs. The spectrum of these CFTs contain a finite set of primary fields, which close under Operator Product Algebra and which are listed in the so-called Kac Table. When these models are integrable, the correction to scaling are therefore determined by fields inside the Kac table. In the pure percolation CFT, the (relevant) energy density ε field, $\varepsilon = V_{1,2}$ generate by fusion with itself an infinite series of irrelevant fields with dimension

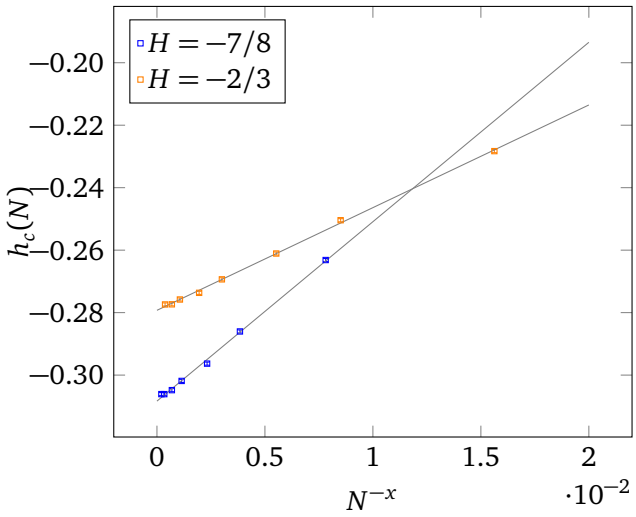

Figure 19: Values of $h_c(N)$ obtained from the crossing of the curves $r_N^{\mathrm{Bin}}(h)$ and $r_N^{\mathrm{Bin}}(h)$, defined in (58). Measurements have been taken for the surface (52).

$\Delta_{1,n}$, $n = 3, 4, \ldots$ (note that we have used the standard minimal model notation $V_{r,s}$ and $\Delta_{r,s}$ for the field and conformal dimension). In the case of pure percolation, which is an integrable model, the value of ω is therefore expected to be given by the lowest irrelevant thermal field dimension, $\omega = 2\Delta_{1,3} = 2$. A discussion of this exponent can be found for instance in Appendix D of [73]. In the case of pure percolation, we find indeed $\omega = 2$. We observe in Table 11 that, when $H \neq -1$, a non-universal correction with $\omega \sim 1$ to the scaling dominates. v

B.2 Fractal dimension D_f

At the critical point $h = h_c$, the level clusters have fractal dimension D_f. This dimension determines the scaling of the average mass (i.e. number of points) $\mathcal{A}_l$ of a level cluster with respect to its length l, $\mathcal{A}_l \sim l^{D_f}$. The length of a level cluster can be defined as its radius of gyration. One effective way to measure D_f is to consider the percolating level cluster whose size is of the same order of the system size, $l \sim N$. To determine D_f, we use then the following relation:

$$\mathbb{E}[\#\text{ sites of the p.l.c.}] \sim N^{D_f}, \quad \text{p.l.c.=percolating level cluster.} \tag{62}$$

A representative example of a numerical measurement of the above average is shown in Figure 20a, for $H = -2/3$. To remove the small sizes effects, we perform fits with the successive lower sizes removed, and expect the best fit parameter to converge to the fractal dimension, as in Figure 20b. The values $D_f^{(1)}$ obtained are given in Table 12.

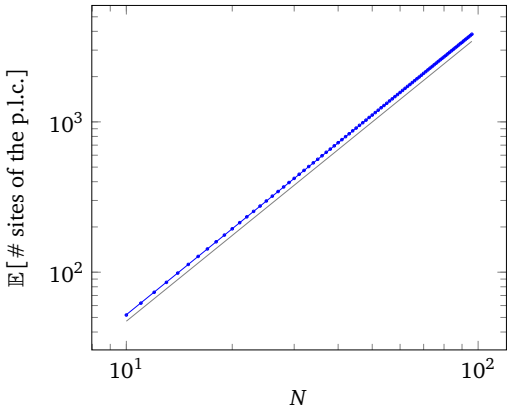

(a) Average mass of the percolating level cluster for $H = -2/3$, and the best fit line which has slope ~ 1.90. The gray line corresponds to the percolation value $D_f = 91/48 \sim 1.8958$.

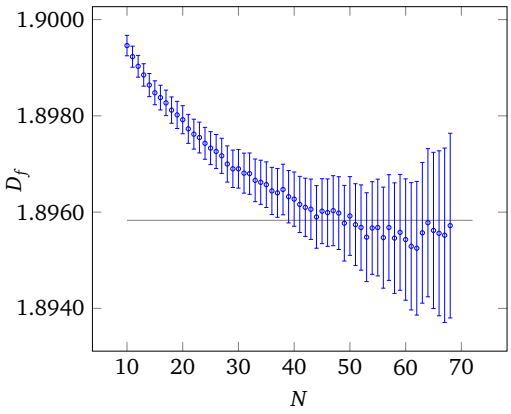

(b) Convergence of the best fit parameter for the fractal dimension when the lowest size points are removed. Here it converges to the percolation value shown as a grey line.

Figure 20

Table 12: Fractal dimensions obtained (1) from the scaling of the largest cluster (62) and (2) from the power-law decay of the two-point connectivity (11), and comparison with previous numerical work [25].

H	$D_f^{(1)}$	$D_f^{(2)}$	D_f [25]
-7/8	1.8955(5)	1.8945(2)	1.8964(2)
-2/3	1.8960(10)	1.893(1)	
-5/8	1.8955(6)	1.892(1)	1.8950(3)
-21/40	1.8965(10)	1.8910(5)	
-19/40	1.8955(8)	1.8897(5)	
-3/8	1.904(1)	1.8970(5)	1.9006(4)
-1/4	1.917(1)	1.906(1)	1.9128(5)

References

[1] A. L. Efros, *Physics and geometry of disorder: Percolation theory*, Science for Everyone. Mir Publishers, ISBN 0828532915,9780828532914 (1987).

[2] S. A. Molchanov and A. K. Stepanov, *Percolation in random fields. I*, Theor. Math. Phys. **55**, 478 (1983), doi:10.1007/BF01015808.

[3] M. B. Isichenko and J. Kalda, *Statistical topography. I. Fractal dimension of coastlines and number-area rule for Islands*, J. Nonlinear Sci. **1**, 255 (1991), doi:10.1007/BF01238814.

[4] S. Prakash, S. Havlin, M. Schwartz and H. Eugene Stanley, *Structural and dynamical properties of long-range correlated percolation*, Phys. Rev. A **46**, R1724 (1992), doi:10.1103/PhysRevA.46.R1724.

[5] V. Beffara and D. Gayet, *Percolation of random nodal lines*, Publ. math. IHES **126**, 131 (2017), doi:10.1007/s10240-017-0093-0.

[6] A. Rivera and H. Vanneuville, *The critical threshold for Bargmann–Fock percolation*, Annales Henri Lebesgue **3**, 169 (2020), doi:10.5802/ahl.29.

[7] A. Rivera, *Statistical mechanics of Gaussian fields*, Ph.D. thesis (2018).

[8] A. Ali Saberi, *Recent advances in percolation theory and its applications*, Phys. Rep. **578**, 1 (2015), doi:10.1016/j.physrep.2015.03.003.

[9] M. Barnsley, R. Devaney, B. Mandelbrot, H.-O. Peitgen, D. Saupe and R. Voss, *The science of fractal images*, Springer-Verlag, Berlin, Heidelberg, ISBN 0387966080 (1988).

[10] R. J. Adler and J. E. Taylor, *Random fields and geometry*, Springer monographs in Mathematics, Springer (2007).

[11] D. Stauffer and A. Aharony, *Introduction to percolation theory*, Oxford University Press, New York (1971).

[12] J. Schmittbuhl, J. -P Vilotte and S. Roux, *Percolation through self-affine surfaces*, J. Phys. A: Math. Gen. **26**, 6115 (1993), doi:10.1088/0305-4470/26/22/014.

[13] S. A. Molchanov and A. K. Stepanov, *Percolation in random fields. II*, Theor. Math. Phys. **55**, 592 (1983), doi:10.1007/BF01015170.

[14] S. A. Molchanov and A. K. Stepanov, *Percolation in random fields. III*, Theor. Math. Phys. **67**, 434 (1986), doi:10.1007/BF01118150.

[15] J. L. Lebowitz and H. Saleur, *Percolation in strongly correlated systems*, Phys. A: Stat. Mech. Appl. **138**, 194 (1986), doi:10.1016/0378-4371(86)90180-9.

[16] J. Aru, T. Lupu and A. Sepúlveda, *First passage sets of the 2D continuum Gaussian free field*, Probab. Theory Relat. Fields **176**, 1303 (2019), doi:10.1007/s00440-019-00941-1.

[17] L. Schoug, A. Sepúlveda and F. Viklund, *Dimension of two-valued sets via imaginary chaos* (2019), arXiv:1910.09294.

[18] A. Rosso, R. Santachiara and W. Krauth, *Geometry of Gaussian signals*, J. Stat. Mech. L08001 (2005), doi:10.1088/1742-5468/2005/08/l08001.

[19] R. Santachiara, F. Stauffer and D. C. Cabra, *Entanglement properties and momentum distributions of hard-core anyons on a ring*, J. Stat. Mech. L05003 (2007), doi:10.1088/1742-5468/2007/05/l05003.

[20] A. Zoia, A. Rosso and M. Kardar, *Fractional Laplacian in bounded domains*, Phys. Rev. E **76**, 021116 (2007), doi:10.1103/physreve.76.021116.

[21] A. Weinrib, *Long-range correlated percolation*, Phys. Rev. B **29**, 387 (1984), doi:10.1103/PhysRevB.29.387.

[22] H. Vanneuville, *Private communivation* .

[23] D. Beliaev, S. Muirhead and A. Rivera, *A covariance formula for topological events of smooth Gaussian fields* (2018), arXiv:1811.08169.

[24] A. Rivera and H. Vanneuville, *Quasi-independence for nodal lines*, Ann. Inst. H. Poincaré Probab. Statist. **55**, 1679 (2019), doi:10.1214/18-AIHP931.

[25] J. Zierenberg, N. Fricke, M. Marenz, F. P. Spitzner, V. Blavatska and W. Janke, *Percolation thresholds and fractal dimensions for square and cubic lattices with long-range correlated defects*, Phys. Rev. E **96**, 062125 (2017), doi:10.1103/physreve.96.062125.

[26] C. P. de Castro, M. Luković, G. Pompanin, R. F. S. Andrade and H. J. Herrmann, *Schramm-Loewner evolution and perimeter of percolation clusters of correlated random landscapes*, Sci. Rep. **8**, 5286 (2018), doi:10.1038/s41598-018-23489-x.

[27] J. Kalda, *Oceanic coastline and super-universality of percolation clusters* (2002), arXiv:cond-mat/0210650.

[28] M. V. Berry, *Regular and irregular semiclassical wavefunctions*, J. Phys. A: Math. Gen. **10**, 2083 (1977), doi:10.1088/0305-4470/10/12/016.

[29] E. Bogomolny and C. Schmit, *Random wavefunctions and percolation*, J. Phys. A: Math. Theor. **40**, 14033 (2007), doi:10.1088/1751-8113/40/47/001.

[30] J. Cardy, *Conformal invariance and percolation* (2001), arXiv:math-ph/0103018.

[31] S. Smirnov, *Critical percolation in the plane: conformal invariance, Cardy's formula, scaling limits*, Comptes Rendus de l'Académie des Sciences - Series I - Mathematics **333**, 239 (2001), doi:10.1016/S0764-4442(01)01991-7.

[32] Vl. S. Dotsenko and V. A. Fateev, *Conformal algebra and multipoint correlation functions in 2D statistical models*, Nucl. Phys. B **240**, 312 (1984), doi:10.1016/0550-3213(84)90269-4.

[33] H. Saleur, *Conformal invariance for polymers and percolation*, J. Phys. A: Math. Gen. **20**, 455 (1987), doi:10.1088/0305-4470/20/2/031.

[34] P. di Francesco, H. Saleur and J. B. Zuber, *Relations between the Coulomb gas picture and conformal invariance of two-dimensional critical models*, J. Stat. Phys. **49**, 57 (1987), doi:10.1007/BF01009954.

[35] J. L. Cardy, *Critical percolation in finite geometries*, J. Phys. A: Math. Gen. **25**, L201 (1992), doi:10.1088/0305-4470/25/4/009.

[36] P. Mathieu and D. Ridout, *Logarithmic minimal models, their logarithmic couplings, and duality*, Nucl. Phys. B **801**, 268 (2008), doi:10.1016/j.nuclphysb.2008.02.017.

[37] R. Nivesvivat and S. Ribault, *Logarithmic CFT at generic central charge: from Liouville theory to the Q-state Potts model* (2020), arXiv:2007.04190.

[38] L. Grans-Samuelsson, L. Liu, Y. He, J. Lykke Jacobsen and H. Saleur, *The action of the Virasoro algebra in the two-dimensional Potts and loop models at generic Q* (2020), arXiv:2007.11539.

[39] M. Picco, S. Ribault and R. Santachiara, *A conformal bootstrap approach to critical percolation in two dimensions*, SciPost Phys. **1**, 009 (2016), doi:10.21468/SciPostPhys.1.1.009.

[40] J. L. Jacobsen and H. Saleur, *Bootstrap approach to geometrical four-point functions in the two-dimensional critical Q-state Potts model: a study of the s-channel spectra*, J. High Energ. Phys. **01**, 084 (2019), doi:10.1007/JHEP01(2019)084.

[41] M. Picco, S. Ribault and R. Santachiara, *On four-point connectivities in the critical 2d Potts model*, SciPost Phys. **7**, 044 (2019), doi:10.21468/SciPostPhys.7.4.044.

[42] Y. He, L. Grans-Samuelsson, J. L. Jacobsen and H. Saleur, *Geometrical four-point functions in the two-dimensional critical Q-state Potts model: connections with the RSOS models*, J. High Energ. Phys. **05**, 156 (2020), doi:10.1007/jhep05(2020)156.

[43] Y. He, J. L. Jacobsen and H. Saleur, *Geometrical four-point functions in the two-dimensional critical Q-state Potts model: The interchiral conformal bootstrap* (2020), arXiv:2005.07258.

[44] K. J. Schrenk, N. Posé, J. J. Kranz, L. V. M. van Kessenich, N. A. M. Araújo and H. J. Herrmann, *Percolation with long-range correlated disorder*, Phys. Rev. E **88**, 052102 (2013), doi:10.1103/PhysRevE.88.052102.

[45] D. Bernard, G. Boffetta, A. Celani and G. Falkovich, *Conformal invariance in two-dimensional turbulence*, Nat. Phys. **2**, 124 (2006), doi:10.1038/nphys217.

[46] M. Bauer and D. Bernard, *2D growth processes: SLE and Loewner chains*, Phys. Rep. **432**, 115 (2006), doi:10.1016/j.physrep.2006.06.002.

[47] X. Cao, A. Rosso and R. Santachiara, *Conformal invariance of loop ensembles under Kardar-Parisi-Zhang dynamics*, Europhys. Lett. **111**, 16001 (2015), doi:10.1209/0295-5075/111/16001.

[48] S. Sheffield and W. Werner, *Conformal loop ensembles: the Markovian characterization and the loop-soup construction*, Ann. Math. **176**, 1827 (2012), doi:10.4007/annals.2012.176.3.8.

[49] B. Duplantier and H. Saleur, *Exact fractal dimension of 2D Ising clusters*, Phys. Rev. Lett. **63**, 2536 (1989), doi:10.1103/PhysRevLett.63.2536.

[50] N. Javerzat, M. Picco and R. Santachiara, *Two-point connectivity of two-dimensional critical Q-Potts random clusters on the torus*, J. Stat. Mech. 023101 (2020), doi:10.1088/1742-5468/ab6331.

[51] R. J. Adler, E. Moldavskaya and G. Samorodnitsky, *On the existence of paths between points in high level excursion sets of Gaussian random fields*, Ann. Probab. **42**, 1020 (2014), doi:10.1214/12-aop794.

[52] A. Kapitulnik, Y. Gefen and A. Aharony, *On the Fractal dimension and correlations in percolation theory*, J. Stat. Phys. **36**, 807 (1984), doi:10.1007/BF01012940.

[53] J. Cardy, *Scaling and renormalization in statistical physics*, Cambridge University Press, ISBN 9780521499590 (1996), doi:10.1017/CBO9781316036440.

[54] N. Javerzat, M. Picco and R. Santachiara, *Three- and four-point connectivities of two-dimensional critical Q-Potts random clusters on the torus*, J. Stat. Mech. 053106 (2020), doi:10.1088/1742-5468/ab7c5e.

[55] J. Lykke Jacobsen, *Loop models and boundary CFT*, in Conformal Invariance: an Introduction to Loops, Interfaces and Stochastic Loewner Evolution, Springer Berlin Heidelberg, ISBN 9783642279331 (2012), doi:10.1007/978-3-642-27934-8_4.

[56] H. W. J. Blöte, J. L. Cardy and M. P. Nightingale, *Conformal invariance, the central charge, and universal finite-size amplitudes at criticality*, Phys. Rev. Lett. **56**, 742 (1986), doi:10.1103/PhysRevLett.56.742.

[57] P. Di Francesco, P. Mathieu and D. Senechal, *Conformal field theory* (1997).

[58] K. K. Mon, *Direct calculation of absolute free energy for lattice systems by Monte Carlo sampling of finite-size dependence*, Phys. Rev. Lett. **54**, 2671 (1985), doi:10.1103/PhysRevLett.54.2671.

[59] M. Krech and D. P. Landau, *Casimir effect in critical systems: A Monte Carlo simulation*, Phys. Rev. E **53**, 4414 (1996), doi:10.1103/PhysRevE.53.4414.

[60] P. J. M. Bastiaansen and H. J. F. Knops, *Monte Carlo method to calculate the central charge and critical exponents*, Phys. Rev. E **57**, 3784 (1998), doi:10.1103/PhysRevE.57.3784.

[61] W. M. Koo and H. Saleur, *Representations of the Virasoro algebra from lattice models*, Nucl. Phys. B **426**, 459 (1994), doi:10.1016/0550-3213(94)90018-3.

[62] R. Couvreur, J. Lykke Jacobsen and R. Vasseur, *Non-scalar operators for the Potts model in arbitrary dimension*, J. Phys. A: Math. Theor. **50**, 474001 (2017), doi:10.1088/1751-8121/aa7f32.

[63] X. Tan, R. Couvreur, Y. Deng and J. Lykke Jacobsen, *Observation of nonscalar and logarithmic correlations in two- and three-dimensional percolation*, Phys. Rev. E **99**, 050103 (2019), doi:10.1103/physreve.99.050103.

[64] S. Ribault, *Conformal field theory on the plane* (2014), arXiv:1406.4290.

[65] Vl. S. Dotsenko and V. A. Fateev, *Four-point correlation functions and the operator algebra in 2D conformal invariant theories with central charge $C \leq 1$*, Nucl. Phys. B **251**, 691 (1985), doi:10.1016/S0550-3213(85)80004-3.

[66] Vl. S. Dotsenko and V. A. Fateev, *Operator algebra of two-dimensional conformal theories with central charge $C \leq 1$*, Phys. Lett. B **154**, 291 (1985), doi:10.1016/0370-2693(85)90366-1.

[67] A. Zamolodchikov and Al. Zamolodchikov, *Conformal bootstrap in Liouville field theory*, Nucl. Phys. B **477**, 577 (1996), doi:10.1016/0550-3213(96)00351-3.

[68] S. Migliaccio and S. Ribault, *The analytic bootstrap equations of non-diagonal two-dimensional CFT*, J. High Energ. Phys. **05**, 169 (2018), doi:10.1007/jhep05(2018)169.

[69] B. Estienne and Y. Ikhlef, *Correlation functions in loop models* (2015), arXiv:1505.00585.

[70] C. P. de Castro, M. Luković, R. F. S. Andrade and H. J. Herrmann, *The influence of statistical properties of Fourier coefficients on random Gaussian surfaces*, Sci. Rep. **7**, 1961 (2017), doi:10.1038/s41598-017-02135-y.

[71] H. Saleur and B. Derrida, *A combination of Monte Carlo and transfer matrix methods to study 2D and 3D percolation*, J. Phys. France **46**, 1043 (1985), doi:10.1051/jphys:019850046070104300.

[72] H. W. J. Blöte and M. P. M. den Nijs, *Corrections to scaling at two-dimensional Ising transitions*, Phys. Rev. B **37**, 1766 (1988), doi:10.1103/PhysRevB.37.1766.

[73] N. G. Fytas, V. Martín-Mayor, G. Parisi, M. Picco and N. Sourlas, *Evidence for supersymmetry in the random-field Ising model at D=5*, Phys. Rev. Lett. **122**, 240603 (2019), doi:10.1103/physrevlett.122.240603.

SUMMARY AND OUTLOOK

SUMMARY

In this thesis we have explored new bootstrap solutions describing geometric observables of critical percolation phenomena. We studied these systems in the scaling limit, in a field theory framework, by assuming that probabilities of non-local nature can be described by correlations of local quantum fields. Our approach relied on the exploitation of the universal finite size effects induced by a toroidal geometry, together with the constraints imposed by conformal symmetry and self-consistency of the theory.

This approach provided exact results on the critical behaviour of two families of correlated percolation models, the $Q-$state Potts model and the model of percolation of random surfaces. For the $Q-$state Potts model we obtained the topological corrections to the two-, three- and four-point connectivities. These results provide notably new predictions for universal observables of critical pure percolation. Moreover we tested the consistency of the recent bootstrap solution [44–49] on the torus.
For the random surfaces models, where conformal invariance remained debated, we provided strong evidence that the percolation clusters are conformally invariant. We also verified the important conjecture of Weinrib that the system remains in the pure percolation universality class when the roughness of the surface $H \in [-1, -3/4]$. This verification was done at the level of highly non-trivial observables, and goes beyond the matching of the main critical exponents. In addition we obtained the first features of the unknown CFT describing this line of critical points. We expect this CFT to be a new bootstrap solution, offering new challenges in our understanding of the space of consistent conformal field theories. Indeed as we mentioned in Chapter 5, these correlated percolation systems can be considered as systems with quenched, long-range correlated disorder. One can therefore expect the corresponding CFT to display features of geometric phenomena (it could be for instance logarithmic), as well as new features coming from the presence of disorder.
All in all, it is manifest that the space of two-dimensional CFTs is far from being completely charted.

OUTLOOK

Besides the follow-up issues listed at the end of the respective chapters, we would like to point at especially interesting, more general open questions arising from our results.

Bulk and boundaries of correlated percolation clusters

It is established that the fractal dimensions of the bulk and boundaries of the clusters in the $O(n)$ models are related [41], all of them being continuous functions of the central charge of the corresponding CFT.

Surprisingly, this does not seem to hold for the clusters of the random surface models, as discussed in Chapter 5. Indeed several numerical works support the fact that the boundaries are described by SLE_κ curves, so that their fractal dimensions match those of the loops of the $O(n)$ models. Conversely, the observed behaviour of the bulk fractal dimension, as well as our results on the two-point connectivity, exclude that the clusters belong to the $O(n)$ universality class. One can then wonder if the bulk and boundaries of the clusters are described by the same CFT.
In the conclusion of Chapter 5 we highlighted a few research avenues to make progress on this issue, and notably on how to obtain estimates of the central charge, which is a crucial parameter (albeit not sufficient) in the identification of a CFT. It would be interesting to investigate the relations between the bulk and boundary of clusters in other families of percolation models, see notably next project below.

Disordered Potts model

Many interesting open problems in two dimensions concern the effect of quenched disorder on critical behaviour [132]. As we have recalled above, the correlated percolation model of Chapter 5 corresponds to a system with long-range correlated disorder, whose effect is to drive the system to new universality classes. A simpler model to study such effects is provided by the $Q-$state Potts model with uncorrelated disorder [133]. Many results have been obtained for this model, both from perturbative and numerical analyses as reviewed in details in [134]. In particular these critical points are believed to be conformally invariant, and several critical exponents have been determined, as well as the central charge. The central open question today is the identification of the CFT describing this family of models.
In this context we propose an analytic and numerical approach to the problem, based on the study of the torus connectivities, which would notably allow to determine the spin-spin-energy structure constants of this CFT. We would like to numerically measure the torus connectivities of the disordered model and obtain numerical estimates of the CFT data (structure constants, central charge and multiplicities), following the analysis of Chapter 5. In addition, in this simpler problem we can in principle compute perturbatively some of this CFT data, and compare with the numerical results.
Besides obtaining new results on this unkown CFT, this analysis would also make connection with the preceeding question, in that it would allow to compare the statistical properties of the clusters with what is known of their boundaries from previous studies.

To complete the loop started in the introduction, critical phenomena are, two centuries after their discovery, more fascinating and challenging than ever. It is quite astonishing to look how far the progress in their description has come, unveiling beautiful mathematical structures as well as making connections with high energy or quantum physics. Chances are, there will be more to discover !

Part III

APPENDIX

A

ELLIPTIC FUNCTIONS

The elliptic theta functions are defined as:

$$\theta \begin{bmatrix} a \\ b \end{bmatrix} (z|\tau) = \sum_{n\in\mathbb{Z}} q^{\frac{1}{2}(n-a/2)^2} e^{2\pi i(z-b/2)(n-a/2)}, \quad a, b = 0, 1 \tag{A.1}$$

where q is the elliptic nome

$$q = e^{2\pi i\tau}. \tag{A.2}$$

The usual notation is:

$$\theta_1 = \theta \begin{bmatrix} 1 \\ 1 \end{bmatrix} \quad \theta_2 = \theta \begin{bmatrix} 1 \\ 0 \end{bmatrix} \tag{A.3}$$

$$\theta_3 = \theta \begin{bmatrix} 0 \\ 0 \end{bmatrix} \quad \theta_4 = \theta \begin{bmatrix} 0 \\ 1 \end{bmatrix}. \tag{A.4}$$

We define also the Dedekind eta function:

$$\eta(\tau) = q^{1/24} \prod_{n=1}^{\infty} (1 - q^n). \tag{A.5}$$

We will give here a few useful properties of these functions. A complete list can be found for example in [135].
From the product representation of the theta functions:

$$\theta_1(z|\tau) = 2q^{1/8} \sin(\pi z) \prod_{n=1}^{\infty} (1 - q^n)(1 - q^n e^{2\pi iz})(1 - q^n e^{-2\pi iz}), \tag{A.6a}$$

$$\theta_2(z|\tau) = 2q^{1/8} \cos(\pi z) \prod_{n=1}^{\infty} (1 - q^n)(1 + q^n e^{2\pi iz})(1 + q^n e^{-2\pi iz}), \tag{A.6b}$$

$$\theta_3(z|\tau) = \prod_{n=1}^{\infty} (1 - q^n)(1 + q^{n-1/2} e^{2\pi iz})(1 + q^{n-1/2} e^{-2\pi iz}), \tag{A.6c}$$

$$\theta_4(z|\tau) = \prod_{n=1}^{\infty} (1 - q^n)(1 - q^{n-1/2} e^{2\pi iz})(1 - q^{n-1/2} e^{-2\pi iz}), \tag{A.6d}$$

we deduce that:

$$\partial^{(2k)} \theta_1(z|\tau)|_{z=0} = 0 \tag{A.7a}$$

$$\partial^{(2k+1)} \theta_\nu(z|\tau)|_{z=0} = 0, \quad \nu = 2, 3, 4. \tag{A.7b}$$

A useful identity is:

$$\partial_z \theta_1(z|\tau)|_{z=0} \equiv \theta_1' = 2\pi\eta^3(\tau). \tag{A.8}$$

BIBLIOGRAPHY

[1] Bertrand Berche, Malte Henkel, and Ralph Kenna. "Fenômenos críticos: 150 anos desde Cagniard de la Tour." In: *Revista Brasileira de Ensino de Física* 31.2 (2009), 2602.1–2602.4. ISSN: 1806-1117. DOI: 10.1590/s1806-11172009000200015. arXiv: 0905.1886 [physics.hist-ph].

[2] P. W. Anderson. "More Is Different." In: *Science* 177.4047 (1972), pp. 393–396. ISSN: 0036-8075. DOI: 10.1126/science.177.4047.393. eprint: https://science.sciencemag.org/content/177/4047/393.full.pdf.

[3] Baron Cagniard de la Tour. "Exposé de quelques résultats obtenus par l'action combinée de la chaleur et de la compressionsur certains liquides, tels que l'eau, l'alcool, l'éther sulfurique et l'essence de pétrole rectifiée." In: *Annales de chimie et de physique* 20 (1822), p. 127. URL: ark:/12148/bpt6k65688981.

[4] Chemistry Demo Lab Ohio State University. *Critical opalescence in mixture of methanol and cyclohexane (video)*. URL: https://youtu.be/DIGdbmJvFUw.

[5] Bjørnholm Thomas Mouritsen Ole G. Nielsen Lars K. "Fluctuations caught in the act." In: *Nature* 404.6776 (2000), p. 352. DOI: 10.1038/35006162.

[6] H.E. Stanley. *Introduction to Phase Transitions and Critical Phenomena*. International series of monographs on physics. Oxford University Press, 1987. ISBN: 9780195053166. URL: https://books.google.fr/books?id=C3BzcUxoaNkC.

[7] John Cardy. "Conformal Field Theory and Statistical Mechanics." In: (2008). arXiv: 0807.3472 [cond-mat.stat-mech].

[8] Lars Onsager. "Crystal Statistics. I. A Two-Dimensional Model with an Order-Disorder Transition." In: *Phys. Rev.* 65 (3-4 1944), pp. 117–149. DOI: 10.1103/PhysRev.65.117.

[9] C. N. Yang. "The Spontaneous Magnetization of a Two-Dimensional Ising Model." In: *Phys. Rev.* 85 (5 1952), pp. 808–816. DOI: 10.1103/PhysRev.85.808.

[10] Tai Tsun Wu, Barry M. McCoy, Craig A. Tracy, and Eytan Barouch. "Spin-spin correlation functions for the two-dimensional Ising model: Exact theory in the scaling region." In: *Phys. Rev. B* 13.1 (1976), pp. 316–374. DOI: 10.1103/PhysRevB.13.316.

[11] M P M den Nijs. "A relation between the temperature exponents of the eight-vertex and q-state Potts model." In: *Journal of Physics A: Mathematical and General* 12.10 (1979), pp. 1857–1868. DOI: 10.1088/0305-4470/12/10/030.

[12] B Nienhuis, E K Riedel, and M Schick. "Magnetic exponents of the two-dimensional q-state Potts model." In: *Journal of Physics A: Mathematical and General* 13.6 (1980), pp. L189–L192. DOI: 10.1088/0305-4470/13/6/005.

[13] Bernard Nienhuis. "Coulomb gas description of 2-D critical behaviour." In: *Phase transitions and critical phenomena*. Ed. by Cyril Domb, Melville S. Green, Joel Louis Lebowitz, Gerhard Gompper, Michael Schick, B Schmittmann, and R. K. P. Zia. Vol. 11. Academic Press, 1972, pp. 731–761. ISBN: 0122203119.

[14] B. Duplantier and H. Saleur. "Exact fractal dimension of 2D Ising clusters." In: *Phys. Rev. Lett.* 63.22 (1989), pp. 2536–2536. DOI: 10.1103/PhysRevLett.63.2536.

[15] H. Saleur and B. Duplantier. "Exact Determination of the Percolation Hull Exponent in Two Dimensions." In: *Phys. Rev. Lett.* 58.22 (1987), pp. 2325–2328. DOI: 10.1103/PhysRevLett.58.2325.

[16] Michael Aizenman, Bertrand Duplantier, and Amnon Aharony. "Path-Crossing Exponents and the External Perimeter in 2D Percolation." In: *Physical Review Letters* 83.7 (1999), 1359–1362. ISSN: 1079-7114. DOI: 10.1103/physrevlett.83.1359.

[17] Alexander M. Polyakov. "Conformal symmetry of critical fluctuations." In: *JETP Lett.* 12 (1970), pp. 381–383.

[18] A. A. Belavin, Alexander M. Polyakov, and A. B. Zamolodchikov. "Infinite conformal symmetry in two-dimensional quantum field theory." In: *Nucl. Phys.* B241 (1984), pp. 333–380.

[19] David Poland and David Simmons-Duffin. "The conformal bootstrap." In: *Nature Physics* 12 (2016), p. 535. DOI: 10.1038/nphys3761.

[20] Sylvain Ribault. "Conformal field theory on the plane." In: (2014). arXiv: 1406.4290 [hep-th].

[21] Vladimir S. Dotsenko. "Série de Cours sur la Théorie Conforme."

[22] P. Di Francesco, P. Mathieu, and D. Senechal. *Conformal field theory*. 1997.

[23] Daniel Friedan, Zongan Qiu, and Stephen Shenker. "Conformal Invariance, Unitarity, and Critical Exponents in Two Dimensions." In: *Phys. Rev. Lett.* 52 (18 1984), pp. 1575–1578. DOI: 10.1103/PhysRevLett.52.1575.

[24] A. Cappelli and J. Zuber. "A-D-E Classification of Conformal Field Theories." In: *Scholarpedia* 5.4 (2010). revision #90926, p. 10314. DOI: 10.4249/scholarpedia.10314.

[25] V.S. Dotsenko and V.A. Fateev. "Four Point Correlation Functions and the Operator Algebra in the Two-Dimensional Conformal Invariant Theories with the Central Charge c < 1." In: *Nucl. Phys. B* 251 (1985), pp. 691–734. DOI: 10.1016/S0550-3213(85)80004-3.

[26] V.S. Dotsenko and V.A. Fateev. "Operator Algebra of Two-Dimensional Conformal Theories with Central Charge C <= 1." In: *Phys. Lett. B* 154 (1985), pp. 291–295. DOI: 10.1016/0370-2693(85)90366-1.

[27] Vincent Pasquier. "Two-dimensional critical systems labelled by Dynkin diagrams." In: *Nuclear Physics B* 285 (1987), pp. 162 –172. ISSN: 0550-3213. DOI: https://doi.org/10.1016/0550-3213(87)90332-4.

[28] V Pasquier. "Operator content of the ADE lattice models." In: *Journal of Physics A: Mathematical and General* 20.16 (1987), pp. 5707–5717. DOI: 10.1088/0305-4470/20/16/043.

[29] Wendelin Werner. *Percolation et modèle d'Ising*. Société Mathématique de France, Paris, 2009. ISBN: 978-2-85629-276-1.

[30] Hugo Duminil-Copin. "La percolation, jeu de pavages aléatoires." In: *Images des Mathématiques, CNRS* (2012). URL: https://images.math.cnrs.fr/La-percolation-jeu-de-pavages-aleatoires.html?lang=fr.

[31] J. L. Cardy. "Critical percolation in finite geometries." In: *Journal of Physics A Mathematical General* 25 (Feb. 1992), pp. L201–L206. DOI: 10.1088/0305-4470/25/4/009. arXiv: hep-th/9111026.

[32] John Cardy. "SLE for theoretical physicists." In: *Annals of Physics* 318.1 (2005), 81–118. ISSN: 0003-4916. DOI: 10.1016/j.aop.2005.04.001.

[33] Stanislav Smirnov. "Critical percolation in the plane: Conformal invariance, Cardy's formula, scaling limits." In: *Comptes Rendus de l'Académie des Sciences-Series I-Mathematics* 333.3 (2001), pp. 239–244. arXiv: 0909.4499 [math.PR].

[34] Stanislav Smirnov. *Conformal invariance in random cluster models. I. Holomorphic fermions in the Ising model*. 2007. arXiv: 0708.0039 [math-ph].

[35] Clément Hongler and Stanislav Smirnov. *The energy density in the planar Ising model*. 2010. arXiv: 1008.2645 [math-ph].

[36] Dmitry Chelkak, Clément Hongler, and Konstantin Izyurov. *Conformal Invariance of Spin Correlations in the Planar Ising Model*. 2012. arXiv: 1202.2838 [math-ph].

[37] Eveliina Peltola. "Toward a conformal field theory for Schramm-Loewner evolutions." In: *Journal of Mathematical Physics* 60.10 (2019), p. 103305. ISSN: 1089-7658. DOI: 10.1063/1.5094364.

[38] Gregory F. Lawler, Oded Schramm, and Wendelin Werner. *Values of Brownian intersection exponents II: Plane exponents*. 2000. arXiv: math/0003156 [math.PR].

[39] Stanislav Smirnov and Wendelin Werner. *Critical exponents for two-dimensional percolation*. 2001. arXiv: math/0109120 [math.PR].

[40] John L. Cardy. "Conformal invariance and surface critical behavior." In: *Nuclear Physics B* 240.4 (1984), pp. 514 –532. ISSN: 0550-3213. DOI: https://doi.org/10.1016/0550-3213(84)90241-4.

[41] Bertrand Duplantier. "Conformally Invariant Fractals and Potential Theory." In: *Physical Review Letters* 84.7 (2000), 1363–1367. ISSN: 1079-7114. DOI: 10.1103/physrevlett.84.1363.

[42] D. Stauffer and A. Aharony. *Introduction to Percolation Theory*. Oxford University Press, New York, 1971.

[43] Gesualdo Delfino and Jacopo Viti. "On three-point connectivity in two-dimensional percolation." In: *J.Phys.* A44 (2011), p. 032001. DOI: 10.1088/1751-8113/44/3/032001. arXiv: 1009.1314 [hep-th].

[44] Marco Picco, Sylvain Ribault, and Raoul Santachiara. "A conformal bootstrap approach to critical percolation in two dimensions." In: *SciPost Phys.* 1.1 (2016), p. 009. DOI: 10.21468/SciPostPhys.1.1.009. eprint: 1607.07224.

[45] Jesper Jacobsen and Hubert Saleur. "Bootstrap approach to geometrical four-point functions in the two-dimensional critical Q-state Potts model: a study of the s-channel spectra." In: *Journal of High Energy Physics* 2019 (Jan. 2019). DOI: 10.1007/JHEP01(2019)084. arXiv: 1809.02191 [math-ph].

[46] Marco Picco, Sylvain Ribault, and Raoul Santachiara. "On four-point connectivities in the critical 2d Potts model." In: *SciPost Phys.* 7.4 (2019), p. 44. DOI: 10.21468/SciPostPhys.7.4.044.

[47] Yifei He, Jesper Lykke Jacobsen, and Hubert Saleur. *Geometrical four-point functions in the two-dimensional critical Q-state Potts model: The interchiral conformal bootstrap*. 2020. arXiv: 2005.07258 [hep-th].

[48] Rongvoram Nivesvivat and Sylvain Ribault. *Logarithmic CFT at generic central charge: from Liouville theory to the Q-state Potts model*. 2020. arXiv: 2007.04190 [hep-th].

[49] Linnea Grans-Samuelsson, Lawrence Liu, Yifei He, Jesper Lykke Jacobsen, and Hubert Saleur. *The action of the Virasoro algebra in the two-dimensional Potts and loop models at generic Q*. 2020. arXiv: 2007.11539 [hep-th].

[50] Nina Javerzat, Raoul Santachiara, and Omar Foda. "Notes on the solutions of Zamolodchikov-type recursion relations in Virasoro minimal models." In: *JHEP* 08 (2018), p. 183. DOI: 10.1007/JHEP08(2018)183. arXiv: 1806.02790 [hep-th].

[51] Nina Javerzat, Marco Picco, and Raoul Santachiara. "Two-point connectivity of two-dimensional critical Q-Potts random clusters on the torus." In: *Journal of Statistical Mechanics: Theory and Experiment* 2020.2 (2020), p. 023101. DOI: 10.1088/1742-5468/ab6331. arXiv: 1907.11041 [hep-th].

[52] Nina Javerzat, Marco Picco, and Raoul Santachiara. "Three- and four-point connectivities of two-dimensional critical Q-Potts random clusters on the torus." In: *Journal of Statistical Mechanics: Theory and Experiment* 2020.5 (2020), p. 053106. DOI: 10.1088/1742-5468/ab7c5e. arXiv: 1912.05865 [hep-th].

[53] Abel Weinrib. "Long-range correlated percolation." In: *Phys. Rev. B* 29.1 (1984), pp. 387–395. DOI: 10.1103/PhysRevB.29.387.

[54] Nina Javerzat, Sebastian Grijalva, Alberto Rosso, and Raoul Santachiara. "Topological effects and conformal invariance in long-range correlated random surfaces." In: *SciPost Phys.* 9 (4 2020), p. 50. DOI: 10.21468/SciPostPhys.9.4.050. arXiv: 2005.11830.

[55] Vl.S. Dotsenko. "Critical behaviour and associated conformal algebra of the Z3 Potts model." In: *Nuclear Physics B* 235.1 (1984), pp. 54 –74. ISSN: 0550-3213. DOI: https://doi.org/10.1016/0550-3213(84)90148-2.

[56] M. Henkel. *Conformal invariance and critical phenomena*. June 1999.

[57] Shoichi Kanno, Yutaka Matsuo, and Shotaro Shiba. "Analysis of correlation functions in Toda theory and AGT-W relation for SU(3) quiver." In: *Phys. Rev.* D82 (2010), p. 066009. DOI: 10.1103/PhysRevD.82.066009. arXiv: 1007.0601 [hep-th].

[58] John L. Cardy. *Scaling and renormalization in statistical physics*. 1996.

[59] David Simmons-Duffin. *TASI Lectures on the Conformal Bootstrap*. 2016. arXiv: 1602.07982 [hep-th].

[60] Al. B. Zamolodchikov. "Conformal symmetry in two-dimensional space: Recursion representation of conformal block." In: *Theoret. and Math. Phys.* 73 (1987), pp. 1088–1093.

[61] Alexander B. Zamolodchikov. *Physics Reviews. vol. 10, pt. 4: Conformal field theory and critical phenomena in two-dimensional systems*. Ed. by Alexei B. Zamolodchikov and I.M. Khalatnikov. 1989.

[62] Sylvain Ribault. "On 2d CFTs that interpolate between minimal models." In: *SciPost Physics* 6.6 (2019). ISSN: 2542-4653. DOI: 10.21468/scipostphys.6.6.075.

[63] Vladimir Belavin, Benoit Estienne, Omar Foda, and Raoul Santachiara. "Correlation functions with fusion-channel multiplicity in $\mathcal{W}_3$ Toda field theory." In: *JHEP* 06 (2016), p. 137. DOI: 10.1007/JHEP06(2016)137. arXiv: 1602.03870 [hep-th].

[64] Alexander B. Zamolodchikov and Alexei B. Zamolodchikov. "Structure constants and conformal bootstrap in Liouville field theory." In: *Nucl. Phys.* B477 (1996), pp. 577–605. DOI: 10.1016/0550-3213(96)00351-3. eprint: hep-th/9506136.

[65] Benoit Estienne and Yacine Ikhlef. "Correlation functions in loop models." In: (2015). arXiv: 1505.00585 [math-ph].

[66] Santiago Migliaccio and Sylvain Ribault. "The analytic bootstrap equations of non-diagonal two-dimensional CFT." In: (2017). arXiv: 1711.08916 [hep-th].

[67] P. Di Francesco, H. Saleur, and J.B. Zuber. "Critical Ising correlation functions in the plane and on the torus." In: *Nuclear Physics B* 290 (1987), pp. 527 –581. ISSN: 0550-3213. DOI: https://doi.org/10.1016/0550-3213(87)90202-1.

[68] P. Di Francesco, H Saleur, and J.-B Zuber. "Correlation Functions of the Critical Ising Model on a Torus." In: *Europhysics Letters (EPL)* 5.2 (1988), pp. 95–99. DOI: 10.1209/0295-5075/5/2/001.

[69] H. Saleur. "Correlation functions of the critical Ashkin-Teller model on a torus." In: *Journal of Statistical Physics* 50.3 (1988), 475–508. ISSN: 1572-9613. DOI: 10.1007/BF01026488.

[70] T. Eguchi and H. Ooguri. "Conformal and current algebras on a general Riemann surface." In: *Nuclear Physics B* 282 (1987), pp. 308–328. DOI: 10.1016/0550-3213(87)90686-9.

[71] V. A. Fateev and A. V. Litvinov. "On AGT conjecture." In: *JHEP* 02 (2010), p. 014. DOI: 10.1007/JHEP02(2010)014. arXiv: 0912.0504 [hep-th].

[72] Wendelin Werner. *Conformally Invariant Models - Parte 1, Escola de Altos Estudos (6:30-7:30)*. URL: https://youtu.be/Rv7NLVslPkQ?t=390.

[73] I Rushkin, E Bettelheim, I A Gruzberg, and P Wiegmann. "Critical curves in conformally invariant statistical systems." In: *Journal of Physics A: Mathematical and Theoretical* 40.9 (2007), pp. 2165–2195. DOI: 10.1088/1751-8113/40/9/020.

[74] Gesualdo Delfino and Jacopo Viti. "Potts q-color field theory and scaling random cluster model." In: *Nucl. Phys.* B852 (2011), pp. 149–173. DOI: 10.1016/j.nuclphysb.2011.06.012. arXiv: 1104.4323 [hep-th].

[75] R. M. Ziff, J. J. H. Simmons, and P. Kleban. "Factorization of correlations in two-dimensional percolation on the plane and torus." In: *Journal of Physics A Mathematical General* 44.6, 065002 (Feb. 2011), p. 065002. DOI: 10.1088/1751-8113/44/6/065002. arXiv: 1011.1101 [cond-mat.dis-nn].

[76] Marco Picco, Raoul Santachiara, Jacopo Viti, and Gesualdo Delfino. "Connectivities of Potts Fortuin-Kasteleyn clusters and time-like Liouville correlator." In: *Nucl.Phys.* B875 (2013), pp. 719–737. DOI: 10.1016/j.nuclphysb.2013.07.014. arXiv: 1304.6511 [hep-th].

[77] Pierre Mathieu and David Ridout. "From percolation to logarithmic conformal field theory." In: *Physics Letters B* 657.1-3 (2007), 120–129. ISSN: 0370-2693. DOI: 10.1016/j.physletb.2007.10.007. arXiv: 0708.0802 [hep-th].

[78] Pierre Mathieu and David Ridout. "Logarithmic minimal models, their logarithmic couplings, and duality." In: *Nuclear Physics B* 801.3 (2008), 268–295. ISSN: 0550-3213. DOI: 10.1016/j.nuclphysb.2008.02.017. arXiv: 0711.3541 [hep-th].

[79] Romain Couvreur, Jesper Lykke Jacobsen, and Romain Vasseur. "Non-scalar operators for the Potts model in arbitrary dimension." In: *Journal of Physics A: Mathematical and Theoretical* 50.47 (2017), p. 474001. ISSN: 1751-8121. DOI: 10.1088/1751-8121/aa7f32.

[80] Victor Gorbenko and Bernardo Zan. *Two-dimensional O(n) models and logarithmic CFTs*. 2020. arXiv: 2005.07708 [hep-th].

[81] V. Gurarie. "Logarithmic operators and logarithmic conformal field theories." In: *Journal of Physics A Mathematical General* 46, 494003 (Dec. 2013), p. 4003. DOI: 10.1088/1751-8113/46/49/494003. arXiv: 1303.1113 [cond-mat.stat-mech].

[82] Matthijs Hogervorst, Miguel Paulos, and Alessandro Vichi. "The ABC (in any D) of logarithmic CFT." In: *Journal of High Energy Physics* 2017.10 (2017). ISSN: 1029-8479. DOI: 10.1007/jhep10(2017)201.

[83] R. Santachiara and J. Viti. "Local logarithmic correlators as limits of Coulomb gas integrals." In: *Nuclear Physics B* 882 (May 2014), pp. 229–262. DOI: 10.1016/j.nuclphysb.2014.02.022. arXiv: 1311.2055 [hep-th].

[84] J. Cardy. "Logarithmic conformal field theories as limits of ordinary CFTs and some physical applications." In: *Journal of Physics A Mathematical General* 46, 494001 (Dec. 2013), p. 4001. DOI: 10.1088/1751-8113/46/49/494001. arXiv: 1302.4279 [cond-mat.stat-mech].

[85] Victor Gorbenko, Slava Rychkov, and Bernardo Zan. "Walking, Weak first-order transitions, and Complex CFTs II. Two-dimensional Potts model at $Q > 4$." In: *SciPost Phys.* 5.5 (2018), p. 50. DOI: 10.21468/SciPostPhys.5.5.050. arXiv: 1808.04380 [hep-th].

[86] R J Baxter. "Potts model at the critical temperature." In: *Journal of Physics C: Solid State Physics* 6.23 (1973), pp. L445–L448. DOI: 10.1088/0022-3719/6/23/005.

[87] B. Nienhuis, A. N. Berker, Eberhard K. Riedel, and M. Schick. "First- and Second-Order Phase Transitions in Potts Models: Renormalization-Group Solution." In: *Phys. Rev. Lett.* 43.11 (1979), pp. 737–740. DOI: 10.1103/PhysRevLett.43.737.

[88] Hugo Duminil-Copin, Vladas Sidoravicius, and Vincent Tassion. "Continuity of the Phase Transition for Planar Random-Cluster and Potts Models with $1 \leq q \leq 4$." In: *Communications in Mathematical Physics* 349.1 (2016), 47–107. ISSN: 1432-0916. DOI: 10.1007/s00220-016-2759-8.

[89] Dmitry Chelkak and Stanislav Smirnov. *Universality in the 2D Ising model and conformal invariance of fermionic observables*. 2009. arXiv: 0910.2045 [math-ph].

[90] R.J. Baxter. *Exactly solved models in statistical mechanics*. 1982. ISBN: 978-0-486-46271-4.

[91] Jesper Jacobsen. "Loop Models and Boundary CFT." In: (). Ed. by Malte Henkel and Dragi Karevski.

[92] Bernard Nienhuis. "Exact Critical Point and Critical Exponents of O(n) Models in Two Dimensions." In: *Phys. Rev. Lett.* 49.15 (1982), pp. 1062–1065. DOI: 10.1103/PhysRevLett.49.1062.

[93] L P Kadanoff. "Lattice Coulomb gas representations of two-dimensional problems." In: *Journal of Physics A: Mathematical and General* 11.7 (1978), pp. 1399–1417. DOI: 10.1088/0305-4470/11/7/027.

[94] P. di Francesco, H. Saleur, and J. B. Zuber. "Relations between the coulomb gas picture and conformal invariance of two-dimensional critical models." In: *Journal of Statistical Physics* 49.1-2 (1987), 57–79.

[95] Vladimir Dotsenko and Vladimir Fateev. "Operator algebra of two-dimensional conformal theories with central charge $C \leq 1$." In: *Physics Letters B* 154 (1985), p. 291. DOI: 10.1016/0370-2693(85)90366-1.

[96] Yacine Ikhlef, Jesper Lykke Jacobsen, and Hubert Saleur. "Three-Point Functions in $c \leq 1$ Liouville Theory and Conformal Loop Ensembles." In: *Phys. Rev. Lett.* 116.13 (2016), p. 130601. DOI: 10.1103/PhysRevLett.116.130601. arXiv: 1509.03538 [cond-mat.stat-mech].

[97] Alexei B. Zamolodchikov. "On the three-point function in minimal Liouville gravity." In: (2005). eprint: hep-th/0505063.

[98] Yifei He, Linnea Grans-Samuelsson, Jesper Lykke Jacobsen, and Hubert Saleur. "Four-point geometrical correlation functions in the two-dimensional Q-state Potts model: connections with the RSOS models." In: *Journal of High Energy Physics* 2020.156 (2020). DOI: 10.1007/JHEP05(2020)156. arXiv: 2002.09071 [hep-th].

[99] Jean-François Richard and Jesper Lykke Jacobsen. "Character decomposition of Potts model partition functions, I: Cyclic geometry." In: *Nuclear Physics B* 750.3 (2006), 250–264. ISSN: 0550-3213. DOI: 10.1016/j.nuclphysb.2006.05.028.

[100] Nina Javerzat. *CFT-notebooks*. URL: https://github.com/NinaJaverzat/CFT-notebooks.

[101] S. Ribault and R. Santachiara. "Liouville theory with a central charge less than one." In: *Journal of High Energy Physics* 8, 109 (Aug. 2015), p. 109. DOI: 10.1007/JHEP08(2015)109. arXiv: 1503.02067 [hep-th].

[102] Sylvain Ribault. *The non-rational limit of D-series minimal models*. 2019. arXiv: 1909.10784 [hep-th].

[103] A L. Efros. *Physics and Geometry of Disorder : Percolation Theory*. Mir Publishers, 1986. Chap. 10.

[104] Abbas Ali Saberi. "Recent advances in percolation theory and its applications." In: *Physics Reports* 578 (2015). Recent advances in percolation theory and its applications, pp. 1 –32. ISSN: 0370-1573. DOI: https://doi.org/10.1016/j.physrep.2015.03.003.

[105] Hernán A. Makse, José S. Andrade, and H. Eugene Stanley. "Tracer dispersion in a percolation network with spatial correlations." In: *Phys. Rev. E* 61.1 (2000), pp. 583–586. DOI: 10.1103/PhysRevE.61.583.

[106] A. D. Araújo, A. A. Moreira, R. N. Costa Filho, and J. S. Andrade. "Statistics of the critical percolation backbone with spatial long-range correlations." In: *Phys. Rev. E* 67.2 (2003), p. 027102. DOI: 10.1103/PhysRevE.67.027102.

[107] D. Bernard, G. Boffetta, A. Celani, and G Falkovich. "Conformal invariance in two-dimensional turbulence." In: *Nature Physics* 2 (2006), p. 124.

[108] Hernán A. Makse, Shlomo Havlin, and H. Eugene Stanley. "Modelling urban growth patterns." In: *Nature* 377 (1995), p. 608.

[109] E. Bogomolny and C. Schmit. "Percolation Model for Nodal Domains of Chaotic Wave Functions." In: *Physical Review Letters* 88.11 (2002). ISSN: 1079-7114. DOI: 10.1103/physrevlett.88.114102.

[110] Alexander B. Zamolodchikov. ""Irreversibility" of the flux of the renormalization group in a 2D field theory." In: *JETP Letters* 43 (1986), p. 730.

[111] Joseph Polchinski. "Scale and conformal invariance in quantum field theory." In: *Nuclear Physics B* 303.2 (1988), pp. 226 –236. ISSN: 0550-3213. DOI: https://doi.org/10.1016/0550-3213(88)90179-4.

[112] H. E. Hurst et al. "The problem of long-time storage in reservoirs." In: *International Association of Scientific Hydrology. Bulletin* 1.3 (1956), pp. 13–27. DOI: 10.1080/02626665609493644.

[113] Robert O. Collins. "In Search of the Nile Waters, 1900–2000." In: *The Nile: Histories, Cultures, Myths*. Ed. by Haggai Erlich and Israel Gershoni. Lynne Rienner Publishers, 2000, p. 256. ISBN: 1555876722.

[114] Hugo Vanneuville. "Percolation in the plane : dynamics, random tilings and nodal lines." Thesis. Université de Lyon, Nov. 2018. URL: https://tel.archives-ouvertes.fr/tel-02067958.

[115] Dmitry Beliaev, Stephen Muirhead, and Alejandro Rivera. *A covariance formula for topological events of smooth Gaussian fields*. 2018. arXiv: 1811.08169 [math.PR].

[116] K. J. Schrenk, N. Posé, J. J. Kranz, L. V. M. van Kessenich, N. A. M. Araújo, and H. J. Herrmann. "Percolation with long-range correlated disorder." In: *Phys. Rev. E* 88.5 (2013), p. 052102. DOI: 10.1103/PhysRevE.88.052102.

[117] Johannes Zierenberg, Niklas Fricke, Martin Marenz, F. P. Spitzner, Viktoria Blavatska, and Wolfhard Janke. "Percolation thresholds and fractal dimensions for square and cubic lattices with long-range correlated defects." In: *Physical Review E* 96.6 (2017). ISSN: 2470-0053. DOI: 10.1103/physreve.96.062125.

[118] Sona Prakash, Shlomo Havlin, Moshe Schwartz, and H. Eugene Stanley. "Structural and dynamical properties of long-range correlated percolation." In: *Phys. Rev. A* 46.4 (1992), R1724–R1727. DOI: 10.1103/PhysRevA.46.R1724.

[119] J Schmittbuhl, J P Vilotte, and S Roux. "Percolation through self-affine surfaces." In: *Journal of Physics A: Mathematical and General* 26.22 (1993), pp. 6115–6133. DOI: 10.1088/0305-4470/26/22/014.

[120] Joel L. Lebowitz and H. Saleur. "Percolation in strongly correlated systems." In: *Physica A: Statistical Mechanics and its Applications* 138.1 (1986), pp. 194 –205. ISSN: 0378-4371. DOI: https://doi.org/10.1016/0378-4371(86)90180-9.

[121] Juhan Aru, Titus Lupu, and Avelio Sepúlveda. *First passage sets of the 2D continuum Gaussian free field*. 2017. arXiv: 1706.07737 [math.PR].

[122] Lukas Schoug, Avelio Sepúlveda, and Fredrik Viklund. *Dimension of two-valued sets via imaginary chaos*. 2019. arXiv: 1910.09294 [math.PR].

[123] Leo P. Kadanoff and Franz J. Wegner. "Some Critical Properties of the Eight-Vertex Model." In: *Phys. Rev. B* 4 (1971), pp. 3989–3993. DOI: 10.1103/PhysRevB.4.3989.

[124] Gesualdo Delfino. "Exact Results for Quenched Bond Randomness at Criticality." In: *Phys. Rev. Lett.* 118.25 (2017), p. 250601. DOI: 10.1103/PhysRevLett.118.250601.

[125] Gesualdo Delfino and Elena Tartaglia. "On superuniversality in the $Q-$state Potts model with quenched disorder." In: *Journal of Statistical Mechanics: Theory and Experiment* 2017.12 (2017), p. 123303. ISSN: 1742-5468. DOI: 10.1088/1742-5468/aa9bad.

[126] C. P. de Castro, M. Luković, G. Pompanin, R. F. S. Andrade, and H. J. Herrmann. "Schramm-Loewner evolution and perimeter of percolation clusters of correlated random landscapes." In: *Scientific Reports* 8.1 (2018). ISSN: 2045-2322. DOI: 10.1038/s41598-018-23489-x. arXiv: 1712.03115 [cond-mat.stat-mech].

[127] N. Posé, K. J. Schrenk, N. A. M. Araújo, and H. J. Herrmann. "Schramm–Loewner evolution of the accessible perimeter of isoheight lines of correlated landscapes." In: *International Journal of Modern Physics C* 29.01 (2018), p. 1850008. DOI: 10.1142/S0129183118500080. eprint: https://doi.org/10.1142/S0129183118500080.

[128] Vincent Beffara. "Hausdorff dimensions for SLE6." In: *The Annals of Probability* 32.3B (2004), 2606–2629. ISSN: 0091-1798. DOI: 10.1214/009117904000000072.

[129] C. P. de Castro, M. Luković, R. F. S. Andrade, and H. J. Herrmann. "The influence of statistical properties of Fourier coefficients on random Gaussian surfaces." In: *Scientific Reports* 7.1 (2017). ISSN: 2045-2322. DOI: 10.1038/s41598-017-02135-y.

[130] Xiangyu Cao, Alberto Rosso, and Raoul Santachiara. "Conformal invariance of loop ensembles under Kardar-Parisi-Zhang dynamics." In: *EPL (Europhysics Letters)* 111.1 (2015), p. 16001. ISSN: 1286-4854. DOI: 10.1209/0295-5075/111/16001.

[131] E. Bogomolny and C. Schmit. "Random wavefunctions and percolation." In: *Journal of Physics A Mathematical General* 40 (Nov. 2007), pp. 14033–14043. DOI: 10.1088/1751-8113/40/47/001. arXiv: 0708.4335 [nlin.CD].

[132] Viktor Dotsenko. *Introduction to the Replica Theory of Disordered Statistical Systems*. Vol. 55. Jan. 2001. DOI: 10.1017/CBO9780511524592.

[133] A. W. W. Ludwig. "Critical behavior of the two-dimensional random q-state Potts model by expansion in (q - 2)." In: *Nuclear Physics B* 285 (1987), pp. 97–142. DOI: 10.1016/0550-3213(87)90330-0.

[134] Bertrand Berche and Christophe Chatelain. *Phase transitions in two-dimensional random Potts models*. 2002. arXiv: cond-mat/0207421 [cond-mat.dis-nn].

[135] Elias Kiritsis. *String theory in a nutshell*. USA: Princeton University Press, 2019. ISBN: 978-0-691-15579-1, 978-0-691-18896-6.

université PARIS-SACLAY
ÉCOLE DOCTORALE
Physique en l'Île-de-France (PIF)

TITRE : Nouvelles solutions de bootstrap conforme et modèles de percolation sur le tore

MOTS CLÉS : bootstrap conforme, modèles critiques, géométrie d'ensembles fractals

RÉSUMÉ : Les propriétés géométriques des phénomènes critiques ont généré un intérêt croissant en physique théorique ainsi qu'en mathématiques au cours des trente dernières années. Les systèmes de percolation sont l'exemple par excellence de tels phénomènes géométriques, où la transition de phase est caractérisée par le comportement de degrés de liberté non-locaux, les amas de percolation. Au point critique, ces amas sont des exemples d'objets aléatoires dont la mesure est invariante conforme, c'est à dire invariante sous tout changement d'échelle local. Nous ne savons en général pas caractériser complètement ces amas, ni même pour le modèle le plus simple de la percolation pure. En deux dimensions, la présence de la symétrie conforme a des conséquences particulièrement importantes. Dans cette thèse nous examinons les implications de cette symétrie sur les propriétés universelles des systèmes critiques bidimensionels, en utilisant une approche dite de bootstrap conforme.
La première partie détaille les implications générales de l'invariance conforme, en examinant ses conséquences sur les fonctions de corrélation. Sont considérés en particulier les effets induits par une topologie de tore, ce qui est appliqué dans la deuxième partie de la thèse à l'étude de modèle statistiques particuliers. Nous discutons également les propriétés analytiques des fonctions de corrélation et présentons des résultats sur des questions techniques liées à l'implémentation de méthodes numériques de bootstrap conforme en deux dimensions. La seconde partie est dédiée à l'étude de deux familles particulières de modèles critiques de percolation avec des corrélations de longue portée : le modèle d'amas aléatoires de Potts à Q états, et un modèle de percolation de surfaces aléatoires. Nous explorons les propriétés percolatoires de ces modèles en étudiant les propriétés de connectivité des amas, c'est à dire les probabilités que des points appartiennent au même amas. Nous avons réalisé que les connectivités sur le tore représentent des observables très intéressantes. En les décrivant comme fonction de corrélation de champs quantiques dans une théorie des champs conforme, nous obtenons de nouveaux résultats sur les classes d'universalité de ces modèles.

TITLE: New conformal bootstrap solutions and percolation models on the torus

KEYWORDS: conformal bootstrap, critical phenomena, geometry of fractal sets

The geometric properties of critical phenomena have generated an increasing interest in theoretical physics and mathematics over the last thirty years. Percolation-type systems are a paradigm of such geometric phenomena, their phase transition being characterised by the behaviour of non-local degrees of freedom: the percolation clusters. At criticality, such clusters are examples of random objects with a conformally invariant measure, namely invariant under all local rescalings. Even in the simplest percolation model –pure percolation, we do not know how to fully characterise these clusters. In two dimensions, the presence of conformal symmetry has especially important implications. In this thesis we investigate the consequences of this symmetry on the universal properties of two-dimensional critical statistical models, by using a conformal bootstrap approach.
The first part details the general implications of conformal invariance, by examining its consequences on correlation functions. Are addressed in particular the effects induced by the torus topology, applied in the second part to the study of specific statistical models. We also examine the analytic properties of correlation functions and present results on technical questions related to the implementation of numerical conformal bootstrap methods in two dimensions. The second part is devoted to the study of two specific families of critical long-range correlated percolation models: the random cluster $Q-$state Potts model and the percolation of random surfaces. We investigate the percolative properties of these models by studying the clusters connectivity properties, namely the probability that points belong to the same cluster. We find that the connectivities on a torus represent particularly interesting observables. By describing them as correlation functions of quantum fields in a conformal field theory, we obtain new results on the universality classes of these models.

Université Paris-Saclay
Espace Technologique / Immeuble Discovery
Route de l'Orme aux Merisiers RD 128 / 91190 Saint-Aubin, France